

Structural and functional studies on GTPases involved in eukaryal translation initiation

Dissertation

zur Erlangung des mathematisch-naturwissenschaftlichen Doktorgrades

„Doctor rerum naturalis“

der Georg-August-Universität Göttingen

im Promotionsprogramm „Grundprogramm Biologie“

der Georg-August University School of Science (GAUSS)

vorgelegt von

Bernhard Kuhle

aus Göttingen

Göttingen, 2014

Betreuungsausschuss

Prof. Dr. Ralf Ficner, Abteilung für Molekulare Strukturbiologie, Institut für Mikrobiologie und Genetik, Georg August Universität Göttingen

Prof. Dr. Marina Rodnina, Abteilung für Physikalische Biochemie, Max Planck Institut für Biophysikalische Chemie, Göttingen

Mitglieder der Prüfungskommission

Referent:

Prof. Dr. Ralf Ficner, Abteilung für Molekulare Strukturbiologie, Institut für Mikrobiologie und Genetik, Georg August Universität Göttingen

Korreferent:

Prof. Dr. Marina Rodnina, Abteilung für Physikalische Biochemie, Max Planck Institut für Biophysikalische Chemie, Göttingen

Weitere Mitglieder der Prüfungskommission

Prof. Dr. Reinhard Lührmann, Abteilung für Zelluläre Biochemie, Max Planck Institut für Biophysikalische Chemie, Göttingen

Prof. Dr. Heinz Neumann, Angewandte Synthetische Biologie, Institut für Mikrobiologie und Genetik, Georg August Universität Göttingen

Prof. Dr. Holger Stark, Abteilung für Dreidimensionale Kryo-Elektronenmikroskopie, Max Planck Institut für Biophysikalische Chemie, Göttingen

Prof. Dr. Jörg Stülke, Abteilung für Allgemeine Mikrobiologie, Institut für Mikrobiologie und Genetik, Georg August Universität Göttingen

Tag der mündlichen Prüfung: 16. Oktober 2014

Preface

The following thesis summarizes my work on translational GTPases and the mechanism of eukaryal translation initiation, which was performed at the University of Göttingen under the supervision of Prof. Dr. Ralf Ficner. The work led to the following publications:

“eIF5B employs a novel domain release mechanism to catalyze ribosomal subunit joining”, *Kuhle, B. and Ficner, R.*, 2014, *The EMBO Journal*, 33: 1177–1191.

“A monovalent cation acts as structural and catalytic cofactor in translational GTPases”, *Kuhle, B. and Ficner, R.*, 2014, *The EMBO Journal*, in press.

“Structural insight into the recognition of amino-acylated initiator tRNA by eIF5B in the 80S initiation complex”, *Kuhle, B. and Ficner, R.*, 2014, *BMC Structural Biology*, accepted.

“Translation initiation factor eIF3b contains a nine-bladed beta-propeller and interacts with the 40S ribosomal subunit”, *Liu, Y., Neumann, P., Kuhle, B., Monecke, T., Schell, S., Chari, A., & Ficner, R.*, 2014, *Structure*, 22: 1-8.

“Analysis of the interaction network between eIF2 and eIF5 and its implications for the process of eukaryal translation initiation”, *Kuhle, B., Valerius, O. and Ficner, R.*, 2014, manuscript in preparation.

“Analysis of the interaction network between eIF2 and eIF2B ϵ and its implications for the mechanism of nucleotide exchange”, *Kuhle, B., Valerius, O. and Ficner, R.*, 2014, manuscript in preparation.

“The crystal structures of eIF2B β and eIF2B δ provide new insights into the regulatory subcomplex of eIF2B, the guanine nucleotide exchange factor for eIF2”, *Kuhle, B., and Ficner, R.*, 2014, manuscript in preparation.

With the exception of Liu *et al.* (2014), these publications are included in this present thesis, although not in chronological but in topical order. The contributions of the individual authors are given at the beginning of the respective chapters.

Contents

<i>Summary</i>	1
<i>Chapter 1 • Introduction</i>	5
1.1 The ribosome and the universal mechanism of translation	6
1.2 Translation initiation	10
1.2.1 Cap-dependent translation initiation in eukarya	10
1.3 GTPases involved in translation	12
1.3.1 The eukaryal translation initiation factor 2 (eIF2)	16
1.3.1.1 eIF2 and the recognition of the Met-tRNA _i	16
1.3.1.2 eIF5 regulates the activity of eIF2.....	19
1.3.1.3 Recycling of eIF2·GDP by eIF2B.....	22
1.3.2 The eukaryal translation initiation factor 5B (eIF5B)	23
<i>Chapter 2 • Interaction network between eIF2 and eIF5</i>	25
2.1 Introduction	26
2.2 Results	29
2.3 Discussion	60
2.4 Materials and Methods.....	69
2.5 Supplementary information	81
<i>Chapter 3 • Interaction network between eIF2 and eIF2Bε</i>	87
3.1 Introduction	88
3.2 Results.....	91
3.3 Discussion	103
3.4 Materials and Methods.....	112
3.5 Supplementary information	116
<i>Chapter 4 • Structural analysis of eIF2Bβ and eIF2Bδ</i>	119
4.1 Introduction	120
4.2 Results.....	123
4.3 Discussion	136
4.4 Materials and Methods.....	141
<i>Chapter 5 • The domain release mechanism of eIF5B</i>	145

5.1	Introduction	146
5.2	Results	149
5.3	Discussion	162
5.4	Materials and Methods	170
5.5	Supplementary information.....	172
Chapter 6 • Recognition of amino-acylated initiator tRNA by eIF5B in the 80S IC.....		185
6.1	Background.....	186
6.2	Results and Discussion	190
6.3	Methods.....	201
Chapter 7 • A monovalent cation as cofactor in translational GTPases		203
7.1	Introduction	204
7.2	Results	207
7.3	Discussion	221
7.4	Materials and Methods	228
7.5	Expanded View.....	232
Chapter 8 • Synopsis and outlook.....		247
References.....		251
Acknowledgements		263
Curriculum vitae		264

Summary

Translation, the process of mRNA-encoded protein biosynthesis, is one of the fundamental processes that are universally conserved in extant cellular life. In all its major stages, namely initiation, elongation, termination and recycling, translation depends on a dynamic interplay between the ribosome as the principle place of protein synthesis, mRNA, tRNAs and a number of accessory proteins called translation factors. A subgroup of these translation factors belongs to the universally conserved family of translational GTPases (trGTPases) that use the free energy of GTP hydrolysis to ensure the necessary speed and accuracy of protein synthesis on the ribosome. One of the most complex processes supported by trGTPases, namely by the eukaryal translation initiation factors 2 (eIF2) and 5B (eIF5B), is the intricate mechanism of cap-dependent translation initiation in eukaryal cells.

The current thesis focuses on the structural and functional characterization of the trGTPases eIF2 and eIF5B. The first part of this thesis (chapters 2-4) is dedicated to eIF2, a structurally unusually complex trGTPase that is responsible for the GTP-dependent delivery of the unique initiator tRNA to the ribosome, and the auxiliary initiation factors that regulate the guanine-nucleotide cycle of eIF2, namely the specialized GTPase activating protein (GAP) eIF5 and the guanine-nucleotide exchange factor (GEF) eIF2B. The second part of the thesis (chapters 5-7) encompasses a structural and functional analysis of eIF5B, a universally conserved trGTPase that catalyzes ribosomal subunit joining in a GTP-dependent manner to form elongation-competent ribosomes.

Throughout the thesis, the methodological focus lies on the specific mechanistic aspects of eIF2 and eIF5B function during translation initiation. Both initiation factors will thereby be treated individually in their respective functional contexts of the initiation process, with each of the six chapters dedicated to particular questions at hand. The natural framework for the analysis of the presented findings is however provided by the origin of the functional properties of eIF2 and eIF5B

Summary

in the historical settings of molecular evolution as a compromise between the innovative processes of structural adaption to biological constellations and the conservative preservation of underlying functional principles. Based on this framework, the specific findings for either trGTPase are used for generalizations in the larger context of translation as an evolved process.

The first chapter forms a general introduction into the mechanism of translation, with a particular focus on the processes that underlie translation initiation in eukarya, to provide an overview of the general mechanistic settings into which eIF2 and eIF5B are placed. More specific introductions into the particular questions addressed in the present work are given individually in each chapter.

Chapter 2 focuses on the analysis of the interaction network between eIF2 and its multifunctional effector protein eIF5. A combination of complimentary high- and low-resolution structural approaches with mutational and biochemical methods is used to show how eIF5 forms three main contacts with the eIF2 complex, and how these interactions affect the contacts of both proteins with initiation factors eIF1 and eIF3c. A high-resolution crystal structure of the eIF2 β N-terminal tail in complex with the eIF5-CTD and Trp quenching experiments show how the recruitment of eIF5 to its substrate eIF2 is mediated by a flexible peptide-domain interaction that provides the means for the dynamic interplay between eIF2, eIF5 and other eIFs in the course of the initiation process. A second interaction was found to be formed between the eIF5-NTD and the GTP-binding eIF2 γ subunit. Finally, the third interaction occurs between the eIF5-CTD and eIF2 γ next to the nucleotide binding pocket, indicating that this contact might be responsible for the previously reported function of eIF5 in stabilizing the bound guanine-nucleotide on eIF2. Together, the presented findings provide a more complete and refined picture of the intricate interactions between eIF2 and eIF5 that play central roles at various stages of the initiation process.

Chapter 3 focuses on the interactions between eIF2 and the catalytic ϵ -subunit of its GEF eIF2B. A combination of structural and biochemical methods was used to gain insight into the interactions between eIF2B ϵ and its substrate eIF2 to understand the molecular basis for nucleotide exchange. This analysis indicates that the catalytic eIF2B ϵ -CTD contacts its substrate eIF2 via two main interfaces: a nucleotide-independent high-affinity interaction with the eIF2 β subunit, and a nucleotide-dependent direct contact to the γ -subunit, which is responsible for the

destabilization of the bound nucleotide, most likely in a manner analogous to the mechanisms used by other GEFs. One of the central aspects of the presented findings is their qualitative comparison to those reported for the eIF2·eIF5 interaction in chapter 2. The observation of a high degree of structural and functional similarities between the regions in eIF2B ϵ and eIF5 that contact eIF2 to modulate its affinity to guanine nucleotides results in the hypothesis that these similarities are not merely the result of mechanistic analogies between both proteins but might in fact be the result of an evolutionary homology.

Chapter 4 focuses on structural aspects of the regulatory subcomplex of the eIF2-specific exchange factor eIF2B which is composed of subunits α , β and δ and which is involved in the regulation of translation by modulating the exchange activity of the eIF2B complex. In this chapter the first high-resolution crystal structures of the isolated eIF2B β and eIF2B δ subunits are presented together with a protocol for the recombinant purification and *in vitro* reconstitution of the complete eIF2B $\alpha\beta\delta$ complex from the fungus *Chaetomium thermophilum*.

In chapter 5, the question is addressed how GTP binding and hydrolysis by eIF5B mediate its catalytic role during ribosomal subunit joining. Six high resolution crystal structures of eIF5B in its apo, GDP- and GTP-bound form are presented. Together with an analysis of the thermodynamics of nucleotide binding, they provide a detailed picture of the nucleotide cycle performed by eIF5B. The data suggest that GTP binding induces significant conformational changes in eIF5B that activate the factor for ribosome binding and subunit joining. Based on these observations, a domain release mechanism for eIF5B activation is proposed, which represents a novel variation from the classical paradigm of GTPase function and suggests a unified picture of subunit joining by a/eIF5B and its bacterial ortholog IF2.

Chapter 6 addresses the specific aspect of how domain IV in eIF5B and IF2 interacts with the acceptor stem of the initiator tRNA in the ribosomal context, an interaction that is central to subunit joining as the last checkpoint for the formation of functional ribosomes. A reinterpretation of a 6.6 Å resolution cryo-EM structure of the yeast 80S initiation complex using the newly determined crystal structures of eIF5B from *C. thermophilum* shows that eIF5B domain IV interacts extensively with the initiator tRNA, which includes direct recognition of the methionylated 3' CCA-end. The presented findings provide the basis for a possible scenario for the evolution of the

Summary

structurally homologous translational β barrel folds in eIF5B/IF2 and EF-Tu/aIF2 γ and their interactions with tRNAs.

Chapter 7 is dedicated to the presentation of the hypothesis of monovalent cation (M^+) dependency among trGTPases, according to which an M^+ ion acts as structural and catalytic cofactor in trGTPases. The fundament for this hypothesis is formed by biochemical and high-resolution structural data that demonstrate that eIF5B, the archaeal elongation factor aEF1A and its bacterial ortholog EF-Tu in their GTP-bound form coordinate an M^+ in their active sites. In sequence and structure, the coordination shell for the M^+ ion is highly conserved among trGTPases from bacteria to human, suggesting a universal mechanism of M^+ -dependent conformational switching and GTP-hydrolysis among trGTPases, which provides considerable explanatory power for previously unresolved questions concerning the function and evolution of trGTPases.

Chapter 8 finally forms a brief synopsis for the presented findings and gives an outlook into the prospects for future work on the various questions that were addressed in the course of this thesis.

Chapter 1 • Introduction

The metabolism of living organisms depends on an intricate network of mutually interdependent reactions that serve the accumulation of energy and the synthesis of cell material. As functionally most versatile macro molecules, proteins play the central role as catalysts of chemical reactions, for cellular transport or as storage molecules. The synthesis of functional proteins according to genetically encoded information thus constitutes one of the key processes in the metabolism of extant cellular life.

During the biosynthesis of proteins, the flow of the genetic information follows a common principle in all living cells, consisting of two major steps: In the first step, called transcription, the DNA-encoded genetic information is copied to a messenger RNA (mRNA), representing a short-lived mobile version of the genetic information. In the second step, called translation, this mRNA serves as template for protein synthesis, during which the triplet codons of the mRNA are translated into amino-acids that become covalently condensed into the growing polypeptide chain. The principle site of protein synthesis is the ribosome, a large multi-protein-RNA complex, whose activity is complemented by an apparatus of additional proteins, the so-called translation factors that ensure the necessary accuracy and speed during the four major stages of translation: initiation, elongation, termination and recycling. As the critical step of the information flow, in which the level of the genetic information intersects with the functional level of proteins, translation thus depends on the concerted interplay between ribonucleic acids and proteins. The key role of this process for cellular life becomes apparent from the universal evolutionary conservation of the translation machinery in the three domains of life, indicating that the underlying principles of extant protein synthesis evolved long before the onset of speciation.

1.1 The ribosome and the universal mechanism of translation

Protein synthesis is carried out by the ribosome, a large ribonucleo-protein assembly of 2.5 and 4 MDa in size in bacteria/archaea and eukarya, respectively, composed of about two-thirds ribosomal RNA (rRNA) and one-third protein (Fig. 1.1) [2-4]. The overall architecture as well as the structural and functional core of the ribosome is universally conserved throughout evolution from bacteria to human [5, 6]. The Ribosome comprises two subunits: The small subunit (30S in bacteria/archaea, 40S in eukarya) contains the mRNA binding channel and decoding center (DC), and is responsible for fidelity and processivity of the translation process. The large subunit (50S in bacteria/archaea, 60S in eukarya) contains the peptidyl transferase center (PTC), which constitutes the active site for peptide bond formation on the ribosome from which the nascent peptide chain is ultimately released through an exit tunnel at the back of the large subunit. Together, small and large ribosomal subunits form the complete 70S or 80S ribosome in bacteria/archaea and eukarya, respectively, that becomes reversibly assembled on mRNAs for protein synthesis [7].

The delivery of amino-acids to the ribosome occurs through transfer RNAs (tRNAs) which successively bind to three tRNA binding sites that are shared between both subunits: the amino-acyl (A), peptidyl (P), and exit (E) site. The A site accommodates the incoming amino-acylated tRNA (aa-tRNA) with its anticodon stem-loop (ASL) oriented toward the mRNA in the DC of the small ribosomal subunit, while the acceptor end with the attached amino-acyl group is positioned next to the PTC of the large subunit (Fig. 1.1). The P site accommodates the peptidyl-tRNA from which the nascent peptide chain is transferred to the A site tRNA. Finally, the E site binds the deacylated tRNA before it dissociates from the ribosome [7, 8].

Like the ribosome itself, the principles that underlie the process of ribosomal protein synthesis with its subdivision into initiation, elongation, termination, and recycling are one of the major commonalities of cellular life (Fig. 1.2) [7].

The initiation phase covers all the steps between the dissociation of the ribosomal subunits after a previous translation cycle and its reassembly at the start site of an mRNA with a unique charged initiator tRNA in its P site, a process that is supported by a set of auxiliary initiation factors (IFs). The major steps that have to be accomplished by the initiation machinery are the recruitment of the initiator tRNA and the mRNA to the small ribosomal subunit, identification of the correct

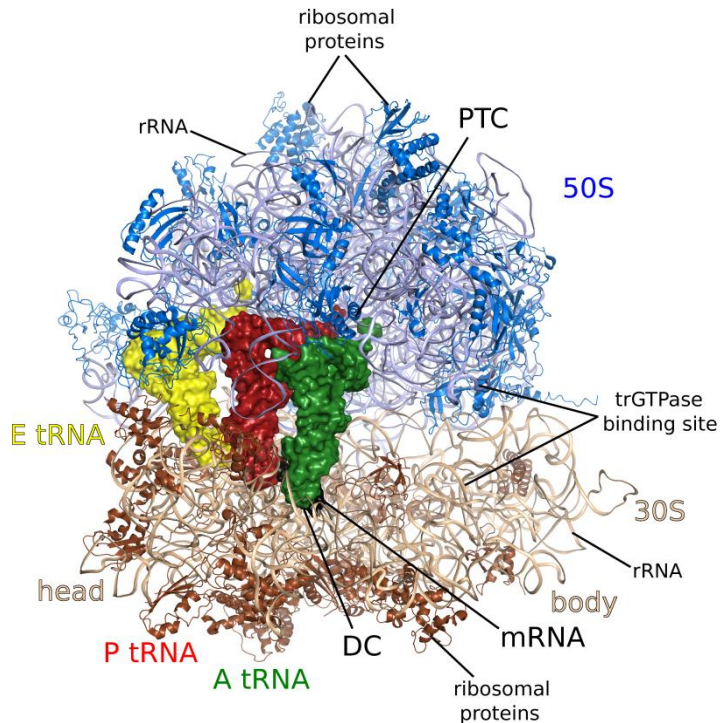


Figure 1.1: Structure of the Ribosome. Overall structure of the bacterial 70S ribosome with mRNA (black) in the decoding center (DC), and tRNAs in A-, P- and E-site (green, red and yellow, respectively) (PDB: 2WDL, 2WDK). The ribosomal RNA (rRNA) and ribosomal proteins are shown in light blue and dark blue for the large 50S ribosomal subunit, and in beige and brown for the small 30S subunit, respectively. The acceptor ends of A- and P-site tRNAs are positioned in the peptidyl-transferase center (PTC) of the 50S subunit, while the anticodon loop of the P site tRNA occupies the DC of the 30S subunit.

start site for translation, and finally the joining of the two ribosomal subunits at the start site. The ultimate result is the formation of an elongation-competent ribosome, ready to accept the first elongator aa-tRNA for peptide bond formation [7, 9]. The critical importance of this process lies in the fact that it sets the reading frame for the subsequent elongation phase and thus decides over the functionality of the synthesized protein.

The elongation phase of translation is a dynamic cyclic process in which tRNAs deliver amino-acids to the ribosome as specified by the mRNA template and sequentially move through the ribosome from the A site to the P site and finally to the E site, thereby adding their amino-acid to the nascent polypeptide chain (Fig. 1.2).

The first step of this cycle is the binding of an aa-tRNA to the ribosomal A site to form a cognate codon-anticodon interaction with the mRNA in the DC of the small subunit. This is followed by peptide bond formation in the PTC between the aa-tRNA in the A site and the peptide attached to the P site-bound tRNA, accompanied by transfer of the peptidyl group to the A site aa-tRNA. Subsequently, in a series of coordinated movements, the mRNA-tRNA complex is translocated by one codon on the ribosome, thereby moving the deacylated tRNA to the E site, while the newly formed peptidyl-tRNA is moved from the A to the P site, leaving the A site free for a new aa-tRNA. In all domains of life, this elongation cycle is supported by two ubiquitous translational GTPases,

namely elongation factors (EFs) 1A/EF-Tu and 2/EF-G, which are responsible for the delivery of cognate aa-tRNAs to the ribosome and to promote the translocation of the mRNA-tRNA complex on the ribosome, respectively [8, 10].

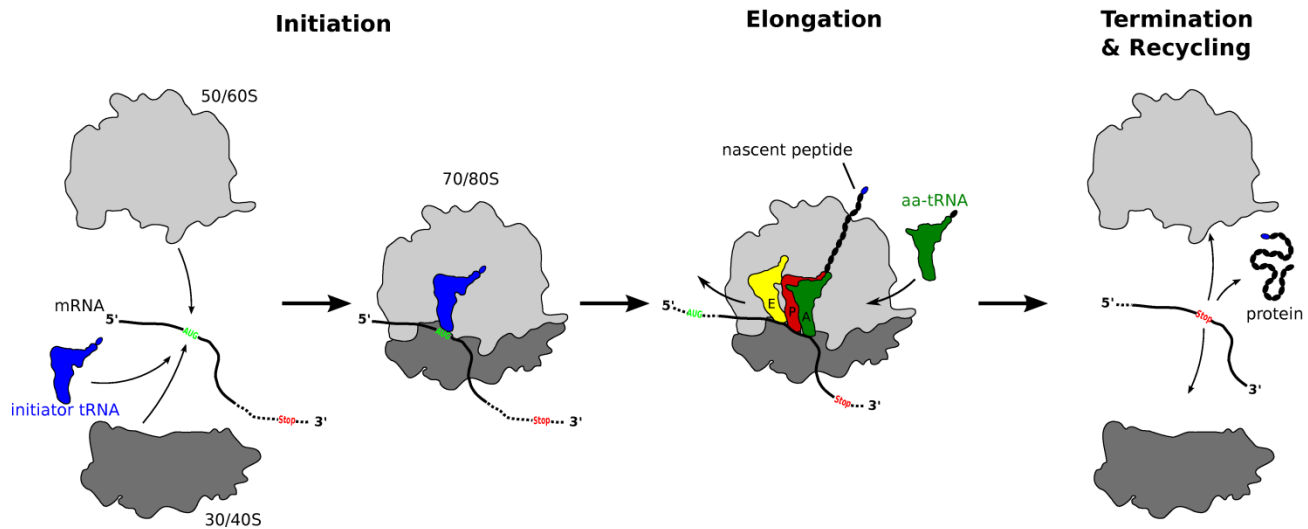


Figure 1.2: Schematic presentation of the basic processes of translation in the three domains of life. The process of translation can be subdivided into initiation, elongation, termination, and recycling. During initiation, the two ribosomal subunits and the specialized initiator tRNA (blue) are recruited to the mRNA to assemble the 70S/80S ribosome with the initiator tRNA positioned in the P site, base paired to the AUG start codon (light green). The 70S/80S ribosome then enters the elongation phase, a cyclic process during which tRNAs (aa-tRNA) deliver amino-acids to the ribosome and move through the ribosome from the A (green) to the P (red) and finally to the E site (yellow), thereby adding their amino-acid to the nascent polypeptide chain as specified by the mRNA template. Translation is terminated upon the encounter of a stop codon (red 'stop') on the mRNA, which results in the release of the synthesized protein and finally in the recycling of the ribosome by dissociation into the individual subunits. During all its stages, the translation process is supported by translation factors, including a number of translational GTPases to ensure the necessary accuracy and speed (not shown for clarity).

Termination of the translation process occurs upon the encounter of an in-frame stop codon in the mRNA, which is recognized by specialized release factors (RFs) to catalyze the hydrolysis of the newly synthesized polypeptide chain from the P site-tRNA. The translation cycle ends in the recycling step with the dissociation of the two ribosomal subunits, which become thus available for a new round of translation initiation (Fig. 1.2) [7, 11].

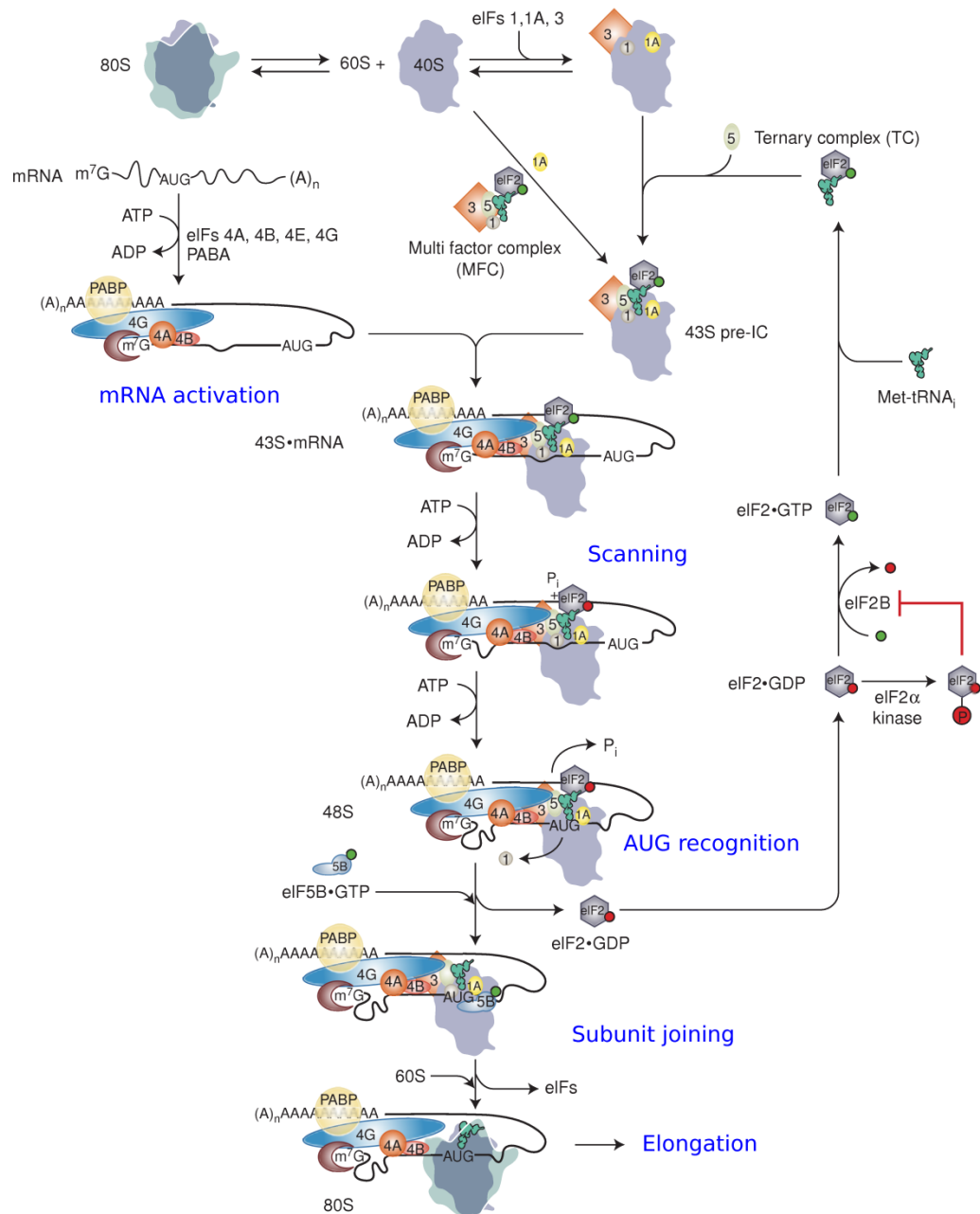


Figure 1.3: Schematic presentation of cap-dependent translation initiation. The mechanism of eukaryal translation initiation covers all steps between dissociation of the 80S ribosome from a preceding translation cycle and its reassembly at the start codon of an mRNA. The initiation process starts with the formation of the eIF2·GTP·Met-tRNA_i TC, which is subsequently recruited to the 40S subunit with the help of eIFs 1, 1A, 3 and 5 to form the 43S pre-IC. The 43S pre-IC then attaches to the 5' proximal region of the mRNA through interactions with the cap binding complex eIF4F and facilitated by the helicase eIF4A. Once bound, the 43S pre-IC starts to scan the 5'-UTR of the mRNA in a 5'-to-3' direction until it reaches the correct AUG start codon. Recognition of the start codon arrests the scanning process and results in the displacement of eIF1 and the eIF5-stimulated hydrolysis of eIF2-bound GTP. eIF2·GDP then dissociates from the pre-IC together with eIFs 1, 5, 3 and 4F. Joining of the 60S subunit is finally promoted by eIF5B·GTP, followed by ribosome-induced GTP hydrolysis on eIF5B and the dissociation of eIF5B·GDP and eIF1A to yield the elongation-competent 80S ribosome. The figure was modified from Hinnebusch & Lorsch [12].

1.2 Translation initiation

Among the different steps of the translation process, translation initiation incurred by far the most extensive divergence in the three domains of life. Hereby, the main differences are found in the mechanisms by which the initiator tRNA and mRNA are recruited to the small ribosomal subunit and the recognition of the correct start site [9, 13]. In prokaryotes, mRNA recruitment entails the direct recognition of the translation initiation region by the 30S subunit through annealing of the Shine-Dalgarno (SD) motif on the mRNA with the complementary anti-SD sequence at the 3' end of the 16S rRNA, placing the start codon directly in the ribosomal P site [13, 14]. In bacteria, this process, together with the recruitment of the initiator tRNA and joining of the 50S subunit is modulated by three monomeric accessory initiation factors, namely IF1, IF2 and IF3 [15]. In eukarya binding of most mRNAs to the 40S subunit does not rely on direct mRNA-rRNA recognition, but instead involves the recruitment of the 40S subunit to the capped mRNA 5' end and a subsequent scanning of the mRNA in the 3' direction until the correct start site is encountered. Although eukaryal cells contain orthologs of bacterial IF1 and IF2 as well as a functional counterpart to IF3, the eukaryal initiation machinery relies on at least 9 additional initiation factors (eIFs) (Table 1.1), many of which are multimeric protein complexes, that together mediate the recruitment of initiator tRNA and mRNA to the 40S subunit, scanning, start codon recognition and finally the joining of the 60S subunit [9, 16].

1.2.1 Cap-dependent translation initiation in eukarya

Cap-dependent translation initiation in eukarya can be subdivided into several, partly parallel occurring steps that are orchestrated by the concerted action of the initiation factors (Fig. 1.3) [9, 12, 16]. In a first step, the heterotrimeric GTPase eIF2 in its GTP-bound form specifically recognizes and binds the methionylated initiator tRNA (Met-tRNA_i) to form a ternary complex (TC). Supported by eIFs 1, 1A, 5 and the multisubunit eIF3 complex, the TC binds to the 40S subunit to form the 43S pre-initiation complex (pre-IC), placing the Met-tRNA_i in the ribosomal P site. The 43S pre-IC is then recruited to the 5'-7-methylguanosine cap of the mRNA in a way facilitated by eIF3, the poly(A) binding protein (PABP) and the multimeric cap-binding complex eIF4F. Once attached to the 5' proximal region of the mRNA, the pre-IC starts to scan the 5' untranslated region (5' UTR) in a 5'-3'

Table 1.1: Translation factors involved in translation in eukarya, archaea and bacteria

Eukaryal initiation factor	Archaeal homolog	Bacterial homolog	Function of the eukaryal homolog
eIF1	aIF1	IF3*	Promotes binding of the eIF2-GTP-Met-tRNA _i complex to the 40S subunit together with eIF1A; promotes ribosomal scanning and ensures the fidelity of start codon recognition; prevents premature accommodation of Met-tRNA _i in the P site; its dissociation is coupled to eIF5-induced GTP hydrolysis by eIF2 and P _i release.
eIF1A	aIF1A	IF1	Promotes binding of the eIF2-GTP-Met-tRNA _i complex to the 40S subunit together with eIF1; stimulates ribosomal scanning and promotes start codon recognition cooperatively with eIF1.
eIF2	aIF2		Consists of three subunits (eIF2 $\alpha\beta\gamma$); specifically recognizes Met-tRNA _i to form an eIF2-GTP-Met-tRNA _i TC; recruits Met-tRNA _i to the P site of the 40S subunit; hydrolyzes GTP upon start codon recognition.
eIF2B			Consists of five subunits (eIF2B $\alpha\beta\gamma\delta\epsilon$); guanosine-nucleotide exchange factor (GEF) that promotes exchange of GDP against GTP on eIF2.
eIF3			Consists of 13 subunits in mammals; interacts with eIF1, eIF5 and eIF2 to form a multi-factor complex; stimulates recruitment of the eIF2-GTP-Met-tRNA _i TC to the 40S subunit; promotes attachment of 43S pre-IC to mRNA; is involved in ribosome dissociation and anti-association, preventing premature joining of 40S and 60S subunits.
eIF4A	aIF4A		ATP-dependent DEAD-box RNA helicase that unwinds secondary structures in the 5' leader of the mRNA.
eIF4B			Enhances the ATPase and helicase activity of eIF4A
eIF4E			Binds to the 5'-cap structure of the mRNA
eIF4H			Homologous to the N-terminal domain of eIF4B; enhances the ATPase and helicase activity of eIF4A
eIF5			Binds eIF1, eIF2 and eIF3; forms nucleation point for the MFC; promotes recruitment of eIF2-GTP-Met-tRNA _i TC to the 40S subunit and stimulates start codon recognition; acts as GTPase activating protein (GAP) that induces hydrolysis of eIF2-bound GTP upon start codon recognition.
eIF5B	aIF5B	IF2	Ribosome-dependent GTPase that catalyzes ribosomal subunit joining
eIF6			Anti-association factor that binds the 60S subunit and prevents its association to the 40S subunit.

* The grouping of IF3 with a/eIF1 is based on their functional homology and the structural similarity of a/eIF1 to the C-terminal domain of IF3 [17, 18] and not on a common evolutionary descent.

direction for the AUG start codon. This process is supported by the small monomeric eIFs 1 and 1A, which bind close to the mRNA channel of the 40S subunit and stabilize the 43S pre-IC in an 'open' conformation that is competent for processive movement along the mRNA, thereby allowing the P site-bound Met-tRNA_i to sample each of the successive mRNA triplets by using complementarity with its anticodon[19-21]. Base-pairing between anticodon of the Met-tRNA_i and the AUG start codon in the ribosomal P site arrests the scanning process and triggers rearrangements within the pre-IC involving eIFs 1, 1A, 2 and 5 that result in the irreversible hydrolysis of the eIF2-bound GTP by the gated release of the orthophosphate (P_i) from eIF2, triggered by the GTPase activating protein (GAP) eIF5. Conversion of eIF2 to its GDP-bound form commits the pre-IC to the downstream events of the initiation process: The inactive eIF2·GDP has a reduced affinity to the Met-tRNA_i, resulting in its release together with eIF5 and eIF1 from the 40S subunit. Joining of the 60S ribosomal subunit is finally catalyzed by the ribosome-dependent GTPase eIF5B. Supported by eIF1A, eIF5B binds to the scanning-arrested 43S pre-IC in a GTP-dependent manner and promotes the association of the large 60S ribosomal subunit. 60S binding triggers the GTPase activity in eIF5B, resulting in the concerted dissociation of eIF5B·GDP and eIF1A from the 80S initiation complex (IC) which is thus ready to enter the elongation phase of translation.

1.3 GTPases involved in translation

Translation is one of the most fundamental cellular processes that are regulated by guanine nucleotide-binding (G) proteins (GTPases). Apart from translation, G proteins such as the small Ras-like GTPases or G_α proteins are involved in a wide variety of mechanisms from signal transduction to nucleocytoplasmic transport. The unifying characteristic of G proteins, which share a common evolutionary origin[22], is their function as molecular switches that alternate between an 'inactive' GDP-bound state and a structurally distinct 'active' GTP-bound state, characterized by the interaction of two conserved dynamic structural elements, switch 1 and switch 2, with the γ-phosphate of the bound GTP molecule (Fig. 1.4A) [23-25]. Only the active GTP-bound conformation of the G protein is able to interact productively with effector molecules or complexes and is therefore a prerequisite for its biological function (Fig. 1.4B). Conversion of the active to the inactive state to 'switch off' the G protein requires the hydrolysis of the bound GTP molecule,

which is achieved by stimulation of the usually low intrinsic GTPase activity. Common features of these activation mechanisms are the stabilization of the catalytic machinery of the GTPase in a conformation that is productive for GTP hydrolysis and the introduction of additional catalytic elements into the GTPase center that stabilize the transition state of the hydrolysis reaction [23, 25].

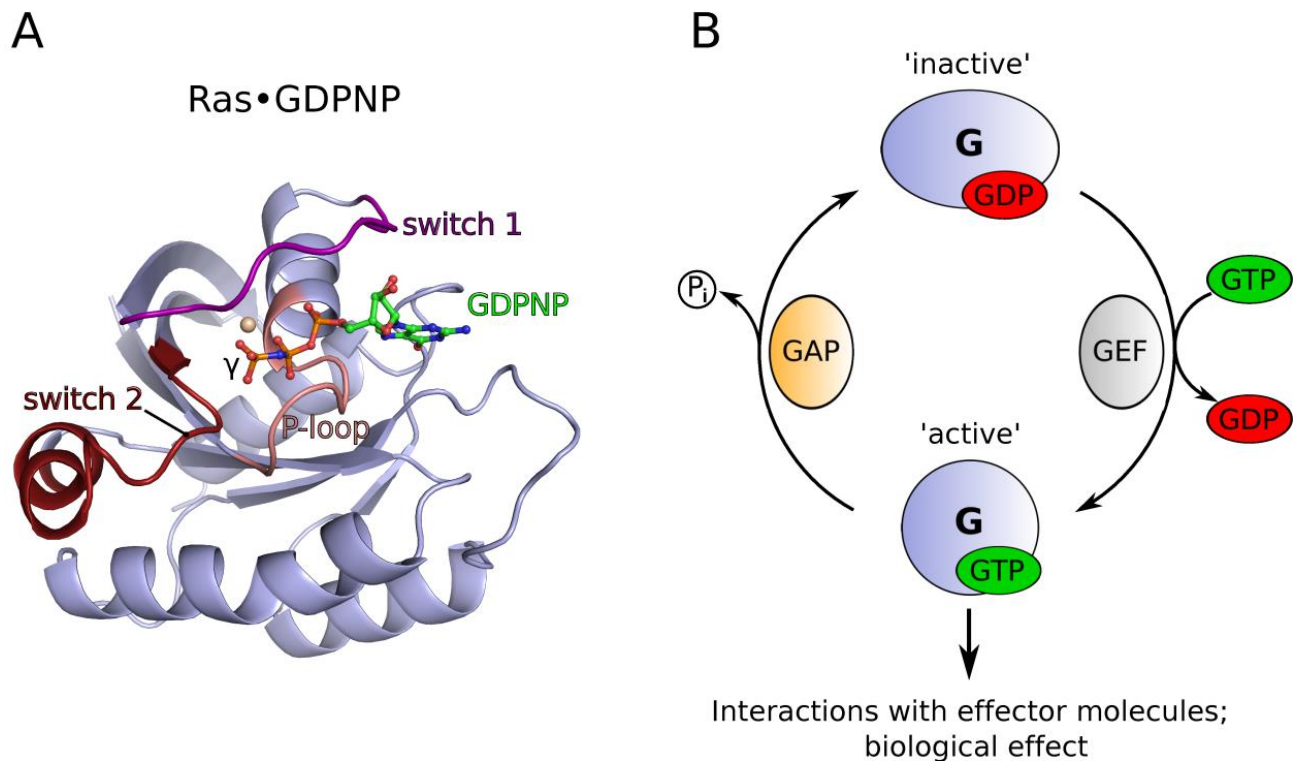


Figure 1.4: G proteins as molecular switches. A) Crystal structure of human Ras (light blue; PDB: 5P21) bound to GDPNP. Ras belongs to the family of small GTPases that consist only of the G domain itself. The phosphate binding loop (P loop), switch 1 and switch 2 are colored in light red, magenta and dark red, respectively. Switch 1 and switch 2 are highly conserved structural elements that specifically recognize the nucleotide state of the G domain by forming direct contacts to the GTP γ -phosphate; both switch elements become thus stabilized in a defined conformation that renders the G domain active for interactions with effector molecules. **B)** Schematic presentation of the conventional guanine-nucleotide cycle of G proteins. To convert the 'inactive' form of the G protein to its 'active' state, GDP has to be replaced by GTP; in some cases (e.g. Ras, EF-Tu and eIF2 γ) this step is accelerated by guanine-nucleotide exchange factors (GEFs). GTP-binding induces the 'active' conformation of the G domain, in which it binds to effector molecules and is able to carry out its biological function in the cell. The GTPase reaction to convert the G protein back to its GDP-bound form is usually slow and has to be accelerated by external factors that complement and/or stabilize the active site (here indicated by the collective term GAP for GTPase activating protein).

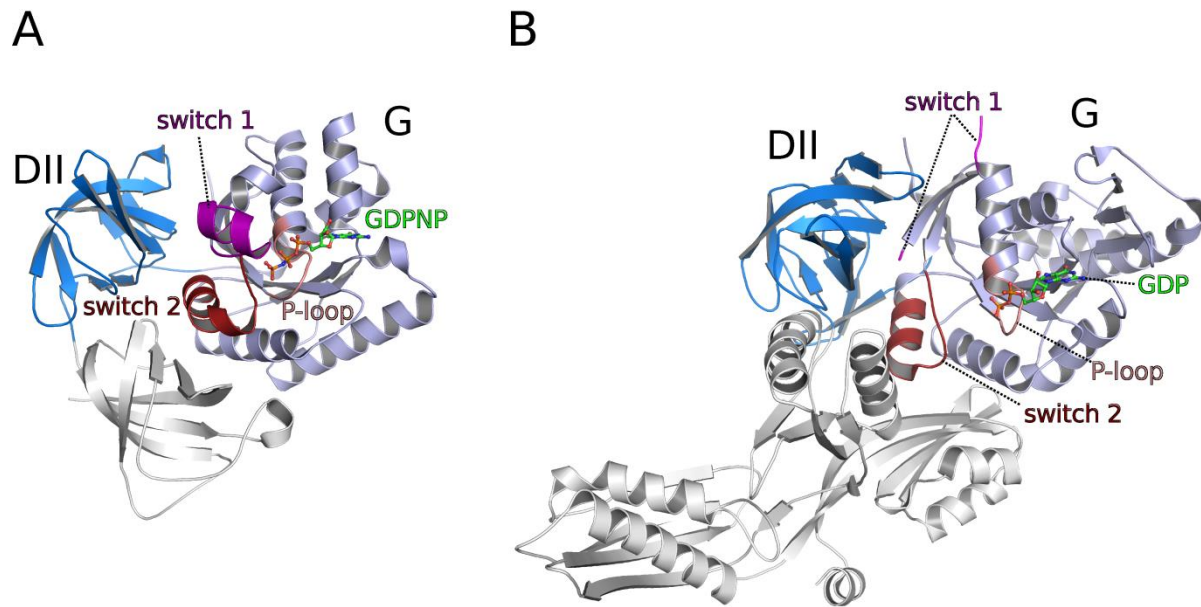


Figure 1.5: The universally conserved structural core in translational GTPases. A, B) Crystal structures of GDPNP-bound EF-Tu (A) and GDP-bound EF-G (B) from *Thermus thermophilus* (PDBs: 1EXM; 1FNM). Both bacterial elongation factors contain a G domain (G; coloring as in Fig. 1.4A) homologous to Ras-like G proteins and a β -barrel domain with greek-key topology (DII; dark blue), which are shared with all other trGTPases. G domain and domain II are supplemented with additional domains (shown in grey), which are required for factor specific functions and not evolutionarily universally conserved across the trGTPase lineages.

In all its basic sub-processes from initiation to ribosome recycling, the translation apparatus depends on auxiliary trGTPases (Table 1.2). Three of these factors, namely initiation factor α /eIF5B/IF2 and elongation factors α /eEF1 α /EF-Tu and α /eEF2/EF-G, are ubiquitous in the three kingdoms of life and are therefore likely to represent the minimal set of trGTPases necessary for mRNA translation that evolved before the emergence of the three primary lineages bacteria, archaea and eukarya [22]. Elongation factor SelB constitutes a special case, as it is represented with homologs in all three domains of life, but not ubiquitously distributed among all species. Additional trGTPases that are not found in all three domains apparently evolved later from the lineages of either α /eEF1 α /EF-Tu or α /eEF2/EF-G [22, 26]. These include the initiation factor α /eIF2, which is only found in archaea and eukarya and the release factors RF3 and eRF3 in bacteria and eukarya, respectively. Despite their different functions during translation, all trGTPases share a common evolutionarily conserved structural core, composed of the G domain and domain II, which is supplemented with additional factor specific domains (Fig. 1.5). The G domain, which is related

to the G domains of other Ras-related GTPases, forms the functional center in trGTPases that couples GTP binding and its hydrolysis to the specific biological function of the factor during translation. The ribosomal complexes on which the different trGTPases fulfill their role hereby act as the GTPase activating element, which stimulates the usually low intrinsic GTPase activity of trGTPases [27].

Table 1.2: Translational GTPases in eukarya, archaea and bacteria

Eukaryal initiation factor	Archaeal homolog	Bacterial homolog	Function
eIF2 γ	aIF2 γ		Forms the central subunit of the heterotrimeric eIF2 complex; recognizes Met-tRNA _i to form the eIF2-GTP-Met-tRNA _i TC to recruit the initiator tRNA _i to the 40S subunit; hydrolyzes GTP upon start codon recognition.
eIF5B	aIF5B	IF2	Catalyzes ribosomal subunit joining; the bacterial ortholog also promotes binding of the fMet-tRNA ^{fMet} to the 30S subunit.
eEF1A	aEF1A	EF-Tu	Delivers aa-tRNAs to the ribosome during elongation.
eEF2	aEF2	EF-G	Translocation of the mRNA/tRNA complex on the ribosome during elongation.
eSelB	aSelB	bSelB	Delivers Sec-tRNA ^{sec} to the ribosome during elongation.
eRF3		RF3	Class-2 release factor; binds class 1 release factors and promotes termination of the translation process.
		LepA	Thought to promote back-translocation on the ribosome.

Two trGTPases that exemplify this split between structural adaptation to new biological constellations and the simultaneous preservation of the underlying principles of function are the eukaryal initiation factors eIF2 and eIF5B. On the one hand, eIF2 constitutes an example for a

tightly regulated trGTPase, in which the G protein forms a constitutive complex with two accessory subunits, and which requires various additional effector proteins to perform its role during translation initiation. eIF5B, on the other hand, is an example for a monomeric, universally conserved trGTPase that fulfills its role during subunit joining without the absolute requirement for additional effector molecules apart from the ribosome itself. Notwithstanding these differences, both proteins follow the basic paradigms of G protein function as molecular switches.

1.3.1 The eukaryal translation initiation factor 2 (eIF2)

eIF2 is responsible for the delivery of the Met-tRNA_i to the 40S ribosomal subunit and plays a key role during the identification of the correct start site for translation (Fig. 1.3). Like other G proteins, eIF2 thereby oscillates between an 'active' GTP-bound form, in which it is able to specifically recognize and bind the Met-tRNA_i and an 'inactive' GDP-bound form, in which eIF2 dissociates from the scanning arrested 43S pre-IC. During this nucleotide cycle, eIF2 function is dependent on two accessory protein factors, namely eIF5 and eIF2B. While eIF5 is essential for eIF2 TC binding to the 40S subunit and required to trigger the hydrolysis of eIF2-bound GTP, eIF2B functions as guanine nucleotide exchange factor (GEF) that recycles eIF2·GDP back into its GTP-bound form.

1.3.1.1 eIF2 and the recognition of the Met-tRNA_i

eIF2 is a heterotrimeric G protein, comprising the subunits eIF2 α , - β , and - γ . All three eIF2 subunits have orthologs in archaea, namely aIF2 α , - β , and - γ , whereas no counterparts are known from bacteria [28]. With the exception of eIF2 α , structural information about eIF2 is limited to its archaeal orthologs (Fig. 1.6). The a/eIF2 α -subunit is composed of two domains: an N-terminal domain that is subdivided into an S1-like OB-fold that forms a rigid body with the following small α -helical subdomain, and a C-terminal α/β domain which contains an additional acidic extension only in the eukaryal orthologs (Fig. 1.6A) [29, 30]. The C-terminal domain of eIF2 α is responsible for direct interactions with the γ -subunit of eIF2 [31-33]. The body of a/eIF2 β is composed of two conserved sub-domains, an N-terminal α/β sub-domain and a zinc binding sub-domain (ZBD), that are preceded by a single N-terminal α -helix (α 1) which is responsible for stable binding to the eIF2 γ (Fig. 1.6B) [31, 32, 34]. Only the eukaryal eIF2 β ortholog contains an additional long N-terminal

extension, which harbors three conserved lysine-rich patches (K-boxes) that are involved in interactions with aromatic/acidic boxes (AA-boxes) in the C-terminal domains of the eIF2 effectors eIF5 and eIF2B ϵ (see next sections) which are likewise not found in archaeal cells [35, 36]. Within the a/eIF2 complex, the α - and β -subunits do not interact directly with each other, but both bind independently to the central γ -subunit [31, 32]. a/eIF2 γ is the G protein within the complex, homologous to the elongation factors EF-Tu, eEF1A and SelB, and accordingly adopts a three-domain architecture composed of a G domain (domain I) and two β -barrel domains (domains II and III) with greek key topology (Fig. 1.6C). Crystal structures of aIF2 γ , obtained either in its apo state, in complex with GDP or with the nonhydrolyzable GTP analog GDPNP revealed that the three domains invariably adopt a 'closed' conformation similar to that of the active GDPNP-bound EF-Tu and in stark contrast to the 'open' conformation in GDP-bound EF-Tu [33, 37-39]. A number of eukaryal orthologs contain an additional non-conserved N-terminal extension, which was, however, shown to be dispensable for eIF2 function *in vivo*[40]. Like in other G proteins, the G domain of a/eIF2 γ harbors the guanine-nucleotide binding site with the highly conserved nucleotide binding motifs [24]. This includes the two mobile switch 1 and switch 2 elements that are thought to change their conformation upon the transition from the GDP-bound form to the GTP-bound state of the G domain, thereby promoting the binding of Met-tRNA_i by eIF2. GTP-bound a/eIF2 γ alone is able to bind the Met-tRNA_i directly [32]. However, the affinity of the eIF2·GTP complex for the Met-tRNA_i is significantly increased (~100-fold) by each of the accessory subunits eIF2 α and eIF2 β [32, 41]. Structural analyses suggest that binding of the C-terminal domain of aIF2 α to domain II of GTP-bound aIF2 γ allosterically opens a channel between switch 1 of the G domain and domain II, thereby allowing the accommodation of the ACC acceptor stem with the attached methionyl group [42, 43]. Further aIF2 α - or GTP-induced domain rearrangements are limited and significantly smaller than those observed for the transition between GDP- and GTP-bound forms of EF-Tu. Consistently, it was found that the affinity of Met-tRNA_i is only ~10-fold greater for eIF2·GTP than for the GDP-bound form, and that the affinities of eIF2·GTP and eIF2·GDP to deacylated tRNA_i is about equal to that of eIF2·GDP for Met-tRNA_i[44, 45]. This indicates that the thermodynamic coupling between the binding of GTP and Met-tRNA_i mainly depends on the methionyl moiety, whereas the rest of the binding interface is virtually

unperturbed [44]. However, the first base pair of the tRNA_i acceptor stem (A1:U72), together with the G31:C39 pair in the anticodon stem loop (ASL) and bases within the T loop form additional signature elements in the initiator tRNA that enhance Met-tRNA_i binding to eIF2·GTP and allow its discrimination against elongator tRNAs[46, 47].

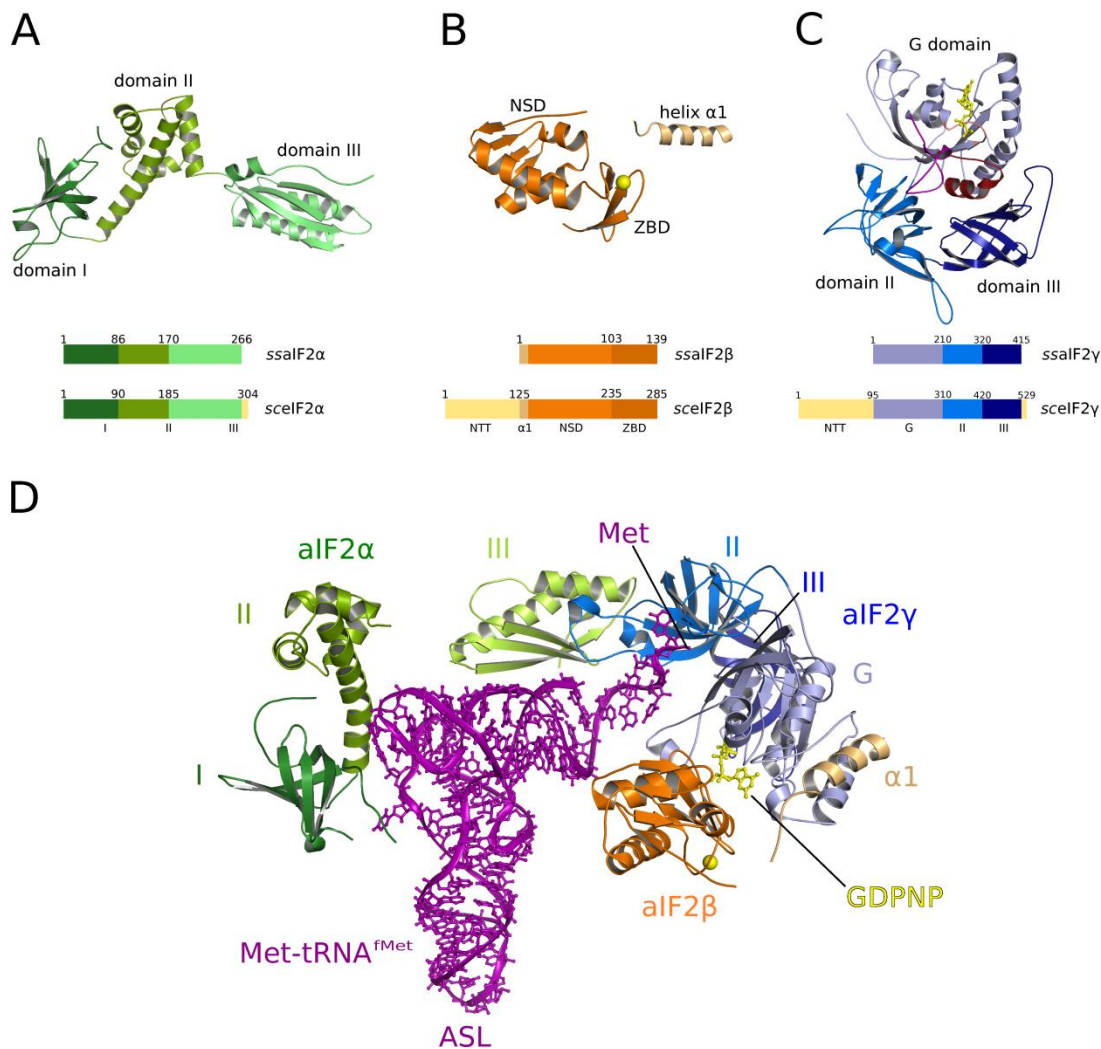


Figure 1.6: Structure of a/eIF2. A-C) NMR solution structure of human eIF2α (A) and crystal structures of aIF2β (B) and GDP-bound aIF2γ (C) as found in the heterotrimeric aIF2 complex from *S. solfataricus* (PDBs: 1Q8K; 2QMU). A comparison of the domain architectures in the eukaryal (sc: *S. cerevisiae*) and archaeal (ss: *S. solfataricus*) orthologs is schematically shown below the structures with corresponding color codes; regions idiosyncratic to the eukaryal lineages are indicated in yellow. The zinc ion in aIF2β is shown as yellow sphere; the GDP molecule bound to aIF2γ is shown as yellow balls and sticks; G domain and domain II of aIF2γ are colored as their homologous domains in EF-Tu and EF-G in Fig. 1.5. **D)** Cartoon representation of the ternary complex of *S. solfataricus* aIF2 with GDPNP and Met-tRNA^{fMet}. The C-terminal domain of aIF2β is not visible in the crystal structure (PDB: 3V11) and was therefore modeled into aIF2 according to its position in 2QMU. The color code for the individual subunits corresponds to that in A-C; the Met-tRNA_i is colored in magenta.

The crystal structure of the TC formed between α IF2·GDPNP and *E. coli* Met-tRNA^{fMet} revealed that α IF2 most likely binds the tRNA_i in a manner significantly different from that observed for elongator tRNA binding by EF-Tu (Fig.1.6D) [42, 48]. The ACC end with the methionyl group is bound in a pocket between switch 1 of the G domain and domain II of α IF2 γ in the same way as in TCs of EF-Tu. However, a kink in the acceptor stem reorients the rest of the tRNA_i dramatically relative to α IF2 γ , thereby preventing the direct interaction between domain III of α IF2 γ and the T stem minor groove of the tRNA as observed in EF-Tu TCs. Instead, the acceptor arm and the T-loop of the tRNA form direct contacts with the C-terminal and N-terminal domains of α IF2 α , respectively. Although similar interactions to eIF2 α were not found for the eIF2·GTP·Met-tRNA_i complex in directed hydroxyl radical footprinting experiments [49], mutational analyses for eIF2 γ , as well as the cryo-electron microscopy (cryo-EM) model of the mammalian 43S pre-IC suggest a similar mode of Met-tRNA_i binding in the eIF2 TC, with the difference that the N-terminal S1-like OB-fold domain of eIF2 α seems to form no direct contact to tRNA_i but instead contacts the 40S subunit [45, 50]. How the β -subunit is positioned in the TC and how it might contribute to Met-tRNA_i binding by α /eIF2 is still not known.

1.3.1.2 eIF5 regulates the activity of eIF2

eIF5 consists of two distinct structural domains (Fig. 1.7). The N-terminal domain (eIF5-NTD) shares sequence and structural homology with the C-terminal portion of α /eIF2 β and can be further subdivided into an N-terminal α / β sub-domain (NSD) and a zinc binding subdomain (ZBD) [51]. Unique features of the eIF5-NTD that are not found in α /eIF2 β are a short sequence insertion in the NSD which bears some resemblance with a Walker A box motif (P-loop) of nucleotide-binding proteins, and a flexible N-terminal tail of ~20 residues that contains a highly conserved arginine residue (Arg15), which was proposed to act as catalytic arginine-finger to trigger the GTPase activity in eIF2 on the 43S pre-IC (see below) [52, 53]. The C-terminal domain of eIF5 (eIF5-CTD) adopts a globular atypical HEAT repeat fold [1, 54], which is connected to the eIF5-NTD through a long mainly negatively charged linker region (eIF5-LR). The overall sequence conservation within the eIF5-CTD is low with the exception of two regions (AA-boxes) that are rich in aromatic and

acidic side chains and together form a large negatively charged surface area (area I) that is required for interactions with the three lysine-rich K-boxes in the N-terminal domain of eIF2 β [35, 55].

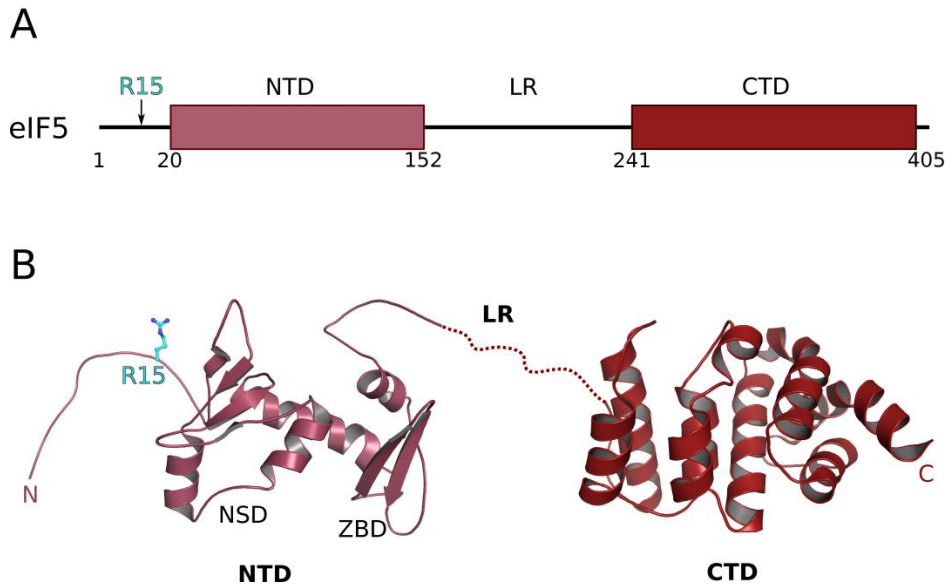


Figure 1.7: Domain architecture of eIF5. **A)** Schematic presentation of the domain architecture in eIF5. eIF5 is thought to fold into an N-terminal domain (NTD; colored wine-red) that contains the putative arginine-finger (R15) in the N-terminal extension, and a HEAT-repeat like C-terminal domain (CTD; colored in dark red). Both domains are connected via a flexible linker region (LR). **B)** NMR solution structure of the human eIF5-NTD (left; PDB: 2G2K) and the yeast eIF5-CTD (right; PDB: 2FUL), connected by the flexible linker region (dashed line). The putative arginine-finger (R15) is shown as sticks. N-terminal subdomain (NSD) and zinc binding domain (ZBD) of the eIF5-NTD are homologous to those in the C-terminal domain of eIF2 β (see Fig. 1.6B). The color code is the same as in (A).

As mentioned above, eIF5 supports the recruitment of eIF2 TCs to the 40S ribosomal subunit during 43S pre-IC formation [56-58]. Binding of the isolated TC to the 40S subunit is slow and its efficient recruitment thus depends on the assistance by other factors, namely eIFs 1, 1A, 5 and the eIF3 complex [56, 57, 59]. With the exception of eIF1A, these factors together with the TC preassemble into a multifactor complex (MFC) in yeast, plants and mammals [59-61] through a network of physical interactions with each other, thereby mutually promoting their binding and the recruitment of the TC to the 40S subunit for 43S pre-IC formation. Hereby, the eIF5-CTD plays a key role as nucleation point for the other factors by forming a platform for direct and partially cooperative interactions with the N-terminal domains of eIF2 β (through the K-boxes) and subunit c of the eIF3 complex, as well as with eIF1 [56, 57, 59]. Consistently, mutations that disrupt any of

these interactions result in impaired 43S pre-IC formation and reduced growth rates in a manner that can be suppressed through the overexpression of the TC, highlighting their importance for TC recruitment [58, 62].

After 43S pre-IC formation and its recruitment to the 5' end of the mRNA, the interaction between eIF2 and eIF5-CTD continues to play a role in scanning and start codon recognition by antagonizing eIF1 binding to the 43S pre-IC, thereby promoting the 'closed' scanning arrested conformation of the pre-IC [21, 63]. However, the main role of eIF5 during scanning and start site recognition is to trigger the intrinsic GTPase activity of eIF2·GTP in its capacity as GTPase activating protein (GAP). Several studies suggested that the eIF5-NTD acts as classical GAP that provides an arginine-finger (Arg15) *in trans* which is introduced into the active site of eIF2 in the context of the scanning 43S pre-IC and stabilizes the transition state of the GTP hydrolysis reaction [52, 53]. This was supported by the finding that substitutions of the invariant Arg15 in the unstructured N-terminal tail of eIF5 are lethal and abolish the eIF5-dependent GTPase activation without reducing the ability of eIF5 to bind eIF2 [51-53, 64]. However, this activating effect of eIF5-NTD strongly depends on the structural context of the pre-IC, suggesting that eIF5 may also contribute allosterically to GTPase activation in eIF2 γ in the scanning pre-IC [64]. Finally, it was reported that the eIF5-NTD is able to bind isolated eIF2 γ only in the absence of eIF2 β [65], which in turn is known to suppress the intrinsic GTPase activity of eIF2 γ through its ZBD [21, 66, 67]. Based on these observations it was proposed that the eIF5-ZBD may displace the structurally homologous eIF2 β -ZBD from eIF2 γ , thereby simultaneously removing the inhibitory effect of eIF2 β and providing the catalytic Arg15 with access to the nucleotide binding site [21]. AUG recognition would then have to trigger the removal of the eIF5-NTD to allow the gated release of the orthophosphate from eIF2·GDP/P_i, which would thus be connected to the release of eIF1 from the P-site and accommodation of the Met-tRNA_i, promoted by the interaction between eIF5-CTD and eIF2 β -NTT.

After P_i release, eIF2·GDP is thought to dissociate from the 43S pre-IC in a tight complex with eIF5 [68]. Recent studies suggested that within this eIF5·eIF2·GDP complex the flexible eIF5-LR between N- and C-terminal domains forms a direct contact to eIF2 in addition to that between eIF5-CTD and eIF2 β -NTT [69]. This interaction was shown to mediate the stabilization of GDP on eIF2. Based on this finding and the observation that a large fraction of cytosolic eIF2 is present in a

complex with eIF5, it was proposed that eIF5 might serve an additional role as guanine-nucleotide dissociation inhibitor (GDI) that antagonizes the GEF function of eIF2B by physically competing with the catalytic eIF2B ϵ -CTD (see below) and by suppressing spontaneous GDP release, thereby preventing eIF2·GDP recycling and reducing the levels of eIF2 TCs in the cell [68, 69].

1.3.1.3 Recycling of eIF2·GDP by eIF2B

After its release from the 43S pre-IC, eIF2·GDP has to be recycled back to eIF2·GTP to allow a new round of Met-tRNA_i binding and translation initiation. Like various other Ras-related G proteins, eIF2 binds GDP tightly with an affinity in the low nanomolar range, and the rates of spontaneous GDP release are too slow to allow efficient TC formation and translation initiation [44]. Guanine-nucleotide exchange on eIF2 is therefore catalyzed by the GEF eIF2B, which promotes GDP release from eIF2·GDP and thereby facilitates its replacement by GTP [70, 71]. eIF2B is composed of five non-identical subunits (α , β , γ , δ , and ϵ) and was recently proposed to form a functional decamer of ~600 kDa in solution containing two copies of each subunit [72, 73]. The minimal catalytically active region of the eIF2B complex was mapped to the ~20 kDa C-terminal domain of eIF2B ϵ , which adopts an atypical HEAT repeat fold homologous to that of the eIF5-CTD (Fig. 1.8) [1, 74]. Like eIF5-CTD, the eIF2B ϵ -CTD contains two conserved AA-boxes at its C-terminus that are required for strong interactions with the K-boxes of the eIF2 β -NTT and are thus implicated in the recruitment of the substrate eIF2 to its GEF [35]. Moreover, eIF2B ϵ -CTD was found to interact directly with eIF2 γ through its N-terminal portion, which was shown to contribute directly to nucleotide exchange on eIF2 and is thus considered to form the catalytic center [70, 71, 75, 76]. Together with eIF2B γ , eIF2B ϵ forms the 'catalytic' subcomplex of eIF2B, in which the γ subunit serves an accessory role by promoting the nucleotide exchange activity of the ϵ subunit. A regulatory subcomplex is formed by the homologous α , β , and δ subunits, which contribute to eIF2·GDP binding through interactions with eIF2 α [77].

Due to its central position in the guanine-nucleotide cycle of eIF2, eIF2B is one of the major targets for the regulation of translation initiation. One of the best studied pathways of eIF2B inhibition is the phosphorylation of eIF2 α at Ser51 (eIF2 α -P) by eIF2 α kinases, which in turn

become activated in response to stress conditions to down-regulate general translation (Fig. 1.1) [78-80].

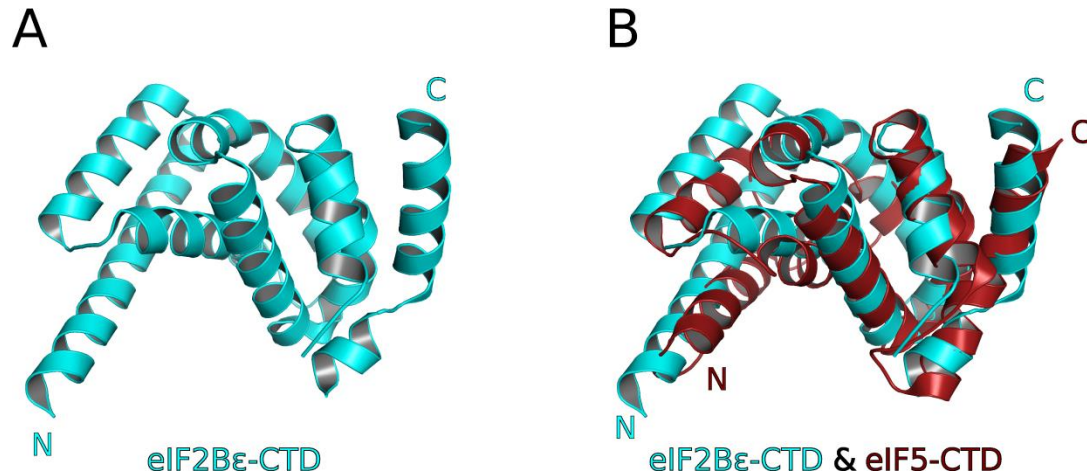


Figure 1.8: Structure of the catalytic domain in eIF2Bε. **A)** Crystal structure of the human eIF2Bε-CTD (PDB: 3JUI), comprising the minimal catalytically active domain within the heteropentameric eIF2B complex. **B)** Structural comparison of the eIF2Bε-CTD (cyan) with the eIF5-CTD (red). Both proteins adopt a structurally homologous atypical HEAT-repeat fold that provides surfaces for interactions with eIF2.

1.3.2 The eukaryal translation initiation factor 5B (eIF5B)

eIF5B is the second trGTPase involved in translation and, unlike eIF2, universally conserved among the three domains of life with the orthologous aIF5B and IF2 in archaea and bacteria, respectively [81]. Crystal structures of aIF5B and IF2 revealed a four domain architecture for both proteins with an N-terminal G domain followed by domains II to IV (Fig. 1.9) [82-84]. The G domain and domain II form the structural core, which in sequence and structure is homologous to the corresponding domains in other trGTPases such as EF-Tu, EF-G and eIF2γ, whereas the α/β domain III is idiosyncratic to a/eIF5B/IF2. The C-terminal domain IV is connected to the preceding domains through a ~40 Å long α-helix and is structurally homologous to domain II; only the archaeal and eukaryal orthologs contain two additional α-helices at their very C-terminal end, which are packed against the β-barrel fold of domain IV. IF2 and eIF5B contain an additional N-domain of up to 600 residues, which displays little conservation in sequence and length and, although implicated in

mediating interactions with the small ribosomal subunit, was shown to be dispensable for eIF5B function in yeast [85].

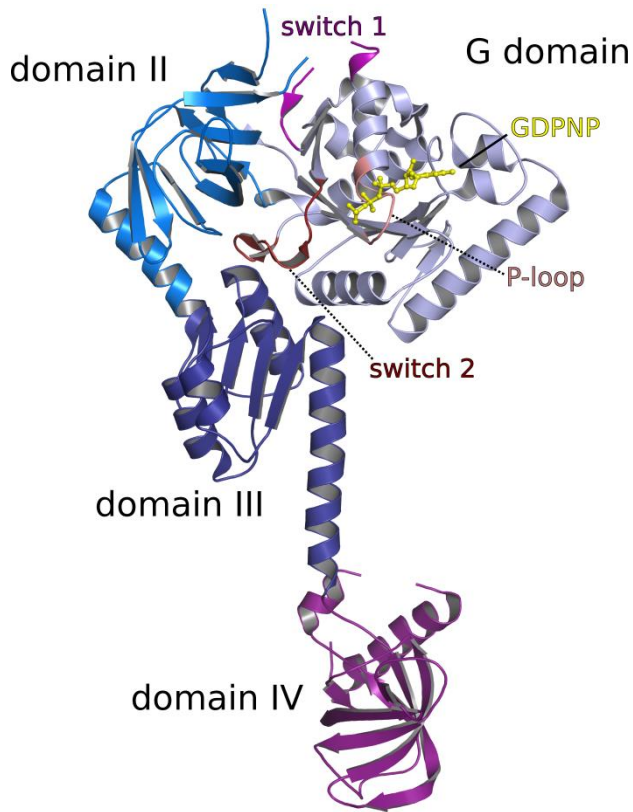


Figure 1.9: Structure of the trGTPase eIF5B. Crystal structure of GDPNP-bound eIF5B from *M. thermoautotrophicum* (PDB: 1G7T). The color code for G domain and domain II are the same as for the homologous domains in EF-Tu, EF-G and eIF2 γ in Fig. 1.6 and 1.7, with P-loop, switch 1 and switch 2 colored light red, magenta and dark red, respectively. GDPNP is shown as yellow balls and sticks. Domains III and IV are colored in dark blue and purple, respectively.

The principle role of eIF5B is to promote subunit joining to form the elongation competent 80S initiation complex. Following the dissociation of eIF2·GDP and most other initiation factors, eIF5B in its GTP-bound form binds to the pre-IC in a manner accelerated by interactions between the C-terminal tail of A site-bound eIF1A and the two α /eIF5B-specific α -helices in domain IV [86-89]. Biochemical studies as well as the recent cryo-EM model of the yeast 80S pre-IC containing a GDPNP-bound eIF5B mutant (T439A) suggest that eIF5B·GTP binds to the 43S pre-IC similar to IF2 on bacterial 30S pre-ICs with domain II interacting with the 40S subunit, while domain IV forms a direct contact to the acceptor stem of the Met-tRNA_i in the P-site [85, 90, 91]. Following its binding to the 43S pre-IC, eIF5B·GTP

promotes the association of the 60S ribosomal subunit, which in turn triggers the intrinsic GTPase activity of eIF5B. GTP hydrolysis and the subsequent transition to the GDP-bound state reduce eIF5B affinity for the 80S ribosome and trigger the concerted release of eIF5B·GDP and eIF1A from the 80 initiation complex [88].

Chapter 2 • Interaction network between eIF2 and eIF5

This manuscript is in preparation for submission

Analysis of the interaction network between eIF2 and eIF5 and its implications for the process of eukaryal translation initiation

Bernhard Kuhle^{1,§}, Oliver Valerius² and Ralf Ficner¹

¹ Abteilung für Molekulare Strukturbiologie, Institut für Mikrobiologie und Genetik, Göttinger Zentrum für Molekulare Biowissenschaften, Georg-August-Universität Göttingen, D-37077 Göttingen, Germany

² Abteilung für Molekulare Mikrobiologie und Genetik, Institut für Mikrobiologie und Genetik, Georg-August-Universität Göttingen, D-37077 Göttingen, Germany

§To whom correspondence should be addressed: bkuhle@gwdg.de

Author contributions:

BK: designed the study and conceived the experiments; performed cloning, protein purification, crystallization, data collection and structure determination, crosslinking experiments, and biochemical studies on nucleotide binding by eIF2; analyzed and interpreted the data; wrote the manuscript. OV: performed mass-spectrometry analysis of crosslinks and helped to analyze MS-data. RF: design of the study; helped to draft the manuscript.

Abstract

Translation initiation results in the accurate assembly of the elongation-competent ribosome with the unique initiator tRNA positioned in its P site, base paired to the AUG start codon of an mRNA. In eukarya, recruitment of the initiator tRNA (Met-tRNA_i) to the ribosome is mediated by the heterotrimeric initiation factor 2 (eIF2), a translational GTPase that requires the multifunctional effector protein eIF5 to carry out its function. Here, we present a structural and biochemical analysis of the interaction network between eIF2 and eIF5. A high-resolution crystal structure of the complex between the eIF5-CTD and the eIF2 β N-terminal tail in combination with Trp quenching experiments shows that recruitment of eIF5 to eIF2 occurs via a flexible peptide-domain interaction that provides a possible explanation for the dynamic interplay between eIF2 and eIF5 and other eIFs that occurs during start site selection on the ribosome. A second direct interaction was mapped between the eIF5-NTD, which is responsible for the stimulation of GTP hydrolysis by eIF2 on the ribosome, and the GTP-binding eIF2 γ subunit. Finally, the third interaction occurs between the eIF5-CTD and eIF2 γ in the direct vicinity to the nucleotide binding pocket, which is likely to be responsible for the previously reported role of eIF5 in stabilizing GDP on eIF2. Together, the presented findings provide a more complete and refined picture of the intricate interactions between eIF2 and eIF5 that play central roles at various stages of the initiation process.

2.1 Introduction

In eukarya, translation is initiated by the formation of an elongation-competent 80S ribosome, assembled with the methionylated initiator tRNA (Met-tRNA_i) in its P-site base-paired to the AUG start codon of an mRNA. This process depends on the concerted action of at least 12 different auxiliary protein factors (eIFs) that mediate the specific binding of mRNA and initiator tRNA, as well as the joining of the two ribosomal subunits by an intricate series of formation, rearrangement, and breaking of interactions and GTP hydrolysis [9, 12].

In the first step of translation initiation, GTP-bound eIF2 binds the Met-tRNA_i to form a ternary complex (TC). Together with eIFs 1, 1A, 5 and the eIF3 complex, the TC is then recruited to the 40S ribosomal subunit and placed over the ribosomal P-site, thereby forming the 43S pre-

initiation complex (pre-IC). Assisted by eIF3 and the eIF4F complex, the 43S pre-IC subsequently binds to the 5'-proximal region of an mRNA, whereby it enters the scanning phase of the initiation process, in which the 5'-untranslated region of the mRNA is searched for the AUG start codon. Upon encounter of the correct initiation site, the scanning process is arrested by the formation of codon-anticodon interactions between the mRNA and initiator tRNA, which triggers a rearrangement of eIF1A, dissociation of eIF1 and finally the irreversible hydrolysis of the eIF2-bound GTP, stimulated by eIF5. GDP-bound eIF2 then dissociates from the scanning-arrested 40S subunit together with eIF5, and is subsequently recycled back to eIF2·GTP by the guanine-nucleotide exchange factor (GEF) eIF2B. Instead of eIF2, GTP-bound eIF5B now binds to the 40S·Met-tRNA_i complex to promote the joining of the large 60S ribosomal subunit, thus forming the 80S pre-IC. Subunit joining finally triggers GTP hydrolysis in eIF5B, resulting in the dissociation of eIF1A together with eIF5B·GDP and the transition of the 80S IC into the elongation phase of translation [9, 12, 16].

The focus of this work lies on the elucidation of the molecular details of the intricate interaction network between the two central initiation factors eIF2 and eIF5. eIF2 is composed of three subunits (eIF2 α , - β , and - γ), each of which has orthologs in archaea (aIF2) but not in bacteria [28]. The eIF2 γ subunit, a paralog of EF-Tu, belongs to the family of Ras-related G proteins and is responsible for the GTP-dependent binding of Met-tRNA_i to form the TC, assisted by the α - and β -subunits [32, 41, 42]. The TC does not bind to the 40S subunit on its own, but instead depends on the concerted action of additional factors, namely eIFs 1, 1A, 3 and 5 [12, 58, 59]. Hereby, the direct interaction between three lysine-rich segments (K-boxes 1-3) in the eukarya-specific N-terminal tail (NTT) of eIF2 β and the negatively charged AA-boxes 1 & 2 in the C-terminal domain (CTD) of eIF5 plays a central role to allow the efficient recruitment of the TC [35]. The eIF5-CTD thereby acts as nucleation core that mediates cooperative interactions between eIF2 β -NTT, eIF1 and the eIF3c-NTD for the formation of an intermediate multi-factor complex (MFC; composed of eIFs 1, 3, 5 and the TC) and finally the proper incorporation of the TC into the 43S pre-IC [56, 57, 59]. Consequently, the loss or weakening of the eIF5-CTD·eIF2 β -NTT interaction results in a significant reduction of TC recruitment to the 40S subunit [35, 57, 92].

Recent studies suggest an additional role for the eIF5-CTD-eIF2 β -NTT interaction during scanning and start site recognition by destabilizing eIF1 binding to the pre-IC that seems to involve the loss of interactions between eIF1 and eIF2 β -NTT and instead the formation of a stronger interaction of the latter to eIF5 in response to start-site recognition [21, 63]. Together with the displacement of the eIF1A C-terminal tail (CTT) from the P-site by the Met-tRNA_i, the resulting release of eIF1 triggers conformational rearrangements of the 40S subunit from an 'open' scanning competent conformation to its 'closed' scanning arrested state, ultimately causing the irreversible hydrolysis of the eIF2-bound GTP by the gated release of P_i[64]. Here, eIF5 again plays a critical role with its N-terminal domain acting as GTPase activating protein (GAP) to trigger the GTPase activity in eIF2, most likely by introducing an arginine-residue (Arg15 in yeast eIF5) as catalytic residue into the GTPase center [52, 53, 64].

After their release from the pre-IC, eIF2·GDP and eIF5 were found to remain tightly associated, giving rise to a large cytosolic pool of eIF2·eIF5 complexes that significantly exceeds the levels of TC in the cell [68]. This observation suggested that eIF5 might serve an additional role in the recycling pathway of eIF2·GDP by antagonizing the guanine-nucleotide exchange (GEF) activity of eIF2B [68, 69]. In line with this assumption an evolutionarily conserved region within eIF5, called DWEAR-motif, was found to be responsible for a reduced rate of GDP dissociation from eIF2. This suggested that eIF5 indeed contains a guanine-nucleotide dissociation inhibitor (GDI) activity, in addition to its ability to compete physically with eIF2B for their common substrate eIF2. Based on these and genetic observations, it was proposed that eIF5 provides a regulatory function under stress conditions by antagonizing spontaneous or GEF-catalyzed recycling of eIF2·GTP and TC formation in addition to the mechanism of eIF2B inhibition by eIF2 α phosphorylation [69].

Over the last years, considerable progress has been achieved in the elucidation of the intricate series of molecular events that govern the involvement of eIF2 and eIF5 in pre-IC formation, start codon recognition and recycling of eIF2 [12]. However, a detailed understanding of these processes is still limited, in part due to the highly dynamic and transient nature of most of the involved interactions that, as a result, escape most biochemical techniques and resist high-resolution structural investigations. By combining different high- and low-resolution structural approaches with mutational and biochemical methods we were able to analyze the complex interaction

network between eIF2 and its multifunctional effector protein eIF5, as well as its influence on the association of eIF1 and eIF3c with the eIF5-CTD. We find that eIF5 forms three major contact sites with the eIF2 complex. One is formed by the N-terminal portion of the eIF5-NTD, which harbors the putative catalytic arginine-finger and specifically contacts the eIF2 γ subunit in the presence and absence of Met-tRNA_i. A second interaction is formed by the eIF5-CTD, which directly contacts the γ -subunit close to the nucleotide binding site of the G domain. Interestingly, we could show that this interface involves the DWEAR-motif, which seems to form an element of the CTD itself and not, as previously assumed, of the flexible linker region between the N- and C-terminal domains. Using fluorescence-labeled nucleotide analogs, we show that this interaction, which is formed irrespective of the nucleotide-state of eIF2 or the presence of Met-tRNA_i, is responsible for the stabilization of eIF2-bound guanine-nucleotides. Finally, the third interaction, which is responsible for the high affinity binding of the two factors, is formed between the AA-boxes in eIF5-CTD and the K-boxes in the eIF2 β -NTT. The first high-resolution crystal structure of an eIF5-CTD·eIF2 β -NTT complex, in combination with fluorescence-based tryptophan quenching and mass-spectrometry-coupled crosslinking experiments, indicates that the two factors interact via a peptide-domain interaction, which allows a dynamic interplay with the simultaneously bound eIF1 and eIF3c. Together, the presented data provide a more complete and refined picture of interactions occurring between eIF2 and its effector protein eIF5, with implications for the chain of molecular events that accompany pre-IC formation, start codon recognition and eIF2 recycling.

2.2 Results

Contributions of the lysine-rich patches K1, K2 and K3 of the eIF2 β -NTT to the interactions with eIF5-CTD

In order to gain insight into the roles of the individual K-boxes for the interactions between eIF2 β -NTT and eIF5-CTD, complex formation between both proteins was monitored by means of tryptophan quenching. For this purpose an eIF5-CTD construct was used comprising residues 241-405 which contains two tryptophan residues, Trp245 and Trp391. According to the previously determined crystal structure of eIF5(241-405)(PDB: 2FUL) [1], the universally conserved Trp391 in AA-box 2 lies close to the C-terminus of the CTD and thereby in direct vicinity to the negatively

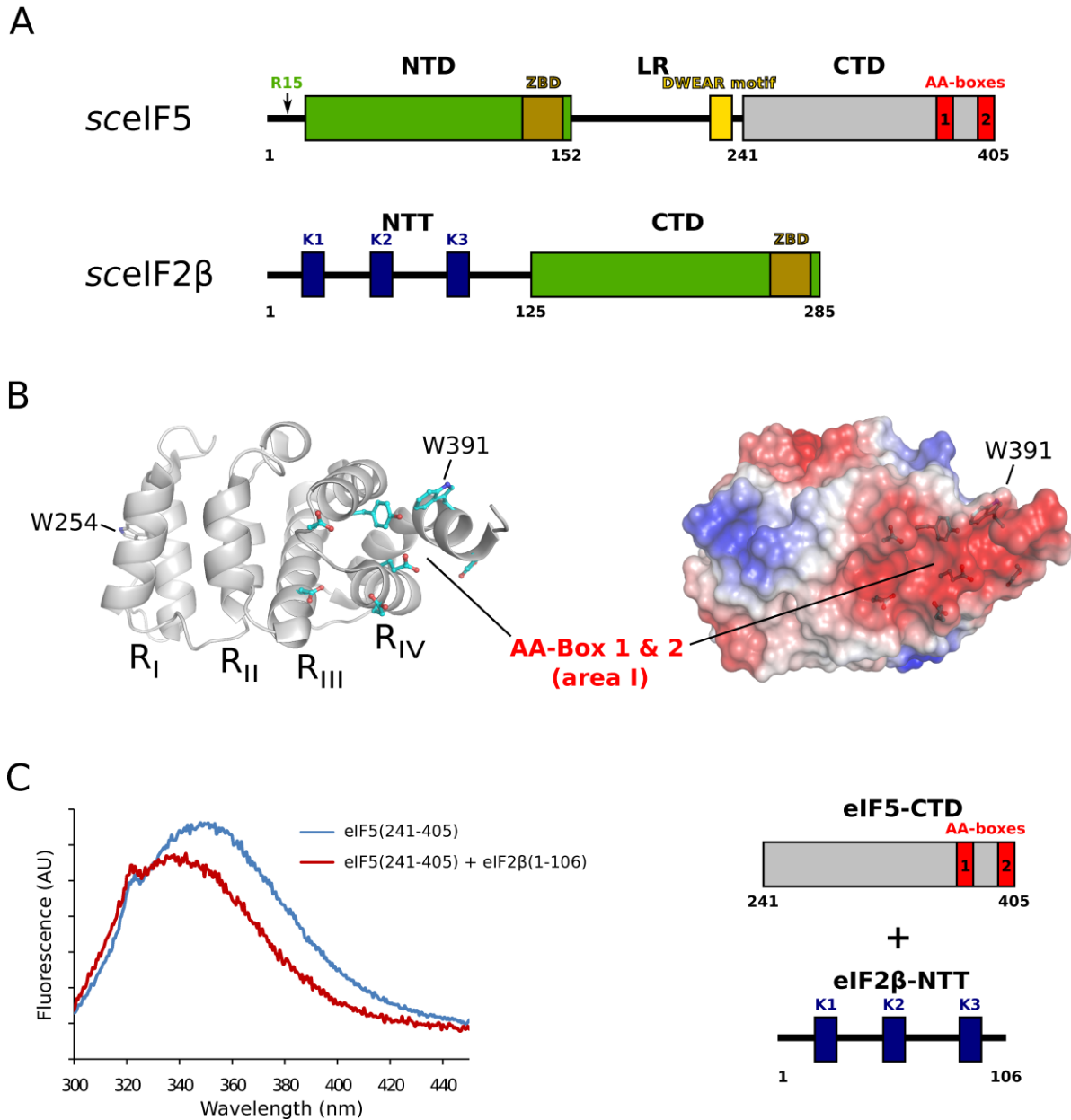


Figure 1. A) Schematic presentation of the proposed domain architecture in eIF5 and eIF2 β . **B)** Crystal structure of the C-terminal HEAT-like domain of eIF5 (residues 241-396) from *S. cerevisiae* (PDB: 2FUL) [1]. The left panel shows the eIF5-CTD in cartoon presentation; the four HEAT-like repeats (R_I-R_{IV}) are indicated, with the conserved Trp245 in R_I and Trp391 in R_{IV}. Next to Trp391, conserved residues of the AA-boxes are shown as balls and sticks. The right panel shows the surface charge distribution of eIF5-CTD (negative, red; positive, blue), revealing the highly negatively charged area I, formed by residues of the two AA-boxes, next to Trp391. **C)** Trp-quenching by eIF2 β on the eIF5-CTD. The chromatogram shows the emission spectrum of eIF5(241-405) upon the excitation of the Trp fluorescence at 280 nm in the absence (blue) and presence (red) of the eIF2 β -NTT.

charged area I, implicated in binding of the K-boxes of eIF2 β (Fig. 1 and S1). We therefore reasoned that binding of the lysine-rich patches of the eIF2 β -NTT in this area should be reflected in the

fluorescence signal of Trp391, either indirectly by its conformational rearrangement or directly through proton transfer from a nearby positioned ϵ -amino group.

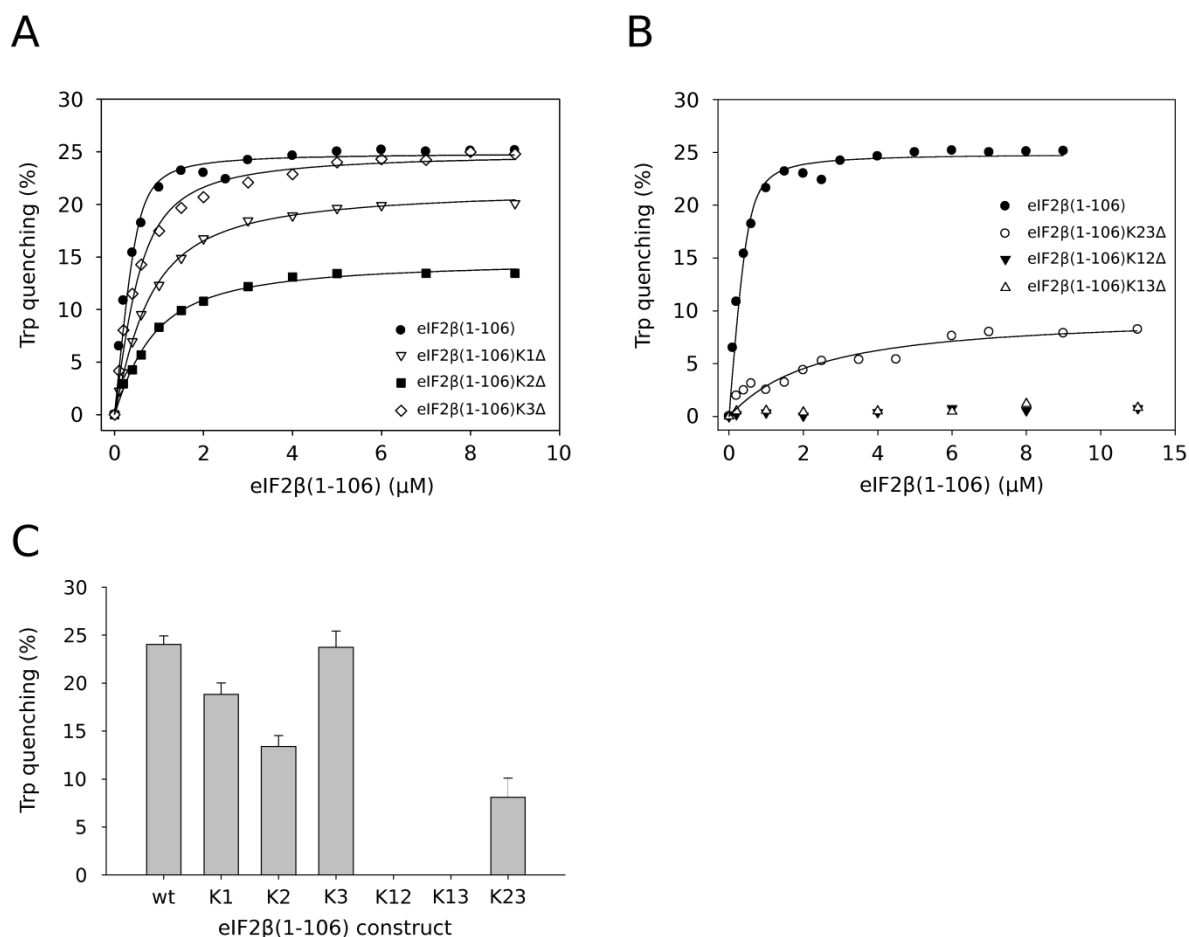


Figure 2. Trp-quenching experiments between eIF5-CTD and eIF2β-NTT. A) Equilibrium titrations of 0.5 μM eIF5(241-405) with increasing amounts of wild-type eIF2 β (1-106) or the three single K-box mutants K1 Δ , K2 Δ , and K3 Δ . The Trp quenching signal (in % of the original fluorescence signal of eIF5(241-405)) was plotted against the concentration of the respective eIF2 β -NTT constructs. The black lines show the fit to the data, using a quadratic one-side binding model. **B)** Equilibrium titration of 0.5 μM eIF5(241-405) with wild-type eIF2 β (1-106) or the three double K-box mutants K12 Δ , K13 Δ , and K23 Δ . **C)** Comparison of the Trp quenching signals for the seven eIF2 β (1-106) constructs. Standard deviations are given as error bars.

In line with this assumption, the addition of eIF2 β (which contains no Trp) to eIF5(241-405) results in a significant decrease in the fluorescence signal at 360 nm (excitation at 290 nm), accompanied by a blueshift of the emission maximum from 350 to 340 nm (Fig. 1C). Both effects are lost in the eIF5(241-405)W391F mutant (Fig. S2). Titration of eIF5(241-405) with increasing amounts of eIF2 β gives an estimate for the K_d of ~ 100 nM and a maximum of $\sim 25\%$ quenching of

Chapter 2

the initial fluorescence signal at saturating eIF2 β concentrations. Similar values are obtained with N-terminal fragments of eIF2 β , containing either residues 1-148 (K_d = 95 nM and ~24% quenching) or 1-106 (K_d = 70 nM and ~24% quenching) (Fig. 2A and Table 1). These values are consistent with the assumption that the NTT provides the entire binding region for interactions of eIF2 β to eIF5-CTD and are in good agreement with the reported affinity (K_d = 40 nM) between eIF5-CTD and the heterotrimeric eIF2 complex [21, 35, 36]. We therefore used the shortest fragment containing all three K-boxes (eIF2 β (1-106)) for the subsequent mutational analysis.

Table 1. Trp quenching experiments between eIF5(241-405) and eIF2 β .

eIF2 β construct	K_d (nM)	Reduction of affinity relative to wt	Quenching signal (%)
eIF2 β (FL)wt	100 \pm 44	--	25
eIF2 β (1-148)wt	95 \pm 24	--	24
eIF2 β (1-106)wt	70 \pm 20	--	24
eIF2 β (1-106)K1 Δ	825 \pm 55	12-fold	19
eIF2 β (1-106)K2 Δ	550 \pm 45	8-fold	13
eIF2 β (1-106)K3 Δ	200 \pm 19	3-fold	24
eIF2 β (1-106)K12 Δ	N.D.		No signal
eIF2 β (1-106)K13 Δ	N.D.		No signal
eIF2 β (1-106)K23 Δ	2200 \pm 400	30-fold	8

K_d is the equilibrium dissociation constant.

N.D., not determined due to the absence of a detectable quenching signal.

Either one or two of the K-boxes in the eIF2 β -NTT (Fig. 1A) were deleted by mutation to alternating Ala and Ser residues. Among the single K-box mutants, the most severe effect was observed for K1 Δ exhibiting a ~12-fold increase in the dissociation constant (K_d = 825 nM) and a simultaneous loss of nearly 20% of the quenching signal (Fig. 2A/C and Table 1). K2 Δ resulted in an ~8-fold loss of binding affinity (K_d = 550 nM), accompanied by a loss of nearly 50% of the quenching signal. Finally, K3 Δ exhibited the smallest effect with an only 3-fold reduction in binding affinity (K_d = 200 nM) and no effect at all on the quenching signal.

Among the double K-box mutants only K23 Δ exhibited a quenching signal (~30% of the signal observed for wild-type eIF2 β), allowing an estimate of 2.2 μ M for the K_d , corresponding to a ~30-fold reduction in binding affinity (Fig. 2B/C and Table 2). By contrast, neither K12 Δ nor K13 Δ exhibited any quenching signal upon addition to eIF5(241-405). For K23 Δ and K12 Δ these observations are compatible with the effects of the single K-box deletions. However, it is interesting to note that both, the loss of binding affinity and the quenching signal for the K23 Δ double mutant are slightly larger than an entirely additive contribution by K2 and K3 would suggest. Moreover, the sole presence of K2 (in K13 Δ), which according to the single mutations contributes significantly to the binding affinity and ~50% of the total quenching signal, results in no signal at all. Thus, K3 actually does seem to provide contributions in K1 Δ and K2 Δ , which, however, do not become apparent from its single-deletion.

These results demonstrate that K1 and K2 provide the principal contact surface for eIF5-CTD, both with immediate effects on the surrounding of Trp391. This central role of Trp391 in the interactions with the eIF2 β -NTT is further supported by the complete loss of the quenching signal and a severe negative impact on the interactions in GST-pull-down assays with eIF5(241-405)W391A, -W391F (Fig. S2). At the same time, K3 seems to provide only a small contribution – at least in the presence of K1 and K2 –, which, moreover, does not involve a direct effect on Trp391. Although in this kind of experiments no quenching signal is not necessarily indicative of no binding, our results suggest that K2 binding is partially assisted by either K1 or K3 for its full binding affinity, and that K3 is able to partially substitute for the loss of K2 in the K2 Δ mutant, possibly by binding to similar surface residues on eIF5-CTD in the absence of K2.

Crystal structure of eIF2 β (39-106) bound to eIF5(201-405)

Despite the critical role which the eIF5-CTD plays as nucleation point for other eIFs during MFC and pre-IC assembly, scanning and start codon recognition, no structural information that would allow direct insight into the molecular details of any of these interactions was so far available. We therefore intended to determine the structure of the eIF5-CTD in complex with the eIF2 β -NTT by means of X-ray crystallography. Based on the results from the Trp-quenching experiments we were particularly interested in the mode of binding of K3, as the contributions of this lysine-patch

Table 2. Data collection and refinement statistics for the structure of the eIF5(201-405)·eIF2β(39-106) complex from *S. cerevisiae*

Crystallization	
Condition	0.8 M (NH ₄)SO ₄ , 0.3 M LiSO ₄
Temperature (°C)	20
Data Collection	
Space Group	P3 ₂ 12
Unit Cell	a = 74.3 Å b = 74.3 Å c = 124.8 Å
	α = 90° β = 90° γ = 120°
Resolution (Å)	2.0 (2.1-2.0)
Observed reflections	359597 (87743)
Unique reflections	48223 (11831)
Completeness (%)	99.9 (99.8)
<I>/σ	22.3 (3.9)
R _{sym} (%)	8.9 (42.8)
Refinement	
R _{work} /R _{free} (%)	17.4/20.1
Rmsd from Strd. Stereochemistry	
Bond length (Å)	0.007
Bond angles (°)	0.98
Ramachandran Plot Statistics	
Most favored (%)	98.5
Allowed regions (%)	1.5
Disallowed regions (%)	0

Values in parentheses refer to the highest resolution shell.
R_{work} and R_{free} factors are calculated using the formula $R = \frac{\sum_{hkl} |F(obs)_{hkl}| - |F(calc)_{hkl}|}{\sum_{hkl} |F(obs)_{hkl}|}$, where F_(obs)_{hkl} and F_(calc)_{hkl} are observed and measured structure factors, respectively. R_{work} and R_{free} differ in the set of reflections they are calculated from: R_{free} is calculated for the test set, whereas R_{work} is calculated for the working set.

seemed to be contingent on the overall binding situation, apparently at odds with its universal conservation among eIF2β orthologs across the eukaryal lineages. We therefore purified N-terminal fragments of *S. cerevisiae* eIF2β containing either all three K-boxes (residues 1-106) or only K2 and K3 (residues 39-106) in complex with the C-terminal domain of *S. cerevisiae* eIF5 (containing either residues 241-405 or 201-405) from *E. coli* cells. The longer construct of eIF5 including residues 201-240 was chosen in order to gain additional insight into the structural arrangement of the highly conserved 'DWEAR-motif' (residues 220-238), previously assigned to the flexible linker region between eIF5-NTD and -CTD and proposed to stabilize GDP binding by eIF2 in eIF2·eIF5 complexes[69] (Fig. S1).

Among the four purified combinations, only the eIF5(201-405)·eIF2β(39-106) complex yielded crystals of sufficient quality to allow structure determination. The final model, refined at a resolution of 2.0 Å, contains two eIF5-CTD copies per asymmetric unit including residues 201 to 399 (with the additional vector-encoded residues PGLGS at the N-terminus) (Details of data collection and

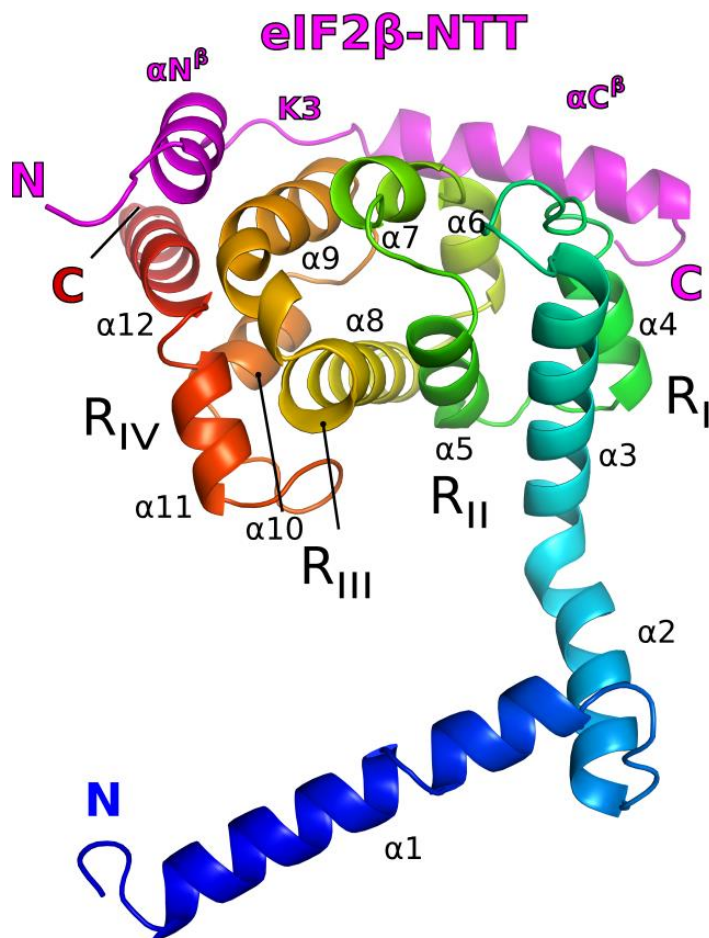


Figure 3. Crystal structure of an eIF2 β -NTT fragment bound to the eIF5-CTD. The eIF5(201-399)-eIF2 β (66-106) complex is shown in cartoon presentation with eIF2 β colored pink and the eIF5-CTD shown in rainbow coloring (N-terminus, blue; C-terminus, red). The body of the eIF5-CTD is formed by ten α -helices (α 3- α 12), folding into four atypical HEAT repeats R_I - R_{IV} (compare Fig. 1B). The N-terminal helices α 1 and α 2 protrude from the HEAT-like domain and form crystal contacts to symmetry related molecules. The bound eIF2 β -NTT fragment folds into two α -helices (αN^β and αC^β) connected by a loop region containing K-box 3 (K3). The eIF2 β -NTT thereby adopts an extended conformation in which it wraps around the eIF5 HEAT-like domain, placing its N-terminus (residue 66) at repeat R_{IV} , while the C-terminus (residue 106) is placed atop of R_I .

refinements statistics are summarized in Table 2). Residues 241-399 of both eIF5 molecules adopt a fold composed of four antiparallel helical repeats (R_I - R_{VI}) (Fig. 3) that is virtually identical to that of the previously reported yeast eIF5-CTD structure (rmsd of 0.8 Å over 133 C_α atoms) [1]. The remaining N-terminal residues (201-240) fold into two additional α -helices (α 1 and α 2) that protrude from the globular part of the eIF5B-CTD and form extensive contacts to symmetry related molecules in the crystal packing. Only one of the two eIF5-CTD molecules binds a fragment of eIF2 β which includes only residues 66-106 and folds into two amphipathic α -helices (hereafter termed αN^β and αC^β), connected by a loop formed by K-box 3 (Fig. 4). Residues 39 to 65, including K2, are not defined in the electron density.

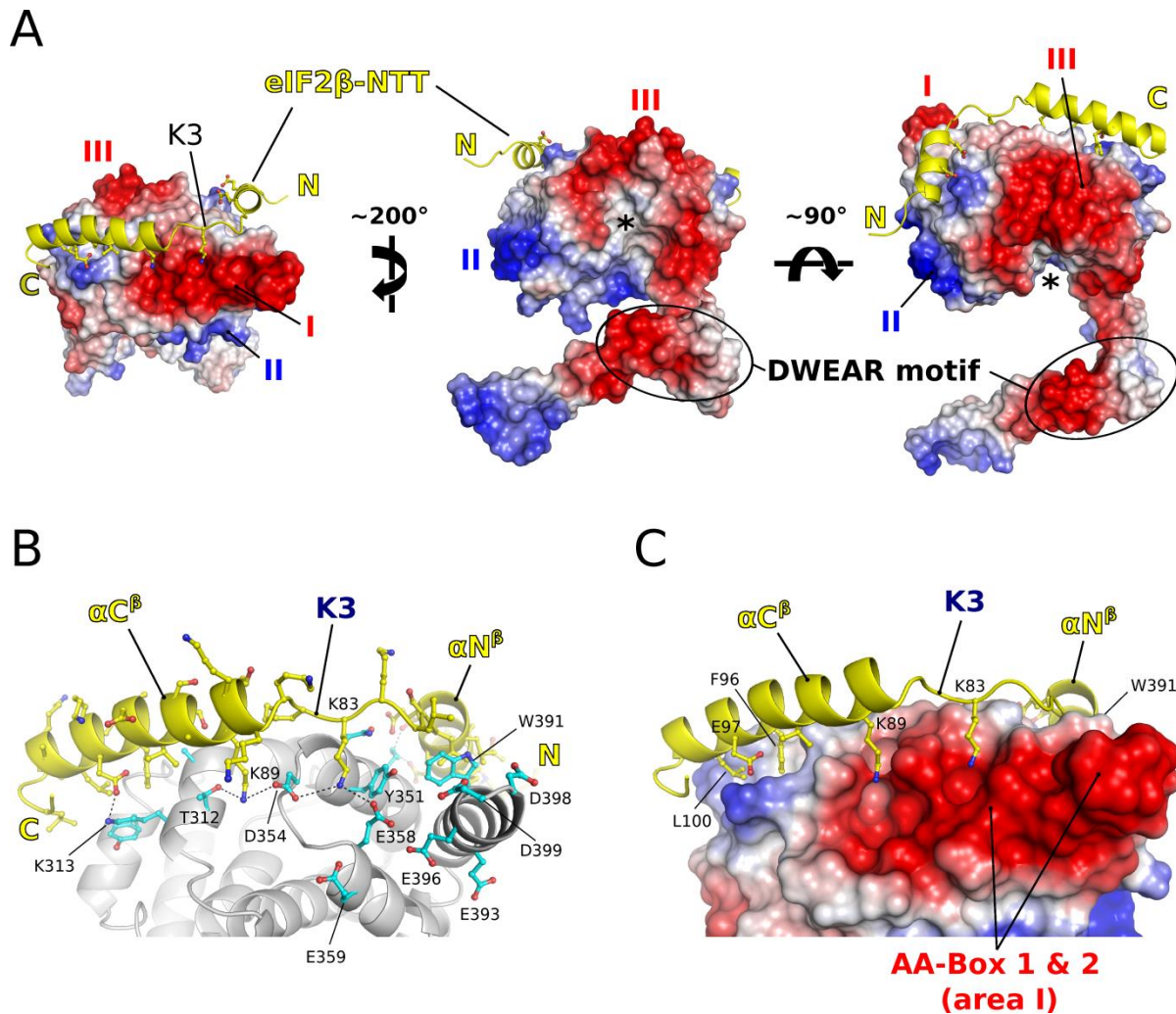


Figure 4. Peptide-domain interaction between the eIF2 β -NTT and eIF5-CTD. **A)** The eIF5(201-399)-eIF2 β (66-106) complex from different orientations. The eIF5-CTD is shown with surface charge presentation (negative, red; positive, blue), demonstrating how the eIF2 β -NTT (yellow cartoon) adopts an extended conformation to associate with the regions between the charged areas I-III through the amphipathic helices αN^{β} and αC^{β} , thereby placing K-box 3 (K3) in direct vicinity to the negatively charged area I. The middle and right panel reveal the existence of a hydrophobic cleft adjacent to area III (asterisk). **B)** Details of the interactions between K-box 3 of eIF2 β (yellow) and the AA-boxes of eIF5 (grey, with conserved AA-box residues and residues involved in direct contacts with eIF2 β shown as balls and sticks in cyan). Among the seven lysine residues of K-box 3, only Lys83 and Lys89 form stable polar interactions with AA-box 1 (indicated by black dashed lines). **C)** The surface charge distribution of eIF5-CTD reveals that Lys83 and Lys89 are inserted into negatively charged pockets from the periphery of area I, while the major part of the negative surface area remains available for interactions with K-boxes 1 and 2 (not present in the crystal structure).

Helix αN^{β} (residues 69-79) lies between helices $\alpha 9$ and $\alpha 12$ of eIF5, on one side contacting Lys345 of eIF5 through Asp88 and Glu91 and on the other side forming a hydrophobic interface with Pro344, Ile348, Pro387, Phe388 and Trp391. Following helix αN^{β} , K3 comes to lie at the very C-terminus of helix $\alpha 9$ of eIF5-CTD and thereby in immediate vicinity to the negatively charged

surface formed by the two conserved AA-boxes in eIF5 (area I) (Fig. 4). However, only two of the seven lysine residues, Lys83 and Lys89, form a direct contact to AA-box 1, with Lys83 lying in a pocket formed by Tyr351, Asp354 and Glu358, and Lys89 lying between Thr312 and Asp354 (Fig. 4B/C). The remaining lysine residues of K-box 3 are poorly resolved in the electron density, indicating that they either do not participate in the interactions with eIF5 or that the formation of stable interactions is prevented by the relatively high salt concentrations at which the crystals were obtained (400 mM $(\text{NH}_4)_2\text{SO}_4$); this may as well be responsible for the inability of K-box 2 to form a stable interaction under these conditions. In agreement with the absence of a strong contribution to the quenching signal in the fluorescence experiments, no lysine residue in K-box 3 is stably positioned in the direct vicinity to Trp391. Finally, helix αC^β of eIF2 β -NTT (Lys89-Ala103) is packed on top of and orthogonal to helices $\alpha 7$ and $\alpha 4$ of eIF5, with Phe96 and Leu100 positioned in a hydrophobic pocket on the eIF5-CTD surface formed by Val270, Tyr273, Ala309 and the aliphatic part of the Lys313 side chain, whose ϵ -amino group additionally forms a salt bridge to Glu97 of eIF2 β (Fig. 4B/C).

Thus, the co-crystallized portion of the eIF2 β -NTT adopts an elongated conformation containing secondary structure elements but no tertiary structure, thereby allowing an extended interaction interface that reaches half around the eIF5-CTD (Fig 4A). Interestingly, the eIF2 β -NTT thereby only peripherally contacts the negatively charged area I of eIF5 through K-box 3 and mainly occupies those regions lying between the negatively charged areas I and III and the positively charged area II, which is thought to provide the main interface for interactions with eIF3c and eIF1 [57]. K-box 3 thereby leaves most of area I available for interactions with K1 and K2, including the highly negatively charged C-terminal end (Glu393-Glu405), as well as Glu358 and Glu359 in AA-box 1, both of which are critical for high affinity binding of the eIF2 β -NTT [57, 93]. This proposed binding interface for the eIF2 β -NTT is in good agreement with the previously reported contact sites for a human eIF2 β -NTT fragment containing K-boxes 2 and 3 on *h*eIF5-CTD, determined by NMR chemical shift assays[63] (Fig. S3B/C).

The DWEAR-motif as transient element of the eIF5-CTD.

An interesting and yet unrecognized characteristic of charge distribution and morphology on the surface of eIF5-CTD is a broad, mainly hydrophobic cleft lying parallel to helix $\alpha 3$ and ending on one side in the acidic area III (Fig. 4A and S3A). The comparison of the available eIF5-CTD structures shows that this cleft is conserved between fungi and mammals and may thus play a functional role. In the human ortholog the lower half of the cleft (next to the N-terminus of helix $\alpha 3$) is occupied by an α -helix formed by 11 residues of the extended C-terminal end (Fig. S4A). However, this extension is idiosyncratic to the human ortholog and not found in fungal eIF5, where the C-terminal end is physically incapable of reaching this far, suggesting an alternative role for the hydrophobic cleft. Our structure of yeast eIF5(201-405) suggests that this role may in fact be the – at least transient – accommodation of helix $\alpha 2$ (residues 229-241) in a manner antiparallel to helix $\alpha 3$ (Fig. 5).

To test this possibility, we took advantage of the technique of genetic code expansion which allows the incorporation of unnatural amino-acids such as the UV-inducible crosslinker p-benzoyl-L-phenylalanine (Bpa) into specific positions of a protein[94]. The idea was that the accommodation of helix $\alpha 2$ into the hydrophobic cleft of the eIF5-CTD should be reflected in a specific crosslinking pattern, where the internal crosslink would be manifested in a faster migration speed during SDS-PAGE due to the formation of the more compact internal lariat topology of the primary structure. For this purpose Bpa was individually introduced in a number of positions of eIF5 along the DWEAR-motif (Asp220, Asp221, Trp223, Ala234, Glu238), and in area III (Glu261) (Fig. 5B). The purified eIF5(201-405)Bpa constructs were exposed to UV-radiation and the crosslinking products were analyzed by SDS-PAGE. In line with our assumption, UV-exposure resulted in the emergence of additional bands migrating faster than the original eIF5(201-405)Bpa constructs (Fig. 5C). No additional bands appeared at higher molecular weight, indicating the absence of dimer or oligomer formation. While no crosslinking was observed for the position Asp220, the strongest crosslink bands were obtained in the cases of E238-, A234-, E261Bpa and to a lesser extent, although still significant, for D221- and W223Bpa. Importantly, MS analysis confirmed that these bands are the product of internal crosslinks in eIF5(201-405), and the search for the target peptide of the crosslink suggests proximity of A234- and E238Bpa to helix $\alpha 8$

(³³⁰RF³³¹) and the loop preceding helix α 11 (³⁷²FVPK³⁷⁵), while E221Bpa in area III was found to crosslink to the C-terminal half of helix α 8 (³³⁵HK³³⁶) (Fig. 5B and Table 3).

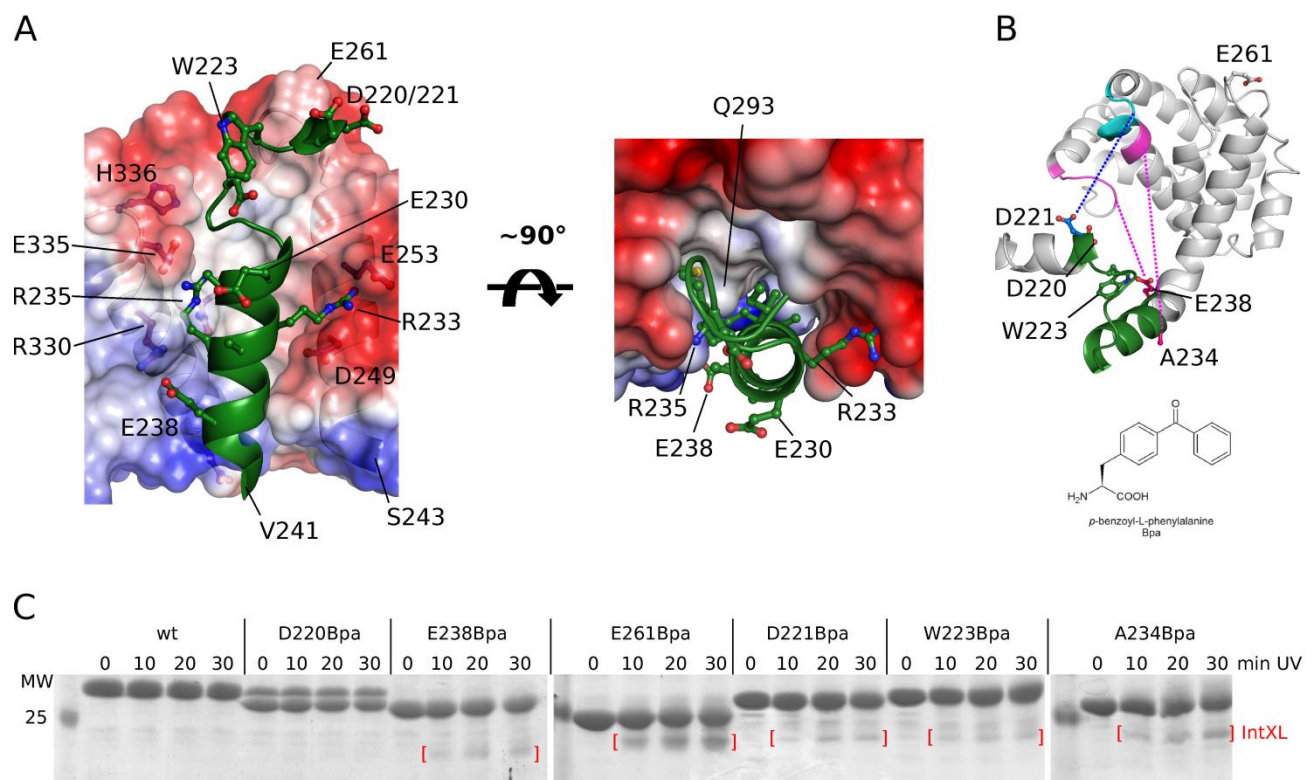


Figure 5. The DWEAR-motif as transient element of the eIF5-CTD. A) Proposed model of the DWEAR-motif (green) as part of the C-terminal HEAT-like domain of eIF5. According to this model, the amphipathic helix α 2 is accommodated into the hydrophobic cleft between helices α 3, α 5 and α 8, thereby allowing the conserved Arg233, Arg235 and Glu238 of the DWEAR-motif to form ionic interactions with Glu253, Glu335 and Arg330, respectively. At the same time, Met227, Ile232, Ala236, and Leu239 of helix α 1 point toward helix α 3 thus forming a continuous hydrophobic interface within the cleft. This places the N-terminus of the DWEAR-motif with Asp220, Asp221, Trp223, Asp226, and Glu230 next to Glu261, resulting in an extended negatively charged area III. Arg330, Glu335 and His336 indicate positions within helix α 8 that were identified as target peptides for Bpa-crosslinks from Asp221 and Glu238 (see B). Compare also Fig. S4C. **B)** Positions in eIF5-CTD where the UV-inducible crosslinker p-benzoyl-L-phenylalanine (Bpa) was introduced (substituted residues are shown as sticks). The DWEAR-motif is colored green. Peptides that were identified as targets for internal crosslinks from Ala234/Glu238 and Asp221 are colored pink and cyan, respectively (see also Table 3). **C)** SDS-gels showing the UV- and time-dependent formation of internal crosslink bands (IntXL) for the eIF5(201-405)Bpa constructs (5 μ M of the protein were exposed to UV light for the indicated time on ice); crosslinks are indicated by red brackets.

Table 3. Internal crosslinks in eIF5(201-405)Bpa constructs.

Crosslinked peptides						
Construct	Bpa peptide	Target peptide	Site	Mass (Da)	Error (ppm)	m/z
D221Bpa	VKD <u>b</u> EWAVDMSE	<u>QIK</u>	205-207	1962.9116	-1.9	555.7913
	<u>b</u> EWAVD	FLGLE <u>HK</u>	336-337	1712.8161	-1.0	571.6102
A234Bpa	<u>b</u> RAKELE	<u>FVPKEVSK</u>	372-373	1929.0430	-2.0	483.0162
	<u>b</u> RAKELE	<u>RFLGLEHK</u>	330-331	1747.0014	2.0	583.0053
	<u>b</u> R	<u>FVPKEVSK</u>	375-379	1358.7377	0.1	453.5840
	EAIR <u>b</u> R	FGT <u>K</u>	367	1346.7144	0.0	449.5763
	EAIR <u>b</u> R	FGT <u>K</u>	367	1346.7144	0.3	673.8601
	<u>b</u> R	KFV <u>P</u> K	374-375	1043.5966	0.1	348.5370
	<u>b</u> R	FV <u>P</u> K	374-375	915.5028	-0.3	458.2550
E238Bpa	<u>b</u> LEVNSE	KFV <u>P</u> K	374-375	1558.8025	-0.4	779.9049
	<u>b</u> LE	<u>FVPKEVSK</u>	372-374	1444.7627	-0.6	482.2590
	<u>b</u> LEVNSE	<u>FVPK</u>	374-375	1430.7201	-0.2	715.8637
	AK <u>b</u> LE	FV <u>P</u> K	374	1200.6663	0.0	600.8367

The likely target positions in the target peptides are underlined.

In the resulting structural model, Ile232, Ala236, and Leu239 point toward helix $\alpha 5$, thus forming a continuous hydrophobic interface, while the outward pointing charged residues of the amphipathic helix $\alpha 2$ would allow the formation of polar interactions to the adjacent regions in helices $\alpha 3$ and $\alpha 8$ and the loop preceding $\alpha 11$. Interestingly, as helix $\alpha 2$ is formed by the C-terminal half of the DWEAR-motif ($^{231}\text{AIRARAKEL}^{239}$) [69], this structural role would provide an explanation for the high degree of conservation of residues such as Arg233, Arg235 and Glu238. At the same time, the N-terminal mainly negatively charged half of the motif ($^{220}\text{DDEWAVDMSEE}^{230}$) would come to lie between the C-terminal ends of helices $\alpha 3$ and $\alpha 8$, respectively, thereby complementing the acidic area III. Importantly, independent support for the manually generated model presented in Figure 5 is provided by the modeling server CluPro[95, 96], which predicts two very similar solutions, when the isolated helix $\alpha 2$ was provided as ligand for the isolated eIF5-CTD (Fig. S4C).

Taken together, these observations indicate that, in contrast to previous assumptions [68, 69], helix $\alpha 2$ and the DWEAR-motif form an at least transient element of the eIF5-CTD rather than of the preceding flexible linker region (Fig. 1A and 5A). This would in part provide an explanation for its high degree of conservation among eIF5 orthologs via a structural role for some of its residues (Fig. S1). At the same time this suggests that the C-terminal domain itself, not the linker region, is involved in the stabilization of the guanine nucleotide bound to the γ -subunit of eIF2. In order to assess this possibility the effect of different eIF5 constructs on the nucleotide binding properties of eIF2 were studied using fluorescent derivatives of GDP and GTP (see below).

Mant-GDP and -GTP as fluorescence-labeled GDP/GTP analogs to study nucleotide binding by eIF2

Derivatives of guanine nucleotides, in which the fluorescent mant group is attached to the 2' or 3' positions of the ribose ring, have been widely used to study the nucleotide binding properties of a variety of GTP-binding proteins. The binding reaction of a mant-nucleotide to a protein can be monitored either by direct excitation of the mant group itself (at 355 nm), in which case the binding event is manifested in a change in the quantum yield of the fluorophore at its emission wavelength (440 nm) due to an environmental change, or indirectly by Foerster Resonance Energy Transfer (FRET) from a nearby tryptophan residue (excited at 280 nm) to the mant-nucleotide.

Despite their widespread use, no study exists so far in which mant-nucleotides were used to monitor guanine nucleotide binding to eIF2. To test the feasibility of such experiments, both options for the excitation of the mant group were tested for mant-GDP and mant-GTP in the presence of eIF2 (Fig. 6). For both nucleotide derivatives, their binding to eIF2 resulted in a significant fluorescence change upon direct excitation. Likewise, a substantial energy transfer between tryptophan residues and the mant group was observed, which was accompanied by a simultaneous decrease in tryptophan fluorescence at ~ 350 nm. Importantly, both fluorescence signals obtained either by direct or by indirect excitation were lost upon the addition of excess unlabeled GDP or GTP but not with ADP or ATP. Thus, mant-nucleotides seem to bind specifically to the nucleotide binding pocket of eIF2 where they can be replaced by the unmodified ligand.

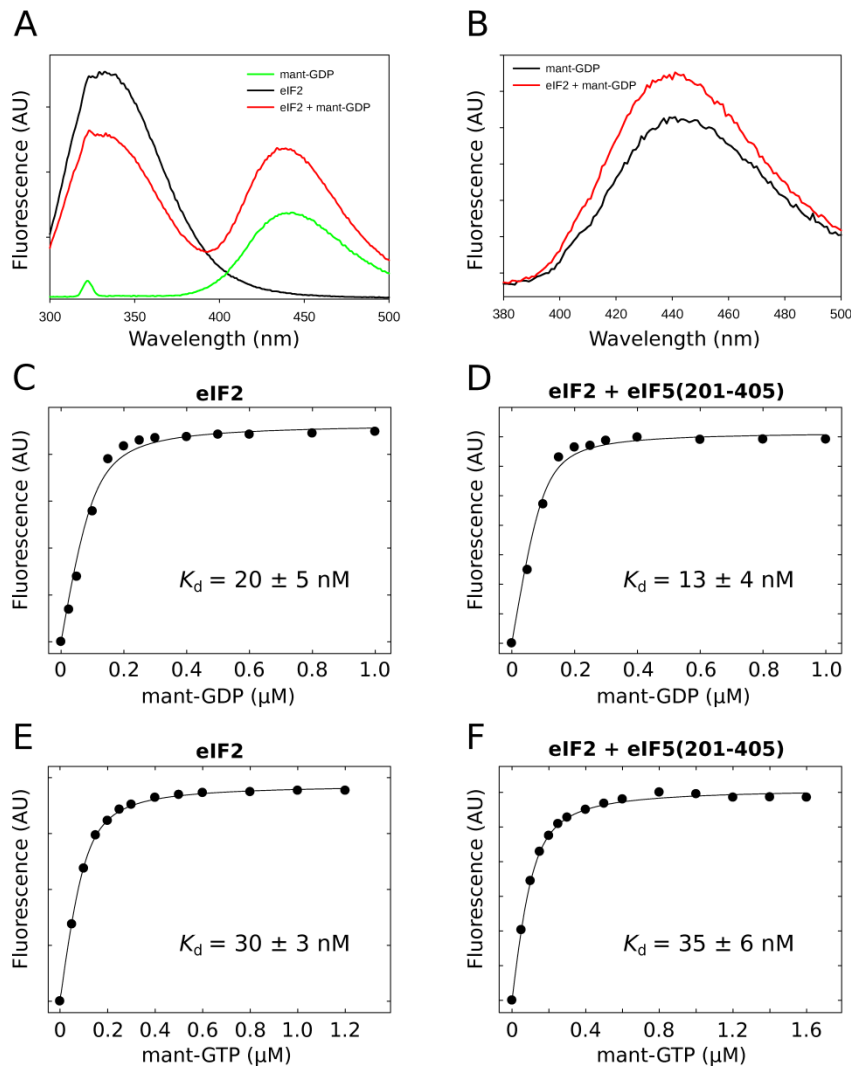


Figure 6. Fluorescence experiments for the interaction between eIF2 and mant-labeled guanine-nucleotides.

A) Emission spectra for 50 nM eIF2 (black), mant-GDP (green) and eIF2 in the presence of mant-GDP (red) upon excitation at 280 nm. **B)** Emission spectra for mant-GDP (black) and 50 nM of eIF2 in the presence of mant-GDP (red) upon direct excitation of the mant-group at a wavelength of 355 nm. **C-D)** Equilibrium titrations of 100 nM eIF2 with mant-GDP either alone (C) or in the presence of 5 mM eIF5(201-405) (D). The binding reaction was monitored by FRET between eIF2 (excited at 280 nm) and the mant-group of the nucleotide (emission monitored at 440 nm). The black line shows the fit to the data, using a quadratic one-side binding model. **E-F)** Equilibrium titrations of 100 nM eIF2 with mant-GTP alone (E) or in the presence of 5 mM eIF5(201-405) (F). K_d values are summarized in Table 4.

Equilibrium titrations of eIF2 with the mant-nucleotides give equilibrium dissociation constants (K_d) of ~ 20 and ~ 30 nM for mant-GDP and mant-GTP, respectively (Fig. 6C/E and Table 4). For mant-GDP this value is very close to that previously measured for GDP by nitrocellulose filtration (20 ± 5 nM)[97]. However, the value obtained for mant-GTP is significantly (57-fold) lower than that reported for GTP (1700 ± 1000 nM) [97]. Previous studies have shown that nucleotide binding by GTP-binding proteins, including the eIF2 γ paralog EF-Tu, is not perturbed by the mant-group [98-100]. It is therefore possible that the high value previously reported for GTP might be due to the used method of nitrocellulose filtration in combination with the relatively fast dissociation rates (k_{off}) of GTP compared to those for GDP (see below).

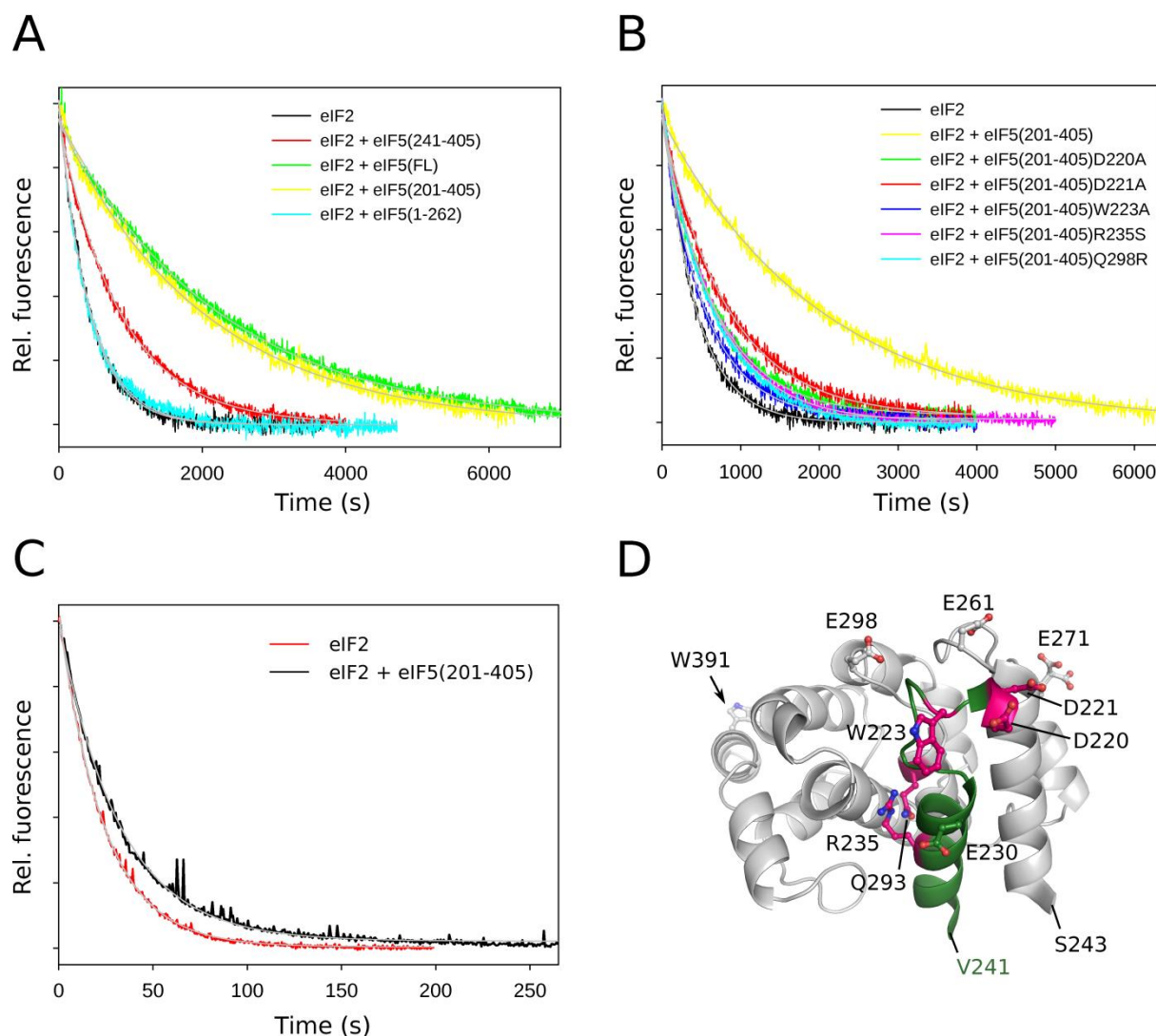


Figure 7. Influence of eIF5 on the dissociation of mant-nucleotides from eIF2. **A)** Time courses for the dissociation of mant-GDP from eIF2 (100 nM eIF2 with 125 nM mant-GDP, followed by the addition of 5 μ M unlabeled GDP) in the absence (black) or in the presence of different eIF5 constructs (5 μ M): Full-length eIF5 (green), eIF5(201-405) (yellow), eIF5(241-405) (red) and the point mutant eIF5(1-262) (cyan). The grey lines represent single-exponential fits which yielded the respective apparent rate constants k_{app} . **B)** Time courses for the dissociation of mant-GDP from eIF2 (100 nM eIF2 with 125 nM mant-GDP, followed by the addition of 5 μ M unlabeled GDP) in the absence (black) or in the presence of 5 μ M eIF5(201-405) (yellow), eIF5(241-405)D220A (green), eIF5(241-405)D221A (red), eIF5(241-405)W223A (blue), eIF5(241-405)R235S (pink) and eIF5(241-405)Q298R (cyan). **C)** Time courses for the dissociation of mant-GTP from eIF2 (100 nM eIF2 with 125 nM mant-GTP, followed by the addition of 5 μ M unlabeled GDP) in the absence (red) or in the presence (black) of eIF5(201-405) (5 μ M). **D)** Structure of the eIF5-CTD (with the DWEAR-motif in green modeled as part of the CTD as shown in Fig. 5A). Positions of point mutations used in the mant-GDP dissociation experiments are shown as sticks.

Dissociation rate constants for mant-GDP and mant-GTP were determined by chase experiments with excess of unlabeled GDP (Fig. 7). Under these conditions, every mant-nucleotide that dissociates from eIF2 is immediately replaced by GDP, while the rate of mant-nucleotide

Table 4. Influence of eIF5 constructs on the binding of mant-GDP and mant-GTP by eIF2

	Nucl.	k_{off} (min^{-1})	k_{app} (min^{-1}) ^a	k_{on} ($\text{M}^{-1} \text{min}^{-1}$) ^b	K_{d} (Nucl.) (nM) ^c	$K_{1/2}$ (eIF5) (nM) ^d
eIF2	mGDP	0.14 ± 0.05		7×10^6	20 ± 5	
	mGTP	2.32 ± 0.11		7.7×10^7	30 ± 3	
+ eIF5(FL)						
wt	mGDP	0.068 ± 0.004				
+ eIF5(201-405)						
wt	mGDP	0.06 ± 0.005	0.061 ± 0.002	4.6×10^6	13 ± 4	123 ± 28
wt	mGTP		2.0 ± 0.1	5.7×10^7	35 ± 6	
A309E	mGDP	0.064 ± 0.004				209 ± 66
K313E	mGDP	0.066 ± 0.006				640 ± 125
D220A	mGDP		0.088 ± 0.002			
D221A	mGDP		0.08 ± 0.002			
W223A	mGDP		0.112 ± 0.004			
E230A	mGDP		0.066 ± 0.002			
R235S	mGDP		0.088 ± 0.001			
E261A	mGDP		0.068 ± 0.002			
E271A	mGDP		0.073 ± 0.004			
Q293R	mGDP		0.105 ± 0.003			
E298A	mGDP		0.07 ± 0.002			
+ eIF5(216-405)						
wt	mGDP		0.06 ± 0.005			
+ eIF5(241-405)						
wt	mGDP		0.108 ± 0.006			
+ eIF5(1-262)						
wt	mGDP		0.142 ± 0.01			

^a Obtained from three independent experiments with 100 nM eIF2 in the presence of 5 μM of the respective eIF5 construct.

^b The bimolecular association constant was calculated according to the relation $k_{\text{on}} = k_{\text{off}}/K_{\text{d}}$

^c K_{d} is the equilibrium dissociation constant between eIF2 and mant-GDP or mant-GTP.

^d $K_{1/2}$ is the apparent equilibrium dissociation constant between eIF2 and the eIF5 construct, obtained from the dependency of the k_{app} of mant-GDP dissociation from eIF2 on the eIF5 concentration.

association is negligible. Thus, the rate by which the fluorescence signal decreases corresponds to the dissociation rate constant of the mant-labeled nucleotide. Single-exponential fitting of the resulting time courses gives values of 0.14 min^{-1} and 2.3 min^{-1} for mant-GDP and mant-GTP, respectively (Table 4); both values are similar to those reported previously [44, 69]. In combination with the K_{d} values obtained in equilibrium titration experiments, the obtained k_{off} values give estimates for the bimolecular association constants (k_{on}) of $7 \times 10^6 \text{ M}^{-1} \text{ min}^{-1}$ and $7.7 \times 10^7 \text{ M}^{-1} \text{ min}^{-1}$ for mant-GDP and mant-GTP, respectively. Taken together, these results show that mant-GDP and mant-GTP are suitable fluorescent guanine nucleotide derivatives to study the nucleotide binding properties of eIF2.

The eIF5-CTD interacts directly with the γ -subunit of eIF2 to stabilize the bound nucleotide.

To test the hypothesis that eIF5-CTD is directly involved in the stabilization of eIF2-bound nucleotides, we used fluorescence-based chase experiments with mant-GDP. For this purpose, eIF2·mant-GDP was mixed with excess of unlabeled GDP either in absence or presence of eIF5, and the resulting decrease of fluorescence due to mant-GDP dissociation and replacement by GDP was monitored over time (Fig. 7). In the absence of eIF5, mant-GDP dissociates from eIF2 with an off rate (k_{off}) of 0.14 min^{-1} , which is decreased more than 2-fold to 0.068 and 0.06 min^{-1} in the presence of full-length eIF5 and eIF5(201-405), respectively. At the same time, the K_d for the eIF2·mant-GDP interaction decreased nearly 2-fold to 13 nM, giving a bimolecular association constant (k_{on}) of $\sim 4.6 \times 10^6 \text{ M}^{-1} \text{ s}^{-1}$. For the construct eIF5(216-405), which lacks most of helix $\alpha 1$ but contains the DWEAR-motif and should thus retain the structural integrity of helix $\alpha 2$ in the context of the CTD, k_{off} was identical to that of the longer fragment (0.06 min^{-1}). By contrast, the construct lacking the DWEAR-motif (eIF5(241-405)) showed a significantly reduced but not completely abolished ability to stabilize mant-GDP on eIF2 ($k_{\text{off}} = 0.11 \text{ min}^{-1}$). Finally, the construct eIF5(1-262), which contains the entire N-terminal domain, linker region, DWEAR-motif, and helix $\alpha 3$ of the CTD, showed no stabilizing effect at all ($k_{\text{off}} = 0.142 \text{ min}^{-1}$). These results indicate that, although the DWEAR-motif provides a major contribution to the GDP stabilizing function of eIF5, its effect is dependent on the structural context of the CTD and, moreover, complemented by regions of the CTD that lie C-terminal to Val241 in the primary structure.

Similarly, but to a lesser degree, dissociation of mant-GTP from eIF2 is as well affected by the presence of eIF5 (Fig. 7C). The dissociation rate decreases from 2.32 min^{-1} in the absence of eIF5 to 2.0 min^{-1} in its presence. However, this is not accompanied by an increase in the overall binding affinity ($K_d = 35 \text{ nM}$), indicating that together with the decreased dissociation rate also the association rate is slightly reduced to $\sim 5.7 \times 10^7 \text{ M}^{-1} \text{ min}^{-1}$.

Next, we tested a number of single point mutations of residues lying within the DWEAR-motif (D220A, D221A, W223A, E230A, and R235S) as well as area III and adjacent regions (E261A, E271A, E298A and Q293R), introduced into eIF5(201-405). Among the DWEAR-motif mutants only D220A, D221A, W223A and R235S had a detectable negative effect on nucleotide stabilization ($k_{\text{off}} = 0.088$,

0.8, 0.112 and 0.088 min⁻¹, respectively). E261A and E298A in area III showed very slight effects ($k_{\text{off}} = 0.068$ and 0.071 min⁻¹, respectively). Q293R exhibited a strong negative effect on the ability of the eIF5-CTD construct to stabilize mant-GDP on eIF2 ($k_{\text{off}} = 0.105$ min⁻¹), comparable to W223A. The importance of this observation lies in the fact that Gln293 lies within the hydrophobic pocket that is proposed to accommodate helix $\alpha 2$ (Fig. 5A and 7D). An arginine in this position would necessarily prevent the association of the DWEAR-motif and its placement next to area III due to sterical repulsion, resulting in the loss of the contribution by the DWEAR-motif. Consistently, Q293R shows only a residual activity corresponding to that of the eIF5(241-405) construct without the DWEAR-motif. Trp-quenching and pull-down experiments with the Q293R mutant and the eIF2 β -NTT show that it retains its ability to bind eIF2 β -NTT and therefore seems to be correctly folded in the region C-terminal to Val241 (Fig. S5). It should be noted however that the dissociation rates for all eIF5-CTD point mutants represent only apparent rate constants, obtained at only one eIF5 concentration (5 mM) at which eIF2 is saturated with eIF5(201-405). Thus, the observed effects for some mutants possibly reflect only a reduction in the affinity of eIF5 to eIF2 and not necessarily a direct involvement of the respective residues in the stabilization of the nucleotide.

The next question was whether the eIF5-CTD, including the associated DWEAR-motif, mediates the stabilization of eIF2-bound nucleotides indirectly or through a direct contact to the γ -subunit. For RhoGDIs it is known that the stabilization of the nucleotide is achieved through the formation of direct contacts to the area surrounding the nucleotide binding pocket of the G domain [101]. For eIF5-CTD or the DWEAR-motif, however, no such direct interaction to the eIF2 γ -subunit has so far been demonstrated, most likely due to the transient character of the contacts mediating GDP stabilization. To assess the spatial arrangement of eIF5-CTD relative to eIF2 in the eIF2·eIF5 complex, we performed UV-crosslinking experiments using various eIF5(201-405)Bpa constructs (see above). Among the DWEAR-motif constructs particularly D221Bpa, W223Bpa and A234Bpa were found to form distinct crosslink bands migrating above the 100 kDa marker, which, according to MS analysis, represent specific crosslinks to the γ -subunit of eIF2 (Fig. 8A). Finally, D220Bpa and E238Bpa as well form crosslinks to eIF2 γ , but with significantly reduced efficiency. Importantly, E261Bpa in area III as well produces a strong and distinct crosslink band with the γ -subunit that is comparable to those obtained for positions 221, 223 and 234, supporting the idea

that the DWEAR-motif and area III form a combined surface area (in the following called area III^{ext} for extended area III; see Fig. S4B) for their interaction with eIF2 γ . A number of additional weak bands migrating at an apparent molecular weight of 130 kDa suggest conformational heterogeneity for this position in the eIF2·eIF5-CTD complex (it should be noted here that all the crosslink-products elute from an analytical size exclusion column at the same volume as the uncrosslinked eIF2·eIF5-CTD complex, thus indicating that the change in migration speed on the SDS-PAGE is most likely due to differences in the topology of the denatured crosslinked peptides (e.g. the crosslink occurred either at the end or the center of the target-chain) rather than an actual higher molecular weight). The only position that was found to form specific crosslinks to eIF2 β and not to the γ -subunit was V270Bpa, which produced bands migrating only slightly above that of uncrosslinked eIF2 γ (Fig. 8D, lanes 7-9). This is in good agreement with the crystal structure of the eIF5-CTD·eIF2 β -NTT complex (Fig. 8E) and is further validated by UV-crosslink experiments with eIF2 β (1-106) alone, which show a strong crosslink only from position V270Bpa (Fig. 10B/D).

Using ESI-MS/MS analysis in an Orbitrap mass spectrometer, followed by an analysis of the obtained data with the StavroX software [102], we were able to identify potential target peptides for the crosslinks from positions W223Bpa, A234Bpa, E238Bpa and E261Bpa (Table 5). Several of the linkage sites were identified more than once (e.g. ⁵⁰⁸HWR⁵¹⁰ from position Trp223 or ⁴⁰⁹ADRLV⁴¹³ from positions Ala234 and Glu238), which increases the probability that the assignment of the crosslinked peptides is correct. According to a homology model of eIF2 γ , based on the structure of aIF2 γ from the archaeon *S. solfataricus*, all the identified linkage sites lie in the frontal face of eIF2 γ in domains II and III and in the vicinity of switch 1 and switch 2 of the G domain (Fig. 13A). In line with their spatial proximity in helix α 1 of eIF5(201-405), positions A234Bpa and E238Bpa were found to crosslink predominantly to the same target peptide (⁴⁰⁹ADRLV⁴¹³), which lies at the bottom of the domain II β -barrel in the eIF2 γ homology model, directly below switch 1. The immediately preceding peptide ⁴⁰⁴PTLCR⁴⁰⁸, with Arg408 as likely linkage site, was identified as additional target only for E238Bpa. For W223Bpa and E261Bpa on the other hand, the target sites were found to lie in domain III and in direct vicinity to the switch 2 region, with ⁵⁰⁸HWR⁵¹⁰, the main target for W223Bpa, in the last β -hairpin loop, and ⁴⁴⁴KTD⁴⁴⁶, the identified target for E261Bpa in the extended first β -hairpin loop of domain III.

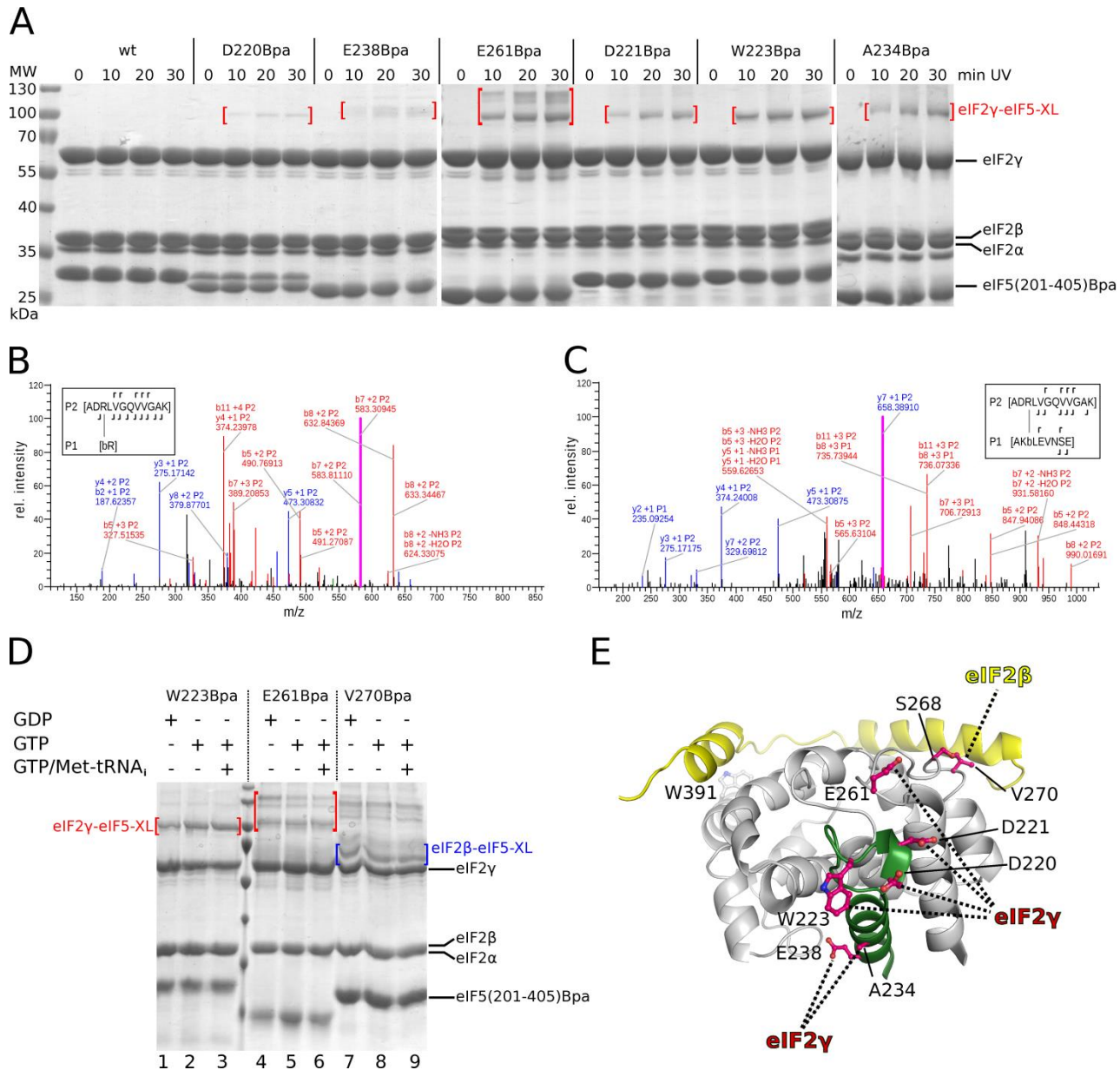


Figure 8. Mapping of the direct interactions between the eIF5-CTD and eIF2γ. **A)** Coomassie stained SDS-gels showing the UV- and time-dependent formation of crosslinks between eIF2γ and the indicated eIF5(201-405)Bpa constructs (crosslink bands are indicated by red brackets). For each experiment, 2 μM eIF2 was mixed with 3 μM GDP and 5 μM eIF5(201-405)Bpa. **B-C)** High-resolution MS2 fragmentation spectra for the crosslinks of A234Bpa (B) and E238Bpa (C) to their target peptide in eIF2γ. A series of b and y product ions were detectable for the peptides involved in the crosslinks; the relative intensity of the observed peaks is plotted against their mass-to-charge ratio (m/z). The inset shows the observed product ions mapped to the sequences of the crosslinked peptides; b stands for Bpa. **D)** SDS-gels showing formation of crosslinks between eIF2 (2 μM) and the indicated eIF5(201-405)Bpa constructs (5 μM) in the presence of 3 μM GDP, 3 μM GTP or 3 μM GTP and 3 μM Met-tRNA_i (crosslink bands are indicated by brackets). **E)** Structure of the eIF5-CTD (with the DWEAR-motif in green modeled as part of the CTD as shown in Fig. 5A) in complex with the eIF2β-NTT (yellow), indicating the positions where Bpa was introduced (residues shown as sticks). The dashed lines indicate the crosslinks to eIF2 formed from the respective positions.

Taken together, these results provide evidence for a direct interaction between the eIF5-CTD and the γ -subunit close to the nucleotide binding pocket in the free eIF2·eIF5 complex. Within eIF5-CTD, this interaction seems to be mediated by a continuous binding interface composed of area III and the associated DWEAR-motif (forming area III^{ext}) that is required for the full nucleotide stabilizing effect on eIF2.

Table 5. Crosslinks between eIF5(201-405)Bpa and eIF2 γ .

Construct	Crosslinked peptides					
	Bpa peptide	Target peptide	Site	Mass (Da)	Error (ppm)	m/z
W223Bpa	DE <u>b</u> AVDMSE	<u>VR</u> KLEPNE	453-454	2111.9518	-2.9	704.65527
	<u>b</u> AVD	K <u>H</u> WRLIGWATIKK	509-510	2063.1183	-2.0	688.37726
	VKDDE <u>b</u> AVD	IE <u>K</u> HWR	507-510	2008.9739	-1.1	670.33099
	<u>b</u> AVD	K <u>H</u> WRLIGWATIK	509-512	1935.0238	-2.0	645.67914
A234Bpa	<u>b</u> R	AD <u>R</u> LVGQVVGAK	411, 413	1637.9127	0.3	410.23355
	<u>b</u> R	AD <u>R</u> LVGQVVGAK	411-413	1637.9132	0.6	546.276
	<u>b</u> R	AD <u>R</u> LVGQVVGAK	411	1619.9042	1.6	540.63959
E238Bpa	AK <u>b</u> LE	AD <u>R</u> LVGQVVGAK	411-413	1923.0703	0.2	641.69495
	AK <u>b</u> LEVSNE	AD <u>R</u> LVGQVVGAK	409-412	2352.2558	0.0	588.82007
	AK <u>b</u> LEVSNE	AD <u>R</u> LVGQVVGAK	411-412	2352.2569	0.5	784.75824
	<u>b</u> LEVSNE	AD <u>R</u> LVGQVVGAK	411-413	2153.1235	-0.1	539.03632
	<u>b</u> LEVSNE	AD <u>R</u> LVGQVVGAK	409-411	2153.1275	1.8	718.38037
	<u>b</u> LE	PT <u>L</u> CR	408	1139.5551	-0.3	570.28119
	<u>b</u> LE	VD <u>P</u> TLCR	408	1296.6265	-2.2	432.88034
E261Bpa	QAG <u>b</u> DKENLPSD	RL <u>L</u> GVKTD <u>G</u> QK	447	2638.3460	-0.4	880.12018
	WILEQAG <u>b</u> DKE	LL <u>G</u> VKTD	444-446	2184.1241	0.8	728.71289

The likely target positions in the target peptides are underlined.

Potential involvement of helix $\alpha^{\text{C}\beta}$ in the eIF2 β -NTT in the pre-organization of the eIF5-CTD relative to eIF2 γ

According to the above results, eIF5-CTD provides two distinct contact surfaces for the heterotrimeric eIF2 complex in solution: On the one hand, the acidic area III^{ext} provides the interface for direct interactions with the γ -subunit. On the other hand, the acidic area I is responsible for high affinity interactions with the eIF2 β -NTT and thus for the efficient recruitment of eIF5 to eIF2. Due to the apparently weak character of the direct contacts between eIF5-CTD and

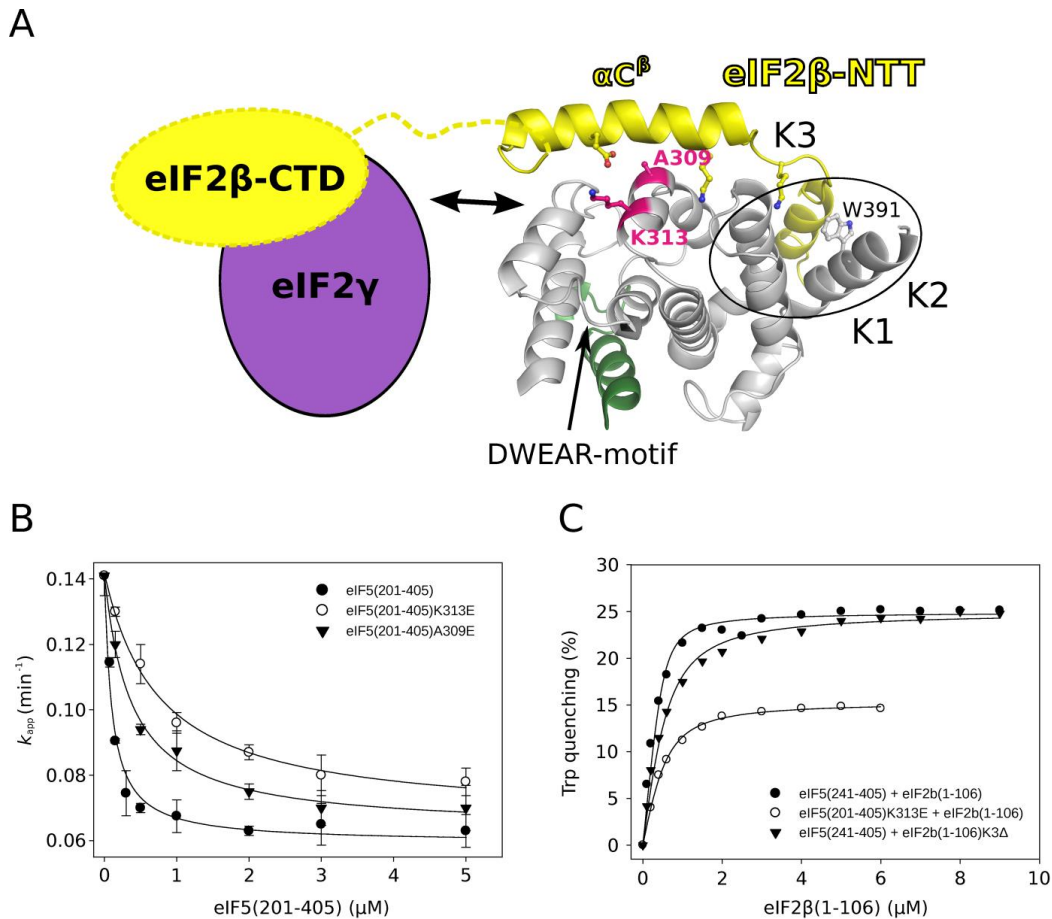


Figure 9. Role of helix αC^{β} in eIF2 β -NTT in the pre-organization of the eIF5-CTD relative to eIF2 γ . **A)** Structure of the eIF5-CTD (the DWEAR-motif (green) is modeled as in Fig. 5A in complex with the eIF2 β -NTT (yellow). The black circle indicates area I of the eIF5-CTD, which forms the contact site for K-boxes 1-3 of eIF2 β . Helix αC^{β} points away from area I, ending atop of repeat R_1 and next to area III^{ext}, which contains residues involved in the interactions with eIF2 γ (see Fig. 8). eIF2 γ and the associated eIF2 β -CTD are shown schematically; the linker between eIF2 β -CTD and eIF2 β -NTT is shown as yellow dashed line. The double arrow indicates the direct interaction between eIF5 and eIF2 γ , which might be promoted by the directionality provided by helix αC^{β} . Ala309 and Lys313 in eIF5 are indicated in pink. **B)** Dependency of k_{app} for dissociation of mant-GDP from eIF2 on the concentration of eIF5(201-405) (closed circles), eIF5(201-405)A309E (closed triangles) and eIF5(201-405)K313E (open circles). Standard deviations, obtained from two independent experiments, are given as error bars. **C)** Equilibrium titrations of 0.5 μ M eIF5(241-405) with increasing amounts of wild-type eIF2 β (1-106) (closed circles) or the K-box mutant K3 Δ (closed triangles) and of 0.5 μ M eIF5(201-405)K313E with wild-type eIF2 β (1-106) (open circles). The Trp quenching signal was plotted against the concentration of the eIF2 β -NTT constructs. The K_d of the eIF5(201-405)K313E-eIF2 β (1-106) complex is 212 ± 30 nM and thus similar to that of the eIF5(241-405)-eIF2 β (1-106)K3 Δ complex (200 nM) and ~ 3 -fold reduced compared to the eIF5(201-405)K313E-eIF2 β (1-106) complex (70 nM). It should be noted that the quenching signal for the eIF5(201-405)K313E-eIF2 β (1-106) complex is reduced compared to the complexes with eIF5(241-405) due to the presence of one additional Trp residue (Trp223) in eIF5(201-405).

eIF2 γ we asked whether the eIF2 β -NTT might indirectly promote these interactions by pre-arranging the eIF5-CTD relative to the rest of eIF2 in addition to its role as a high affinity anchor

point for eIF2. As indicated by the crystal structure of the eIF5-CTD·eIF2 β -NTT complex, this could involve helix αC^{β} , which in full-length eIF2 β is followed by the eIF2 γ -bound eIF2 β -CTD and could thus induce an orientation of eIF5-CTD relative to the γ -subunit that is favorable for their direct contact (Fig. 9A). For this purpose we purified two eIF5(201-405) constructs in which either A309 or K313 were exchanged against glutamate, thereby disrupting the interface for αC^{β} either by sterical or electrostatic repulsion (K313 forms a salt bridge to D114 in αC^{β} ; Fig. 9A and 4). These mutants were then tested for their ability to stabilize mant-GDP on eIF2. Neither of the mutants had a severe negative impact on the GDP-stabilizing effect of the eIF5-CTD, with off rates of 0.065 min⁻¹ and 0.068 min⁻¹ for A309E and K313E, respectively, compared to 0.06 min⁻¹ for the wild-type (Fig. 9B and Table 4). However, the concentration of the respective construct that was necessary to achieve the half maximal stabilizing effect increased relative to the wild-type construct ($K_{1/2}$ = 123 nM) by ~2- and 5-fold for A309E ($K_{1/2}$ = 209 nM) and K313E ($K_{1/2}$ = 640 nM), respectively, indicative of a reduced affinity to eIF2 γ . Trp-quenching experiments showed nearly wild-type affinities of the K313E mutant for eIF2 β (1-106) (Fig. 9C and Table 1), in line with its relative distance from the main interface for K-box binding in surface area I in the crystal structure. Thus, under the assumption that eIF5 interacts with the isolated eIF2 β -NTT in the same way as in the heterotrimeric eIF2 complex, which was supported by the Bpa crosslinking experiments from position Val270, these results indicate that these mutants increase the k_{off}/k_{on} ratio in the direct interface between eIF5-CTD and eIF2 γ , which could be explained by a reduced ability of helix αC^{β} in eIF2 β to pre-arrange eIF5-CTD relative to the γ -subunit.

Interactions between eIF5-CTD, eIF2 β -NTT, eIF1 and eIF3c-NTD

Previous biochemical and genetic studies have identified the C-terminal domain of eIF5 as one of the key components in eukaryal translation initiation as versatile interaction partner for other initiation factors. In recent years particularly the dynamic interplay of the eIF5-CTD with eIF1 and eIF2 came into focus as it was proposed to be pivotal for the fidelity of start codon selection and P_i release from eIF2 [21, 57, 63, 103]. However, the exact nature of the structural rearrangements that are thought to occur between these factors upon the encounter of the AUG start codon have remained controversial, in part due to incomplete or even contradictory data concerning their

relative arrangement on the surface of eIF5-CTD. In light of our data on the interactions of eIF5-CTD with eIF2 β and eIF2 γ , we therefore tried to gain further insight into its interactions with eIF1 and the N-terminal domain of eIF3c. For this purpose we used Bpa incorporated into specific positions of eIF1 or eIF5 by genetic code expansion, to detect spatial proximity by UV-induced crosslinking and subsequent MS analysis.

First, we tested different eIF5(201-405)Bpa constructs for their ability to form crosslinks to eIF1, eIF2 β (1-106) or eIF3c(1-136), respectively (Fig. 10). Bpa incorporated into positions Asp220, Asp221 and Trp223 of the DWEAR-motif showed nearly no crosslinking at all (Fig. 10A-C, lanes 1-4). By contrast, the other Bpa-constructs (Glu238, Glu261, Ser268 and Val270) showed clear UV- and time-dependent crosslink bands for eIF1, eIF2 β -NTT as well as eIF3c-NTD, however, with significant differences in the efficiency (Fig. 10A-C, lanes 5-8). For eIF1 the strongest bands were obtained from positions Glu238 and Val270 (Fig. 10A, lanes 5 and 8, respectively), while slightly weaker bands were observed for Glu261 and Ser268 (Fig. 10A, lanes 6 and 7, respectively). In line with the crystal structure, the eIF2 β -NTT crosslinked efficiently to S268- and V270Bpa (Fig. 10B, lanes 7 and 8, respectively), whereas E238- and E261Bpa showed significantly weaker bands in comparison (Fig. 10B, lanes 5 and 6, respectively). The opposite tendency was observed for eIF3c-NTD, with the strongest crosslink occurring from position Glu238, followed by Glu261 and Val270 and virtually no crosslink from S268 (Fig. 10C, lanes 5, 6, 8, and 7, respectively). These data result in the following main conclusions:

i) E238Bpa lies close to a common binding site for eIF1 and eIF3c-NTD. The internal crosslinks (see above) suggest a position for E238Bpa close to the C-terminus of helix α 8 and the loop preceding helix α 11. This would suggest the conserved basic surface area II as most likely candidate for the interactions with eIF1 and eIF3c-NTD, in line with previous reports that identified this region as primary interface for both factors [57, 104] (e.g. the H336Q-K337Q double mutant in eIF5 was found to reduce binding to eIF3c and eIF1 [57] and the same dipeptide is found in one of the identified target peptides (³³¹FLGLEHK³³⁷) for E238Bpa (Table 3)).

ii) eIF1 not only binds to area II close to Glu238 but is also able to interact with a second interface in direct vicinity to Val270 on the opposite side of eIF5-CTD. This would suggest overlapping interaction interfaces for eIF1 and eIF2 β in this region as proposed by Luna *et al.*[63].

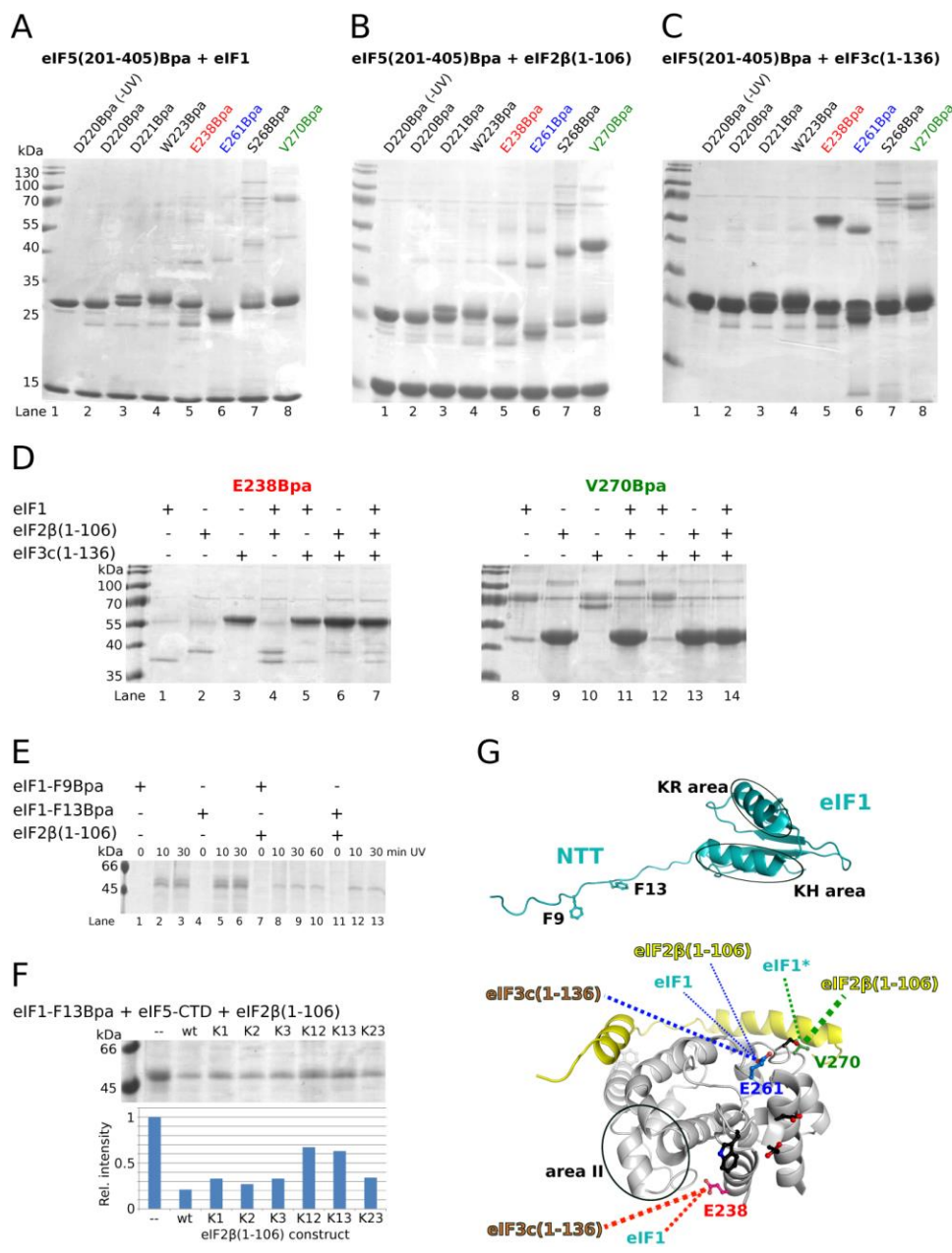


Figure 10. Mapping of the interactions between eIF5-CTD, eIF2β-NTT, eIF1 and eIF3c-NTD by crosslinking. **A-C)** SDS-gels showing the UV-dependent formation of crosslinks for the complexes between different eIF5(201-405)Bpa constructs (Bpa positions indicated above each lane) and eIF1 (A), eIF2β(1-106) (B) and eIF3c(1-136) (C). In all cases (except the -UV samples), samples were exposed to UV light for 30 min on ice.

D) Dependency of the crosslink patterns from positions Glu238 and Val270 in eIF5(201-405) on the composition of the formed complexes.

E) UV- and time dependent formation of crosslinks between eIF1Bpa (with Bpa in positions Phe9 and Phe13) and eIF5(201-405) in the absence (lanes 1-6) or presence of the eIF2β-NTT (lanes 7-13).

F) Influence of K-box mutations on the ability of the eIF2β-NTT to reduce crosslinking between eIF1-F13Bpa and eIF5(201-405). The relative intensities of the crosslink bands were determined using ImageJ.

G) Structures of eIF1 (cyan;

PDB: 2OGH) and the eIF5-CTD (the DWEAR-motif (green) is modeled as in Fig. 5A) in complex with the eIF2β-NTT (yellow), indicating the positions where Bpa was introduced (as sticks). In eIF5, Asp220, Asp221, Trp223 and Ser268 are shown in black; Glu238, Glu261 and Val270 are shown in red, blue and green, respectively. Dashed lines indicate the crosslinks between the components of the minimal MFC formed from the respective positions; the thickness of the dashed lines roughly corresponds to the relative intensity of the crosslink bands shown in A-D. Black circles indicate known interaction surfaces on eIF5 and eIF1: area II on eIF5 was proposed to interact with eIF1 and eIF3c; the KR area on eIF1 interacts with eIF3c and the ribosome; the KH area of eIF1 was shown to interact with the eIF5-CTD and/or with the eIF2β-NTT [55, 57, 104]. The asterisk marks a crosslink that is not formed in the presence of the eIF2β-NTT.

iii) Although all three factors seem to have preferred regions for their interactions with eIF5-CTD, the crosslink data indicate significant overlaps between the contact surfaces in the respective

binary complexes. This necessarily raises the question whether the interactions in these regions can occur simultaneously or are mutually exclusive.

In order to address this question, we repeated the UV-crosslinking experiments, this time forming the respective ternary and quaternary complexes of eIF5(201-405)E238Bpa or -V270Bpa with eIF1, eIF2 β -NTT and/or eIF3c-NTD. Interestingly, diametrically opposite effects were observed for the two tested positions: In case of E238Bpa the simultaneous addition of eIF1 and eIF2 β -NTT, each in 2-fold molar excess over eIF5(201-405)Bpa, increased the crosslinking efficiency to both proteins ~2-fold relative to their respective binary complexes (Fig. 10D, compare lanes 1, 2 and 4). The addition of eIF3c-NTD (equimolar to eIF1) resulted in a significant loss in band intensity for eIF1 as well as eIF2 β ; this negative effect could be slightly but reproducibly compensated in the complexes containing all four components (Fig. 10D, compare lanes 5-7). In stark contrast to these observations, the addition of eIF2 β -NTT to the V270Bpa construct completely abolished any crosslinks to eIF1 or eIF3c-NTD (Fig. 10D, compare lanes 8, 10 and 14), while eIF1 in turn was able to partially suppress the crosslinks to eIF3c-NTD in the eIF5(201-405)Bpa·eIF1·eIF3c-NTD complex (Fig. 10D, compare lanes 8, 10 and 12).

To further test these results, we then introduced Bpa into eIF1 in positions Phe9 and Phe12 of the flexible N-terminal tail (NTT) (Fig. 10G). Both constructs allowed specific crosslinks to eIF5(201-405), with two bands emerging in a UV- and time-dependent manner, migrating close together at ~50 kDa (Fig. 10E, lanes 1-6). The addition of eIF2 β -NTT in 2-fold molar excess over eIF1 caused a significant reduction of both eIF5-CTD·eIF1Bpa crosslinks (Fig. 10E, compare lanes 3 and 6 with lanes 9 and 13). Interestingly, this negative effect of the eIF2 β -NTT on the crosslink efficiency was particularly severe on the upper band which completely disappeared in the ternary complexes. The same experiments in the presence of the single and double K-box mutants of the eIF2 β -NTT showed a clear correlation between their respective affinity to eIF5-CTD and their ability to reduce the crosslink efficiency between eIF1Bpa and eIF5 (Fig. 10F and 2). These observations indicate that the two bands originate from two alternative positions or orientations of eIF1 on the surface of eIF5-CTD with the upper band formed in an interaction that is incompatible with the presence of eIF2 β , while the lower band is formed in an interaction which is not completely abrogated by eIF2 β . It can therefore be speculated that these two interfaces between eIF1 and

EIF5-CTD are the same as those that result in the crosslinks from V270Bpa and E238Bpa to eIF1, respectively.

In combination with the tryptophan quenching and structural data, these observations support a model in which the respective interfaces for the interactions of eIF5-CTD with other initiation factors change significantly depending on the composition of the complex. Particularly interesting is the case of eIF1, for which the crosslink data indicate two distant binding sites on eIF5-CTD. The first binding site (interface I) lies close to Val270 and is completely abrogated by the binding of eIF2 β -NTT, presumably due to an overlap between both binding sites (Fig. 10G). According to Luna *et al.* [63] this interaction is independent of the eIF1-NTT. Thus, eIF1 seems to interact with interface I through its globular core domain, most likely involving residues within the so-called KH area and surrounding Gly97 [63, 104]. The second binding site (interface II) lies close to Glu238 and thus most likely involves the positively charged area II. This binding site is shared with eIF3c-NTD and in stark contrast to interface I this contact is not only compatible with but even slightly strengthened by the presence of the eIF2 β -NTT (Fig. 10D, lane 4). The eIF1-NTT, which is dispensable for the interaction with interface I [63], was shown to be required for the cooperative binding of eIF1 and eIF2 β to eIF5-CTD and assembly of the MFC [55, 104]. This would suggest that the eIF1-NTT, rich in acidic and aromatic side chains, is responsible for the interaction with eIF5-CTD in the positively charged area II (interface II), where it binds simultaneous and in close proximity (or even in direct contact) to eIF3c-NTD. This placement of eIF1-NTT and eIF3c-NTD is, moreover, in good agreement with the crystal structure of eIF2 β (66-106) bound to eIF5-CTD, in which the N-terminus of the former lies directly above area II and thereby in a suitable position to contact both factors through the linker-region between K2 and K3 (Fig. 4A and 10G). Thus, within the eIF5-CTD·eIF2 β -NTT·eIF1·eIF3c-NTD complex, the minimal MFC core, eIF1 would remain directly associated with eIF5-CTD area II only through its NTT. At the same time, the C-terminal domain of eIF1 could remain associated with eIF3c-NTD through the 'KR area' in the N-terminal α -helix, and the KH area of eIF1, after its displacement from eIF5-CTD by the eIF2 β -NTT, would become available for direct interactions with the eIF2 β -NTT itself [104]. Considering the significantly higher affinity of the eIF2 β -NTT for area I compared to that of eIF1, it is conceivable

Chapter 2

that the above described interaction network represents the state in which the four initiation factors are organized in the MFC when it joins the 40S subunit.

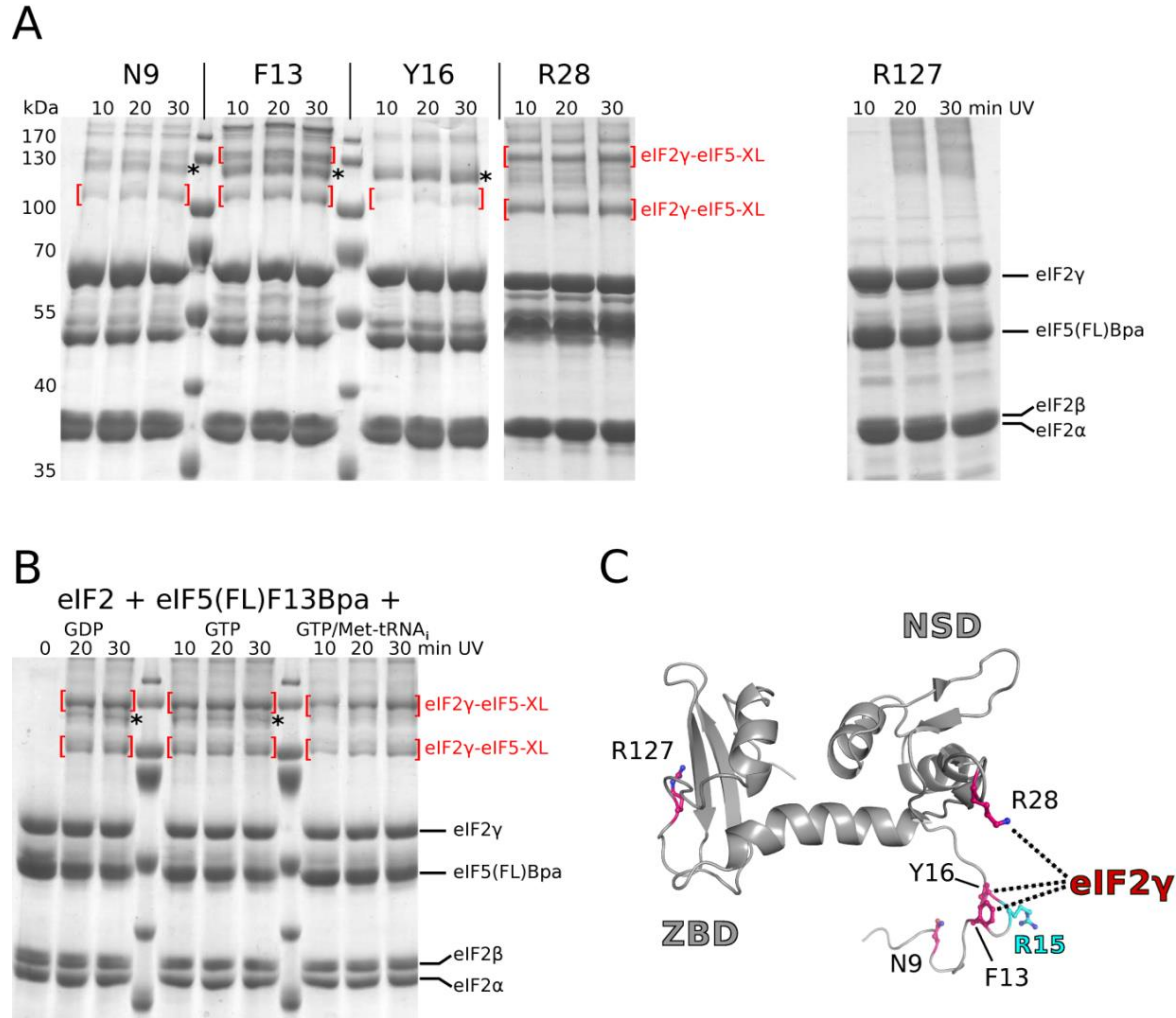


Figure 11. Mapping of the interactions between eIF5-NTD and eIF2 by Bpa crosslinking. **A)** SDS-gels showing the UV-dependent formation of crosslink bands between 5 μ M of the different eIF5(FL)Bpa constructs and 2 μ M eIF2. Crosslinks to eIF2 γ are indicated by red brackets; the strong crosslink bands for positions Asn9, Phe13 and Tyr16 directly below the 130 kDa marker (marked with *) also occur in the absence of eIF2 and are thus likely to originate from a crosslink between two eIF5 molecules. **B)** SDS-gel showing the UV- and time-dependent formation of crosslink bands between eIF2 and eIF5(FL)F13Bpa in the presence of 3 μ M GDP, 3 μ M GTP or 3 μ M GTP/Met-tRNA_i (crosslink bands are indicated by red brackets). **C)** Solution structure of the eIF5-NTD from *H. sapiens* (PDB: 2G2K) indicating the positions where Bpa was introduced in the yeast homolog (residues shown as pink sticks). Arg15 (cyan) in the flexible N-terminal tail corresponds to the putative catalytic arginine-finger [52, 53]. Dashed lines indicate crosslinks to eIF2 γ . The eIF5-NTD is structurally subdivided into N-terminal subdomain (NSD) and the C-terminal zinc binding domain (ZBD).

eIF5-NTD and eIF5-CTD interact with eIF2 γ in the eIF2·GTP·Met-tRNA_i ternary complex

Up to this point all interaction studies were carried out in the absence of Met-tRNA_i. It is therefore unclear, whether the direct contact between eIF5-CTD and eIF2 γ would persist in the presence of the charged initiator tRNA and in the context of the eIF2·GTP·Met-tRNA_i ternary complex. The UV-crosslinking experiments with Bpa constructs of the eIF5-CTD were therefore repeated, this time in the presence of a 2-fold molar excess of Met-tRNA_i over eIF2, equimolar to the Bpa construct. As shown in Figure 8D, the crosslink efficiency for the tested constructs with Bpa in positions Trp223, Glu261 or Val270 remained virtually unchanged upon the addition of the initiator tRNA. This suggests that the underlying direct interactions of eIF5-CTD to the eIF2 γ -subunit and to eIF2 β exist in the complex with free eIF2, as well as with the ternary complex of eIF2·GTP with the Met-tRNA_i.

Next, we studied whether it would also be possible to detect direct interactions between the eIF5-NTD and eIF2 in solution using UV-inducible crosslinking. For this purpose, Bpa was introduced into various positions of the NTD in full-length eIF5. In the flexible N-terminal extension, the Bpa moiety was introduced in positions Asn9, Phe13 and Tyr16 and thus in direct vicinity to Arg15, the potential arginine-finger of eIF5 (Fig. 11C). Moreover, Bpa was introduced in lieu of Arg28 in the first hairpin loop of the N-terminal β -sheet, and Arg127 next to the zinc-finger motif. Among the three N-terminal positions N9Bpa and Y15Bpa resulted only in faint crosslink bands (Fig. 11A), the strongest of which (at ~120 kDa) occurred even in the absence of eIF2 and thus most likely represents a crosslink between two eIF5 molecules. Although the same band also occurred with F13Bpa, here two additional strong crosslink bands emerged at ~100 and ~140 kDa in a UV- and time-dependent manner only in the presence of eIF2 (Fig. 11A). A similar crosslink pattern was observed for R28Bpa, while no clear eIF2-dependent crosslinks could be obtained for position R127Bpa. MS-analysis of the crosslink bands from F13Bpa and R28Bpa revealed that both positions crosslink specifically to eIF2 γ within the eIF2 complex. However, it was so far not possible to identify any target peptides of the crosslink. As the weaker crosslink bands were not analyzed by mass spectrometry, it cannot be ruled out at present that some of them are due to crosslinks to either the α - or β -subunit. Moreover, it should be noted that none of the eIF5-NTD-Bpa constructs were so far tested for their ability to stimulate GTP hydrolysis on eIF2 on the ribosome; it is therefore currently not clear in how far Bpa in the various positions affects the interactions

between eIF5 and eIF2. Nonetheless, the presented results indicate that the eIF5-NTD within the eIF2·eIF5 complex is positioned relative to eIF2 in a way that favors specific crosslinks to the γ -subunit particularly from the N-terminal subdomain (Fig. 11C).

Interestingly, the addition of Met-tRNA_i apparently causes slightly reduced crosslinking efficiency from F13Bpa, which, however, seems to be accompanied by an increase in specificity for the two main crosslinks to eIF2 γ (Fig. 11B). Thus, it seems that the spatial proximity between eIF5-NTD and eIF2 γ persists in the ternary complex. This proximity however was not found to depend strongly on the nucleotide state of eIF2 (except in the case of the increased specificity with the TC), with only slight increases in crosslinking efficiency for F13Bpa and R28Bpa when GTP was present. Moreover, the crosslinks were not affected by the presence of GDP and fluoroaluminates (Fig. S6). This observation is in line with the absence of any additional fluorescence signal due to the addition of AlF_x to the eIF2·mant-GDP·eIF5 complex, and in line with the assumption that the Arg15 of eIF5 requires the structural context of the scanning 43S pre-IC to perform its role.

The eIF5-CTD competes with eIF2B ϵ -CTD for the interaction interface on eIF2 γ .

Previous studies revealed a high degree of structural homology between eIF5-CTD and the C-terminal domain of eIF2B ϵ (residues 524-712), which forms the minimal catalytically active domain of the guanine nucleotide exchange factor eIF2B [1, 54, 74]. Mutational and biochemical studies demonstrated that this GEF activity is mediated by residues within the first two α -helices (repeat R_i) of the eIF2B ϵ -CTD, whose mutagenesis directly affects its interactions to eIF2 γ . In light of our own data, this indicates that eIF2B ϵ -CTD and eIF5-CTD contact eIF2 γ through structurally corresponding regions in R_i and R_i/area III, respectively. It is therefore conceivable that both domains interact with a common interface on the eIF2 γ -subunit (between G domain, domain II and domain III, close to the nucleotide binding pocket) to mediate either the stabilization (eIF5) or the destabilization (eIF2B ϵ) of the bound nucleotide. It has recently been proposed that eIF2B γ , the second catalytically relevant subunit within the eIF2B complex, acts as a GDI displacement factor (GDF) that promotes the release of eIF5. This role of eIF2B γ was proposed to be necessary to allow productive binding of eIF2B ϵ , which on its own was unable to compete efficiently with eIF5 for interactions with eIF2 [105]. This raises the question whether the DWEAR-motif in eIF5-CTD and its

direct contact to eIF2 γ is required for the efficient competition with eIF2B ϵ for their common substrate, which in turn would indicate that the role of eIF2B γ as GDF is to force the eIF5-CTD out of its direct interaction with eIF2 γ .

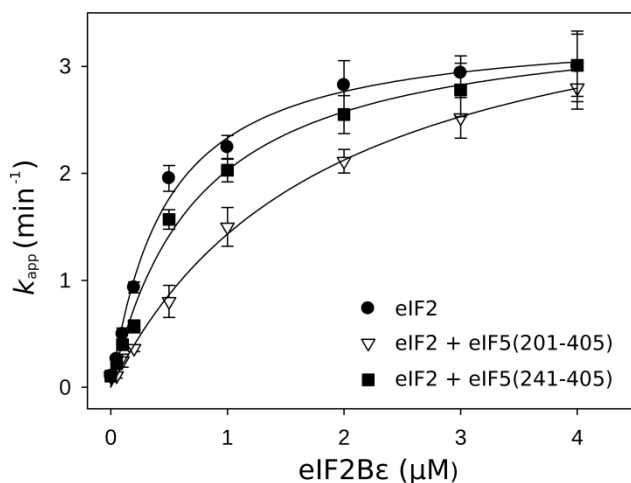


Figure 12. The DWEAR motif in the eIF5-CTD is required for efficient competition with eIF2B ϵ -CTD for their common substrate eIF2. The plot shows the dependency of k_{app} values for the dissociation of the eIF2-mant-GDP complex (100 nM eIF2 with 125 nM mant-GDP) on the concentration of the catalytic eIF2B ϵ -CTD either in the absence of eIF5 (closed circles), in the presence of 100 nM eIF5(241-405) (closed square) or in the presence of 100 nM eIF5(201-405) (open triangle). eIF2B ϵ -CTD and unlabeled GDP (5 μM) were added simultaneously to the mixtures of eIF2-mant-GDP and eIF5-CTD. Standard deviations from two independent experiments are given as error bars.

In order to assess this question, the ability of full-length eIF2B ϵ or eIF2B ϵ (524-712) to compete either with eIF5(201-405) or eIF5(241-405) for the interaction with eIF2 was studied under steady-state conditions by monitoring the dissociation of mant-GDP from preformed eIF2-eIF5 complex (eIF5 was added equimolar to eIF2) and increasing amounts of GEF. Both eIF5 constructs interact identically with the eIF2 β -NTT and should therefore be able to compete equally well with eIF2B ϵ for this interaction. However, only eIF5(201-405) contains the DWEAR-motif and therefore the entire interface required to interact with eIF2 γ . Thus, if the above made assumption is correct, eIF5(201-405) should be more efficient than eIF5(241-405) in preventing eIF2B ϵ to promote mant-GDP release. As shown in Figure 12, this is indeed the case. While eIF5(201-405) efficiently prevents the binding of eIF2B ϵ and reduces the apparent K_d ($K_{1/2}$) between eIF2B ϵ and eIF2-mant-GDP nearly 5-fold to 1920 ± 350 nM, eIF5(241-405) is significantly less efficient with an only 2-fold reduction ($K_{1/2}$ of 700 ± 180 nM). However, in contrast to previous reports [105], we observed that the presence of either eIF5 construct had no negative effect on the k_{off} of mant-GDP from the eIF2 complex at saturating eIF2B ϵ concentrations (Fig. 12). This indicates that the GEF at high concentrations (~ 40 -fold excess over eIF5) is able to out-compete eIF5 from its interactions

with eIF2 efficiently, an ability that at low (physiological) GEF concentrations is limited by the direct contact between eIF5 and eIF2 γ .

2.3 Discussion

Using a combination of mutational, biochemical and structural approaches, this work provides new insights into intricate interaction network between eIF2, its multifunctional effector protein eIF5, eIF1 and eIF3c, with a particular focus on the eIF2-eIF5 complex. Due to the central role of these factors during the process of eukaryotic translation initiation, the presented observations have implications for nearly all steps of the initiation pathway from MFC and pre-IC assembly to scanning, start codon recognition and the general regulation of protein biosynthesis.

The eIF5-CTD interacts directly with eIF2 γ in the eIF2-eIF5 complex. Previous studies established that eIF5 folds into two structurally independent domains, the C-terminal and N-terminal domain, connected via a 'linker region' (LR) (Fig. 1A). The eIF5-NTD (in yeast) was defined as the first 152 amino acids and contains the putative arginine-finger (Arg15) that is thought to stimulate GTP hydrolysis by eIF2 in the scanning pre-IC [51-53]. The eIF5-CTD was defined as comprising residues 241-405, which fold into the atypical HEAT motif shown in Figure 1B, and provides interfaces for interactions with other eIFs to promote MFC and pre-IC assembly [1] (see below). The intervening residues 153-240 were proposed to form the flexible and unstructured LR, in which the conserved residues of the DWEAR-motif (residues 220-238) mediate the stabilization of the eIF2-bound GDP molecule [69]. Our own data support this role of the DWEAR-motif. However, they also strongly suggest that the DWEAR-motif does not belong to the LR but in fact forms an at least transient part of the eIF5-CTD. In the resulting structural model, helix $\alpha 2$ is accommodated in the hydrophobic cleft formed by the N-terminal helices of repeats R_I to R_{III}, while residues D220-E230 augment area III (Fig. 5 and S3C). Together, the DWEAR-motif and area III form an extended, mainly negatively charged surface (area III^{ext}) of the eIF5-CTD (Fig. S4B) that directly contacts eIF2 γ and stabilizes the bound guanine-nucleotide (Fig. 7, 8 and 13). This assumption is in line with the observation that the DWEAR-motif stimulates eIF5 binding to excess eIF2 γ (and thus independently of the

recruitment of eIF5 by the eIF2 β -NTT) only in the structural context of the CTD [65, 69], while this ability is lost in a construct comprising residues 1-262 (Table 4).

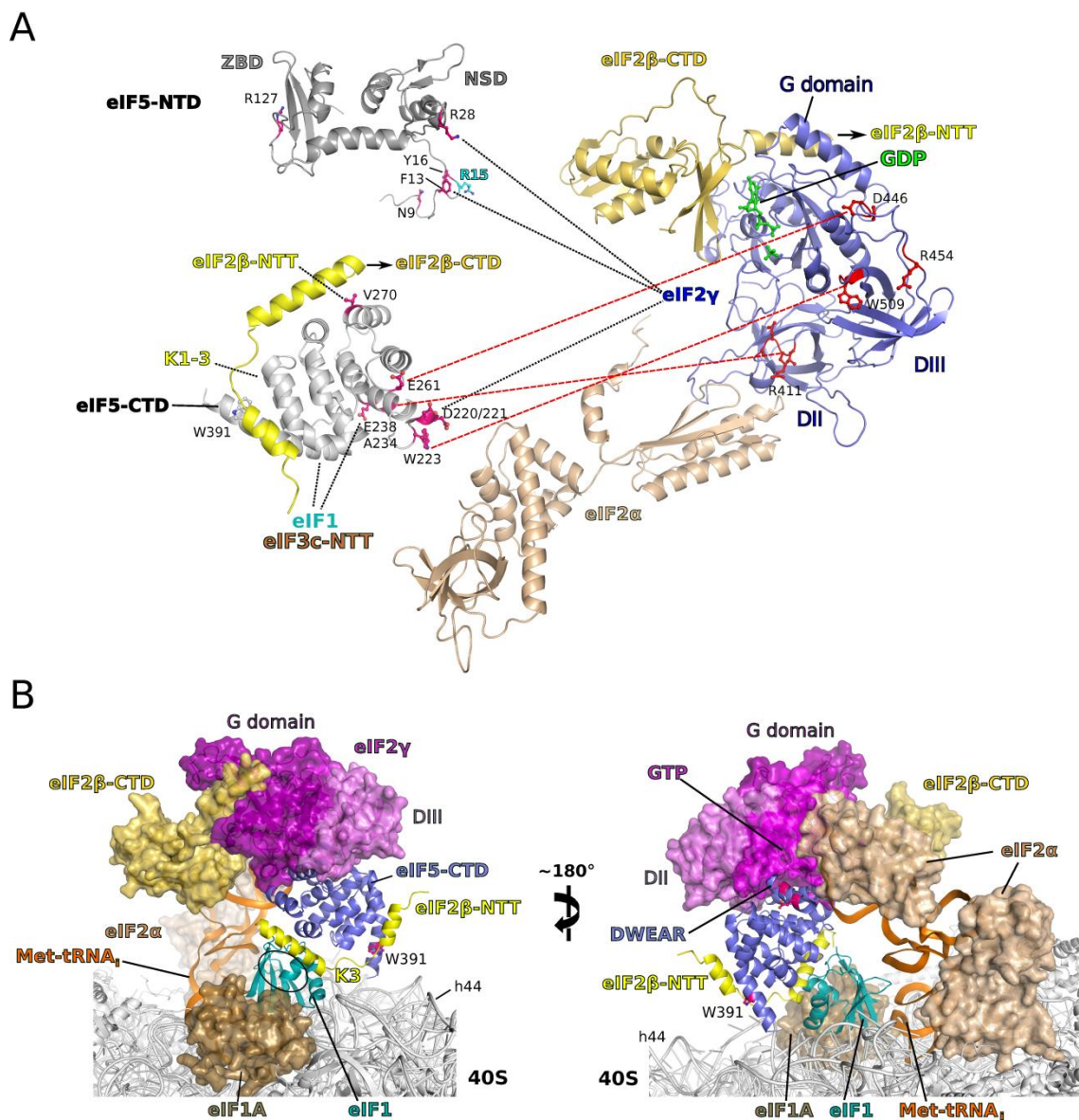


Figure 13. Model of the interactions between eIF5 and eIF2. A) Interaction map between eIF2 and eIF5 obtained by fluorescence and Bpa crosslinking experiments. eIF5-NTD and -CTD are shown in dark and light grey, respectively, with Bpa positions indicated (pink sticks). The eIF2 β -NTT bound to eIF5-CTD and the eIF2 β -CTD bound to eIF2 γ (blue, with GDP in green) are shown in light and dark yellow, respectively. eIF2 α is colored in beige. Red dashed lines indicate identified crosslinks between eIF5-CTD and eIF2 γ , while black dashed lines indicate crosslinks were the target protein but no specific peptide could be identified. The heterotrimeric eIF2 complex was modeled using the structures of the archaeal ortholog (aIF2) and human eIF2 α (PDBs: 3CW2, 1Q8K). **B)** Model of the eIF5-CTD in the context of the 43S pre-IC, based on the cryo-EM map of the mammalian 43S pre-IC (EMDB accession code: 5658), the crystal structures of eIF1 and eIF1A bound to the 40S subunit [19, 50] and the interactions depicted in (A). The eIF5-CTD (blue cartoon) thereby comes to lie in the gap between eIF2 γ (purple) and the platform of the 40S subunit (grey), placing the eIF2 β -NTT and area I in direct vicinity to the binding site for eIF1 (cyan cartoon; the circle indicates the KH area) and close to eIF1A (brown surface).

Central mechanistic questions that arise from the presented data are how eIF5-CTD contacts eIF2 γ and how this interaction stabilizes the bound guanine nucleotide. The mass-spectrometry analysis of the crosslink data shows that particularly the N-terminal residues of the DWEAR-motif, as well as Glu261 from area III lie in direct vicinity to the frontal face of eIF2 γ between G domain, domain II and domain III and thus close to the nucleotide binding pocket (Fig. 8 and 13). It is thus possible that eIF5-CTD stabilizes the nucleotide through direct contacts with the switch regions and/or the P-loop in a manner similar to the N-terminal α -helix bundle of RhoGDIs in complex with Rho proteins [106, 107] or the C-terminal α -helical 'GoLoco' motif in regulators of G protein signaling (RGS) of G α proteins [108-110]. However, although the mutational analysis indicates that the conserved Asp220, Asp221, Trp223 and/or Arg235 in the DWEAR-motif could play a role in nucleotide-stabilization similar to the conserved Asp45 in the RhoGDI Cdc42 [110] or the arginine residues of the GoLoco motif [109], the absence of any effect of eIF5 on the fluorescence signal of eIF2-bound mant-GDP/GTP (excited directly or indirectly by FRET) rather speaks against the introduction of residues directly into the nucleotide binding pocket itself. Moreover, according to our structural model of the DWEAR motif as part of the eIF5-CTD (Fig. 5), the effect of Arg235 mutations on nucleotide stabilization could also be explained by the putative structural role for the formation of the interaction interface within eIF5-CTD. A similar structural role for Asp220, Asp221 and/or Trp223 can also not be excluded. Instead, we assume that the eIF5-CTD acts allosterically by stabilizing the overall eIF2 γ in its nucleotide-bound conformation necessarily forming direct interactions with the P-loop or the switch regions. This would be in agreement with the observation that Bpa-constructs of eIF5-CTD crosslink to eIF2 in its GDP-, GTP- and Met-tRNA_i-bound form with virtually identical efficiency, and that the effect of eIF5-CTD on nucleotide binding is not limited to GDP-bound eIF2 (Fig. 7 and 8D). Both observations indicate that the contact between eIF5-CTD and eIF2 γ does not depend on the conformation of the two switch regions. Moreover, they are in line with the structural studies on the archaeal eIF2 ortholog (aIF2), which indicate that the overall domain arrangement of aIF2 γ remains essentially unchanged between apo, GDP- and GTP-bound states with domains I-III adopting a 'closed' conformation. This conclusion results in the interesting implication that the direct contact of eIF5-CTD to eIF2 γ is not

idiosyncratic to the eIF2·GDP·eIF5 complex but may in fact exist during various stages of the initiation process, including assembly of pre-ICs, as well as the scanning process (see next section).

Role of the direct interaction between eIF5-CTD and eIF2 γ : Although the DWEAR-motif is highly conserved among eukaryotes from yeast to human (Fig. S1), suggesting an important role in eIF5 function, this role is still elusive. Hence, a critical question that arises from our own and previous data concerns the physiological relevance of the direct interaction between the eIF5-CTD and eIF2 γ .

Originally, the DWEAR-motif was identified as a region within eIF5 that stabilizes eIF2-bound GDP [69]. Based on this observation it was proposed that eIF5 on the one hand physically antagonizes the GEF function of eIF2B by competing for their common substrate eIF2. On the other hand, it has been suggested that eIF5 might act as guanine-nucleotide dissociation inhibitor (GDI) for eIF2 that antagonizes spontaneous GDP dissociation and may be necessary for tight translational control [69]. With the central difference that we assume the DWEAR-motif to belong to the eIF5-CTD itself, our own results support both effects *in vitro*, showing that eIF5 reduces the dissociation rate of eIF2-bound GDP by more than 2-fold (Fig. 7 and Table 4) and antagonizes eIF2B ϵ -catalyzed GDP-dissociation at low GEF concentrations in a manner dependent on the presence of the DWEAR-motif (Fig. 12). This could indeed support a role for the eIF5-CTD·eIF2 γ contact as physical antagonist of eIF2B association and nucleotide exchange.

However, the claim of physiological relevance for these effects is problematic: The role of eIF5 as physical antagonist for eIF2B was recently questioned by the finding that eIF2B γ provides a second activity within the eIF2B catalytic subcomplex as ‘GDI displacement factor’ (GDF) that effectively displaces eIF5 from eIF2 under physiological conditions [105]. The data presented in Figure 12 suggest that eIF2B γ may destabilize the direct contact of the eIF5-CTD to eIF2 γ and thereby supports the entry of the eIF2B ϵ catalytic domain even at low (physiological) GEF concentrations. For the role of the DWEAR-motif, this poses the question for the cause-and-effect relation between the eIF5-CTD and eIF2B γ . The fact that eIF2B can effectively displace eIF5 under normal as well as starvation conditions (with phosphorylated eIF2 α) argues against a functionally relevant role for eIF5 as physical antagonist [73]. In turn, this indicates that the GDF activity of

eIF2B evolved to antagonize the direct eIF5-CTD·eIF2 γ contact, which would thus have to serve a different function at an earlier stage in the nucleotide cycle of eIF2. One of these possible functions is the inhibition of spontaneous GDP release from free eIF2, thereby allowing a tighter control of translation initiation under stress conditions [73] where an efficient stress response is dependent on the reduction of eIF2-TC levels [80]. Originally, this assumption was based on the observation that the W391F mutation in eIF5, which reduces the GDI activity, confers a Gcn $^{-}$ phenotype due to its inability to induce *GCN4* translation under starvation conditions [69] (see introduction of chapter 4 for an explanation of the Gcn $^{-}$ phenotype). However, our own as well as previous data show that Trp391 is directly involved in the interactions with the eIF2 β -NTT (Fig. 2)[35], indicating that its mutation reduces the presumed GDI function indirectly by destabilizing the entire eIF2·eIF5 complex. It is thus problematic to assign the observed Gcn $^{-}$ phenotype to the GDI function alone, as the W391F mutation is likely to affect MFC- and pre-IC formation, as well as start codon recognition. As a consequence, W391F might confer a Gcn $^{-}$ phenotype due to leaky-scanning on uORF1 on the *GCN4* mRNA leader, similar to other eIF5 mutations that destabilize its contacts to the eIF2 β -NTT [58]. Moreover, the same study found that the eIF5^{LR7A} mutation, in which seven of the conserved DWEAR-motif residues were mutated to Ala, had an even stronger negative effect on the *in vitro* GDI activity of eIF5, however, without conferring a Gcn $^{-}$ phenotype; this supports the idea that the loss of GDI function is not the primary origin underlying the reported W391F phenotype. Another indication for the relevance of the GDI activity is, according to Jennings and Pavitt [69], provided by the observation that the W391F and LR7A mutations in eIF5 suppress the lethality of the N249K mutation in eIF2B ϵ [105]. This was explained by the bypass of the GEF deficiency in eIF2B by an increase in spontaneous GDP dissociation from eIF2 due to a reduced GDI activity in eIF5. The central problem with this interpretation is that it is not known how the N249K mutation affects the GEF function by eIF2B *in vivo*. The isolated eIF2B ϵ -N249K mutant catalyzes nucleotide exchange as efficiently as the wild-type protein [71], arguing against a direct effect on the GEF activity. Instead, the deletion of the corresponding N-terminal region within eIF2B ϵ (residues 93-358) has a severe negative impact on the interactions with other eIF2B subunits, in line with its implication in interactions with eIF2B γ and the formation of the $\gamma_2\epsilon_2$ tetrameric core of the functional eIF2B decamer [105]. Consequently, N249K most likely reduces GEF activity *in vivo*

negatively affecting eIF2B ϵ complex formation, which is essential for productive interactions with eIF2 and the GDF function of eIF2B γ [105]. The W391F and LR7A mutations in eIF5 would thus suppress the phenotype of eIF2B ϵ -N249K by allowing the partially inactive eIF2B complex to compete more efficiently for their common substrate eIF2 and not due to increased spontaneous GDP dissociation. In line with this interpretation, W391F and LR7A are unable to rescue growth of the eIF2B ϵ -E569D mutant, in which complete GEF-inactivity is caused by the loss of a key catalytic residue. Thus, the increased spontaneous GDP release is not sufficient to allow efficient translation in the absence of GEF activity. Finally, it should be noted that eIF5 reduces the rate of GDP dissociation only ~2-fold at saturating eIF5 concentration (Fig. 9B and Table 4). As eIF5 and eIF2 are thought to exist in a 1:1 ratio in the cell, this effect on free eIF2 would be additionally reduced to ~1.5-fold. Thus, although the eIF2·eIF5 complex may play a role as stable cytosolic pool for eIF2 similar to the Rho·RhoGDI complex [68, 101] or may be relevant for a channeling process, where the potentially unstable eIF2 is passed on from eIF5 to eIF2B, it is in our opinion unclear to what extent the stabilization of the eIF2-bound guanine nucleotide is actually relevant for translation regulation.

An alternative option is that the moderate nucleotide-stabilizing effect is not a functionally relevant feature of eIF5 but merely the consequence and therefore rather a side effect of the direct interaction between the eIF5-CTD and eIF2 γ , causing an increased internal rigidity of the latter. In this case, the actual mechanistic significance of the interaction may not lie in the delayed GDP release but in the proper arrangement of the eIF5-CTD relative to the G domain of eIF2. This assumption is supported by the observation that GDP-, GTP-, and GTP/Met-tRNA_i-bound eIF2 seem to interact equally well with the eIF5-CTD (Fig. 8D). This suggests that the direct eIF5-CTD·eIF2 γ contact exists not only in solution with the GDP-bound form, but may as well be formed at other stages of the initiation process in which eIF2 exists in its active GTP-bound form. Hereby, a central aspect is the observation that the DWEAR-motif does not belong to the flexible linker region as previously assumed, but instead forms an element of the CTD itself – possibly stabilized in the eIF5·eIF2 complex. Thus, the eIF5-CTD·eIF2 γ interaction might play a functional role in the context of the interactions between eIF5-CTD, the eIF2 β -NTT, eIF1, eIF1A and eIF3c and their involvement in pre-IC formation, scanning and start codon recognition (see below). Interestingly, such a contact

would be compatible with the recently reported cryo-EM model of the 43S pre-IC, in which the eIF5-CTD can be accommodated between eIF2 γ of the TC and the 40S subunit (Fig. 13B). In agreement with previous suggestions [21, 63] this would position the eIF5-CTD within contact distance of the 40S subunit and with areas I and II in direct vicinity to the binding sites of eIF1 and eIF1A. It is thus possible that the conserved eIF5-CTD·eIF2 γ interaction may play a subordinate role in the communication between the ribosome, ribosome-associated initiation factors eIF1 and eIF1A, and the γ -subunit of eIF2. This suggestion is clearly tentative and will have to be tested experimentally in the context of the initiation machinery; however, it would be in line with the newly identified key role for the eIF5-CTD in scanning and start-codon recognition and the requirement for a factor that mediates between the rearrangements occurring on the ribosome and the detached G domain of eIF2 γ , where P_i release occurs in response to the formation of the codon-anticodon interaction between mRNA and initiator tRNA, reorganization of eIF1A and the dissociation of eIF1 from the P-site[21, 63, 64].

The eIF5-NTD interacts directly with eIF2 γ in the eIF2·eIF5 complex. Another central aspect of the processes of scanning and start-site selection is the role of the eIF5-NTD, the GAP domain of eIF5. A previous study proposed direct interactions between the eIF5-NTD and eIF2 γ [65]. However, the designated eIF5-NTD of this study included residues 1-279, containing the NTD, the linker region as well as the DWEAR-motif and R_i of the CTD. Although the eIF5(1-262) construct is unable to stabilize the guanine nucleotide (Table 4) and is therefore most likely unable to stably contact the γ -subunit, it is unclear what effect the presence of the complete R_i repeat would have. Hence, it cannot be ruled out that the observed direct contact between eIF5(1-279) and eIF2 γ was at least partially mediated by its C-terminal portion and not through the actual NTD. We reassessed this question and found that the eIF5-NTD in the complex with eIF2 is indeed positioned in direct proximity to the γ -subunit in a way that allows specific crosslinks from positions Phe13 next to the putative arginine-finger (Arg15) in the N-terminal tail, and from Arg28 in the first β -hairpin loop of the N-terminal subdomain, but not from Arg127 in the zinc binding domain (ZBD) (Fig. 11 and 13A). As for eIF5-CTD, the crosslinks occur with free eIF2 as well as the eIF2-TC, indicating that the underlying interactions are independent of or even slightly more specific in the presence of bound

Met-tRNA_i (Fig. 11B). However, a dependency of the interactions on the presence of GTP or the transition state mimic GDP+AlF_x could not be observed (Fig. S6), which stands in contrast to previous reports for the mammalian factors [53] but is consistent with the dependency of GTPase activation by eIF5 on the structural context of the 43S pre-IC [21]. It is thus likely that the direct interactions between eIF5 and eIF2 γ that result in the observed crosslinks are of a transient nature and require additional initiation factors or the 40S subunit itself to be stabilized for productive interactions with the eIF2 γ G domain to carry out its GAP activity.

The interaction network between eIF5-CTD, eIF2 β -NTT, eIF1 and eIF3c-NTD. The crystal structure of the eIF5(201-405)·eIF2 β (66-106) complex in combination with tryptophan quenching studies suggest a highly dynamic mode of interactions between eIF5 and eIF2 β with distinct roles for each of the three conserved K-boxes. K1 and K2 seem to be mainly responsible for the high affinity interactions with a K_d of \sim 100 nM that center on the negatively charged area I close to Trp391 of eIF5-CTD and involve residues of both AA-boxes (Fig. 2, 4 and SC). By contrast, K3 is positioned in the periphery of area I and contributes only marginally to the overall affinity (Fig. 2 and Table 1), but might, together with the adjacent helix αC^{β} , serve a role by pre-arranging the eIF5-CTD relative to eIF2 in order to promote the weak direct interaction between area III^{ext} and eIF2 γ (Fig. 9).

As indicated by the mutational studies, the contributions of individual K-boxes to the interactions with eIF5-CTD are mainly additive; this indicates that the eIF2 β -NTT, which is presumably unfolded in the unbound state [111], does not adopt a distinct tertiary domain fold upon binding to eIF5. Instead, it seems to form a peptide-domain interaction with eIF5-CTD, in which only some parts adopt a secondary structure such as αN^{β} and αC^{β} flanking K-box 3 (Fig. 3 and 4). This mode of segmented peptide-domain contact provides a number of context-dependent advantages over the rigid domain-domain interaction. On the one hand, it allows rapid evolution and adaptation to interactions with varying partners, as the peptide sequence is constrained only by the need to conserve residues directly involved in these interactions and can be easily extended in length to provide new interfaces. On the other hand, it introduces the means for a high degree of internal variability in the interactions, as each interacting segment (i.e. the K-boxes) can be released and/or reorganized individually, while the remaining segments are unaffected in their

contacts and retain reasonable affinity. This is conceivable particularly in the case of the lysine-rich K-boxes in the eIF2 β -NTT, for which the disorder-to-order transition upon binding to eIF5-CTD is most likely accompanied by a particularly large loss of internal conformational entropy, which is paid individually by the K-boxes and not collectively by the entire interface. This unfavorable entropic contribution results in an uncoupling of binding strength from specificity, giving rise to specific interactions that are at the same time relatively weak and thus reversible.

Functional relevance for this mode of interaction most likely lies in the complex series of rearrangements between eIF5-CTD, eIF2 β -NTT and other initiation factors such as eIF1, eIF1A, and eIF3c, which underlie the formation of the scanning-competent pre-IC and start codon recognition. In yeast cells, formation of the MFC is thought to provide a major intermediate step for the efficient recruitment of the eIF2-TC to the 40S subunit and pre-IC assembly. The stability of the MFC and consequently its ability to promote TC recruitment was shown to depend on an intricate interaction network between eIF5-CTD, eIF2 β -NTT, eIF1 and eIF3c-NTD, in which the loss of one of these factors negatively affects the incorporation of the others into the 43S pre-IC. In this context, the eIF2 β -NTT appears to play a central role for the nucleation of MFC assembly through its tight interactions with the eIF5-CTD and the promotion of eIF1 and eIF3c binding to eIF5-CTD. In line with this scenario, our structural and biochemical studies show how the eIF2 β -NTT can interact with area I of eIF5-CTD (Fig. 2 and 4), while at the same time supporting the binding of the eIF1-NTT and eIF3c-NTD in area II (Fig. 10). By contrast, the second binding site on the eIF5-CTD for eIF1, which lies in the vicinity of Val270, is incompatible with the simultaneous binding of the eIF2 β -NTT (Fig. 10). A possible mechanistic significance of this latter observation is unclear, as the loss of this eIF1-binding interface due to the mutagenesis of eIF5 causes the retention of eIF1 within the pre-IC and a suppressor of *sui⁻* (*Ssu⁻*) phenotype (due to an increased stringency of AUG selection) rather than increased dissociation rates, most likely due to the simultaneous disruption of the binding interface between eIF5 and eIF2 β -NTT (see below)[21].

Apart from its involvement in cooperative MFC formation, the eIF2 β -NTT is as well involved in the stabilization of eIF1 on the 40S subunit in its open, scanning competent conformation. However, this interaction is thought to be destabilized upon the encounter of the AUG start codon in a manner that depends on a displacement of eIF1 from the eIF2 β -NTT by the eIF5-CTD [21, 63].

Thus, in light of the proposed mode of peptide-domain interaction, this could indicate that one segment of the eIF2 β -NTT interacts with eIF5-CTD throughout the process of pre-IC formation, scanning and start-site selection, whereas a second region switches between eIF5-CTD and eIF1 in a context-dependent manner, with eIF1 as the preferred interaction partner in the open, scanning competent pre-IC, while this preference switches to eIF5-CTD upon the encounter of the AUG start codon and initiator tRNA-induced displacement of eIF1 from the P-site [21]. In this context, the critical aspect of the nature of the peptide-domain interaction between eIF2 β -NTT and eIF5-CTD would be the independency of TC stabilization in the pre-IC from these rearrangements, while they at the same time provide a high degree of flexibility and the means for a tightly balanced dynamic interplay with other factors in a changing structural context. Interestingly, the placement of the eIF5-CTD in the cryo-EM structure of the mammalian 43S pre-IC based on the crosslinking data, would be compatible with such rearrangements, as it would position the eIF2 β -NTT directly between the eIF5-CTD and eIF1 bound adjacent to the ribosomal P-site (Fig. 13B).

2.4 Materials and Methods

Cloning

DNA fragments corresponding to the open reading frames of eIF1 (encoded by the *TIF1* gene in *S. cerevisiae*), eIF2 β (*SUI2*), eIF5 (*TIF5*) and eIF2B ϵ (*GCD6*) or truncations thereof were amplified by PCR using yeast genomic DNA as template and a corresponding pair of primers. These fragments were digested using restriction enzymes for which the restriction sites had been incorporated into the amplification primers. The digested DNA fragments were then ligated into the desired vectors cut with the same restriction enzymes. The ligation mixture was subsequently transformed into XL1-Blue *E. coli* cells (Stratagene) and plated out on LB agar plates containing the appropriate antibiotics. Several colonies of each plate were picked and subjected to a test PCR to identify positive clones, which were then individually grown over night in LB medium supplemented with antibiotics to purify the plasmid by the Qiaprep Spin Miniprep Kit (Qiagen) according to the manufacturer's instructions. The sequences of the selected constructs were verified by DNA sequencing.

Single or multiple point mutants of the different constructs were generated by the QuickChange technique (Stratagene) using appropriate mutagenesis primers. For the incorporation of the genetically encoded unnatural amino-acid p-benzoyl-L-phenylalanine (Bpa) into a protein chain, the amber stop codon TGA was introduced into the desired position along the coding sequence. In the case of the eIF5 constructs, this was preceded by the replacement of the endogenous TGA stop codon by TAA. Plasmid preparation and verification of the correct sequence were performed as described above.

Protein expression and purification

All constructs except those for the incorporation of Bpa (see below) were expressed in *E. coli* BL21(DE3) Rosetta II cells (Novagene). Cells containing the respective plasmid were grown in 2xYT (supplemented with antibiotics) at 37 °C with shaking at 220 rpm until they reached an OD₆₀₀ of ~0.8 and were subsequently transferred to 16 °C. After 20 min the expression was induced by the addition of isopropyl- β -D-thiogalactopyranosid (IPTG) to a final concentration of 0.5-1 mM. The cells were harvested after 16 hours at 16 °C.

For the expression of proteins containing the genetically encoded unnatural amino-acid Bpa, the mutant constructs were transformed into the expression strain BL21(DE3)+pSupBpa (provided by Heinz Neumann)[94]. The cells were grown in 300 ml cultures of LB medium, supplemented with antibiotics and 1 mM Bpa (provided by Heinz Neumann), and grown at 37 °C until an OD₆₀₀ of ~0.6 was reached. The cultures were then transferred to 25 °C and the expression induced by the addition of 1 mM IPTG. The cells were harvested 15 hours after induction.

Purification of eIF1: eIF1 (wild-type and Bpa constructs) were expressed without affinity tag. The cells were resuspended in L-150 buffer (150 mM NaCl, 20 mM HEPES (pH 7.5), 5% glycerol, 1 mM EDTA, 4 mM β -mercaptoethanol) supplied with a mixture of protease inhibitors including aprotinin, leupeptin, pepstatin (ALP), and PMSF. The cells were lysed in a microfluidizer (Microfluidics, USA) and cell debris was removed by centrifugation for 30 min at 30,000 xg. The supernatant was applied to an SP Sepharose column (GE Healthcare) equilibrated in L-150 buffer. After loading the sample and washing the column with four column volumes of L-150 buffer, the bound protein was eluted with a linear gradient of high salt buffer (1 M NaCl, 20 mM HEPES (pH

7.5), 5% glycerol, 4 mM β -mercaptoethanol). Fractions containing eIF1 (a single peak at \sim 300 mM NaCl) were pooled and the salt concentration reduced to \sim 150 mM NaCl by dilution with L-150 buffer containing no NaCl. The diluted protein was applied to a HiLoad Heparin Sepharose column (GE Healthcare) equilibrated in L-150 buffer. Elution was started with a linear gradient into high salt buffer. Fractions containing eIF1 were pooled and applied to a Superdex S-75 size exclusion column (GE Healthcare) equilibrated in GF-150 buffer (150 mM KCl, 10 mM HEPES (pH 7.5), 5% glycerol, 2 mM DTT). Fractions containing the pure protein were pooled, concentrated and flash-frozen. The identity of eIF1 was verified by mass spectrometry analysis.

Purification of eIF2 β and eIF3c-NTD: Full-length eIF2 β was expressed as GST-fusion protein. Cell lysis was carried out as described above with the difference that L-500 buffer (500 mM NaCl, 20 mM HEPES (pH 7.5), 5% glycerol, 0.1 mM EDTA, 4 mM β -mercaptoethanol) was used instead of L-150 buffer. After centrifugation, the supernatant was loaded onto a GSTrap column (GE Healthcare) equilibrated in L-500 buffer. After loading of the sample the column was washed with 2 column volumes of L-500 buffer and the bound fusion protein was eluted by washing the column with elution buffer (L-500 buffer with 30 mM reduced glutathione). Fractions containing the target protein were pooled and incubated over night at 4 °C with PreScission protease (GE Healthcare) in a 1:100 weight ratio of protease to fusion protein to remove the GST tag. After a desalting step in 200 mM NaCl, 20 mM HEPES (pH 7.5), 5% glycerol, 4 mM β -mercaptoethanol, the cleaved GST, PreScission protease and uncleaved protein were removed by a second GSH Sepharose step. The flow-through containing the cleaved eIF2 β was pooled, concentrated and applied to a Superdex S-200 column (GE Healthcare) equilibrated in GF-150 buffer. Fractions containing the pure protein were pooled, concentrated and flash-frozen. All eIF2 β truncations and eIF3c(1-136) (eIF3c-NTD) were purified according to the same protocol described for full-length eIF2 β (the plasmid used for the expression of eIF3c(1-136) was obtained from S. Khoshnevis).

Purification of eIF5-CTD and eIF2B ϵ -CTD constructs: All C-terminal eIF5 constructs and eIF2B ϵ (524-712) were expressed as GST-fusion protein and purified similar to eIF2 β with some differences: After loading the supernatant onto the first GSTrap column and washing with L-500 buffer, the column was equilibrated in low salt buffer (100 mM NaCl, 10 mM HEPES (pH 8), 5% glycerol, 4 mM β -mercaptoethanol) before the bound fusion protein was eluted with low salt

Chapter 2

buffer plus 30 mM reduced glutathione. After PreScission protease treatment, the cleaved protein was loaded onto a Source 30Q column (GE Healthcare) equilibrated in low salt buffer. While GST and the protease eluted in the flow-through, the target proteins bound to the column and were eluted with a linear gradient into high salt buffer (1 M NaCl, 10 mM HEPES (pH 7.5), 5% glycerol, 4 mM β -mercaptoethanol). Fractions containing the target protein were pooled and loaded onto a Superdex S-75 column equilibrated in GF-150 buffer. Fractions containing the pure protein were pooled, concentrated and flash-frozen for storage at $-80\text{ }^{\circ}\text{C}$.

Purification of full-length eIF5 and eIF5(1-262): Full-length eIF5 and eIF5(1-262) were expressed as N-terminally polyhistidine-tagged proteins. Cell resuspension and lysis were carried out essentially as described above for eIF2 β with the difference that L-500-His buffer additionally contained 20 mM imidazole and no EDTA. After centrifugation the supernatant was loaded onto a HisTrap column (GE Healthcare) equilibrated in L-500-His buffer. The column was then washed with 2 column volumes of L-500-His buffer and bound protein was eluted with a linear gradient into elution buffer (L-500-His buffer with 300 mM imidazole). Fractions containing the target protein were pooled and incubated over night at $4\text{ }^{\circ}\text{C}$ with TEV protease in a 1:100 weight ratio of protease to target protein to remove the His-tag. After a desalting step in 250 mM NaCl, 20 mM HEPES (pH 7.5), 5% glycerol, 2 mM β -mercaptoethanol and 15 mM imidazole, the cleaved His-tag, TEV protease and uncleaved protein were removed by a second Ni-NTA step. The flow-through containing the cleaved eIF5 was pooled, concentrated and applied to a Superdex S-200 column equilibrated in GF-150 buffer. Fractions containing the pure protein were pooled, concentrated and flash-frozen for storage at $-80\text{ }^{\circ}\text{C}$.

Purification of eIF2: Polyhistidine-tagged eIF2 was overexpressed in *S. cerevisiae* strain GP3511 (a gift from G. Pavitt) containing a high-copy plasmid for the expression of all three subunits of eIF2 (*SUI2* (eIF2 α), *SUI3* (β), and His-tagged *GCD11* (γ)) [112]. For expression, 15 1-L cultures of YPD media were each inoculated with 1 ml of an overnight culture and grown for ~ 16 hours at $30\text{ }^{\circ}\text{C}$ with shaking at 220 rpm. The cells were harvested, resuspended in lysis buffer (500 mM KCl, 50 mM HEPES (pH 7.5), 5% glycerol, 20 mM imidazole, 1 mM MgCl_2 , 4 mM β -mercaptoethanol) containing protease inhibitors ALP and PMSF, flash-frozen in liquid nitrogen and disrupted in an ultra centrifugal rotor mill (Retsch ZM200, # 20.823.0001). After thawing of the cell

powder, the lysate was clarified by centrifugation at 45,000 xg for 45 minutes. The supernatant was filtered and applied to a HisTrap column equilibrated in lysis buffer. After washing the column with 4 column volumes of lysis buffer, bound protein was eluted with lysis buffer containing 300 mM imidazole. Fractions containing eIF2 were pooled and the salt concentration reduced to ~250 mM KCl by dilution with buffer containing 20 mM HEPES (pH 7.5), 5% glycerol and 4 mM β -mercaptoethanol. The diluted sample was then loaded onto a HiLoad Heparin Sepharose column equilibrated in 300 mM KCl, 20 mM HEPES (pH 7.5), 10% glycerol and 4 mM β -mercaptoethanol. The column was washed with low salt buffer and bound protein was eluted with a linear gradient of high salt buffer (1 M KCl, 20 mM HEPES (pH 7.5), 10% glycerol, 4 mM β -mercaptoethanol). Fractions containing eIF2 were pooled, concentrated and loaded onto a Superdex S-200 column equilibrated in GF-150 buffer. The absence of residual guanine nucleotides in the eIF2 preparations was verified by HPLC on a NUCLEOSIL 4000-7 PEI column (Macherey-Nagel). Nucleotide-free eIF2 complex was concentrated, flash-frozen and finally stored at -80 °C.

Purification of the yeast Methionyl-tRNA Synthetase: Yeast Methionyl-tRNA Synthetase was expressed in *S. cerevisiae* as GST-fusion protein from a plasmid containing a TRP auxotrophic marker (a gift from J. Lorsch). 15 1-L cultures of synthetic complete medium lacking tryptophan (SC-Trp medium) were inoculated from an overnight culture of yeast cells containing the plasmid for expression of GST-MetRS and were grown at 30 °C for 12 hours. Harvesting and lysis of the cells was carried out as described for eIF2 (see above), except for a different lysis buffer (500 mM NaCl, 50 mM HEPES (pH 7.5), 5% glycerol, 2 mM β -mercaptoethanol). The cleared lysate was loaded onto a GSTrap column equilibrated in lysis buffer. After washing the column with 4 column volumes of lysis buffer, the bound protein was eluted with 20 mM reduced glutathione. The fractions containing the GST-MetRS were pooled, concentrated and loaded onto a Superdex S-200 column equilibrated in 100 mM KCl, 40 mM Tris/HCl (pH 7.4), 10 mM MgCl₂, 5% glycerol, 2 mM DTT. The pure GST-MetRS was flash-frozen in liquid nitrogen and stored at -80 °C.

Purification, crystallization and structure determination of the eIF5(201-405)-eIF2 β (39-106) complex

The individual proteins, eIF2 β (39-106) and eIF5(201-405), were purified as described above. The complex was formed by mixing eIF5(201-405) with a 1.5-fold molar excess of eIF2 β (39-106). After incubation for 30 min at 20 °C the complex was separated from excess eIF2 β (39-106) by size exclusion chromatography on a Superdex S-75 equilibrated in GF-150 buffer and finally concentrated to ~20 mg/ml. Other complexes that did not yield any crystals suitable for structure determination were purified by the same protocol.

Initial crystals of the eIF5(201-405)-eIF2 β (39-106) complex grew at 20 °C within one day under a condition containing 0.4 M (NH₄)₂SO₄ and 0.05 M Li₂SO₄. After optimization, the best diffracting crystals were finally obtained with 12 mg/ml protein in 0.4 M (NH₄)₂SO₄ and 0.08 M Li₂SO₄ at 10 °C.

X-ray diffraction data were collected at BL 14.1 (HZB, BESSY, Berlin) [113]. The obtained data set was processed in space group P3₂12 using XDS [114] and scaled to a final resolution of 2.0 Å. The phase problem was solved by molecular replacement using the program PHASER [115] with the atomic coordinates of yeast eIF5(241-396) (PDB: 2FUL) as search model. The initial structural model comprised two eIF5(241-396) molecules per asymmetric unit. Missing regions of the eIF5 construct (residues 201-240) and eIF2 β were built manually in Coot [116]. The final model was obtained gradually by iterative rounds of refinement in PHENIX [117], followed by manual model building.

Synthesis and purification of Met-tRNA_i

Yeast initiator tRNA was synthesized by *in vitro* transcription. As template, a 142 nucleotides long DNA was used that contained the T7 promoter (underlined) and a hammer-head (HH) ribozyme (italic), followed by the sequence for the tRNA itself (bold) (purchased from Sigma Aldrich), as previously described [97, 118]:

5'TAATACGACTCACTATAGGGGAGACGCTCTGATGAGTCCGTGAGGACGAAACGGTACCCGGTACCGTC**AGC**
GCCGTGGCGCAGTGGAAAGCGCGCAGGGCTCATAACCCTGATGTCCTCGGATCGAAACCGAGCGGCGCTA
CCA3'

The use of the HH-ribozyme in front of the target RNA allows the transcription to begin with GGG instead of AGC, which results in a higher efficiency of the T7-RNA polymerase (T7-RNAP) [118]. After synthesis of the HH-tRNA fusion, the HH-ribozyme cleaves itself off in a Mg^{2+} -dependent reaction, leaving the native tRNA sequence.

The DNA template was amplified by PCR using 5'GGAGCCTAATACGACTCACTATAG3' as forward primer and 5'T^mG^mGTAGCGCCGCTCGGTTTC3' as reverse primer. T^m and G^m are 2'-O methylated nucleotides to reduce the occurrence of 3' heterogeneities due to addition of nontemplated nucleotides by the T7 polymerase [119]. The amplified template was purified by ethanol precipitation and dissolved in water.

The optimal conditions for the transcription reaction were determined in analytical scale by varying the Mg^{2+} concentration or the ratio of T7-RNAP to the DNA template. Preparative transcription reactions (7 ml final volume) contained 1 x Tris buffer, 5 mM DTT, 30 mM $MgCl_2$, 75 μ g/ml T7-RNAP, 0.54 μ M DNA template, and 2.5 mM of each NTP. The reaction was allowed to continue for 4 hours at 37 °C. The mixture was then filtered and applied to a 1-ml Mono Q column (GE Healthcare). After washing the column with buffer A (400 mM Na-acetate, 0.2 mM EDTA, 100 mM Tris/HCl (pH 6.9)), the elution was started by applying a 50-ml gradient from 0-100% buffer B (1.5 M Na-acetate, 0.2 mM EDTA, 100 mM Tris/HCl (pH 7.3)). The run was analyzed on a urea gel, showing that the cleaved tRNA_i eluted in a single peak containing small contaminations of HH-ribozyme. Uncleaved HH-tRNA and the DNA template eluted in a peak at higher salt concentrations, while the T7-RNAP eluted in the flow-through (according to SDS-PAGE analysis). Fractions containing the tRNA_i were pooled, concentrated to ~2 ml volume and applied to a Superdex S200 (16/60) column equilibrated in 25 mM Tris/HCl (pH 7.5), 30 mM KCl and 1 mM DTT. The tRNA_i eluted in a single peak, free of HH-ribozyme. The pure tRNA_i was stored at -80 °C.

In an alternative procedure, tRNA_i was *in vitro* transcribed and purified without HH-ribozyme as a potential origin for a partial missfolding of the tRNA. A critical drawback of this strategy is that the T7-RNAP has to start at AGC instead of the optimal GGG in the HH-ribozyme, which results in lower initial yields. However, this is partially compensated by the fact that the Mg^{2+} concentration has to be optimized for the transcription efficiency alone and does not have to take the activity of the ribozyme into account as well. Moreover, no tRNA product is lost due to incomplete cleavage

Chapter 2

of the HH-tRNA_i fusion. For this purpose, the above reverse primer and 5'AGCCTAATACGACTCACTATAAGCGCCGTGGCGCAGTGG3' as forward primer were used to generate the new DNA template:

5'AGCCTAATACGACTCACTATAAGCGCCGTGGCGCAGTGGGAAGCGCGCAGGGCTCATAACCCTGATGTCC
TCGGATCGAAACCGAGCGGCGCTACCA3'

The optimal condition for the transcription reaction was found to be 16 mM MgCl₂, 50 µg/ml T7-RNAP and 0.68 µM DNA template. The preparative reaction and subsequent purification was carried out as described above for the purification with HH-ribozyme. From the same volume of preparative reaction mixture, the final yield of pure tRNA_i was usually about 25% lower than for the reaction with HH-ribozyme.

Preparative charging of the tRNA_i with methionine was carried out essentially as described previously [97]. The stoichiometric charging reaction mixture contained 25 mM Tris/HCl (pH 7.6), 10 mM Mg(OAc)₂, 1 mM DTT, 2 mM ATP, 200 µM methionine, 5 µM tRNA_i and 3 µM MetRS in a total volume of 4 ml. For 'hot' control reactions that were carried out parallel to the stoichiometric charging reaction, radiolabeled L-[³⁵S]methionine (Hartmann Analytic) was used to assess the amount of produced [³⁵S]methionyl-tRNA_i and thus the charging efficiency [97]. The reaction mixture was incubated at 30 °C for 20 min, the time point at which the maximal charging efficiency, usually 34-36%, had been reached according to the control reaction. The charged Met-tRNA_i was then once extracted with buffered phenol and once with chloroform, followed by the addition of 0.3 M NaOAc (pH 5) and an ethanol precipitation for 2 hours at -20 °C. The dried pellet was finally resuspended in H₂O to a final concentration of 30 µM Met-tRNA_i. As the remaining uncharged tRNA_i was reported not to interfere significantly with the initiation process in an *in vitro* reconstituted system [97], a further purification of the charged initiator tRNA was not performed.

UV Crosslinking Experiments with Bpa

Crosslinking was performed by exposing Bpa-containing proteins either alone or in the presence of potential interaction partners to 365 nm UV light at a distance of ~5 cm for 10-30 min on ice (Vilber Lourmat lamp, 2 X 8W, 365 nm tubes, 32 W, 230 V #VL-208.BL). All reactions were performed in standard reaction buffer (100 mM KCl, 20 mM Tris/HCl (pH 7.5), 3 mM MgCl₂ and 2 mM DTT).

Following UV light irradiation, the crosslink products were separated by SDS-PAGE and stained with Coomassie blue. Crosslinking occurred in a UV- and time-dependent manner only in the presence of proteins containing Bpa. Protein bands of interest were excised and in-gel digested with trypsin or a mixture of trypsin and GluC as described [120] for subsequent analysis by ESI-MS/MS2 (see below).

Mass spectrometry analysis with nano LC-nano ESI-MS/MS2

Nano LC - RSLCnano Ultimate 3000 system (Thermo Scientific): Peptides of 1 μ l sample solution were loaded and washed on an Acclaim PepMap 100 column (75 μ m x 2 cm, C18, 3 μ m, 100 \AA , Thermo Scientific) at a flow rate of 25 μ l/min for 6 min in 100% solvent A (98% water, 2% acetonitrile, 0.07% TFA). Analytical peptide separation by reverse phase chromatography was performed on an Acclaim PepMap RSLC column (75 μ m x 25 cm, C18, 3 μ m, 100 \AA , Thermo Scientific) typically running a gradient from 98% solvent A (water, 0.1% formic acid) and 2% solvent B (80% acetonitrile, 20% water, 0.1% formic acid) to 42% solvent B within 95 min and to 65% solvent B within the next 26 min at a flow rate of 300 nl/min (solvents and acids from Fisher Chemicals).

Nano ESI mass spectrometry -OrbitrapVelos Pro (Thermo Scientific): Chromatographically eluting peptides were on-line ionized by nano-electrospray (nESI) using the Nanospray Flex Ion Source (Thermo Scientific) at 2.4 kV and continuously transferred into the mass spectrometer. Full scans within the mass range of 300-1850 m/z were taken from the Orbitrap-FT analyzer at a resolution of 60,000 with parallel data-dependent top 10 MS2-fragmentation with the LTQ Veleo Pro linear ion trap (CID). LCMS method programming and data acquisition was performed with the software XCalibur 2.2 (Thermo Fisher).

MS-data analysis - Protein identification with Proteome Discoverer 1.4: MS/MS2 data processing for peptides was done with the Proteome Discoverer 1.4 software (Thermo Scientific) and the Discoverer Daemon 1.4 software (Thermo Scientific) using the SequestHT and Mascot search engines (Thermo Scientific and Matrix Science, respectively) and a *S. cerevisiae*-specific protein databases (Saccharomyces Genome Database, SGD, Stanford University) extended by the most common contaminants. Oxidation (+ 16 Da) was considered as variable modification of

methionine, carbamidomethylation (+ 57.02146 Da) as static modification of cysteine. False discovery rates of peptide identifications were obtained by decoy database analyses of the MS datasets. FDR was set 0.01 at maximum.

Identification of crosslinked peptides with StavroX: The search for target peptides for UV-induced crosslinks was performed using the program StavroX [102] with the following settings: Precision for precursor comparison, 10 ppm; precision of fragment comparison 0.8 Da; mass limits, 200-800 Da; used enzymes, trypsin and GluC, allowing 2 missed cleavages at Arg, Lys and Glu, and 3 missed cleavages at Asp; static modification on cysteine (carbamidomethylation) and variable modification on methionine (oxidation); peaks were considered only with signal-to-noise ratio (S/N) above 2. The quality of the searches was assessed by a parallel decoy search using the reversed protein sequence to determine the occurrence of false positives, as well as by the calculation of a score, which is calculated from the number of signals above the specified S/N value according to the algorithm given in [102].

Steady-State Fluorescence Measurements

All experiments were carried out on a Fluoromax-3 spectrophotometer (Jobin Yvon Inc., USA) using a quartz cuvette (Hellma Analytics, Germany). All reactions were done at 20 ± 1 °C in the standard reaction buffer (100 mM KCl, 20 mM Tris/HCl (pH 7.5), 3 mM MgCl₂ and 2 mM DTT).

The binding of eIF2 β to eIF5-CTD was monitored by tryptophan quenching experiments. Tryptophan fluorescence in eIF5-CTD was excited at 280 nm, resulting in an emission at 350 nm, which was quenched upon the addition of eIF2 β (full-length and N-terminal domain fragments). Equilibrium dissociation constants (K_d) for the complexes were determined by titrating eIF5-CTD with increasing amounts of eIF2 β , until saturation was reached. The residual fluorescence signal produced by eIF2 β (which contains no tryptophan) alone was determined by blank-titrations into buffer and subsequently subtracted from the binding data.

The binding of mant-labeled guanine nucleotides to eIF2 was monitored either by direct excitation at a wavelength of 355 nm or by Foerster Resonance Energy Transfer (FRET) from tryptophan residues excited at 280 nm and an emission wavelength of 440 nm. Fluorescence emission spectra were recorded after incubating the eIF2·mant-nucleotide complexes for 5 min at

20 °C. To estimate the K_d for eIF2·mant-nucleotide complexes in presence or absence of eIF5, the fluorescence of increasing amounts of mant-nucleotides was measured either in buffer alone or in the presence of 200 nM of eIF2 complex. The dilution was less than 1%. To form the eIF2·eIF5 complex, 20-fold molar excess of eIF5 was added to eIF2 and incubated for 10 min at 20 °C prior to the experiment.

Assuming a one-site binding model for the studied binding reactions, the data obtained from the equilibrium titrations were fitted to a quadratic equation:

$$F = F_0 + \Delta F_{\max} \frac{(X + Y + K_d) - \sqrt{(X + Y + K_d)^2 - 4XY}}{2X}$$

where F is the fluorescence signal of the mant-nucleotide in the absence or presence of eIF2, F_0 is the initial fluorescence signal, ΔF_{\max} is the maximum fluorescence signal, X is the total concentration of eIF2, Y is the total concentration of the added mant-nucleotide and K_d is the equilibrium dissociation constant.

For the determination of the apparent equilibrium dissociation constants of eIF2·mant-GDP to eIF5 from the pre-steady-state experiments (see below), the above equation was modified as follows:

$$k_{\text{app}} = k_a + (k_b - k_a) \frac{(X + Z + K_{1/2}) - \sqrt{(X + Z + K_{1/2})^2 - 4XZ}}{2X}$$

Here, k_{app} is the characteristic apparent rate constant for the dissociation of the mant-nucleotide from eIF2 in the presence of a specific concentration of eIF5, Z is the concentration of eIF5, k_a is the dissociation rate constant of mant-GDP from eIF2 alone, k_b is the dissociation rate constant of mant-GDP from eIF2 in the presence of saturating concentrations of eIF5 and $K_{1/2}$ is the concentration of eIF5 at which the half maximal effect on the dissociation rate of mant-GDP from eIF2 is reached (the apparent equilibrium dissociation constant). Data evaluation was done with the SigmaPlot software.

Pre-Steady-State fluorescence measurements

Pre-steady-state experiments were carried out on a Fluoromax-3 spectrophotometer using a quartz cuvette with stirring magnet to allow fast mixing of the reacting components. All reactions

Chapter 2

were done at 20 ± 1 °C in standard reaction buffer. The fluorescence of mant-nucleotides was excited either directly at 355 nm or via FRET from tryptophan residues excited at 280 nm and monitored at an emission wavelength of 440 nm.

To study the dissociation of nucleotides, 100 nM eIF2·mant-GDP or eIF2·mant-GTP complex was formed by adding 125 nM of the respective mant-nucleotide to 100 nM nucleotide-free eIF2, followed by an incubation for 3 min at 20 °C. To start the reaction, unlabeled GDP was added in excess and the decrease in mant-fluorescence was monitored over time. The data were evaluated by fitting to a single exponential function with the equation:

$$F(t) = F_0 + Ae^{-k_{app}t}$$

where $F(t)$ is the fluorescence at time t , F_0 is the final fluorescence signal, k_{app} is a characteristic apparent time constant and A is the amplitude. Data evaluation was done with the SigmaPlot software.

2.5 Supplementary information

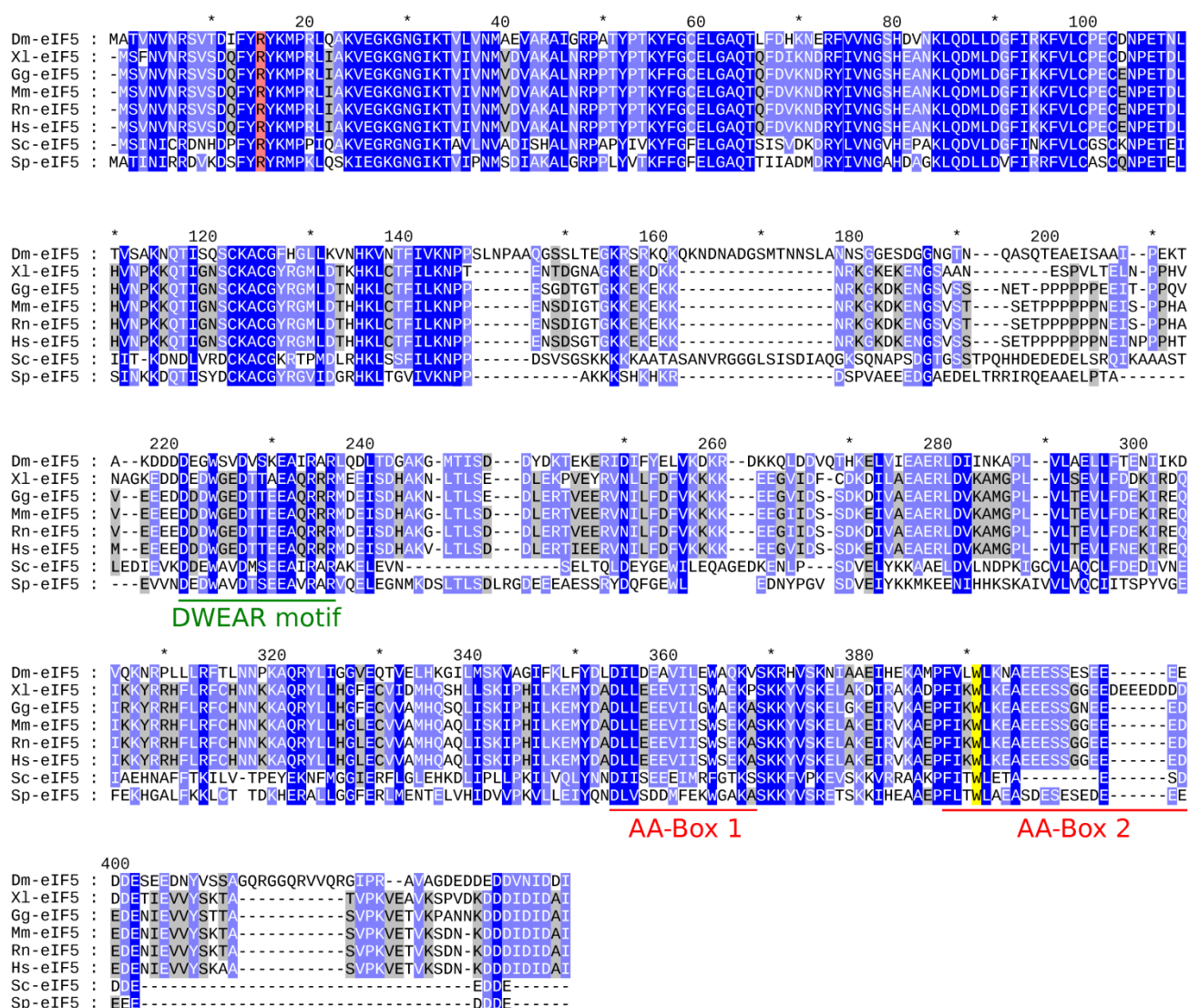


Figure S1. Multiple sequence alignment of eIF5 orthologs. Highly conserved residues are highlighted in dark blue, conserved residues in light blue and variable residues in grey; the putative arginine-finger (Arg15) and Trp391 in AA-box 2 are highlighted in red and yellow, respectively. The numbering above the alignment corresponds to the yeast ortholog (Sc-eIF5); the DWEAR motif and AA-boxes 1 & 2 are indicated below the alignment. Dm, *Drosophila melanogaster*; Xl, *Xenopus laevis*; Gg, *Gallus gallus*; Mm, *Mus musculus*; Rn, *Rattus norvegicus*; Hs, *Homo sapiens*; Sc, *Saccharomyces cerevisiae*; Sp, *Schizosaccharomyces pombe*. The alignment was generated using the clustal omega algorithm.

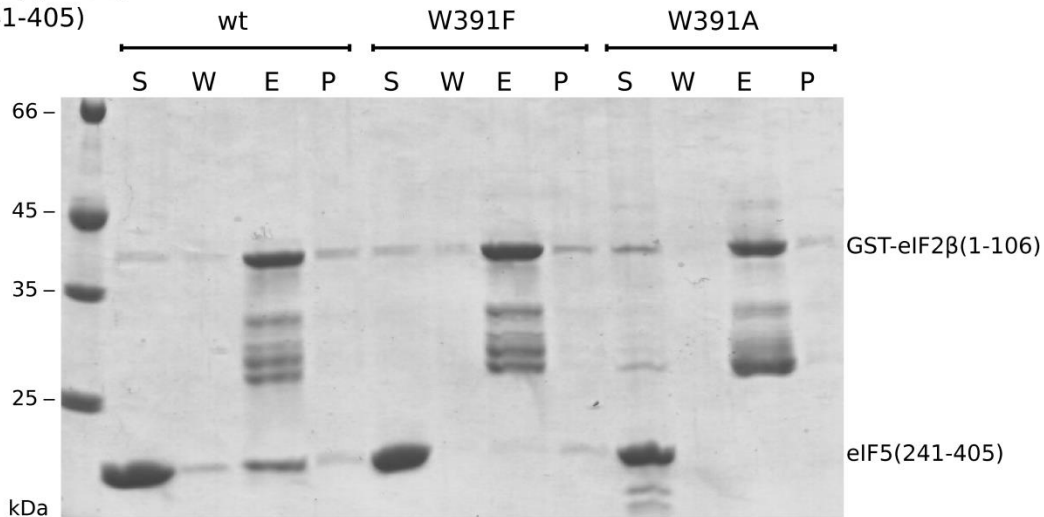
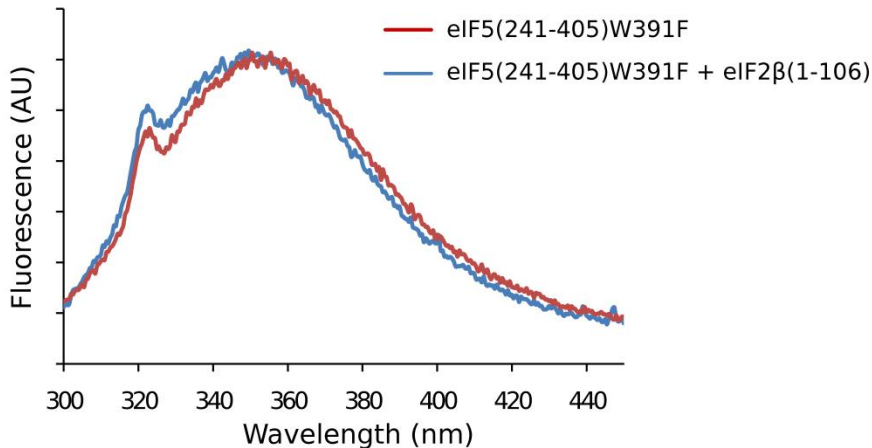
AGST-eIF2 β (1-106) +
eIF5(241-405)**B**

Figure S2. Effect of Trp391 mutations in eIF5 on the interaction with the eIF2 β -NTT. **A)** GST-pull down experiments between GST-eIF2 β (1-106) and eIF5(241-405) wild-type (wt), eIF5(241-405)W391F and eIF5(241-405)W391A. For each experiment, 50 μ g of GST-eIF2 β (1-106) were first immobilized on GSH-Sepharose beads and subsequently incubated for 10 min at 20 $^{\circ}$ C with 100 μ g eIF5(241-405). The beads were then washed three times with washing buffer (100 mM NaCl, 20 mM Hepes (pH 7.5), 5% glycerol, 2 mM DTT) and the bound proteins were finally eluted from the beads with washing buffer containing 20 mM reduced glutathione. S, supernatant after incubation and before washing; W, supernatant after the third washing step; E, supernatant after elution; P, pellet after elution. **B)** Tryptophan quenching experiment between eIF5(241-405)W391F and eIF2 β (1-106). The chromatogram shows the emission spectrum of eIF5(241-405)W391F upon the excitation of the Trp fluorescence at 280 nm in the absence (red) and presence (blue) of the eIF2 β -NTT.

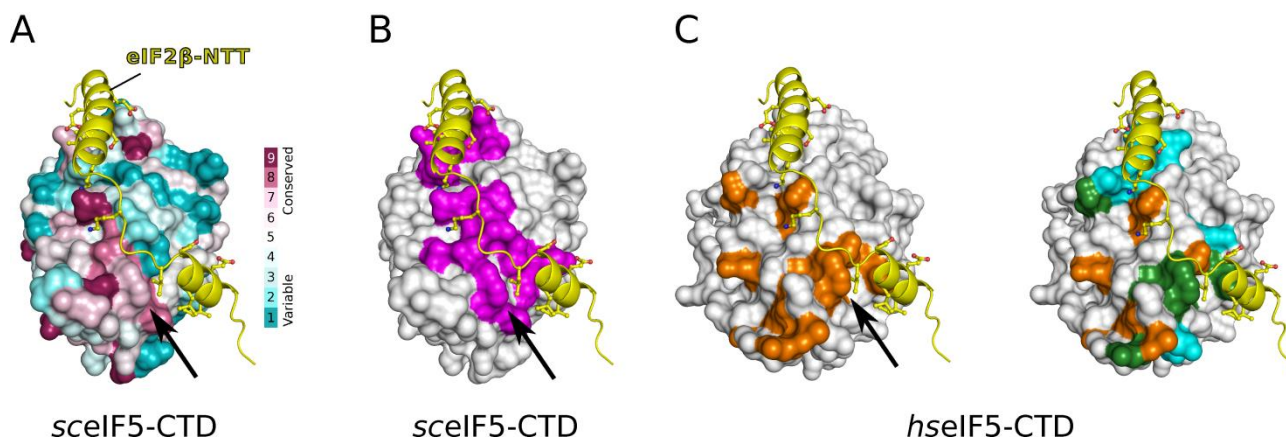


Figure S3. Binding of the eIF2 β -NTT by eIF5-CTD. **A)** The fragment of the eIF2 β -NTT (yellow) binds eIF5-CTD in a comparatively conserved area, with the highest degree of conservation occurring in the vicinity of Trp391 (arrow). **B)** eIF5-CTD is shown as grey surface, with residues directly involved in contacts with the eIF2 β -NTT (yellow) colored pink. **C)** Model of eIF2 β -NTT (yellow) bound to the human eIF5-CTD (PDB: 2IU1) according to the structure of the yeast complex (B). The hseIF5-CTD is shown as grey surface; in the left panel, residues affected by eIF2 β (K2K3) binding in NMR chemical shift assays are colored orange; in the right panel, residues affected only by eIF2 β (K2K3) or eIF1 are colored cyan and orange, respectively, and residues affected by both are colored green [63].

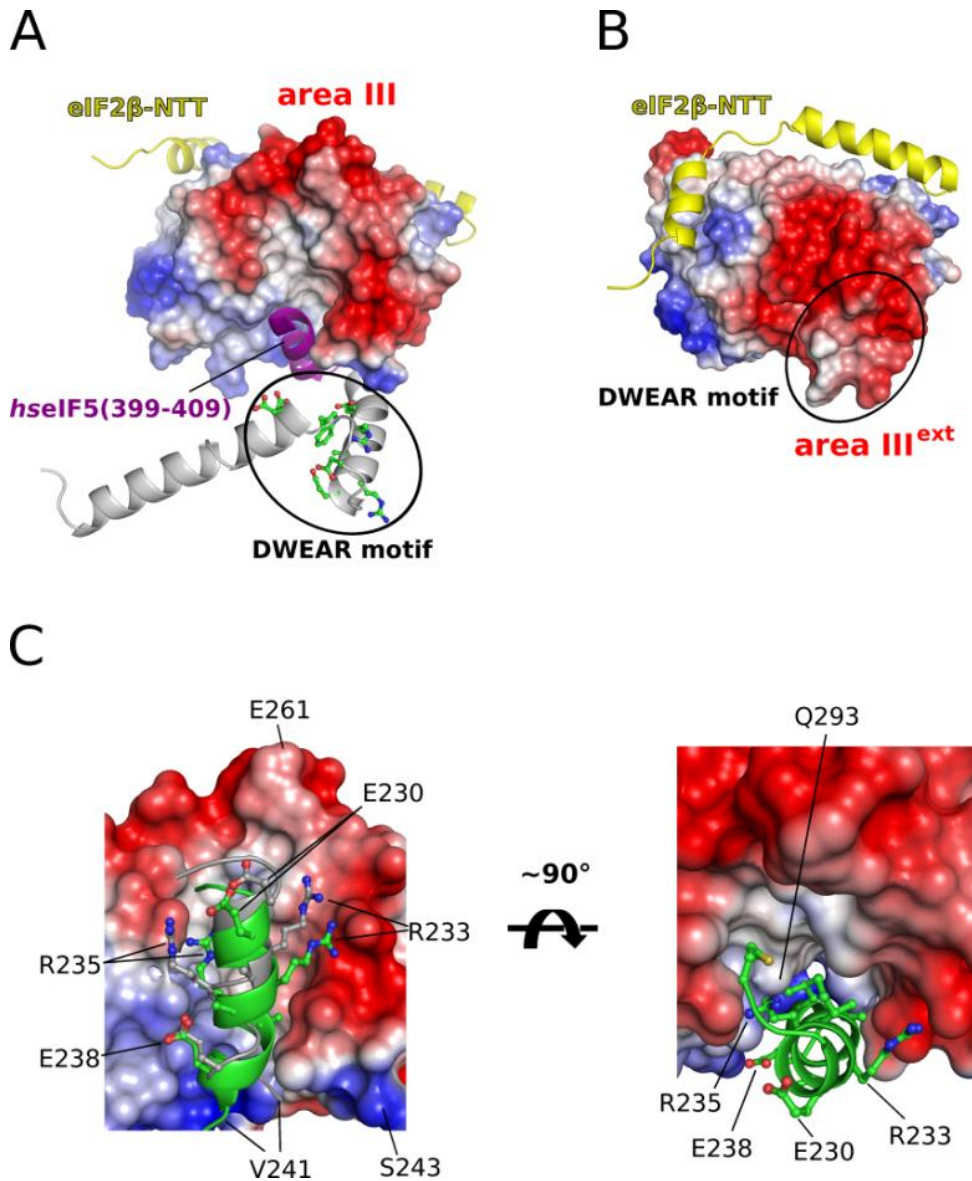


Figure S4. Model of the DWEAR-motif as element of the eIF5-CTD. **A)** Overview of the eIF5-CTD·eIF2 β -NTT complex with residues 241-399 of eIF5 shown in surface charge presentation; helices $\alpha 1$ and $\alpha 2$ are shown as grey cartoon with DWEAR-motif residues as green sticks (circle) and the eIF2 β -NTT as yellow cartoon. In the crystal structure of human eIF5-CTD (PDB: 2IU1), the hydrophobic cleft below area III is partially occupied by an α -helix formed by the C-terminal residues 399-409 (purple), which have no counterpart in yeast (see also Fig. S1). **B)** Surface charge presentation of the eIF5-CTD model presented in Figure 5A, with helix $\alpha 1$ and the DWEAR-motif accommodated in the hydrophobic cleft. As a consequence, the negatively charged N-terminal portion of the DWEAR-motif comes to lie next to area III of the CTD, thereby forming the extended area III^{ext}. **C)** Two models of helix $\alpha 1$ (grey and green, respectively) accommodated in the hydrophobic cleft, generated by the ClusPro server (compare Fig. 5A).

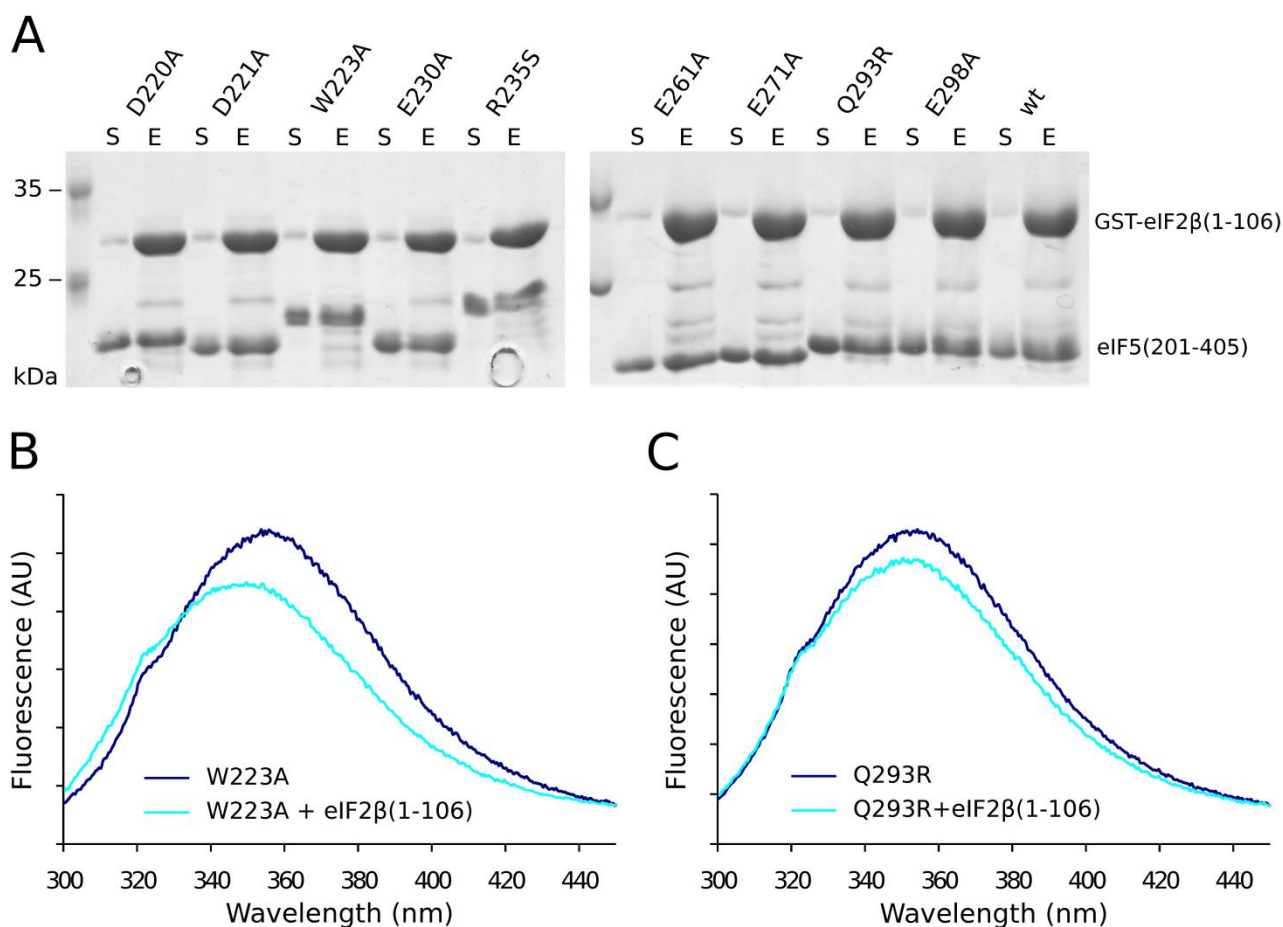


Figure S5. Effect of eIF5-CTD single mutations on the interaction with the eIF2β-NTT. **A)** GST-pull down experiments between GST-eIF2β(1-106) and eIF5(201-405) D220A, D221A, W223A, E230A, R235S, E261A, E271A, Q293R, E298A, and the wild-type protein (wt). For each experiment, 50 μg of GST-eIF2β(1-106) were first immobilized on GSH-Sepharose beads and subsequently incubated for 10 min at 20 °C with 100 μg eIF5(201-405). The beads were then washed three times with washing buffer (100 mM NaCl, 20 mM Hepes (pH 7.5), 5% glycerol, 2 mM DTT) and the bound proteins were finally eluted from the beads with washing buffer containing 20 mM reduced glutathione. S, supernatant after incubation and before washing; E, supernatant after elution. **B-C)** Tryptophan quenching by eIF2β(1-106) upon binding to eIF5(201-405)W223A (B) and eIF5(201-405)Q293R (C). The chromatograms show the emission spectra of the respective eIF5(201-405) construct (1 μM) upon the excitation of the Trp fluorescence at 280 nm in the absence (blue) and presence (cyan) of the eIF2β-NTT (2 μM). It should be noted that the quenching signal for the eIF5(201-405)Q293R is weaker than the one observed for eIF5(201-405)W223A as it contains one additional Trp residues that is not directly involved in the binding reaction with the eIF2β-NTT.

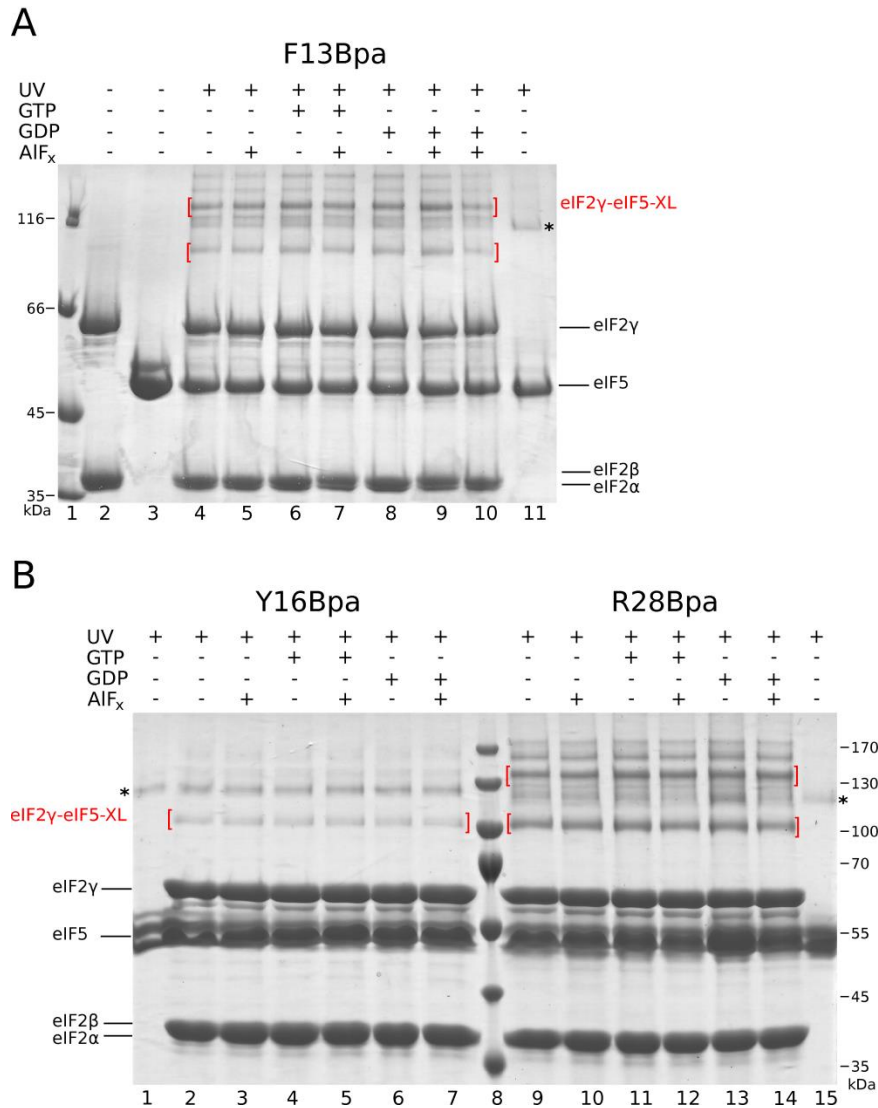


Figure S6. Dependency of the Bpa-crosslinks between the eIF5-NTD and eIF2 on the presence of nucleotides and fluoroaluminates. A) SDS-gel showing the UV-dependent formation of crosslink bands between 5 μ M eIF5(FL)F13Bpa and 2 μ M eIF2 in the absence or presence of GDP (3 μ M), GTP (3 μ M) and/or AIF_x (2 mM AlCl₃/20 mM NaF). Lane 1 contains the molecular weight marker; lane 2 contains only eIF2; lanes 3 and 11 contain only eIF5 without (3) and with (11) UV-irradiation; lanes 4-10 contain eIF2 and eIF5; lane 10 contains the same mixture as lane 9 with the difference that it contains 200 mM KCl instead of 100 mM. **B)** SDS-gel showing the UV-dependent formation of crosslinks between 5 μ M eIF5(FL)Y16Bpa (left) or eIF5(FL)R28Bpa (right) and 2 μ M eIF2 in the absence or presence of GDP (3 μ M), GTP (3 μ M) and/or AIF_x (2 mM AlCl₃/20 mM NaF). Lane 8 contains the molecular weight marker; lanes 2-7 and 9-14 contain eIF2 and eIF5; lanes 1 and 15 contain only eIF5(FL)Y16Bpa (1) or eIF5(FL)R28Bpa after UV-irradiation. For all experiments, crosslinking was performed on ice for 30 min. Crosslinks to eIF2 γ are indicated by red brackets; the strong crosslink bands for positions directly below the 130 kDa marker (marked with *) also occur in the absence of eIF2 and are thus likely to originate from a crosslink between two eIF5 molecules.

Chapter 3 • Interaction network between eIF2 and eIF2Bε

This manuscript is in preparation for submission

Analysis of the interaction network between eIF2 and eIF2Bε and its implications for the mechanism of nucleotide exchange

Bernhard Kuhle^{1,§}, Oliver Valerius² and Ralf Ficner¹

¹ Abteilung für Molekulare Strukturbiologie, Institut für Mikrobiologie und Genetik, Göttinger Zentrum für Molekulare Biowissenschaften, Georg-August-Universität Göttingen, D-37077 Göttingen, Germany

² Abteilung für Molekulare Mikrobiologie und Genetik, Institut für Mikrobiologie und Genetik, Georg-August-Universität Göttingen, D-37077 Göttingen, Germany

[§]To whom correspondence should be addressed: bkuhle@gwdg.de

Author contributions:

BK: designed the study and conceived the experiments; performed cloning, protein purification, crystallization, data collection and structure determination, crosslinking experiments, and biochemical studies on nucleotide binding by eIF2; analyzed and interpreted the data; wrote the manuscript. OV: performed mass-spectrometry analysis of crosslinks and helped to analyze the MS-data. RF: design of the study; helped to draft the manuscript.

Abstract

The eukaryal initiation factor 2 (eIF2) is a heterotrimeric translational GTPase, responsible for the GTP-dependent delivery of the methionylated initiator tRNA to the ribosome. The guanine nucleotide cycle performed by eIF2 during translation initiation is tightly regulated by the opposing effects of the GTPase activating protein (GAP) eIF5 and the guanine-nucleotide exchange factor (GEF) eIF2B. Here, we present a structural and biochemical analysis of the interaction network between eIF2 and eIF2B ϵ , the catalytic subunit of the heteropentameric eIF2B complex, with the aim to gain insight into the mechanism of nucleotide exchange. On the one hand, we show that the main interaction, which is responsible for the recruitment of eIF2B ϵ to eIF2, is mediated by a dynamic peptide-domain interaction between the catalytic eIF2B ϵ -CTD and the eIF2 β N-terminal tail. On the other hand, a second interaction was mapped directly between eIF2B ϵ -CTD and the immediate vicinity of the nucleotide binding pocket on eIF2 γ , an interaction that is most likely responsible for the destabilization of the eIF2-bound nucleotide. Together, the presented findings provide a refined model for the interactions between eIF2B ϵ and its substrate eIF2, which has implications for the mechanism of nucleotide exchange and possibly provides insight into the evolutionary history of the structurally and functionally similar C-terminal domains of eIF2B ϵ and eIF5.

3.1 Introduction

The eukaryal translation initiation factor 2 (eIF2) is a G protein that plays an essential role during the initiation phase of translation in eukarya. In its GTP-bound form, eIF2 specifically recognizes and binds methionylated initiator tRNA (Met-tRNA_i) and delivers it to the 43S pre-initiation complex (43S pre-IC) [12, 16]. Upon the recognition of the correct start site for translation, the GTPase activating protein (GAP) eIF5 triggers the GTPase activity in eIF2, resulting in the irreversible hydrolysis of eIF2-bound GTP. After the release of Met-tRNA_i, the inactive eIF2-GDP dissociates from the ribosome and has to be recycled back to eIF2-GTP for a next round of initiation. Like other Ras-related G proteins, eIF2 binds GDP tightly with an affinity in the lower nanomolar range, and the rate of spontaneous GDP dissociation is too slow to support efficient translation [44]. The exchange reaction is therefore catalyzed by the guanine-nucleotide exchange

factor (GEF) eIF2B, which promotes the dissociation of GDP, followed by binding of GTP due to its ~10-fold higher cellular concentration.

eIF2 is an unusually complex translational GTPase, formed by the three highly conserved non-identical subunits eIF2 α , - β , and - γ [121, 122]. According to biochemical studies and crystal structure analyses of the archaeal ortholog (aIF2), eIF2 α and - β form no direct contact to each other and bind the central eIF2 γ subunit independently [31]. The γ -subunit adopts a three-domain architecture homologous to that of elongation factors EF-Tu and eEF1A, with the nucleotide binding pocket located in the G domain (domain I) [37]. Similar to other G proteins, it is thought that a/eIF2 γ undergoes structural rearrangements when switching from the inactive GDP-bound to the active GTP-bound state, initiated by conformational changes in two conserved dynamic elements of the G domain, termed switch 1 and switch 2, that are responsible for the recognition and binding of the GTP γ -phosphate [31, 33]. The α -subunit was identified as a major factor in protein synthesis control as target for phosphorylation at a universally conserved serine (Ser51) by eIF2 α kinases in response to stress conditions [78, 112]. Phosphorylation of eIF2 α is thought to convert eIF2·GDP from a substrate to a competitive inhibitor of its GEF eIF2B, thereby reducing the rate of translation initiation and thus protein synthesis in general [112, 123, 124].

eIF2B is a large protein complex of five non-identical subunits that was reported to exist as a functional decamer of ~600 kDa in solution [72, 73]. The homologous eIF2B α , - β , and - δ subunits form a regulatory subcomplex that contributes to eIF2 binding through interactions with eIF2 α [77]. These interactions are enhanced by eIF2 α -phosphorylation, thereby abrogating GEF activity by rendering phosphorylated eIF2 a competitive inhibitor of eIF2B [112]. The eIF2B γ and - ϵ subunits form the catalytic subcomplex that mediates the GEF function of eIF2B [112]. Within this catalytic subcomplex, eIF2B ϵ is the actual catalytic subunit, whose activity is stimulated by eIF2B γ .

The minimal catalytically active region within eIF2B was mapped to the C-terminal domain of eIF2B ϵ (residues 524-712 in yeast), which was shown to adopt a HEAT repeat-like domain fold homologous to that of the eIF5-CTD [1, 54, 74]. Like eIF5-CTD, the eIF2B ϵ -CTD contains two conserved aromatic/acidic motifs (AA-boxes) that interact with the lysine-rich K-boxes in the eIF2 β -NTT [35] (Fig. 1 and S1). Moreover, it was found that mutagenesis of Trp699 in AA-box 2 (corresponding to Trp391 in eIF5) confers lethality in yeast by weakening the interaction between

eIF2B ϵ and its substrate eIF2 [75]. A second interaction was mapped between the two N-terminal α -helices of eIF2B ϵ -CTD and eIF2 γ itself, which was proposed to be directly involved in the catalysis of nucleotide exchange [70, 75, 76]. This assumption was based on the observation that mutagenesis of conserved surface residues in the N-terminal α -helices, namely Thr552, Leu568, Glu569 and Ser576, caused growth defects or lethality *in vivo*, accompanied by a reduced or abolished catalytic activity of the eIF2B ϵ mutant *in vitro*. Hereby, particularly Glu569 was identified as key catalytic residue, whose mutagenesis to alanine abolishes GEF activity without affecting the affinity of the construct to eIF2 γ . However, up to now it is unknown how and in which orientation the eIF2B ϵ -CTD enters the eIF2 complex and where the interface on the eIF2 γ subunit lies. Consequently, the actual mechanism of eIF2B ϵ -catalyzed nucleotide exchange and the order of molecular events that accompany GEF-binding, GDP release and GTP rebinding are still enigmatic.

Here we used a combination of structural and biochemical methods to gain insight into the interactions between eIF2B ϵ and its substrate eIF2 to provide a better understanding of the molecular events that result in nucleotide exchange. On the one hand, we studied the interactions between eIF2B ϵ and the N-terminal tail of eIF2 β using tryptophan quenching experiments. These indicate that the eIF2 β -NTT forms a high affinity peptide-domain interaction with the AA-boxes of eIF2B ϵ -CTD very similar to that observed between eIF2 β and the eIF5-CTD (see chapter 2). On the other hand, mass-spectrometry-coupled UV-crosslinking reveals that the N-terminal end of eIF2B ϵ -CTD, containing the catalytic center, contacts the eIF2 γ subunit directly and in the immediate vicinity to the nucleotide binding pocket through an interface that overlaps with that observed for the DWEAR-motif and area III of eIF5-CTD. Finally, the effect of eIF2B ϵ on nucleotide binding and dissociation was studied using fluorescent derivatives of GDP/GTP. Together, the presented findings suggest that the eIF2B ϵ -catalyzed exchange reaction follows a successive series of reversible steps involving the formation of an intermediate unstable eIF2-GDP-eIF2B ϵ ternary complex, in which the GEF promotes nucleotide release by inducing conformational rearrangements in the nucleotide binding pocket in a manner similar to other known GEFs.

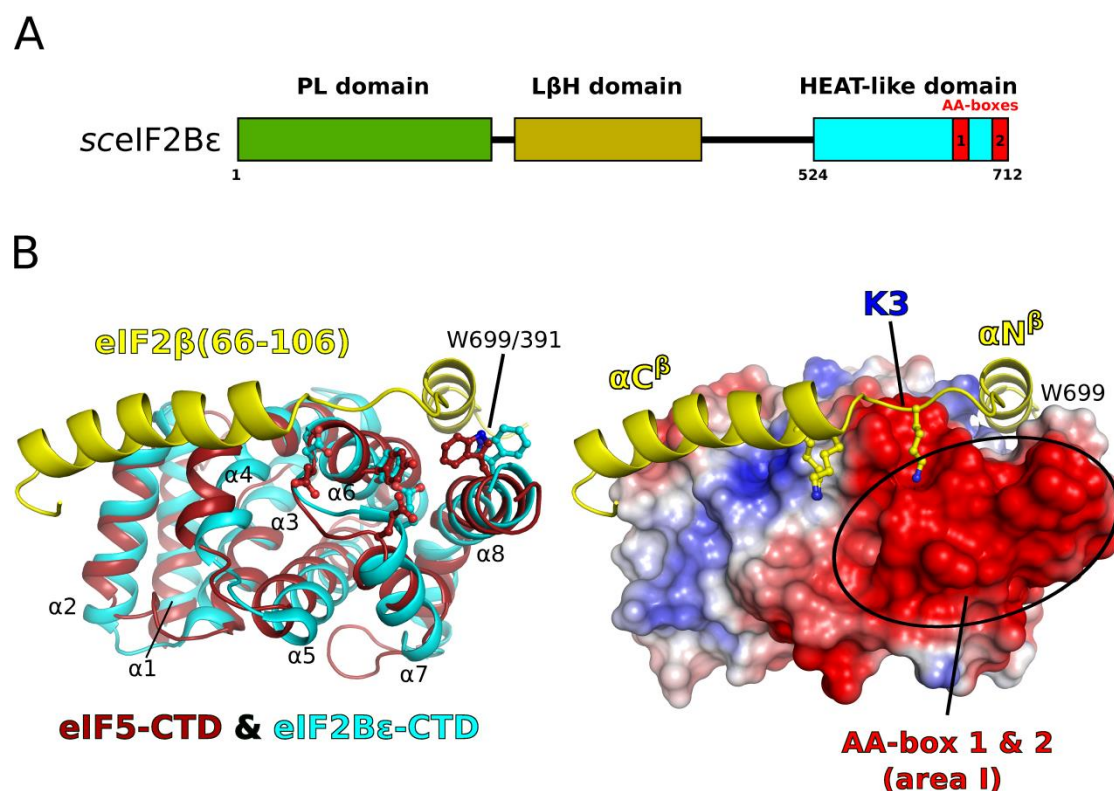


Figure 1. Structure of the eIF2Bε-CTD **A)** Schematic presentation of the proposed domain architecture in eIF2Bε with an N-terminal pyrophosphorylase-like (PL) domain, a central left-handed β-helix (LβH) domain and the C-terminal HEAT-like domain, which constitutes the minimal catalytic domain within the eIF2B complex. **B)** The left panel shows the superposition of the crystal structures of the eIF2Bε-CTD (residues 524-712, colored in cyan; PDB: 3JU1) and eIF5-CTD (red) bound to a fragment of the eIF2β-NTT (yellow) (see chapter 2). Selected conserved residues of AA-boxes 1 and 2 are shown as balls and sticks, including the homologous Trp699 and Trp391 in eIF2Bε and eIF5, respectively. As shown in the right panel, this positions K-box 3 (K3) of the eIF2β-NTT in direct vicinity to the negatively charged area I of eIF2Bε and allows an overall interaction between eIF2Bε-CTD and the eIF2β-NTT very similar to that observed for the eIF5-CTD (compare Figure 4 in chapter 2).

3.2 Results

Model of the eIF2β-NTT bound to the catalytic C-terminal domain of eIF2Bε

The minimal catalytically active domain of eIF2Bε (residues 544-712 in the *S. cerevisiae* ortholog) and the C-terminal domain of eIF5 (residues 241-405) share structural homology over the entire HEAT repeat-like fold (Fig. 1). Despite differences in the structural details [1], this homology is complemented by the presence of the two conserved AA-boxes (1 & 2) close to the C-terminal end, which form the negatively charged area I in the tertiary structure of both proteins. In both cases, this area was found to provide the primary contact surface for the K-box-containing N-terminal tail

of eIF2 β [35]. However, structural information for this interaction is so far not available for eIF2B ϵ and it is not known whether both interactions follow similar or distinct patterns.

Attempts to solve the structure of eIF2B ϵ -CTD in complex with fragments of eIF2 β -NTT analogous to those for the eIF5-CTD·eIF2 β -NTT complex (see chapter 2) were unsuccessful. Instead, part of the eIF2 β -NTT (residues 66-106; including K-box 3) was modeled onto eIF2B ϵ -CTD according to the eIF5-CTD·eIF2 β -NTT complex structure (Fig. 1B). In this model, K-box 3 comes to lie in the periphery of area I, which allows the direct contact of its lysines 83 and 89 with Tyr663, Asp666 and Glu670 in eIF2B ϵ (corresponding to Tyr351, Asp354 and Glu358 in eIF5, respectively). Moreover, the adjacent regions on eIF2B ϵ -CTD would provide mainly hydrophobic surface areas for the binding of helices α N $^{\beta}$ and α C $^{\beta}$ flanking K-box 3, complemented by salt bridges of Lys608 and Arg624 in eIF2B ϵ to acidic side chains in α N $^{\beta}$ and α C $^{\beta}$, similar to those observed in the complex with eIF5. Thus, it is conceivable from this model that the structural homology between eIF2B ϵ - and eIF5-CTD is as well reflected in their respective interaction with the fragment eIF2 β (66-106).

Contributions of the lysine-rich K-boxes 1-3 of the eIF2 β -NTT to the interactions with eIF2B ϵ .

As in the case of eIF5-CTD, eIF2B ϵ -CTD contains a universally conserved solvent exposed tryptophan residue within AA-box 2 (Trp699; Trp391 in eIF5) that was previously shown to be important for interactions with eIF2 β [74, 75]. We therefore assumed that it is possible to determine the relative contributions of K-boxes 1, 2, and 3 in eIF2 β -NTT to its interactions with eIF2B ϵ -CTD by monitoring Trp-quenching upon complex formation. Unlike eIF5(241-405) with its two tryptophan residues, the corresponding eIF2B ϵ (524-712) fragment contains five tryptophan residues. Among these, Trp618, Trp676 and Trp677 are buried within the hydrophobic core, whereas Trp696 and Trp699 lie in direct vicinity to area I on the protein surface. Surprisingly, this larger number of Trp residues did not result in a smaller quenching signal due to an increased background fluorescence by unaffected residues; instead, the addition of full-length eIF2 β or eIF2 β (1-106) to eIF2B ϵ -CTD resulted in a substantial reduction of the emission at 360 nm by ~43% (compared to ~24% for eIF5-CTD), accompanied by a slight blueshift of the emission maximum (Fig. 2). A possible explanation for this rather unexpectedly strong signal is that not only Trp699, but also the less conserved Trp696 and/or Trp677 are directly or indirectly affected by the binding

of eIF2 β . As the mutagenesis of Trp699 to alanine completely abolishes any quenching signal, most likely due to its inability to bind eIF2 β at all, and due to the potential structural role of the other residues, we were not able to determine the relative contributions of the individual Trp residues to the quenching signal. However, the fact that four of the five tryptophan residues are located in helices α 7 and α 8 in the vicinity of the negatively charged area I and Trp699, whereas the fifth tryptophan in helix α 4 is buried in the hydrophobic core suggests that area I provides the main interface for the binding of the three K-boxes.

As observed for eIF5-CTD, eIF2B ϵ -CTD binds eIF2 β (1-106) and full-length eIF2 β with similar affinities (K_d of 100 and 120 nM, respectively) and results in the same quenching signal (Table 1). The following experiments were therefore carried out with the isolated eIF2 β -NTT (residues 1-106), containing either single or double K-box mutations. The single K-box mutations exhibit only a slightly different pattern of contributions in comparison to their interactions to eIF5 (see chapter 2), with 5-, 8- and 1.8-fold reductions in binding affinity for K1 Δ , K2 Δ and K3 Δ , respectively (Fig. 2B/D and Table 1). Thus, again K-boxes 1 and 2 seem to provide the primary interface for eIF2B ϵ binding with only minor contributions by K-box 3. It is, however, interesting to note that the contribution by K-box 1 seems to be less prominent than in the eIF2 β ·eIF5 interaction, which is also reflected by the maintenance of the full quenching signal in K1 Δ . By contrast, K2 Δ results in the loss of nearly 30% of the quenching signal, while K3 Δ shows no effect – in analogy to the observations with eIF5-CTD (see chapter 2). Interestingly, the double mutants show some variations in their pattern of interactions with eIF2B ϵ -CTD compared to those observed for eIF5-CTD (Fig. 2C/D and Table 1). K12 Δ completely abolishes the quenching signal, in line with their strong respective contributions suggested by the single mutants and identical to the observation for eIF5-CTD. K23 Δ shows an entirely additive effect of the K2 Δ and K3 Δ single mutations on the binding affinity ($K_d = 1.4 \mu\text{M}$; 14-fold reduction) and quenching signal (loss of \sim 30%), suggesting that K-box 3 in the interaction with eIF2B ϵ is not able to partially compensate the loss of K-box 2 as proposed for the eIF2 β ·eIF5 interaction. The largest difference is exhibited by the K13 Δ mutation, which still conferred the full quenching signal at a \sim 12-fold reduced binding affinity ($K_d = 1.2 \mu\text{M}$), conform with additive contributions by K1 Δ and K3 Δ .

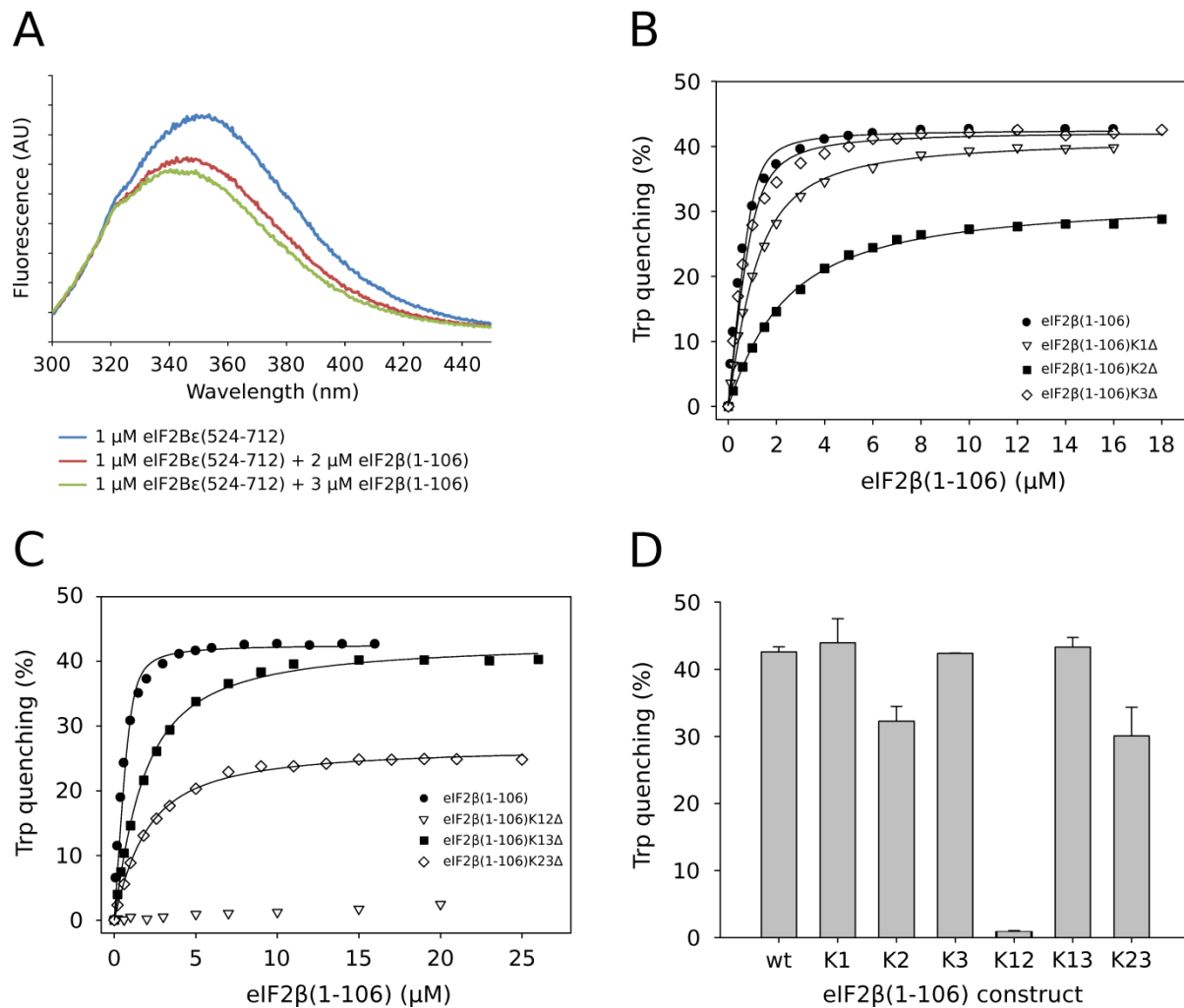


Figure 2. Trp-quenching experiments between eIF2 $\beta\epsilon$ -CTD and eIF2 β -NTT. A) Trp quenching on the eIF2 $\beta\epsilon$ -CTD by the eIF2 β -NTT. The chromatogram shows the emission spectrum of 1 μM eIF2 $\beta\epsilon$ (524-712) upon the excitation of the Trp fluorescence at 290 nm in the absence of eIF2 β -NTT (blue line) or in the presence of 2 (red) or 3 μM (green) eIF2 β (1-106). **B)** Equilibrium titrations of 0.5 μM eIF2 $\beta\epsilon$ (524-712) with increasing amounts of wild-type eIF2 β (1-106) or the three K-box mutants K1 Δ , K2 Δ , and K3 Δ . The Trp quenching signal (in % of the original fluorescence signal of eIF2 $\beta\epsilon$ (524-712)) was plotted against the concentration of the respective eIF2 β -NTT constructs. The black lines represent the fit to the data using a quadratic one-side binding model. **C)** Equilibrium titration of 0.5 μM eIF2 $\beta\epsilon$ (524-712) with wild-type eIF2 β (1-106) or the double K-box mutants K12 Δ , K13 Δ , and K23 Δ . **D)** Comparison of the Trp quenching signals for the seven eIF2 β (1-106) constructs. Standard deviations, obtained from three independent experiments, are given as error bars.

Taken together, these data suggest an interaction between the eIF2 β -NTT and eIF2 $\beta\epsilon$ -CTD similar to that with the eIF5-CTD, which is centered on the area surrounding Trp699 and area I and responsible for high affinity binding between the GEF domain and its substrate. The main

contributions for the interactions are provided by K-boxes 1 and 2, while K-box 3 plays only a subordinate role.

Table 1. Trp quenching experiments between eIF2B ϵ (524-712) and eIF2 β .

eIF2 β construct	K_d (nM)	Reduction of affinity relative to wt	Quenching signal (%)
eIF2 β (FL)wt	90 \pm 41	--	41
eIF2 β (1-106)wt	100 \pm 30	--	43
eIF2 β (1-106)K1 Δ	510 \pm 65	5-fold	44
eIF2 β (1-106)K2 Δ	830 \pm 35	8-fold	32
eIF2 β (1-106)K3 Δ	180 \pm 22	1.8-fold	42
eIF2 β (1-106)K12 Δ	N.D.		1
eIF2 β (1-106)K13 Δ	1230 \pm 430	12-fold	41
eIF2 β (1-106)K23 Δ	1400 \pm 380	14-fold	29

K_d is the equilibrium dissociation constant.

N.D., not determined due to missing quenching signal.

eIF2B ϵ -CTD contacts the γ -subunit of eIF2 directly next to the nucleotide binding pocket.

Within the eIF2B ϵ -CTD, the catalytic center was mapped to the N-terminal helices α 1 and α 2 opposite to Trp699, with Thr552, Leu568, Ser576 and particularly Glu569 as critical catalytic center residues that interact directly with the eIF2 γ -subunit [74, 75]. In order to identify the binding site for the catalytic center of eIF2B ϵ -CTD on eIF2, the photo-inducible crosslinker Bpa was introduced in various positions of eIF2B ϵ (524-712) (Asp544, Gln559, Thr572 and Met575) in the periphery of the proposed catalytic center (Fig. 3C). All four eIF2B ϵ -CTD-Bpa constructs still stimulated GDP dissociation from eIF2, however, with reduced activity when compared to the wild-type protein (Fig. S2). For the first crosslinking experiments, the heterotrimeric eIF2 complex in the presence of GDP was mixed with a 2-fold molar excess of purified eIF2B ϵ (524-712)Bpa and exposed to UV light. UV- and time-dependent crosslink bands emerged for all constructs, however, with significantly different efficiencies depending on the position of the crosslinker (Fig. 3A). According to MS-analysis, all crosslink bands migrating above the 70 kDa marker were directly to the γ -subunit of eIF2.

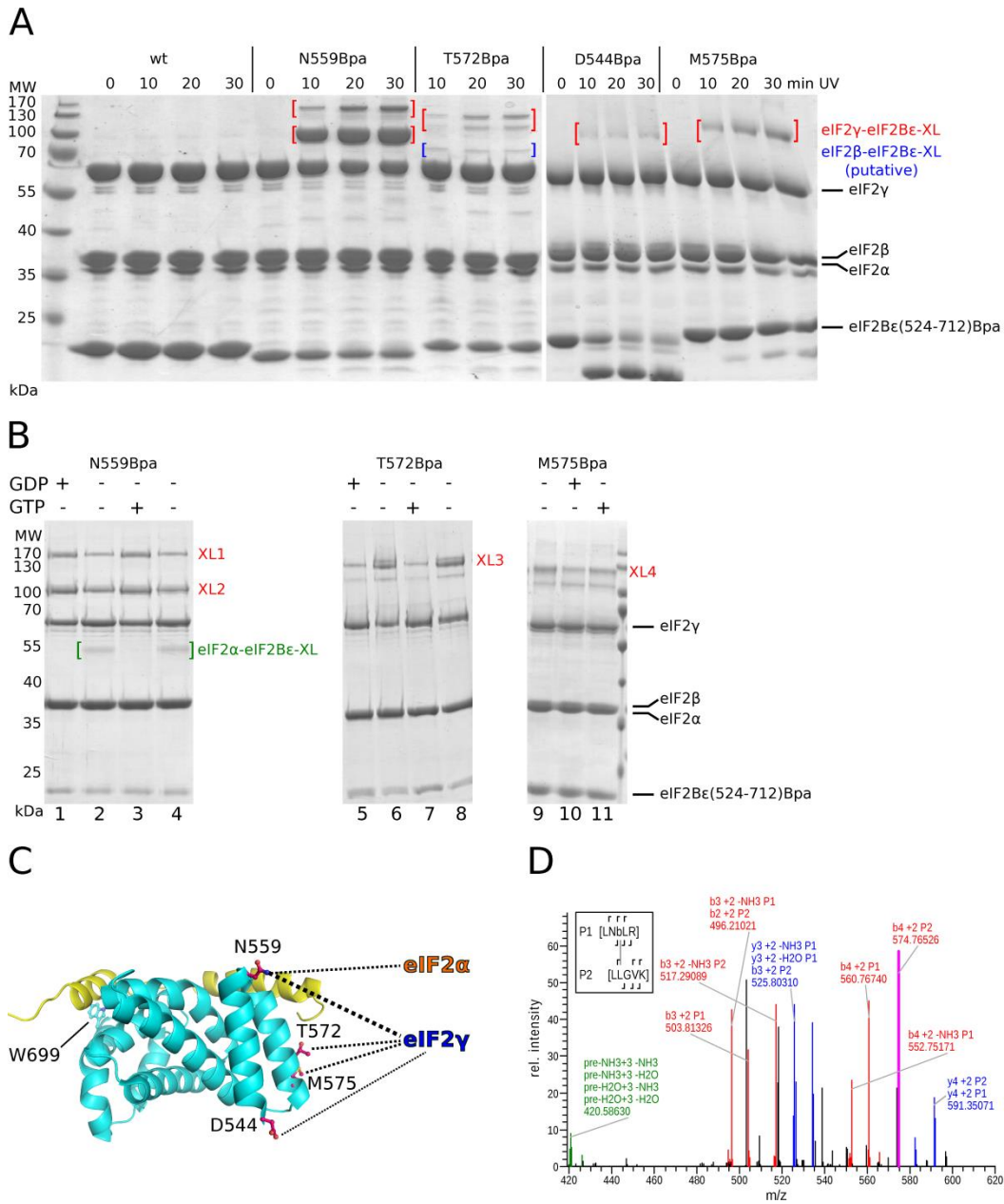


Figure 3. Mapping of the interactions between the eIF2βε-CTD and eIF2 by UV-crosslinking. A) SDS-gels showing the UV- and time-dependent formation of crosslinks between eIF2γ and the indicated eIF2βε(524-712)Bpa constructs (crosslink bands are indicated by brackets). For T572Bpa, the band migrating at ~70 kDa above eIF2γ as well occurs in a UV-dependent manner and is most likely a crosslink between eIF2βε(524-712)T572Bpa and eIF2β; an unambiguous identification of the target molecule was so far not possible. For each experiment, 2 μM eIF2 was mixed with 4 μM eIF2βε(524-712)Bpa. **B)** Nucleotide-dependency of the crosslinks between eIF2βε(524-712)Bpa and eIF2. Crosslinking experiments were carried out with 2 μM eIF2 and 4 μM eIF2βε(524-712)Bpa either in the absence of guanine-nucleotides or in the presence of 4 μM GDP or GTP. **C)** Structure of the eIF2βε(524-712) (with the eIF2β-NTT in yellow modeled as shown in Fig. 1B), indicating the positions where Bpa was introduced (pink sticks). The dashed lines indicate the crosslinks to eIF2 formed from the respective positions. **D)** High-resolution MS2 fragmentation spectra for the crosslink of N559Bpa to a target peptide in eIF2γ. A series of b and y product ions were detectable for the peptides involved in the crosslinks; the relative intensity of the observed peaks is plotted against their mass-to-charge ratio (m/z). The inset shows product ions mapped to the sequences of the crosslinked peptides; b is Bpa.

By far the most efficient crosslink was obtained for the (nearly fully active) N559Bpa construct (Fig. S2) with Bpa at the very C-terminus of helix α 1, which migrated at \sim 130 and \sim 100 kDa, respectively (both elute from the analytical size exclusion column at the same volume as the uncrosslinked eIF2·eIF2B ϵ (524-712) complex). Less efficient but still significant crosslinks to eIF2 γ were observed for T572Bpa and M575Bpa, both of which produced a stronger upper band (\sim 120 kDa) and a weaker lower band (\sim 105 kDa). The least efficient position was D544Bpa, which instead formed a strong internal crosslink.

Table 2. Crosslinks between eIF2B ϵ (524-712) and eIF2 γ .

Construct	Bpa peptide	Crosslinked peptides					
		Target peptide	Site	Mass (Da)	Error (ppm)	m/z	
N559Bpa	XL1a	AME <u>b</u> NHDLDTALLE	ADMAR	484	2285.0215	-0.1	762.3448
	XL1b	AME <u>b</u> NHDLDTALLE	ADmAR	484	2301.0157	-0.2	767.6765
	XL1c	RAME <u>b</u> NHDLDTALLE	<u>P</u> NE	458	2237.0176	-0.1	746.3440
	XL2a	GIATVERAME <u>b</u> NHD	IEIR	361	2223.0868	0.2	556.5271
	XL2a	AmE <u>b</u> NHD	IEIR <u>P</u> GIVTKD	362-367	2223.0881	5.9	556.5274
	XL2b	<u>b</u> NHD	PTLCRAD	408-411	1410.6128	1.5	705.8107
	XL2c	AmE <u>b</u> NHD	PTLCRAD	408-410	1757.7259	0.0	586.5801
T572Bpa	XL3a	LN <u>b</u> LR	LLGVK	441-443	1276.7775	-0.1	432.2674
	XL3b	LN <u>b</u> LR	LLGVKTDGQK	442-443	1806.0260	-0.7	452.2619
	XL3c	LN <u>b</u> LR	LLGVKTDGQK	440	1806.0279	0.3	456.7647
	XL3d	LN <u>b</u> LR	LLGVK	444	1276.7774	-0.2	324.4524
	XL3e	LN <u>b</u> LR	RLLGVKTDGQK	443	1980.1385	-0.2	495.7900
	XL3f	LN <u>b</u> LR	RLLGVK	444	1450.8894	0.1	363.4778
M575Bpa	XL4a	LNTLR <u>b</u> SMNVTYHE	LLGVK	442	1741.8528	-5.2	785.7448
	XL4b	<u>b</u> SMNVTYHEVRIATITALLR	HWR	509-510	2918.5253	0.2	730.3867

Target positions in the target peptides are underlined.

Using ESI-MS/MS analysis in an Orbitrap mass spectrometer, followed by an analysis of the obtained data with the StavroX software [102], we were able to identify potential target peptides for the crosslinks from positions N559Bpa, T572Bpa and M575Bpa (Table 2). For the upper band produced by N559Bpa (crosslink XL1), ⁴⁸⁰ADMAR⁴⁸⁴ and ⁴⁵⁸PNE⁴⁶⁰ were identified as potential target peptides for the crosslink (target positions are underlined). In a homology model of yeast eIF2 γ (based on crystal structures of the archaeal aIF2 γ) both peptides lie at the lower side of domain III adjacent to the cleft to domain II (Fig. 7). The crosslink-peptides for the stronger lower crosslink band (XL2) were found to lie in domain II, with ³⁶¹RPGIVTK³⁶⁷ and ⁴⁰⁸RAD⁴¹⁰ at the bottom of the β -

barrel as target sites. For the upper band of T572Bpa (XL3) ⁴⁴¹LGVK⁴⁴⁴ was identified as main target, which lies in the long flexible loop following the first β -strand of domain III, positioned directly next to the switch 2 region of the G domain (Fig. 7). The same peptide, as well as the adjacent ⁵⁰⁸HWR⁵¹⁰ in domain III could also be identified as targets for M575Bpa (Table 2). For D544Bpa, no target peptides could be clearly identified so far.

eIF2B ϵ -CTD interacts with eIF2 γ in a nucleotide-dependent manner.

An important further question was whether the crosslink pattern would change depending on the nucleotide status of eIF2. For this purpose, the experiments were repeated either in the absence or presence of excess GDP or GTP. Interestingly, N559-, T572- and M575Bpa but not D544Bpa exhibited a strong but non-uniform dependency of their crosslinks on the nucleotide status of eIF2 (Fig. 3B). For T572Bpa and M575Bpa in helix α 2, the most efficient crosslinking was observed with apo eIF2, which significantly decreased in the complex with GDP- or GTP-bound eIF2 (including XL3). The opposite tendency was observed for N559Bpa, where both crosslinks to eIF2 γ (XL1 and XL2) significantly improved in the presence of either nucleotide; only with apo eIF2 an additional crosslink from N559Bpa occurred at \sim 50 kDa at the expense of the upper eIF2 γ -containing bands, which according to MS analysis was a specific crosslink to the α -subunit of eIF2.

These results indicate that the eIF2·eIF2B ϵ -CTD complex undergoes a conformational rearrangement upon the transition of eIF2 from the nucleotide-bound to the apo state, in which the C-terminus of helix α 2 moves into a position that allows more efficient crosslinking to eIF2 γ , while the C-terminus of helix α 1 (with Gln559) moves into a position that allows less efficient crosslinking to eIF2 γ but instead provides access to the α -subunit. These rearrangements, however, are insensitive to the species of the bound nucleotide and occur with GDP and GTP alike.

Influence of eIF2B ϵ on the kinetics of guanine nucleotide binding by eIF2

To study the interactions of eIF2 with eIF2B ϵ and GDP or GTP, we used the fluorescent derivatives of GDP/GTP, mant-GDP and mant-GTP, to monitor binding and dissociation of guanine nucleotides (see chapter 2). The affinities of mant-GDP and -GTP to eIF2 in the presence of eIF2B ϵ were determined by equilibrium titrations (Fig. 4). The dissociation rate constants (k_{off}) were determined

in chase experiments with excess unlabeled GDP (Fig. 5). Finally, the bimolecular association constants (k_{on}) were estimated from K_d and k_{off} according to the relation $K_d = k_{off}/k_{on}$. Previous reports suggested that full-length eIF2B ϵ and the C-terminal fragment eIF2B ϵ (524-712) show the same level of GEF activity [70]; we therefore used the fragment eIF2B ϵ (524-712) in most experiments unless stated otherwise.

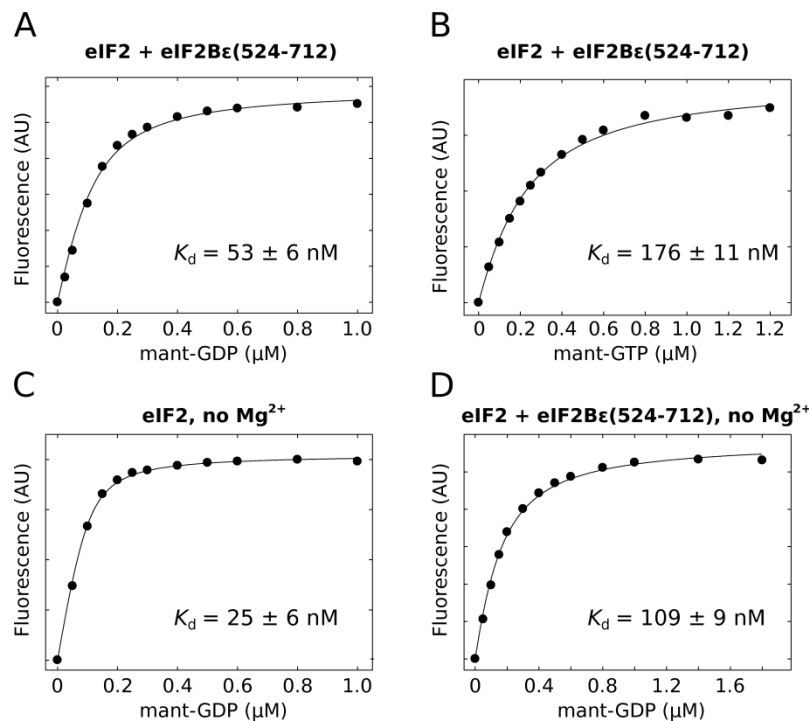


Figure 4. Influence of the eIF2B ϵ -CTD and Mg²⁺ ions on the binding of mant-GDP and mant-GTP by eIF2. A-B) Equilibrium titrations of 100 nM eIF2 with mant-GDP (A) and mant-GTP (B) in the presence of 5 μ M eIF2B ϵ (524-712). **C-D)** Equilibrium titrations of 100 nM eIF2 with mant-GDP without (C) or with (D) 5 μ M eIF2B ϵ (524-712) and in the absence of Mg²⁺. The binding reaction was monitored by FRET between eIF2 (excited at 280 nm) and the mant-group of the nucleotide (emission monitored at 440 nm). The black lines show the fit to the data, using a quadratic one-side binding model; the resulting values are summarized in Table 3.

Mant-GDP bound to the eIF2-eIF2B ϵ -CTD complex with a K_d of 53 nM and thus nearly 3-fold weaker than to the eIF2 complex alone ($K_d = 20$ nM) (Fig. 4 and Table 3). The dissociation rate constant (k_{off}) was determined to be 3.42 min⁻¹, giving an estimate for the k_{on} of 6.5×10^7 M⁻¹ min⁻¹. Thus, the eIF2B ϵ -CTD promotes the dissociation of GDP by \sim 25-fold relative to the non-catalyzed reaction (0.14 min⁻¹) under the used conditions, while simultaneously allowing a \sim 10-fold faster association (Table 3). Likewise, the affinity of eIF2 for mant-GTP was reduced \sim 6-fold from a K_d of 30 nM in the absence to a K_d of 176 nM in the presence of eIF2B ϵ -CTD. As for GDP, this reduction in affinity is accompanied by a significant increase of the dissociation rate ($k_{off} = 2.32$ min⁻¹ for eIF2 alone), which, however, could not be determined reliably due to the limitations of the used technique.

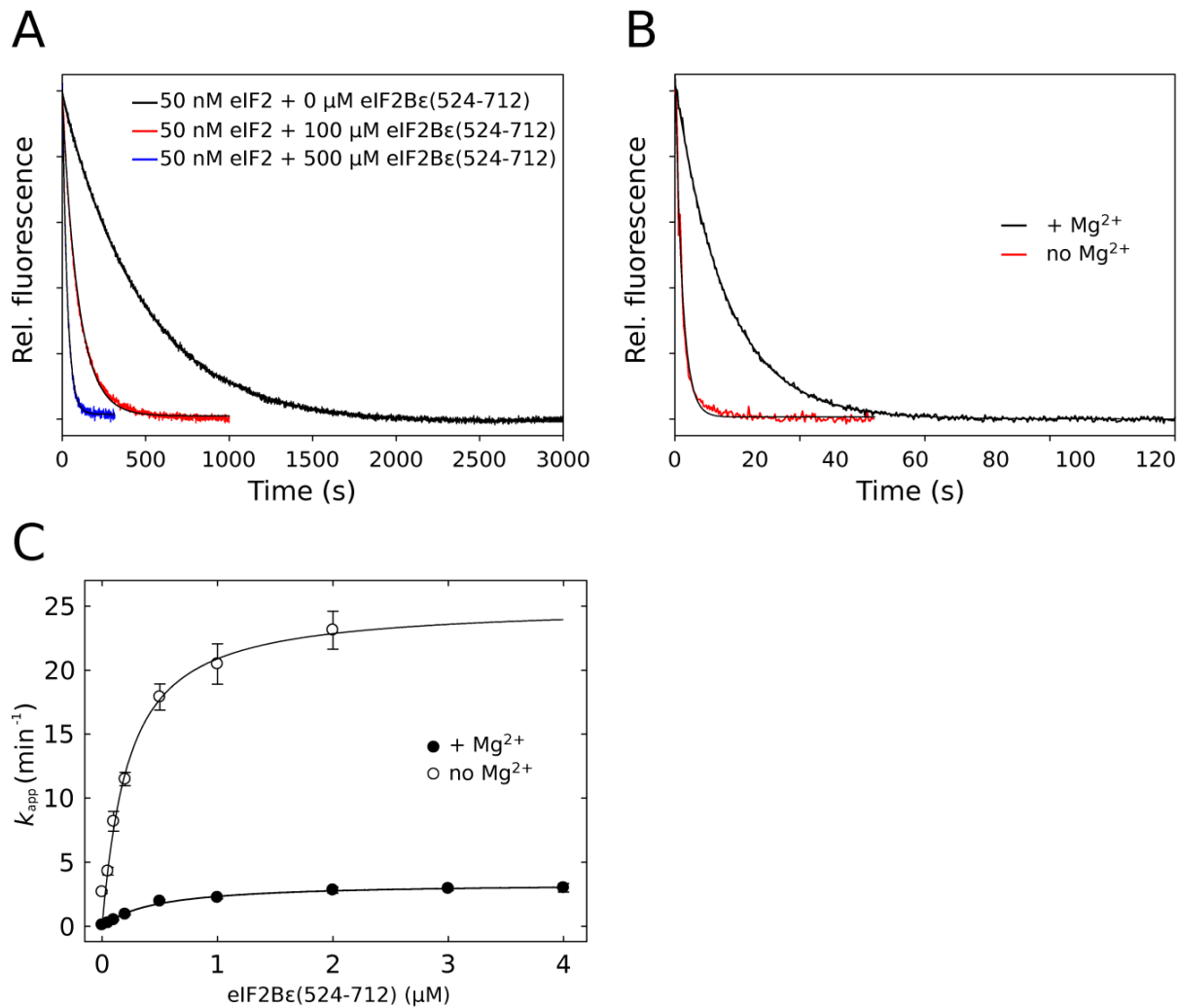


Figure 5. Effect of eIF2B ϵ (524-712) and Mg^{2+} on the dissociation of mant-GDP from eIF2. **A)** Representative time courses for the dissociation of mant-GDP from eIF2 (50 nM eIF2 with 100 nM mant-GDP and 3 μM unlabeled GDP) in the presence of 0 (black), 100 (red) and 500 nM (blue) eIF2B ϵ (524-712). The smooth black lines represent single-exponential fits which yielded the respective apparent rate constants k_{app} . **B)** Time courses for the dissociation of mant-GDP from eIF2 (50nM eIF2 with 100 nM mant-GDP and 3 μM unlabeled GDP) in the presence (black) or in the absence of 2.5 mM Mg^{2+} (red). **C)** Dependency of the dissociation of eIF2·mant-GDP (50 nM) on the concentration of eIF2B ϵ (524-712) either in the presence (closed circles) or absence of 2.5 mM Mg^{2+} ions (open circles).

To determine the approximate affinity between eIF2B ϵ -CTD and GDP-bound eIF2, the apparent off rates (k_{app}) for the dissociation of mant-GDP from eIF2 at increasing concentrations of the GEF were fitted to a quadratic equation, giving an estimate for the $K_{1/2}$ of 423 ± 53 nM (Fig. 4C), which is 2.6-fold larger than the value reported previously for similar conditions (~ 162 nM) [105].

For other GEF-catalyzed nucleotide exchange reactions it is known that the GEF contributes to the destabilization of the guanine nucleotide by destabilizing the coordination of the Mg^{2+} ion. To study the contribution of Mg^{2+} coordination to GDP binding, the affinity and dissociation rate of mant-GDP was determined in the absence of Mg^{2+} and the presence of 1 mM EDTA. Although having only a minor effect on the affinity of mant-GDP to eIF2 determined under steady-state condition ($K_d = 25$ nM), the absence of Mg^{2+} resulted in a ~20-fold increased dissociation rate ($k_{off} = 2.7$ min⁻¹). Consequently, this implies that the association rate constant (k_{on}) as well increases to 1.1×10^8 M⁻¹ min⁻¹. Addition of eIF2Bε-CTD further increased the dissociation rate by a factor of 9.4 to 25.2 min⁻¹ (7.4-fold faster than the catalyzed reaction in the presence of Mg^{2+}), accompanied by a decreased affinity ($K_d = 109$ nM) and an increased association rate constant of 3.9×10^6 M⁻¹ s⁻¹.

Table 3. Influence of eIF2Bε(524-712) on the binding of mant-GDP and mant-GTP by eIF2

	Nucl.	MgCl (mM)	k_{off} (min ⁻¹)	k_{on} (M ⁻¹ min ⁻¹) ^a	K_d (Nucl.) (nM) ^b	$K_{1/2}$ (2Bε) (nM) ^c
eIF2	mGDP	2.5	0.14 ± 0.05	7×10^6	20 ± 5	N.D.
eIF2	mGDP	0	2.7 ± 0.15	1.1×10^8	25 ± 6	N.D.
eIF2	mGTP	2.5	2.32 ± 0.11	7.7×10^7	30 ± 3	N.D.
eIF2 +						
eIF2Bε-CTD	mGDP	2.5	3.42 ± 0.21	6.5×10^7	53 ± 6	432 ± 53
eIF2Bε-CTD	mGDP	0	25.2 ± 0.	2.3×10^8	109 ± 9	195 ± 40
eIF2Bε-CTD	mGTP	2.5	N.D.		176 ± 11	N.D.

^a The bimolecular association constant was estimated according to the relation $k_{on} = k_{off}/K_d$

^b K_d is the equilibrium dissociation constant between eIF2 and mant-GDP or mant-GTP. Values for eIF2 binding to mGDP or mGTP in the presence of $MgCl_2$ are adapted from Table 4 in chapter 2.

^c $K_{1/2}$ is the apparent equilibrium dissociation constant between eIF2 and eIF2Bε(524-712), estimated from the dependency of k_{app} of mant-GDP dissociation from eIF2 on the concentration of eIF2Bε-CTD.

N.D., not determined

An intermediate ternary complex of GEF, eIF2 and the nucleotide is formed during the exchange reaction catalyzed by the eIF2Bε-CTD.

As indicated by the crosslink data, the eIF2-bound nucleotide has the ability to influence the way in which eIF2Bε is arranged relative to eIF2, without abolishing its binding. This suggests that nucleotide and exchange factor can bind simultaneously to eIF2 to form an intermediate ternary complex. To test this assumption, we titrated a given concentration of fluorescently labeled

Chapter 3

eIF2·mant-GDP with increasing amounts of the exchange factor (either full-length or the CTD alone). If the binding of GDP and GEF were mutually exclusive, the latter should be able to compete with the bound mant-nucleotide, resulting in the loss of the fluorescence signal at saturating amounts of eIF2B ϵ .

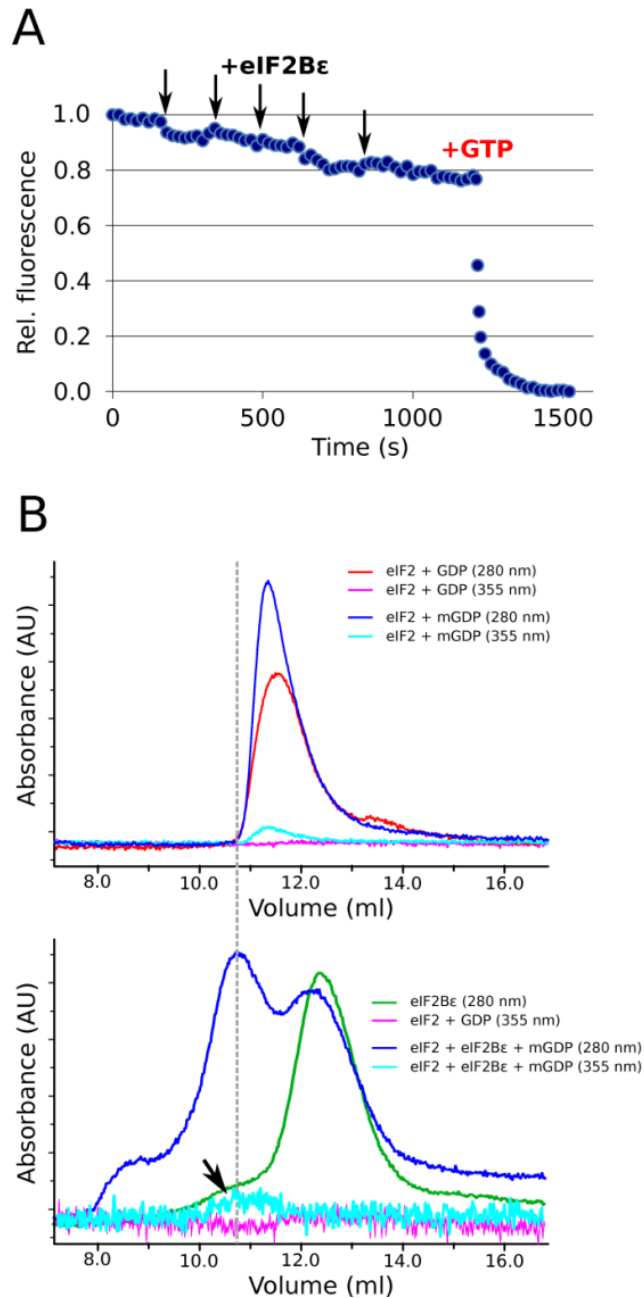


Figure 6. eIF2, guanine-nucleotide and eIF2B ϵ form a ternary complex. **A)** Titration of eIF2·mant-GDP (100 nM eIF2 with 125 nM mant-GDP) with increasing amounts of eIF2B ϵ . Each of the black arrows indicates the addition of 5 μ M eIF2B ϵ , until 25 μ M (250-fold excess) was reached. '+GTP' indicates the time point at which 10 μ M unlabeled GTP was added to the mixture. The mant-fluorescence was excited directly at 355 nm and monitored at 440 nm. **B)** Analytical size exclusion chromatography for eIF2 in complex with guanine-nucleotides and eIF2B ϵ . The upper panel shows the runs of eIF2 either with GDP (red and pink) or with mant-GDP (blue and cyan) with the absorption monitored at 280 and 355 nm. Only for the eIF2·mant-GDP complex, absorption at 280 nm (blue) and at 355 nm (cyan) is observed. The lower panel shows the complex run (blue, 280 nm; cyan, 355 nm) between eIF2·mant-GDP and eIF2B ϵ (the green curve corresponds to eIF2B ϵ alone), in which the main peak is shifted \sim 0.6 ml relative to the eIF2·mant-GDP peak (grey dashed line). In order to highlight the observed absorption by mant-GDP (arrow) in the eIF2·eIF2B ϵ containing peak, the scale for the absorption at 355 nm in the lower panel was reduced three-fold relative to that at 280 nm.

As shown in Figure 6A, eIF2B ϵ causes a slight decrease of the fluorescent signal, indicating either a direct effect on the fluorescence by the mant group or a reduction of the amount of mant-GDP bound to eIF2. After adding a 250-fold excess of eIF2B ϵ over eIF2, which should be sufficient to saturate the latter with the GEF, unlabeled GTP was added in excess to determine the ground-fluorescence of the unbound mant-GDP. According to this final signal, the addition of excess eIF2B ϵ resulted in the loss of only $\sim 20\%$ of the initial fluorescence. Consistent with the crosslinking studies, this indicates that the remaining $\sim 80\%$ originate from mant-GDP still bound to the binary complex of eIF2·eIF2B ϵ .

To further test the existence of an eIF2·mant-GDP·eIF2B ϵ ternary complex we tried to monitor it by analytical size exclusion chromatography. The binary eIF2·mant-GDP complex eluted at ~ 11.4 ml and exhibited a clear peak for the absorption at 355 nm, the excitation wavelength for the mant moiety (Fig. 6B). A corresponding absorption at 355 nm was not observed for the apo eIF2 complex or for eIF2·GDP. We then added excess eIF2B ϵ to the preformed eIF2·mant-GDP binary complex, which should yield the eIF2·mGDP·eIF2B ϵ ternary complex, and loaded it onto the column. As expected, eIF2 and eIF2B ϵ formed a complex which eluted at ~ 10.7 ml (monitored by absorption at 280 nm), corresponding to a 0.7 ml shift relative to eIF2·mant-GDP alone. Importantly, a correspondingly shifted peak was observed for the absorption at 355 nm, indicating that the eIF2·eIF2B ϵ complex still contained mant-GDP and demonstrating the existence of a ternary complex of all three components as an intermediate of the nucleotide exchange reaction (Fig. 6B).

3.3 Discussion

Implications for the mechanism of eIF2B ϵ -catalyzed nucleotide exchange on eIF2.

Like eIF2, a large number of Ras-related G proteins bind GDP with high affinity and have very low rates of spontaneous GDP release. In order to allow nucleotide exchange and thus efficient activation of the G protein for its function in biological time scales, GEFs are used to accelerate GDP release by several orders of magnitude [23, 25]. Although GEFs of different G protein families are structurally unrelated and bind to their substrates in different ways, it was found that they use common principles to destabilize the tightly bound guanine nucleotide, notwithstanding

considerable differences in the molecular details how the underlying problem is solved. Initially, GEFs bind to the GTPase·GDP complex forming an unstable ternary complex in which both, the nucleotide as well as the GEF are bound with low affinity by the G protein. In the majority of cases, GDP-destabilization is primarily achieved by deformation of the nucleotide-binding site in the two switch regions and the P-loop that are responsible for Mg^{2+} coordination and phosphate binding. Usually, the flexible switch 1 becomes displaced by the GEF through steric hindrance, while extensive contacts are formed with switch 2. As a result, switch 2 is usually remodeled in a way that allows the formation of a salt bridge between the aspartate of its conserved DXXG motif and the invariant P-loop lysine, causing the loss of critical contacts for the Mg^{2+} ion and the GDP- β -phosphate. Alternative or additional features are the introduction of side chains *in cis* by the G protein or *in trans* by the GEF that obstruct the binding sites for the Mg^{2+} ion and/or the phosphate moiety. Moreover, some GEFs distort the P-loop backbone, thereby breaking hydrogen bonds that stabilize the β -phosphate. As a consequence of these rearrangements, the GDP molecule is released more rapidly from the unstable ternary complex, followed by the formation of a stable GTPase·GEF complex. Subsequently, a GTP molecule binds, again to form an unstable ternary complex from which the GEF is finally released to yield the GTP-bound G protein [23, 25, 101]. For the exchange reaction on eIF2 it was so far unclear to what extent these basic principles of GEF activity also apply to the guanine-nucleotide exchange reaction catalyzed by eIF2B ϵ .

A structural model for the interactions between the catalytic subdomain of eIF2B ϵ and eIF2

Interactions between eIF2B ϵ and eIF2 β . Using tryptophan quenching experiments, we sought to provide a better understanding of the interaction between eIF2 β and the eIF2B ϵ -CTD, which was proposed to involve interactions between the three K-boxes in eIF2 β and the two conserved AA-boxes in the C-terminal region of eIF2B ϵ [35, 74].

Our experiments show that the eIF2 β -NTT provides a high-affinity binding site for the eIF2B ϵ -CTD within the eIF2 complex with a K_d of ~ 100 nM (Fig. 2, Table 1), in line with the proposed role as docking site for the GEF on its substrate eIF2 [35, 74]. This affinity is dependent on the presence of the three lysine-rich K-boxes, in particular K-boxes 1 and 2, consistent with the idea that ionic interactions with the negatively charged surfaces on eIF2B ϵ play a critical role in the contact. As

indicated by the location of the solvent-exposed tryptophan residues that are likely to contribute most to the quenching signal induced by K-box 2 (Trp677, 696, and 699), area I and the acidic C-terminal tail are the most likely candidates for these interactions, in line with the high degree of conservation of their acidic residues (Fig. 1B and S1). The contributions of the three K-boxes to the overall binding affinity are entirely additive suggesting that they interact with eIF2B ϵ independently from each other via a peptide-domain interaction similar to that proposed for the eIF5-CTD (see chapter 2), in which the eIF2 β -NTT does not adopt a tertiary structure upon binding, but instead adopts an extended conformation to wrap around the eIF2B ϵ -CTD. Consistently, the topology and surface charge properties of the eIF2B ϵ -CTD would be compatible with a mode of binding for K-box 3 and the adjacent α -helices α N $^{\beta}$ and α C $^{\beta}$ similar to that seen in the eIF5-CTD-eIF2 β -NTT complex structure (Fig. 1B). If so, it can be envisaged that α -helix α N $^{\beta}$ serves a similar role in the eIF2-eIF2B ϵ complex as proposed for the complex with eIF5 by prearranging the eIF2B ϵ -CTD relative to eIF2 γ in a way that promotes the direct interactions between the two proteins to mediate nucleotide exchange. This would provide an explanation why K-box 3 is highly conserved among eIF2 β orthologs, despite its relative marginal contribution to the overall affinity and despite the apparent absence of an evolutionary constraint imposed by the necessity to stabilize a tertiary structure fold.

Interactions between eIF2B ϵ and eIF2 γ . In previous studies the interface for direct eIF2B ϵ -eIF2 γ interactions was mapped to the first two α -helices of the eIF2B ϵ -CTD; however, the binding site on eIF2 γ was unknown. We could show that the short-range UV-inducible crosslinker Bpa, introduced in various positions in the periphery of the proposed interface, crosslinks specifically to the γ -subunit of eIF2 (Fig. 3). Moreover, we were able to identify specific target peptides within eIF2 γ for the crosslinks from positions Asn559, Thr572 and Met575 in eIF2B ϵ (Fig. 7, Table 2). These suggest that the eIF2B ϵ -CTD, like eIF5, contacts the frontal face of eIF2 γ , with Thr572 and Met575 in helix α 2 positioned close to residues 440-444 in domain III of eIF2 γ (green surface in Fig. 7), while Asn559 at the C-terminus of α 1 points toward residues 362-367 in domain II and the probable binding site for eIF2 α on eIF2 γ (golden surfaces in Fig. 7). Hence, this orientation would explain why Bpa in lieu of Asn559, but not Thr572 or Met575, is able to crosslink directly not only to eIF2 γ but also to eIF2 α in complexes with apo eIF2 (Fig. 3B). As a consequence,

the catalytic center residues would come to lie atop of the G3 (¹⁹⁴DCPG¹⁹⁷) motif and the switch 2-helix (helix B in EF-Tu [38]), and in the direct vicinity to the binding sites for the β- and γ-phosphates of the bound guanine nucleotide (Fig. 8).

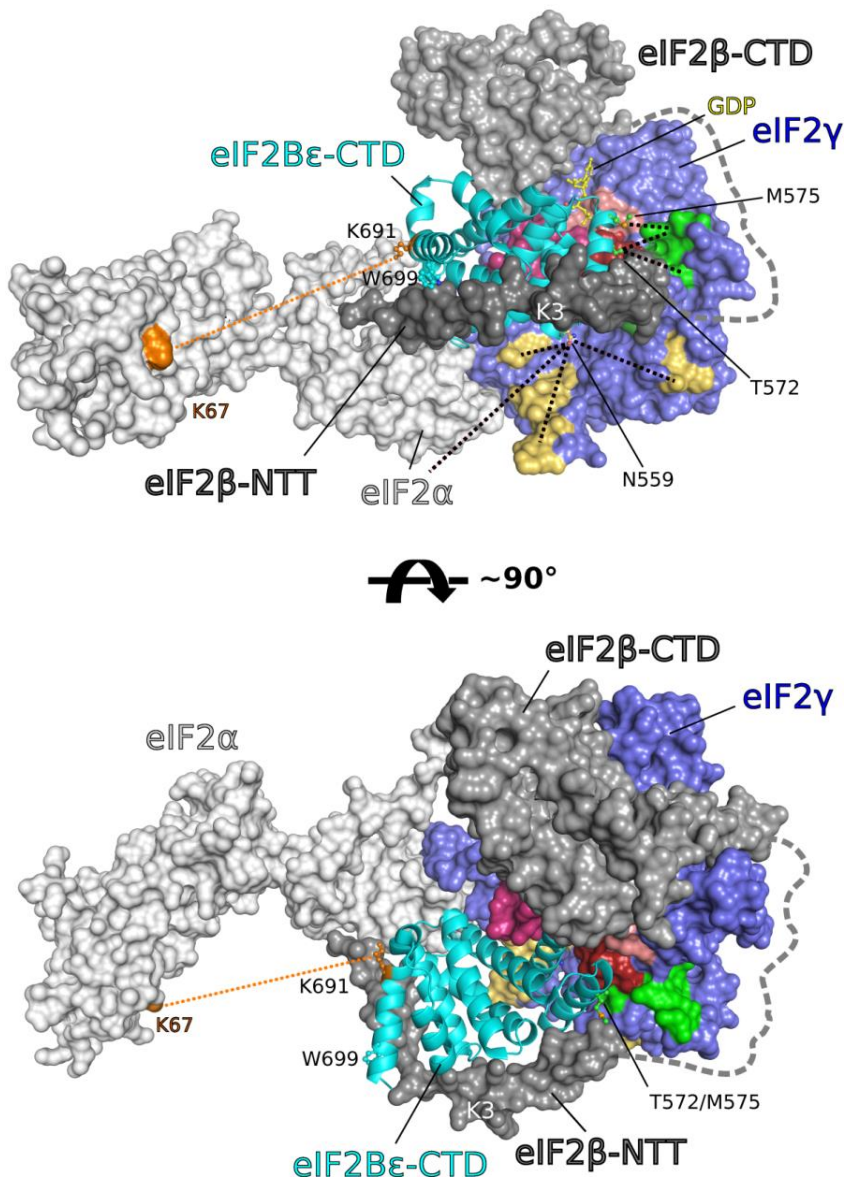


Figure 7. Model for the eIF2-eIF2Bε-CTD complex. The eIF2Bε-CTD is shown as cyan cartoon, between the eIF2β-NTT (dark grey surface) and eIF2γ (blue surface, with the GDP molecule shown as yellow sticks and P-loop, switch 1 and switch 2 in light red, wine red and dark red, respectively). Target peptides for crosslinks (black dashed lines) from positions T572/M575 and N559 are highlighted as green and dark yellow surfaces on eIF2γ, respectively. N559 is oriented toward eIF2α (light grey), as suggested by the direct crosslink observed in the absence of a bound guanine-nucleotide. The linker peptide between the eIF2β-NTT and -CTD is indicated by a thick grey dashed line next to eIF2γ. The orange dashed line between Lys67 in eIF2α (orange surface) and Lys691 on eIF2Bε (orange sticks) indicates a crosslink identified in [73]. According to this model, the eIF2Bε-CTD is clamped between the eIF2β-NTT, which provides the K-boxes for high affinity interactions in the area surrounding Trp699 (pointing away from eIF2γ), and the frontal face of eIF2γ. The putative catalytic center residues of eIF2Bε (located between T572/M575 and N559) in repeat R₁ are thereby positioned next to the nucleotide binding pocket in eIF2γ.

Under the assumption that the eIF2Bε-CTD retains its structural integrity upon binding to eIF2, and that helices α1 and α2 remain associated with the rest of the domain, the resulting

structural model predicts that the C-terminal end of eIF2B ϵ with Trp699 and area I points away from eIF2 γ , which would allow the eIF2 β -NTT to clamp the eIF2B ϵ -CTD between both eIF2-subunits (Fig. 7). As a consequence, the C-terminal end of helix αN^{β} (residues 91-103) points toward domain III of eIF2 γ , supporting the idea that helix αN^{β} might promote the direct eIF2B ϵ ·eIF2 γ interaction by prearranging the eIF2B ϵ -CTD relative to the G protein (see above). The remaining distance of 40-50 Å to helix $\alpha 1$ (residues 127-140) of the eIF2 β -CTD, which anchors eIF2 β to the eIF2 γ G domain, could be readily spanned by a flexible linker formed by the missing 23 residues. Interestingly, it was reported that within the eIF2·eIF2B complex Lys691 of eIF2B ϵ can be crosslinked to Lys67 in the N-terminal domain of eIF2 α using the chemical crosslinker BS3 (spacer length 11.4 Å) [73]. Considering the flexibility of the eIF2 α -NTD relative to the eIF2 γ -bound C-terminal domain, this finding is in excellent agreement with the proposed structural model for the eIF2·eIF2B ϵ -CTD complex, in which Lys691 points away from eIF2 γ and is thus freely accessible for the eIF2 α -NTD (Fig. 7). It should, however, be mentioned that this model is incompatible with the proposal that Trp699 is directly involved in interactions with eIF2 γ and in the catalysis of nucleotide exchange [75, 76]. Instead, our model would favor a scenario in which Trp699 is limited to a critical role in the interactions with the eIF2 β -NTT, where its loss due to mutagenesis weakens the high affinity binding to eIF2 through eIF2 β similar to the W391A/F mutation in eIF5, and thus affects the exchange activity of eIF2B ϵ merely indirectly by abolishing the efficient recruitment of the GEF.

Implications for nucleotide-exchange by eIF2B ϵ

Does the eIF2·eIF2B ϵ interaction follow the common basic principles that underlie most GEF-catalyzed exchange reactions? Positioning of the eIF2B ϵ -CTD relative to eIF2 on the basis of the crosslink data suggests that helices $\alpha 1$ and $\alpha 2$ bind eIF2 γ in the direct vicinity to helix B (switch 2) (Fig. 8). This would indeed indicate that eIF2B ϵ approaches the nucleotide binding pocket from the phosphate-binding side to form contacts to the switch 2 region, similar to those found in complexes of other G proteins with their GEFs [25]. Moreover, eIF2 forms intermediary ternary complexes with guanine-nucleotide and eIF2B ϵ (Fig. 6), however, with a reduced affinity and increased rates of dissociation for the nucleotide (Fig. 4, 5). Although the affinity between eIF2B ϵ and eIF2 γ in these complexes was not quantified directly, the crosslink pattern between the two

proteins was found to depend strongly on the nucleotide state of eIF2, without making a difference between GDP and GTP (Fig. 3B). These observations indicate that the eIF2·eIF2Bε complex undergoes a series of reversible conformational rearrangements from the GDP-bound state to the nucleotide-free state and finally to the GTP-bound state, in which the first and the last state adopt similar arrangements. It is therefore conceivable that the eIF2Bε-catalyzed exchange reaction follows a multi-step process analogous to that on other G proteins, involving two low-affinity ternary complexes, in which the GEF destabilizes the bound nucleotide and *vice versa*, as well as three high-affinity binary complexes with eIF2 bound to GDP, eIF2Bε or GTP, respectively.

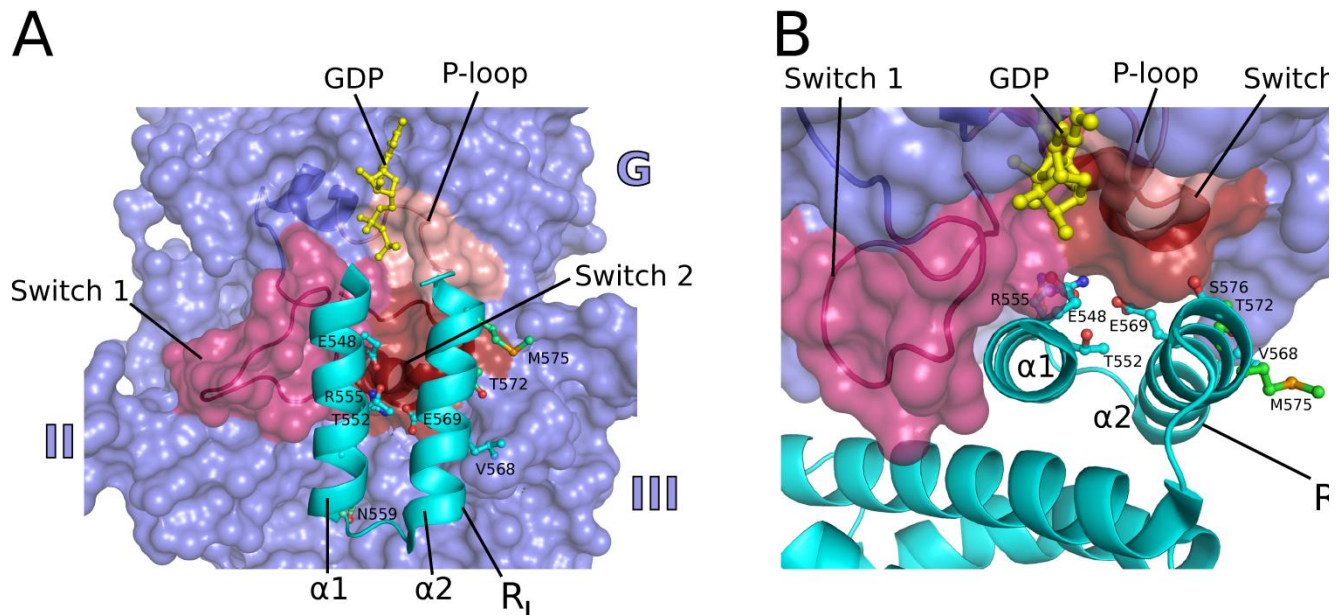


Figure 8. Detail of the modeled interactions between the eIF2Bε-CTD and eIF2γ. **A)** Front view of repeat R₁ of eIF2Bε (cyan cartoon) on the surface of eIF2γ (blue surface with the GDP molecule shown as yellow sticks; P-loop, switch 1 and switch 2 are colored light red, wine red and dark red, respectively). N559, T572 and M575 are shown as green balls and sticks. Residues that are either universally conserved and/or were reported to contribute to the exchange activity of eIF2Bε are shown as balls and sticks in cyan. **B)** Top view of eIF2Bε on the surface of eIF2γ (colored as in A).

One of the salient features of nucleotide destabilization by GEFs is the distortion of the Mg²⁺-binding site [25, 101]. In line with previous reports [125], we found that Mg²⁺ ions stabilize the binding of GDP to eIF2, resulting in a ~20-fold acceleration of GDP release in its absence (Fig. 4, 5, Table 3). The addition of eIF2Bε further accelerates GDP dissociation by ~10-fold, which

corresponds to a 7.4-fold faster GDP release relative to the GEF-catalyzed reaction in the presence of Mg^{2+} ions. This indicates that the removal of Mg^{2+} plays a role in eIF2 β -catalyzed nucleotide release, consistent with the position of helices $\alpha 1$ and $\alpha 2$ in the direct vicinity of switch 2 (Fig. 8). A possible scenario for this effect is that eIF2 β stabilizes the formation of a salt bridge between aspartate 193 of the $^{193}DCPG^{196}(G3)$ motif in switch 2 and the invariant P-loop lysine (Lys114), an interaction that is observed in the apo states and some GDP-bound forms of trGTPases which do not require specialized GEFs, as well as in structures of the eIF2 γ -orthologs eEF1A and EF-Tu in complexes with their respective GEFs eEF1B α and EF-Ts [126, 127].

As indicated by the acceleration of GDP release by eIF2 β in the absence of Mg^{2+} ions, further contributions seem to arise from the deformation of the nucleotide-binding site itself. An interesting observation in this context is that GTP as well as GDP stabilize switch 1 in a way that protects it from proteolytic cleavage (Fig. S3). Thus, efficient GDP destabilization by eIF2 β might require the displacement of switch 1 from the nucleotide binding site. According to the structural model presented in Figure 8, helix $\alpha 1$ could function as a wedge that intercalates between switch 1 and switch 2 and thereby displaces the former, similar to helix $\alpha 14$ of SOS1 in its complex with Ras (PDB: 1BKD). Notably, this positions the highly conserved Glu548 and the catalytically relevant Glu569 close to switch 2 and the Mg^{2+} and phosphate-binding sites, similar to Glu942 in SOS1. At the same time, the invariant Arg555 comes to lie close to the N-terminus of the switch 2-helix, which would allow a stabilizing contact to the invariant Asp198 in switch 2 following the $^{193}DCPG^{196}(G3)$ motif. This might be relevant, as one reoccurring feature of complexes between G proteins and their GEFs is the stabilization of switch 2 by a conserved acidic residue following the G3 (DXXG) motif through ionic interactions with the GEF [128, 129].

Taken together, the proposed placement of eIF2 β -CTD relative to the nucleotide binding site on eIF2 γ places the highly conserved catalytic center residues of the GEF within contact distance to the switch regions and the P-loop and is thus compatible with their direct involvement in GDP release. It should be noted that single mutations of most of the conserved residues within helices $\alpha 1$ and $\alpha 2$, including Glu458 and Arg555, were not found to have a detectable negative impact on yeast cell growth [74, 75]. However, is it in our opinion likely that similar to the mechanism of EF-Ts-catalyzed GDP release on EF-Tu [130], most of the individual interactions

between eIF2 and eIF2B ϵ contribute only marginally to the overall nucleotide release efficiency, but instead contribute synergistically to bring about the GDP destabilization required for its efficient release.

Due to the low resolution of our structural model for the eIF2·eIF2B ϵ complex based on the crosslink data, the assumptions about the contributions by eIF2B ϵ to nucleotide exchange and the involvement of specific residues are necessarily tentative and remain speculative. However, our data clearly favor a mechanism of eIF2B ϵ -induced nucleotide exchange that proceeds via a successive series of reversible steps and the distortion of the Mg²⁺ and phosphate binding sites by the remodeling of the switch regions and/or the P-loop. Hence, our data support the idea that the eIF2B ϵ -CTD-catalyzed exchange reaction follows the common basic principles of nucleotide exchange known from other GEFs.

Implications for the evolution of the C-terminal domains of eIF2B ϵ and eIF5 and their interactions with eIF2

Within the family of trGTPases, only four factors, namely eIF2 and the homologous EF-Tu, eEF1A, and aEF1A, are known to have dedicated protein-GEFs that catalyze nucleotide exchange. For all other trGTPases no GEFs are known, which is consistent with their usually low affinities for GDP and its fast dissociation rates (with the possible exception of RF3, for which the ribosome itself was proposed to act as GEF [131]). In this context, it is interesting to note that all four GEF-dependent trGTPases belong to the same monophyletic clade, with eIF2 γ most likely derived from the EF-Tu lineage [22]. An obvious conclusion would be to expect a common evolutionary history for the respective GEF functions as well. However, this is not the case. All three GEFs, namely EF-Ts, a/eEF1B and eIF2B ϵ , share no mutual sequence or structural homology, and at least for EF-Ts and eEF1B it is known that their structural differences are reflected in very different ways by which they approach and bind their respective substrate trGTPases [126, 127]. Moreover, no GEF is known for the archaeal eIF2 ortholog aIF2. Thus, it seems evident that the catalytic activity of eIF2B ϵ -CTD evolved after the divergence of the archaeal and eukaryal lineages and independently from EF-Ts or a/eEF1B. Similarly, no structural or functional counterpart for the eIF5-CTD is known from archaea, likewise implying a relatively recent evolutionary history.

From the data presented here, it becomes evident that eIF2B ϵ -CTD and eIF5-CTD share two critical interactions with eIF2: On the one hand the high affinity interaction between the conserved AA-boxes and the K-boxes in the eIF2 β -NTT. On the other hand the direct interaction to overlapping interfaces on the frontal face of eIF2 γ , which in both cases involve the regions surrounding repeat R₁ of the HEAT repeat-like fold and which have direct, though opposing, effects on the nucleotide binding properties of their common substrate eIF2 γ . In light of the similarity of these interactions, combined with the structural and partial sequence homology between both proteins (Fig. S1), it is conceivable that eIF2B ϵ -CTD and eIF5-CTD share a common evolutionary origin in an AA-box-containing protein, which already bound eIF2 in a manner similar to the extant proteins and modulated its nucleotide binding properties – although this does not necessarily imply physiological relevance of this effect, similar to the suggestion for eIF5 (see chapter 2). Unfortunately, due to the low degree of sequence conservation between eIF2B ϵ -CTD and eIF5-CTD, their apparently ubiquitous distribution among eukarya, and the absence of homologs in archaea or bacteria which could be used as outgroups for a phylogenetic analysis, it is currently not possible to determine whether the ancestral protein was more eIF5- or eIF2B ϵ -CTD-like, which would provide valuable insight into the process of evolution of the complex eukaryal initiation apparatus.

It has previously been noted that with the exception of the two AA-boxes, eIF5-CTD and eIF2B ϵ -CTD share very little sequence similarity (Fig. S1), which further extends to the details of the overall charge distribution and structural characteristics of the surfaces of both proteins, even in the area surrounding the two AA-boxes [1]. This divergence of sequence and structure in regions that are directly involved in an apparently highly conserved interaction with the eIF2 β -NTT might be surprising at first sight. However, an explanation is provided by the proposed mode of peptide-domain interaction between eIF2 β -NTT and eIF2B ϵ -CTD or eIF5-CTD, respectively. For the eIF2 β -NTT it was proposed that the absence of any obvious sequence conservation outside the K-boxes is due to the absence of any evolutionary constraint that would be imposed by the necessity to adopt a stable tertiary structure fold for interactions with eIF5 or eIF2B ϵ (chapter 2). Similarly, the peptide-domain interaction would also release the peptide-binding sites on both proteins from the evolutionary constraint, which would be imposed by a structurally rigid domain as common

interaction partner for both C-terminal domains. The intrinsically flexible eIF2 β -NTT would not require an in sequence and structure highly conserved interface on both proteins, but instead allows relatively rapid divergence of its two interaction partners. Consistent with this proposal of rapid evolution for eIF2 β -CTD and eIF5-CTD, both proteins show a low degree of sequence similarity not only between each other, but also within each of the two lineages themselves.

3.4 Materials and Methods

Cloning

The DNA fragment corresponding to the open reading frame of eIF2 β (encoded by the *GCD6* gene in *S. cerevisiae*) or truncations thereof were amplified by PCR using yeast genomic DNA as template and a corresponding pair of primers. Cloning, mutagenesis and verification of the different plasmids used in this study were performed as described in chapter 2 (page 69).

Protein expression and purification

Expression of the various constructs and the purification of eIF2 β and eIF2 was performed as described in chapter 2 (pages 70-73).

Purification of eIF2 β -CTD constructs: All C-terminal eIF2 β constructs (residues 524-712), including those containing Bpa, were expressed as GST-fusion protein and purified according to the protocol for the eIF5-CTD constructs described in chapter 2 (page 71).

Purification of full-length eIF2 β : Full-length eIF2 β was expressed without affinity tag. Cell lysis was carried out as described (chapter 2, page 70) in L-150 buffer (150 mM NaCl, 20 mM HEPES (pH 7.5), 5% glycerol, 1 mM EDTA, 4 mM β -mercaptoethanol) supplied with a mixture of protease inhibitors including aprotinin, leupeptin, pepstatin (ALP), and PMSF. The cleared lysate was applied to a Q Sepharose (GE Healthcare) and bound nucleic acids and proteins, including eIF2 β , were eluted with a linear gradient into high salt buffer (1 M NaCl, 20 mM HEPES (pH 7.5), 5% glycerol, 4 mM β -mercaptoethanol). Fractions containing the target protein were pooled and ammonium sulfate added to a final concentration of 1 M. The sample was then loaded onto a phenyl-sepharose column (GE Healthcare) equilibrated in 200 mM NaCl, 1 M (NH₄)₂SO₄, 20 mM HEPES (pH 7), 5% glycerol, 4 mM β -mercaptoethanol. While the flow through contained mainly DNA or RNA,

eIF2B ϵ remained bound to the column and could be eluted with a linear gradient in low salt buffer containing 50 mM HEPES (pH 7.5), 5% glycerol and 4 mM β -mercaptoethanol. Peak fractions containing eIF2B ϵ were pooled and applied to a Superdex S-200 equilibrated in GF-150 buffer. The concentrated protein was flash-frozen in liquid nitrogen and stored at -80 °C.

UV Crosslinking Experiments with Bpa and analysis by mass spectrometry

Crosslinking experiments and the subsequent analysis of the formed crosslinks by mass-spectrometry were performed as described in chapter 2 (pages 76-78).

Steady-State Fluorescence Measurements

All experiments were carried out on a Fluoromax-3 spectrophotometer (Jobin Yvon Inc., USA) using a quartz cuvette (Hellma Analytics, Germany). All reactions were done at 20 ± 1 °C in the standard reaction buffer (100 mM KCl, 20 mM Tris/HCl (pH 7.5), 3 mM MgCl₂ and 2 mM DTT).

The binding of eIF2 β to eIF2B ϵ -CTD was monitored by tryptophan quenching experiments. Tryptophan fluorescence in eIF2B ϵ -CTD was excited at 280 nm, resulting in an emission at 350 nm, which was quenched upon the addition of eIF2 β (full-length and N-terminal domain fragments). Equilibrium dissociation constants (K_d) for the complexes were determined by titrating eIF2B ϵ -CTD with increasing amounts of eIF2 β , until saturation was reached. The residual fluorescence signal produced by eIF2 β (which contains no tryptophan) alone was determined by blank-titrations into buffer and subsequently subtracted from the binding data.

The binding of mant-labeled guanine nucleotides to eIF2 was monitored either by direct excitation at a wavelength of 355 nm or by Foerster Resonance Energy Transfer (FRET) from tryptophan residues excited at 280 nm and an emission wavelength of 440 nm. Fluorescence emission spectra were recorded after incubating the eIF2·mant-nucleotide complexes for 5 min at 20 °C. To estimate the equilibrium dissociation constants (K_d) for eIF2·mant-nucleotide complexes in presence or absence of eIF2B ϵ , the fluorescence of increasing amounts of mant-nucleotides was measured either in buffer alone or in the presence of 200 nM of eIF2 complex. The dilution was less than 1%. To form eIF2·eIF2B ϵ complexes, eIF2B ϵ was added to eIF2 in a 20-fold molar excess and incubated for 10 min at 20 °C prior to the experiment.

Titration of eIF2·mant-GDP with eIF2Bε were carried out by adding increasing amounts of the GEF to 1 ml of 100 nM eIF2·mant-GDP. The solution was carefully mixed and the fluorescence signal at 440 nm (after excitation at 355 nm) measured until a stable value was obtained. At the end of the titration a 200-fold excess of unlabeled GDP was added to determine the contribution of the unbound mant-GDP to the observed fluorescence signal.

Assuming a one-site binding model for all studies reactions, the data obtained from equilibrium titrations were analyzed according to a quadratic binding model:

$$F = F_0 + \Delta F_{\max} \frac{(X + Y + K_d) - \sqrt{(X + Y + K_d)^2 - 4XY}}{2X}$$

where F is the fluorescence signal of the mant-nucleotide in the absence or presence of eIF2, F_0 is the initial fluorescence signal, ΔF_{\max} is the maximum fluorescence signal, X is the total concentration of eIF2, Y is the total concentration of the added mant-nucleotide and K_d is the equilibrium dissociation constant. For the determination of the apparent equilibrium dissociation constants of eIF2·mant-GDP to eIF2Bε, the above equation was modified as follows:

$$k_{\text{app}} = k_a + (k_b - k_a) \frac{(X + Z + K_{1/2}) - \sqrt{(X + Z + K_{1/2})^2 - 4XZ}}{2X}$$

Here, k_{app} is the characteristic apparent rate constant of the mant-nucleotide from eIF2 in the presence of a specific concentration of eIF2Bε (see below), Z is the concentration of eIF2Bε, k_a is the dissociation rate constant of mant-GDP from eIF2 alone, k_b is the dissociation rate constant of mant-GDP from eIF2 in the presence of saturating concentrations of eIF2Bε and $K_{1/2}$ is the concentration of eIF2Bε at which their respective half maximal effect on the dissociation rate of mant-GDP from eIF2 is reached (the apparent equilibrium dissociation constant). Data evaluation was done with the SigmaPlot software.

Pre-Steady-State Fluorescence Measurements

Pre-Steady-State experiments were carried out on a Fluoromax-3 spectrophotometer using a quartz cuvette with stirring magnet to allow fast mixing of the reacting components. All reactions were done at 20 ± 1 °C in standard reaction buffer. The fluorescence of mant-nucleotides was

excited either directly at 355 nm or via FRET from tryptophan residues excited at 280 nm and monitored at an emission wavelength of 440 nm.

To study the dissociation of nucleotides, 50 nM eIF2·mant-GDP or eIF2·mant-GTP complex was formed by adding 100 nM of the respective mant-nucleotide to 50 nM nucleotide-free eIF2, followed by an incubation for 10 min at 20 °C. To start the reaction, unlabeled GDP was added in excess and the decrease in mant-fluorescence was monitored over time. The data were evaluated by fitting to a single exponential function with the equation:

$$F(t) = F_o + Ae^{-k_{app}t}$$

where $F(t)$ is the fluorescence at time t , F_o is the final fluorescence signal, k_{app} is a characteristic apparent time constant and A is the amplitude. The data evaluation was done with the SigmaPlot software.

Interaction studies using analytical size exclusion chromatography

Complex formation between nucleotide-bound eIF2 and eIF2B ϵ was studied by size exclusion chromatography on an analytical Superdex S-200 (10/300) column (GE Healthcare). For runs without eIF2B ϵ , 50 μ g eIF2 complex was incubated for 5 min at 20 °C with 1 mM guanine nucleotide (GDP or mant-GDP) in a total volume of 300 μ l reaction buffer (100 mM KCl, 20 mM Tris/HCl (pH 7.5), 3 mM MgCl₂ and 2 mM DTT). To study complex formation between nucleotide-bound eIF2 and eIF2B ϵ , 50 μ g of preincubated eIF2·nucleotide complexes were incubated for an additional 5 min at 20 °C in the presence of 60 μ g of full-length eIF2B ϵ resulting in a ~2-fold molar excess of the GEF over eIF2. The samples were then loaded onto the column, equilibrated in reaction buffer at 20 °C. The run was monitored at absorption wavelengths of 280, 254 and 355 nm.

3.5 Supplementary information

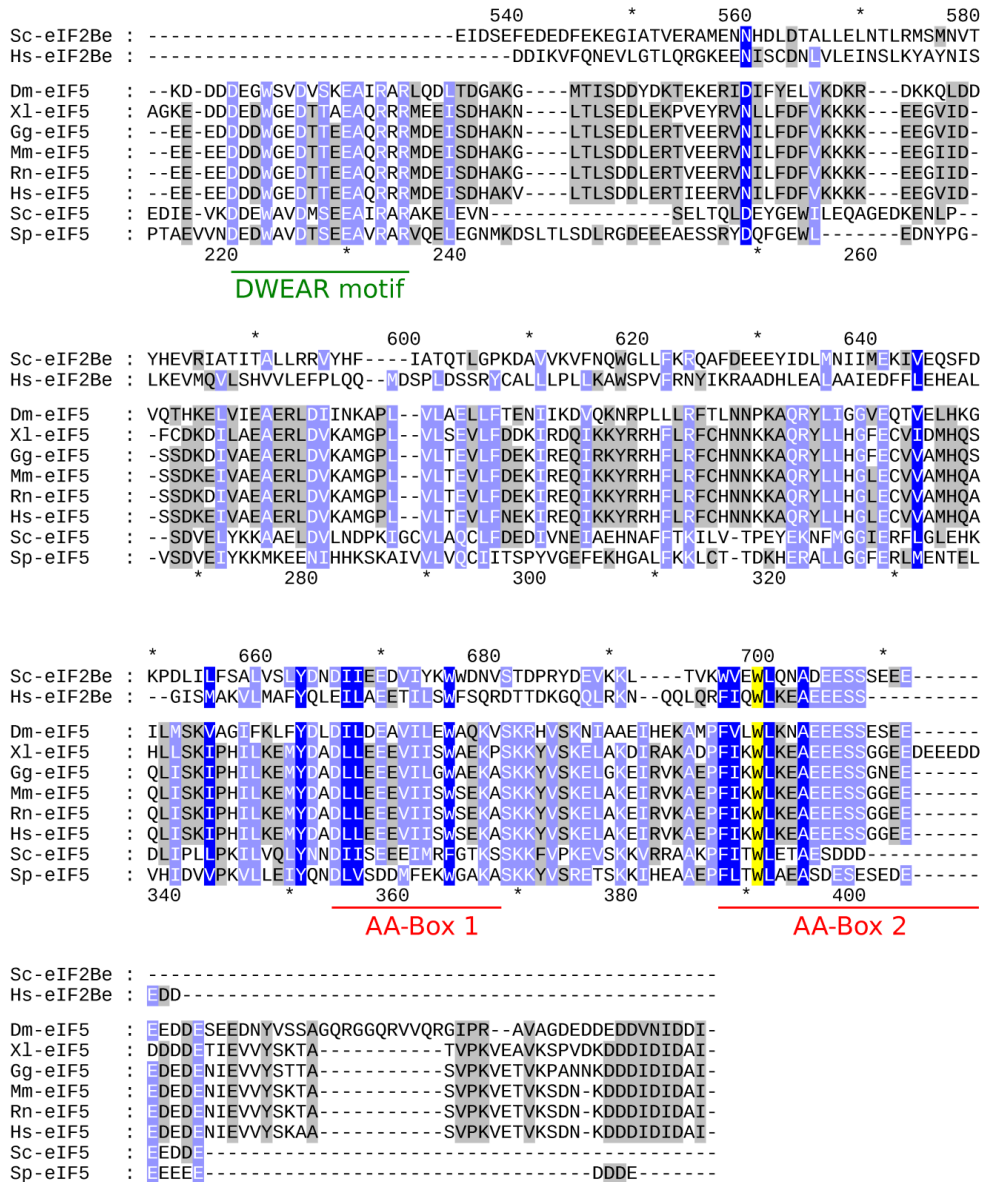


Figure S1. Multiple sequence alignment of the eIF5-CTD with eIF2Bε-CTD. Residues conserved between both proteins are highlighted in dark blue, conserved residues in light blue and variable residues in grey; the universally conserved Trp391 (eIF5) and Trp699 (eIF2Bε) in AA-box 2 is highlighted in yellow. The numbering above the alignment corresponds to the yeast ortholog of eIF2Bε (Sc-eIF2Be), the numbering below the alignment corresponds to the yeast ortholog of eIF5 (Sc-eIF5). The DWEAR motif and AA-boxes 1 & 2 are indicated below the alignment. Sc, *Saccharomyces cerevisiae*; Hs, *Homo sapiens*; Dm, *Drosophila melanogaster*; Xl, *Xenopus laevis*; Gg, *Gallus gallus*; Mm, *Mus musculus*; Rn, *Rattus norvegicus*; Sp, *Schizosaccharomyces pombe*. The alignment was initially generated using the clustal omega algorithm and subsequently corrected manually according to the structural alignment between the yeast orthologs of eIF5-CTD and eIF2Bε-CTD (PDB: 1PAQ).

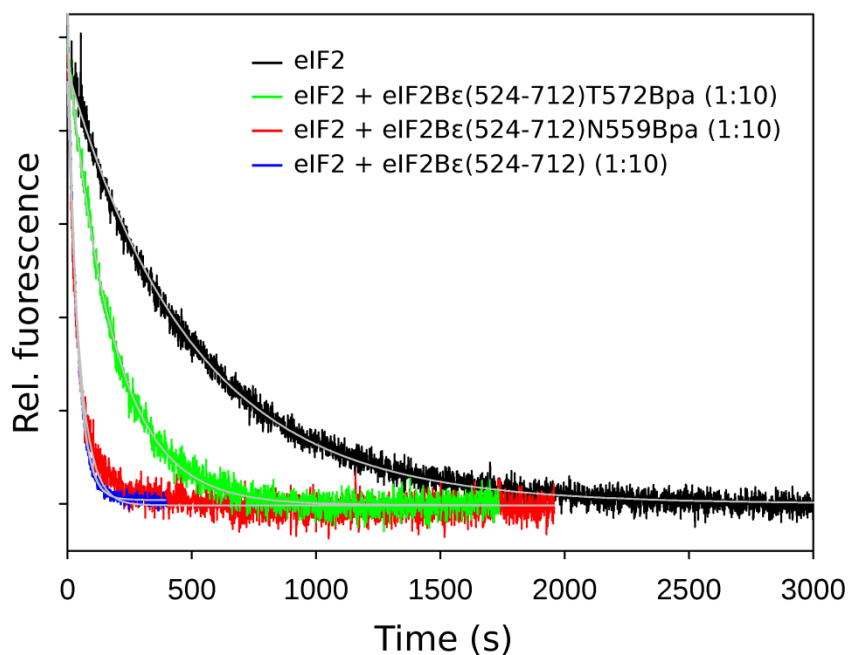


Figure S2. Influence of Bpa mutations on the guanine-nucleotide exchange activity of eIF2Bε-CTD. Time courses for the dissociation of mant-GDP from eIF2 (50 nM eIF2 with 100 nM mant-GDP and 3 μM unlabeled GDP) in the absence of eIF2Bε (black) and in the presence of 500 nM eIF2Bε(524-712)T572Bpa (green), eIF2Bε(524-712)N559Bpa or eIF2Bε(524-712). The smooth black lines represent single-exponential fits which yielded the apparent rate constants (k_{app}) of 0.135 min⁻¹ for eIF2 alone and 0.77 min⁻¹, 1.8 min⁻¹, and 2.3 min⁻¹ for eIF2 with eIF2Bε(524-712) T572Bpa, N559Bpa or wt, respectively.

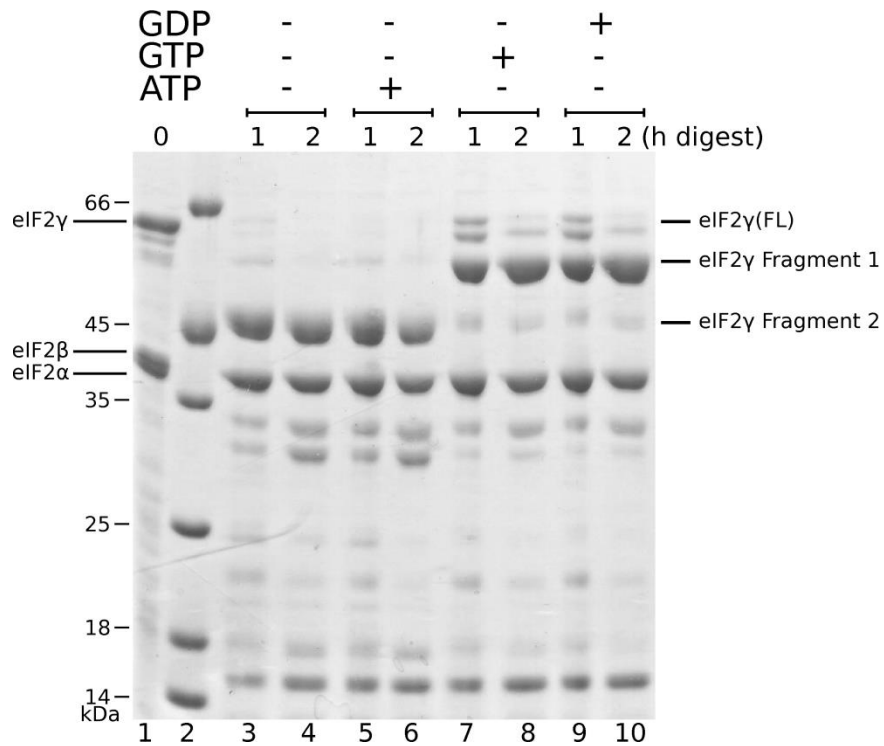


Figure S3. Influence of GDP and GTP on the limited proteolysis of eIF2 by thermolysine. Depending on the presence or absence of GDP and GTP (20-fold excess over eIF2), full-length eIF2 γ (lane 1; running at ~65 kDa) is cleaved either into a fragment running at ~55 kDa (fragment 1) or a fragment running at ~46 kDa (fragment 2). According to MS-analysis, these fragments originate from a cleavage either in front of the G domain (fragment 1) or within switch 1 (fragment 2). While ATP, like in apo eIF2, is unable to protect switch 1 from proteolytic cleavage, GDP and GTP both stabilize switch 1 in a conformation that is not accessible to thermolysine. The cleavage reaction was performed for the indicated time (in hours) in 100 mM KCl, 20 mM Tris (pH 7.5), 5% glycerol, 2.5 mM MgCl₂, 1 mM DTT at 20 °C and in the presence of thermolysine at a ratio of 1:10,000 (w/w) relative to eIF2.

Chapter 4 • Structural analysis of eIF2B β and eIF2B δ

This manuscript is in preparation for submission

Crystal structures of eIF2B β and eIF2B δ provide new insights into the regulatory subcomplex of eIF2B, the guanine nucleotide exchange factor for eIF2

Bernhard Kuhle^{1,§} and Ralf Ficner¹

¹ Abteilung für Molekulare Strukturbiologie, Institut für Mikrobiologie und Genetik, Göttinger Zentrum für Molekulare Biowissenschaften, Georg-August-Universität Göttingen, D-37077 Göttingen, Germany

§ To whom correspondence should be addressed: bkuhle@gwdg.de

Author contributions:

BK: designed the study and conceived the experiments; performed cloning, protein purification, crystallization, data collection and structure determination; analyzed and interpreted the data; wrote the manuscript. RF: design of the study; helped to draft the manuscript.

Abstract

The eukaryal translation initiation factor 2B (eIF2B) acts as guanine nucleotide exchange factor (GEF) for eIF2 and forms a central target for pathways regulating translation initiation. eIF2B consists of five non-identical subunits (α - ϵ), which assemble into a catalytic subcomplex (γ and ϵ) that catalyzes nucleotide exchange on eIF2 and a regulatory subcomplex (α , β and δ) that regulates eIF2B function under stress conditions by tight binding of eIF2. Here, we provide new structural insight into the regulatory subcomplex of eIF2B from the fungus *Chaetomium thermophilum*, obtained by its *in vitro* reconstitution from the individually purified subunits and by solving the first high-resolution crystal structures of eIF2B β and eIF2B δ . These structures confirm the proposed structural homology between the three regulatory subunits, but at the same time reveal critical differences that may be relevant for the assembly of the eIF2B $\alpha\beta\delta$ complex. Based on the presented findings, we propose a structural model for the eIF2B regulatory subcomplex, which constitutes a vantage point for further structural and functional studies on eIF2B.

4.1 Introduction

The initiation of ribosomal protein synthesis in eukarya is a highly regulated process, which requires the concerted action of at least twelve different auxiliary protein factors, called eukaryal translation initiation factors (eIFs) [12]. One of the central hubs for translational regulation during the initiation phase is the eukaryal translation initiation factor 2B (eIF2B), which functions as guanine nucleotide exchange factor (GEF) for eIF2 to regenerate the latter in its GTP-bound form [80, 112].

The translation initiation cycle in eukarya starts when GTP-bound eIF2 specifically forms a ternary complex (TC) with methionylated initiator tRNA (Met-tRNA_i) and, supported by other eIFs, delivers it to the P-site of the 40S ribosomal subunit to form the 43S pre-initiation complex (pre-IC). The 43S pre-IC is subsequently recruited to the 5'-end of an mRNA to be translated and enters the scanning phase of translation initiation, during which it searches the 5'-untranslated region (5'-UTR) of the mRNA for the start site of translation. Upon recognition of the correct AUG start codon, eIF2 hydrolyzes the bound GTP and dissociates from the pre-IC in its GDP-bound form. For a new round of translation initiation eIF2 has to be recycled back into its 'active' GTP-bound form.

Due to the high affinity of the eIF2·GDP complex and the low rate of spontaneous GDP release, the exchange of GDP for GTP on eIF2 depends on the catalytic activity of the GEF eIF2B [12, 112].

Consistent with this central position in the guanine-nucleotide cycle of eIF2, eIF2B is one of the main targets for global regulation of translation in eukarya [132]. The best characterized mechanism to control eIF2B activity is the phosphorylation of serine 51 (S51-P) in the α -subunit of eIF2 (eIF2 α) by kinases in response to stress or starvation conditions [78-80]. eIF2 α phosphorylation results in a significantly increased affinity of eIF2(α -P) for eIF2B, thereby converting eIF2 from a substrate into a competitive inhibitor of its GEF, and giving rise to the formation of non-productive eIF2(α -P)·eIF2B complexes [78, 112, 123, 124]. As a consequence, inhibition of eIF2B function reduces the cellular levels of TCs that are available for translation initiation, thus causing the down-regulation of overall protein synthesis. However, at the same time, eIF2 α phosphorylation causes the up-regulation of certain mRNAs *via* a mechanism called translation re-initiation through upstream open reading frames (uORFs) in the 5'-leader region. One well studied example for such an mRNA is that for the transcription factor GCN4 in the yeast *Saccharomyces cerevisiae*, whose expression is up-regulated due to eIF2 α phosphorylation by the kinase GCN2 in response to amino-acid starvation, and which in turn stimulates the expression of enzymes involved in amino-acid synthesis [79, 80].

Compared to the GEFs of most other Ras-related G proteins, eIF2B is an unusually large and complex exchange factor, comprising five non-identical subunits (α , β , γ , δ , and ϵ) which form two subcomplexes that bind eIF2 independently from each other [112]. eIF2B γ and eIF2B ϵ together form the catalytic subcomplex, in which the C-terminal domain (CTD) of the ϵ -subunit constitutes the minimal catalytically active fragment [65, 74, 112]. The N-terminal regions of eIF2B ϵ exhibit sequence similarity to eIF2B γ and are most likely involved in their mutual interaction [133, 134]. eIF2B α , β , and δ form the regulatory subcomplex of eIF2B [112, 135], in which all three subunits share mutual sequence similarity over the entire length of eIF2B α [136]. While the disruption of the genes for eIF2B β - ϵ is lethal in mammals and yeast, eIF2B α is not essential [137]. However, eIF2B α was found to be critical for the sensitivity of the eIF2B regulatory subcomplex to eIF2 α phosphorylation and thus de-repression of *GCN4* expression in yeast. The essential roles for eIF2B β and δ within the eIF2B complex are still not entirely clear. Apart from their putative structural

roles in complex assembly, eIF2B β was found to promote eIF2 binding and to contribute to the efficiency in nucleotide exchange, while eIF2B δ was proposed to play a role in Met-tRNA_i recruitment to eIF2·GTP [77].

For all five eIF2B subunits, a number of mutations have been identified that affect the activity of the eIF2B complex. Here, two main phenotypes can be distinguished in *S. cerevisiae*. On the one hand, mutations that decrease the GEF activity of eIF2B and thereby lower the cellular TC concentration, resulting in *GCN4* derepression independently of eIF2 α phosphorylation and amino-acid starvation. This phenotype is called general control de-repression (Gcd⁻) and has been found for mutations in all five eIF2B subunits. On the other hand, mutations that prevent the expression of *GCN4* even under stress conditions by rendering eIF2B insensitive to eIF2 α phosphorylation are called general control non-derepressible (Gcn⁻). Such a phenotype was found for mutations in the three subunits of the regulatory subcomplex, which is thought to be indicative of a large interface for eIF2 α binding on the eIF2B $\alpha\beta\delta$ complex [80, 135].

Despite considerable efforts over the last decades to understand eIF2B function, the architecture of the eIF2B complex remains elusive, thereby hampering the interpretation of available biochemical and genetic observations at the molecular level. This is exemplified by the lack of high-resolution structural insight into the eIF2B complex, which is limited to the isolated structures of the C-terminal catalytic domain of eIF2B ϵ from yeast and human and the human eIF2B α subunit. Moreover, until recently it was thought that eIF2B forms a hetero-pentamer containing one copy of each of the five subunits. However, recent studies indicate that eIF2B in yeast and mammals in fact forms a functional decamer in solution that is composed of two eIF2B $\alpha\beta\delta\gamma\epsilon$ hetero-pentamers. The way in which the contact between the two pentamers is mediated is still not clear, as the available data contradict each other in this respect, suggesting that decamerization is either mediated by an eIF2B α_2 dimer [72, 138] or an eIF2B($\gamma\epsilon$)₂ tetramer [73]. Similarly, the proposed arrangement of the individual subunits differs considerably between the studies, illustrating the problem to provide a clear picture of the eIF2B complex and its putative interactions with the substrate eIF2 on the basis of the available data.

The aim of this study was to provide structural insight into the molecular architecture of the eIF2B regulatory subcomplex. We were able to purify the three orthologs of eIF2B α , eIF2B β and eIF2B δ

from the thermophilic fungus *Chaetomium thermophilum*, which allowed us to reconstitute the eIF2B regulatory subcomplex *in vitro*. Analytical size exclusion chromatography experiments suggest that this subcomplex exists as an eIF2B $\alpha_2(\beta\delta)_2$ hexamer in solution, in which an eIF2B α_2 dimer most likely mediates the dimerization of two eIF2B $\alpha\beta\delta$ heterotrimers. Moreover, we solved the first high-resolution crystal structures of eIF2B β and eIF2B δ , which demonstrate their structural homology to each other and to eIF2B α . Using the presented results in combination with previous biochemical and genetic data, we generate a structural model for the eIF2B regulatory subcomplex. The possibility to *in vitro* reconstitute the eIF2B regulatory subcomplex in a pure form and in large amounts, as well as the availability of structural models for eIF2B α , β , and δ provides a promising basis for future structural and functional studies on the eIF2B complex.

4.2 Results

Overall structure of eIF2B $\beta(\Delta 123-148)$

Initial trials to crystallize wild-type eIF2B β from *C. thermophilum* were unsuccessful. We therefore designed a construct lacking residues 123-148 (eIF2B $\beta(\Delta 123-148)$), which, according to secondary structure predictions and sequence comparison with orthologs from other species, form a non-conserved unstructured loop region between two conserved α -helical regions. Unlike the wild-type protein, eIF2B $\beta(\Delta 123-148)$ readily crystallized in a condition containing 100 mM HEPES (pH 6.8) and 1.33 M tri-sodium citrate. The structure of *C. thermophilum*eIF2B $\beta(\Delta 123-148)$ was solved by molecular replacement and refined at a resolution of 2.54 Å (Table 1). The final model contains two eIF2B $\beta(\Delta 123-148)$ molecules (molecules A and B) per asymmetric unit, consisting of an N-terminal α -helical domain (residues 10-202) and a C-terminal Rossmann-fold-like domain (residues 203-419) (throughout the manuscript we will follow the residue-count for wild-type eIF2B β , ignoring the internal deletion) (Fig. 1). The N-terminal domain folds into six α -helices, with helices $\alpha 1$, 2, 4, 5, and 6 assembled around helix $\alpha 3$ through hydrophobic interactions. Residues 1-9 are not resolved in the electron density and are therefore considered to be disordered. Likewise, residues 106-180 are not resolved in molecule B of the asymmetric unit. In molecule A residues 106-112 and 160-174 are not resolved, whereas the region comprising residues 113-122 and 149-159 (in which residues 122 and 149 are directly fused by a peptide-bond) adopt two additional α -helices ($\alpha 5'$ and $\alpha 5''$)

Table 1. Crystallization, X-ray data collection and refinement statistics for structures of *Chaetomium thermophilum* eIF2B subunits β and δ

	eIF2B β Δ 123-148	eIF2B δ (148-443)
Crystallization		
Condition	100 mM HEPES (pH 6.8), 1.33 M tri-sodium citrate	100 mM MES (pH 6.2), 0.8 M (NH ₄) ₂ SO ₄
Temperature (°C)	20	20
Data Collection		
Space Group	R3	P2 ₁ 2 ₁ 2 ₁
Unit Cell	a = 138 Å b = 138 Å c = 146.6 Å $\alpha = \beta = 90^\circ$ $\gamma = 120^\circ$	a = 74.8 Å b = 94.5 Å c = 107.8 Å $\alpha = \beta = \gamma = 90^\circ$
Molecules/asym. unit	2	2
Resolution (Å)	2.54 (2.63-2.54)	2.55 (2.65-2.55)
Observed reflections	134799 (14846)	93747 (10009)
Unique reflections	34537 (3801)	25018 (2697)
Completeness (%)	99.9 (99.9)	97.7 (98.3)
$\langle I \rangle / \sigma$	23.7 (2.6)	16.4 (3.0)
R _{sym} (%)	5.0 (58.4)	5.6 (48.1)
CC(1/2) (%)	99.9 (76.4)	99.7 (73.4)
Refinement		
R _{work} (%)	17.0	18.8
R _{free} (%)	20.3	22.7
Rmsd from Standard Stereochemistry		
Bond length (Å)	0.008	0.004
Bond angles (°)	1.14	0.85
Ramachandran Plot Statistics		
Most favored (%)	98.2	98.7
Allowed regions (%)	1.8	1.3
Disallowed regions (%)	0	0

Values in parentheses refer to the highest resolution shell.

R_{work} and R_{free} factors are calculated using the formula $R = \frac{\sum_{hkl} |F(obs)_{hkl}| - |F(calc)_{hkl}|}{\sum_{hkl} |F(obs)_{hkl}|}$, where F(obs)_{hkl} and F(calc)_{hkl} are observed and measured structure factors, respectively. R_{work} and R_{free} differ in the set of reflections they are calculated from: R_{free} is calculated for the test set, whereas R_{work} is calculated for the working set.

that form contacts to symmetry related molecules in the crystal packing. The C-terminal Rossmann-fold-like domain is composed of a seven-stranded β -sheet with the first six β -strands parallel and the seventh oriented antiparallel to the rest. The β -sheet is sandwiched between six α -helices, three on each side. A second three-bladed antiparallel β -sheet (strands β 5, β 6, and β 8) is

packed against strands β_4 , β_7 , and β_9 of the first β -sheet, with the strands of the two sheets lying orthogonal to each other. An additional α -helix (α_{13}) forms the C-terminal end of eIF2B β . Two loop regions comprising residues 253-258 and 347-373 (denoted the 'arm-region'), respectively, are flexible and mainly disordered in both C-terminal domains of the asymmetric unit.

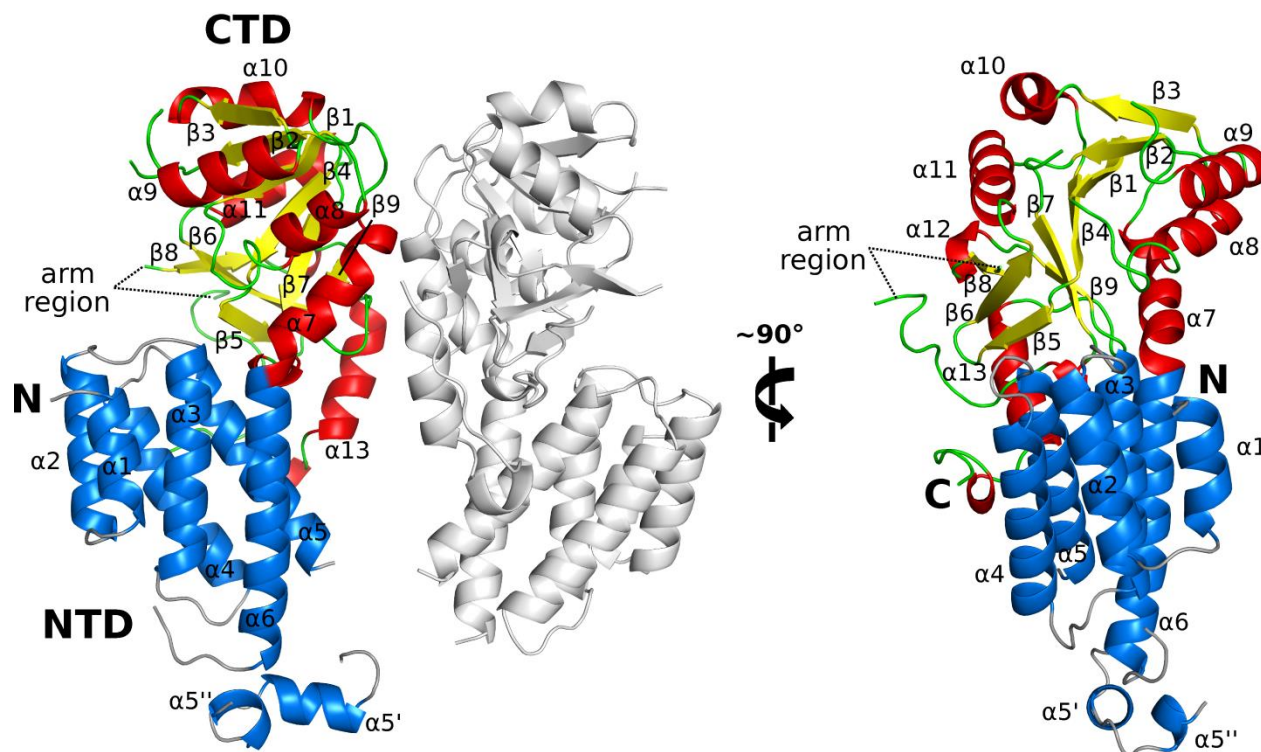


Figure 1. Overall crystal structure of *C. thermophilum* eIF2B β (Δ 123-148). eIF2B β is shown in cartoon presentation with the N-terminal α -helical domain (residues 10-202) colored blue, and the helices and β -sheets of the C-terminal Rossmann-fold-like domain (residues 203-419) are colored red and yellow, respectively. The arm region is only partially resolved in the electron density. In the left panel, the grey colored molecule represents the second copy of eIF2B β in the asymmetric unit, which is omitted in the right panel. Helix $\alpha_{5'}$, which is stabilized through contacts to symmetry related molecules in the crystal packing, contains the fusion between residues 122 and 149.

The two monomers of the asymmetric unit are arranged back-to-back to each other (Fig. 1), with the mainly hydrophobic dimer-interface formed solely by the backside of the C-terminal domains, involving helices α_7 and α_{12} and strand β_9 of the large β -sheet of each monomer. The individual N- and C-terminal domains of the two molecules can be superimposed well with rmsd values of 0.23 Å for 98 C_{α} atoms of the N-terminal domain and 0.28 Å for 145 C_{α} atoms of the C-

terminal domain. The overall proteins differ more significantly (rmsd of 0.59 Å over 270 C_α atoms) due to different angles between N- and C-terminal domains, as indicated by a slight increase in the angle between the connecting helices α6 and α7 from ~40° in molecule A to ~45° in molecule B (Fig. 3B). In both molecules, this conformation is stabilized through hydrophobic, as well as ionic interactions between helices α5 and α6 in the NTD and helix α13 in the CTD. As a consequence, the N- and C-terminal domains together form a deep cleft at the front of the molecule, with a mainly negatively charged platform formed by the connecting α2-α3 and α4-α5 loops in the NTD and a mainly positively charged lid formed by the CTD (Fig 3E).

Overall structure of eIF2Bδ(148-443)

During purification, eIF2Bδ usually degraded into two fragments of ~35 kDa and ~20 kDa according to SDS-PAGE analysis (see Materials and Methods for details). Crystallization trials were performed for the full-length protein, as well as for the 35 kDa fragment. Only the latter yielded high quality crystals that could be used for data collection and allowed the determination of the crystal structure of *C. thermophilum*eIF2Bδ(148-443) by molecular replacement (Table 1). The final model, refined at 2.55 Å resolution, contains two eIF2Bδ(148-443) molecules (molecules A and B) per asymmetric unit, which superimpose well with each other with an rmsd of 0.2 Å over 239 C_α atoms (Fig. 2). Each monomer is formed by an N-terminal α-helical domain (residues 148-266) and a C-terminal Rossmann-fold-like domain (residues 267-443). The N-terminal domain folds into five α-helices that lie nearly parallel to each other, assembled around a hydrophobic core. The N-terminal 147 residues are not resolved in the electron density. As the theoretical masses of this fragment and that of the crystallized protein correspond well to the two degradation fragments observed during purification, we assume that the N-terminal residues were lost during purification due to a proteolytic event, which would also be consistent with the low R-factors of 18.8 and 22.7% (Table 1). The C-terminal Rossmann-fold-like domain is composed of a six-stranded parallel β-sheet (β1-β4, β7 and β9), sandwiched between three α-helices on each side. A second three-bladed antiparallel β-sheet (strands β5, β6, and β8) is packed against strands β4, β7, and β9 of the first β-sheet, with the strands of the two sheets lying orthogonal to each other. The long loop region ('arm-region') comprising residues 402-420 is disordered in both molecules of the

asymmetric unit. Likewise, the C-terminal 23 residues are not resolved in the electron density, indicating that they are either flexible or were lost during purification.

Together with helix α_2 , helices α_5 and α_6 form the $\sim 3800 \text{ \AA}^2$ large interface for homodimer formation between the two molecules of the asymmetric unit, with the helices of one monomer oriented nearly orthogonal to those of the other (Fig. 2, 5A). The most intimate contact is thereby formed at the kink-regions between helices α_5 and α_6 of the two protomers.

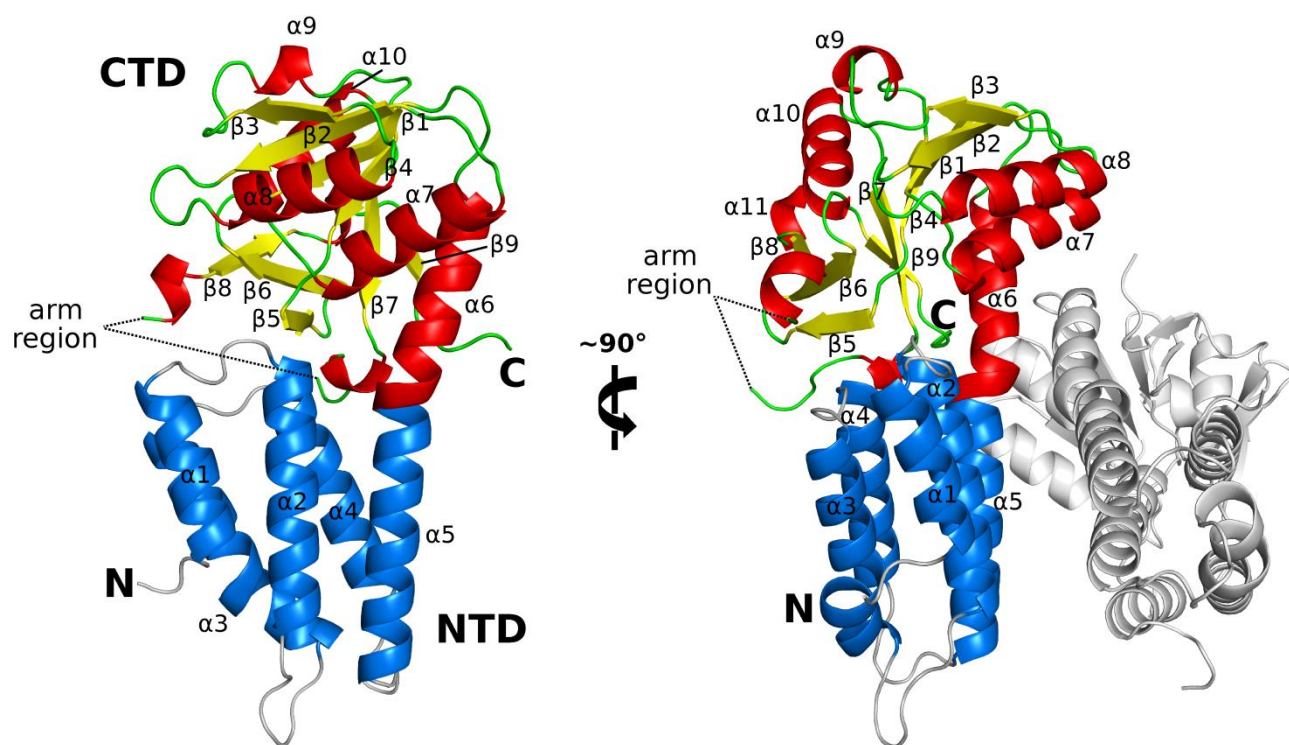


Figure 2. Overall crystal structure of *C. thermophilum*eIF2B δ (148-443).eIF2B δ is shown in cartoon presentation with the N-terminal α -helical domain (residues 148-266) colored blue, and the helices and β -sheets of the C-terminal Rossmann-fold-like domain (residues 267-443) colored red and yellow, respectively. The arm region is mainly disordered and therefore not resolved in the electron density. In the right panel, the grey colored molecule represents the second copy of eIF2B δ in the asymmetric unit, which is omitted in the left panel.

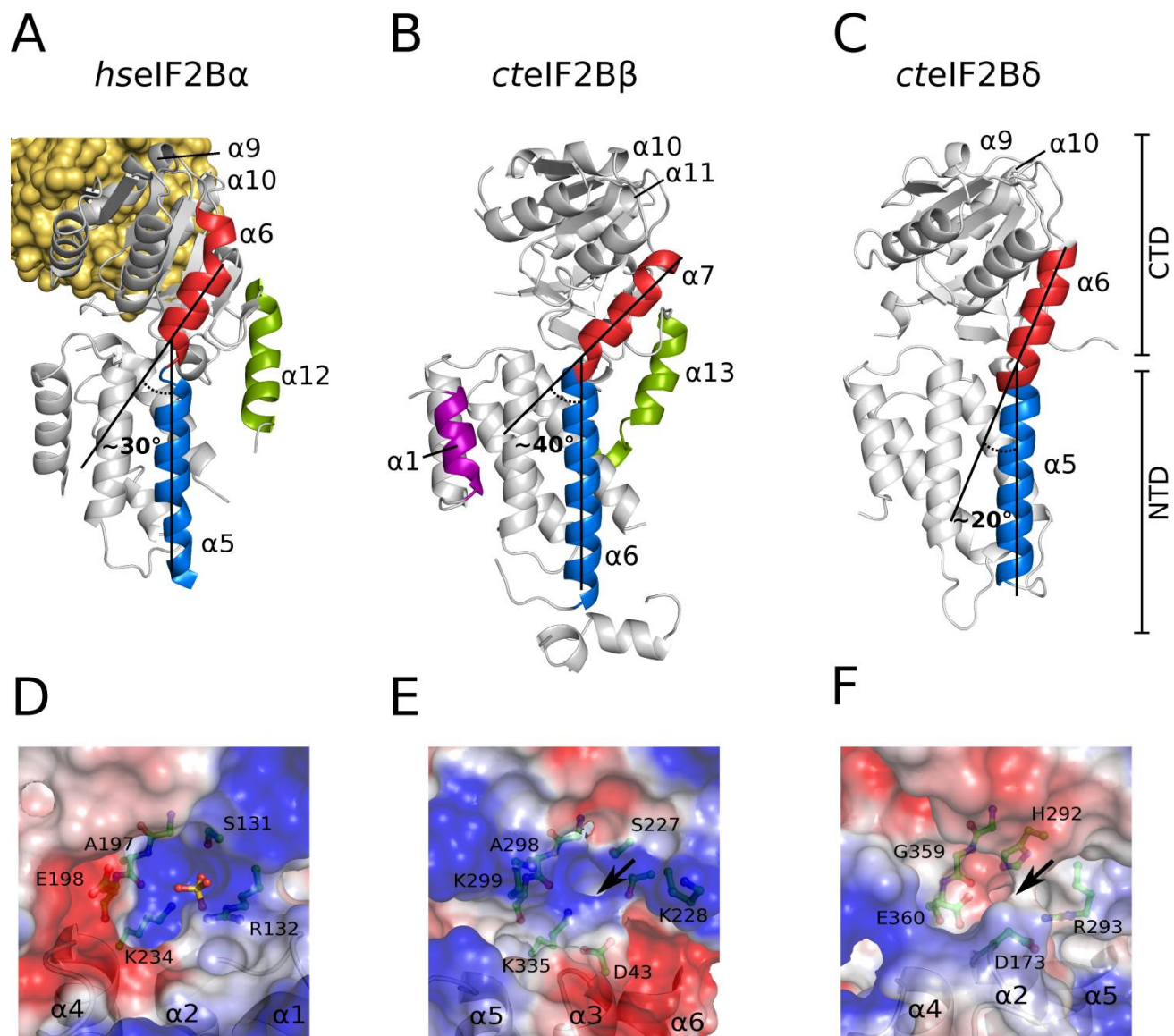


Figure 3. Comparison of the structures of human eIF2Bα with *C. thermophilum* eIF2Bβ and eIF2Bδ. A-C) Compared to *ctelF2Bδ* (C), *hseIF2Bα* (PDB: 3ECS) (A) and *ctelF2Bβ* (B) exhibit significantly increased angles between the two long connecting helices between N- and C-terminal domains (colored blue and red, respectively), which might be dependent on the presence of the additional C-terminal α -helix (green) that forms direct contacts to the NTD and which is absent in the *ctelF2Bδ* structure. *ctelF2Bβ* (B) exhibits an additional N-terminal α -helix ($\alpha 1$; purple), which is not found in *hseIF2Bα* or *ctelF2Bδ*. Homodimer formation by *hseIF2Bα* through helices $\alpha 9$ and $\alpha 10$ of the C-terminal domain is indicated by the second *hseIF2Bα* molecule of the asymmetric unit as golden surface. D-E) Surface charge presentation (negative, red; positive, blue) of the cleft between N- and C-terminal domains in *hseIF2Bα* (D), *ctelF2Bβ* (E) and *ctelF2Bδ* (F). The crystal structure of *hseIF2Bα* accommodates a sulfate ion at the bottom of the cleft, surrounded by positively charged residues. Although some of these residues are conserved also in *ctelF2Bβ* and *ctelF2Bδ*, both structures do not contain a sulfate ion in the corresponding position (arrows).

Structural comparison between the subunits of the eIF2B regulatory subcomplex

Earlier analyses revealed mutual sequence similarities between the three eIF2B α , β , and δ subunits [136]. Consistently, our structural analysis for eIF2B β and eIF2B δ from *C. thermophilum* demonstrate that both subunits share a common overall fold, comprising an N-terminal helix bundle and a C-terminal α/β Rossmann-like fold, which is, moreover, homologous to the previously reported structure of eIF2B α from *Homo sapiens*[139].

Notwithstanding their overall structural similarity, each of the three structures reveals features that are either idiosyncratic among the three proteins, or shared with only one of the other subunits (Fig. 3). One prominent example is the first of the six α -helices of the N-terminal domain in subunit β ($\alpha 1$), which replaces the four-stranded antiparallel β -sheet that usually occupies this position in 5-methylthioribulose 1-phosphate isomerases (5M1PIs), ribose-1,5-bisphosphate isomerases (RBPIs) or archaeal eIF2B-like proteins (e.g. PDBs 1T5O, 1W2W), proteins which were found to be in sequence and structure homologous to eIF2B α , $-\beta$ and $-\delta$ [28, 139, 140]. Neither the additional α -helix nor the β -sheet is observed in the eIF2B α - or δ -subunit. It should be noted, however, that the sequence conservation between eIF2B β orthologs is low in this region [136], suggesting that helix $\alpha 1$ might not be universally conserved.

Another distinctive feature is the relative orientation of the five conserved helices of the N-terminal helix bundle (Fig. 3A-C). In eIF2B β and $-\delta$ all five α -helices lie nearly parallel to each other. A similar arrangement is found in 5M1PIs, RBPIs and eIF2B-like proteins. By contrast, helices $\alpha 1$ - $\alpha 5$ in eIF2B α are significantly less parallel to each other, particularly with helix $\alpha 1$ reoriented relative to the following helices by nearly 50°, thereby allowing a direct contact between the $\alpha 1$ - $\alpha 2$ loop to helix $\alpha 7$ in the C-terminal domain that is not observed in the structurally related homologues [139].

In agreement with the relative high degree of sequence similarity, the C-terminal Rossmann-like domain of the eIF2B subunits exhibits a higher degree of structural homology and only minor differences in the arrangement of helices $\alpha 8$ and $\alpha 9$ ($\alpha 9$ and $\alpha 10$ in *ct*eIF2B β). One of the most prominent distinctive features within the C-terminal domain is the C-terminal α -helix found in the structures of eIF2B α (helix $\alpha 12$) and eIF2B β (helix $\alpha 13$) (Fig. 3A/B). This α -helix is not present in eIF2B δ (Fig. 3C), despite the fact that it contains conserved residues at its C-terminus that would correspond to this α -helix in the other two subunits [136], and despite the fact that the crystal

packing would allow its formation in the same position. In eIF2B α and $-\beta$, this helix forms mainly hydrophobic contacts to the N-terminal domain, thereby stabilizing one of the most salient features of both proteins: the strong kink in the transition of helix α_5 of the NTD to helix α_6 of the CTD (helices α_6 and α_7 in eIF2B β). The angle between the axes through both helices is $\sim 30^\circ$ in eIF2B α and $40\text{--}45^\circ$ in eIF2B β . By contrast, these helices are nearly coaxially fused in eIF2B δ with an angle of close to 20° , suggesting that the contact to the C-terminal α -helix observed in the other two subunits is a requirement for the conformational rearrangement to the kinked state (Fig. 3A-C). This is supported by the structures of 5M1PI/eIF2B-like structures, which usually lack a structural element corresponding to the C-terminal helix in eIF2B α and $-\beta$, resulting in nearly straight connecting helices. An exception from this rule is the RBPI from *Thermococcus kodakarensis*, which contains a homologous C-terminal α -helix that forms contacts to the N-terminal domain as observed in eIF2B α and $-\beta$ and thereby stabilizes an angle of $\sim 50^\circ$ between helices α_5 and α_6 (PDB: 3A11)[141].

As a consequence of the increased angle, the cleft formed by the N- and C-terminal domains is considerably larger in eIF2B α and eIF2B β than in the δ -subunit, which in the case of eIF2B α allows the coordination of a sulfate ion in a pocket of the cleft $\sim 16 \text{ \AA}$ from its entrance [139] (Fig. 3D). Sulfate ions have also been observed in the narrower clefts of several 5M1PI/eIF2B-like proteins. However, in these cases the sulfate ion is positioned significantly closer to the entrance and coordinated by a different set of residues [139]. Although some of the residues responsible for sulfate ion binding in eIF2B α are conserved in subunits β and δ [139], and despite the presence of 0.8 M sulfate ions in the crystallization condition for eIF2B δ (Table 1), neither of the two structures exhibited an electron density in the corresponding position that could be explained by a sulfate ion (Fig. 3E/F). This apparent inability of subunits β and δ to coordinate the sulfate ion can be explained by the fact that eIF2B β and eIF2B δ contain residues (Asp43 and His292, respectively) that would overlap with the putative sulfate ion binding site, causing electrostatic and/or steric repulsion (Fig. 3D-F).

Another important aspect of the newly determined structures is their implication for the oligomeric state of eIF2B β and eIF2B δ . So far studied eIF2B-like proteins, 5M1PIs, as well as RBPIs were found to form homodimers in solution [138, 139]. All crystal structures of these proteins that

have so far been determined revealed a structurally nearly identical dimer interface, in which two adjacent α -helices of the C-terminal domain in one monomer pack against the same helices of the other [138]. Additionally, a structurally conserved loop (the 'arm-region') protrudes from one CTD and packs against the other, thereby extending the large central β -sheet of the Rossmann-like fold. The same dimer interface was found in the crystal structure of *H. sapiens* eIF2B α (Fig. 4A), and recent biochemical studies suggest that eIF2B α uses this interface to form a physiological homodimer in solution [72, 138]. It is therefore noteworthy that the structures of eIF2B β and eIF2B δ presented here constitute an exception among their homologues (eIF2B α /eIF2B-like/5M1PIs/RBPIs) as they apparently do not form stable homodimers along this interface. For eIF2B β , the crystal structure does not suggest an alternative interaction that might allow stable dimerization, in line with our observation that *ct*eIF2B β exists as a monomer in solution (see below). By contrast, *ct*eIF2B δ seems to exist as a mixture of monomers and homodimers in solution (see below), which could indicate that the monomeric form crystallized under the used condition, and that an unstable homodimer could still be formed through the same interface as in eIF2B α . However, unlike eIF2B β , the two monomers in the asymmetric unit of the eIF2B δ structure do interact *via* a large interface formed by helices α_2 , α_5 , and α_6 , which could thus provide an alternative means to form a homodimer in solution (Fig. 5A).

Protein interaction studies by analytical size exclusion chromatography

To study the solution state and interactions between the individual eIF2B subunits α , β , and δ from *Chaetomium thermophilum*, we used analytical size exclusion chromatography (SEC) (Fig. 6).

CteIF2B α exists as a homo-dimer in solution. We found that *ct*eIF2B α (~41 kDa) alone elutes from the analytical SEC column in two peaks. The smaller peak elutes at 10.8 ml, while the main peak elutes at 12.5 ml, corresponding to apparent molecular weights of ~250 and 95 kDa, respectively. No peak was observed at an elution volume that would correspond to a monomer (~14 ml). This suggests that *ct*eIF2B α most likely forms mainly dimers (~82 kDa) in solution, while a small fraction forms higher oligomeric states, possibly homo-tetramers.

CteIF2B β exists as a monomer in solution. In contrast to *ct*eIF2B α , *ct*eIF2B β (~45 kDa) alone elutes from the analytical SEC column in one peak at 14.2 ml, corresponding to an apparent

molecular weight of ~40 kDa, as expected for a monomer. An additional small shoulder elutes at 12.5-13 ml, which could correspond to a small fraction of homo-dimeric *ct*eIF2B β in solution.

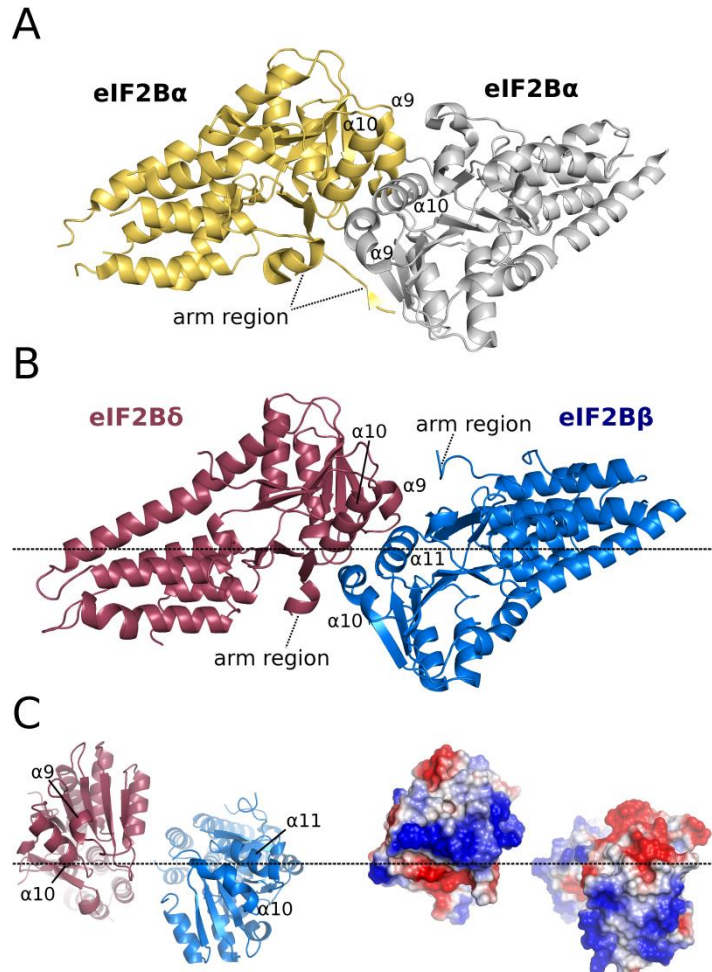


Figure 4. Model for the heterodimer between eIF2B β and eIF2B δ . **A)** The *hseIF2B α* homodimer (PDB: 3ECS). Like in the homologous 5M1PIs and RBPIs, the dimer interface is mainly formed by helices α_9 and α_{10} of the CTD in one monomer, which pack against the same helices of the second molecule. The interface is complemented by the ‘arm-region’, which protrudes from one CTD to extend the large central β -sheet of the Rossmann-like fold in the CTD of the second monomer. **B)** Model for the eIF2B β -eIF2B δ heterodimer along the same interface as seen for eIF2B α . In the structures of the individual subunits, the helices corresponding to α_9 and α_{10} in eIF2B α are not occupied by homodimer formation and are thus available for heterodimer formation. **C)** The left panel shows the view directly onto the hypothetical eIF2B β -eIF2B δ heterodimer interfaces of eIF2B β (blue) and eIF2B δ (dark red), respectively. The right panel shows the same view on both proteins in surface charge presentation (red, negative; blue, positive). The horizon indicated by the dashed line corresponds to that shown in (B), demonstrating that the surface charge distribution on the two proteins would be compatible with heterodimer formation.

CteIF2B δ exists as a mixture of monomers and homo-dimers in solution. Finally, full-length *ct*eIF2B δ (~49 kDa) alone elutes in two main peaks, the first at 12.1 ml and the second at 14.1 ml, corresponding to apparent molecular weights of ~120 and ~40 kDa, respectively. This suggests that *ct*eIF2B δ exists as a mixture in solution of nearly equal amounts of monomers and dimers (~98 kDa), with the equilibrium slightly shifted in favor of dimer-formation.

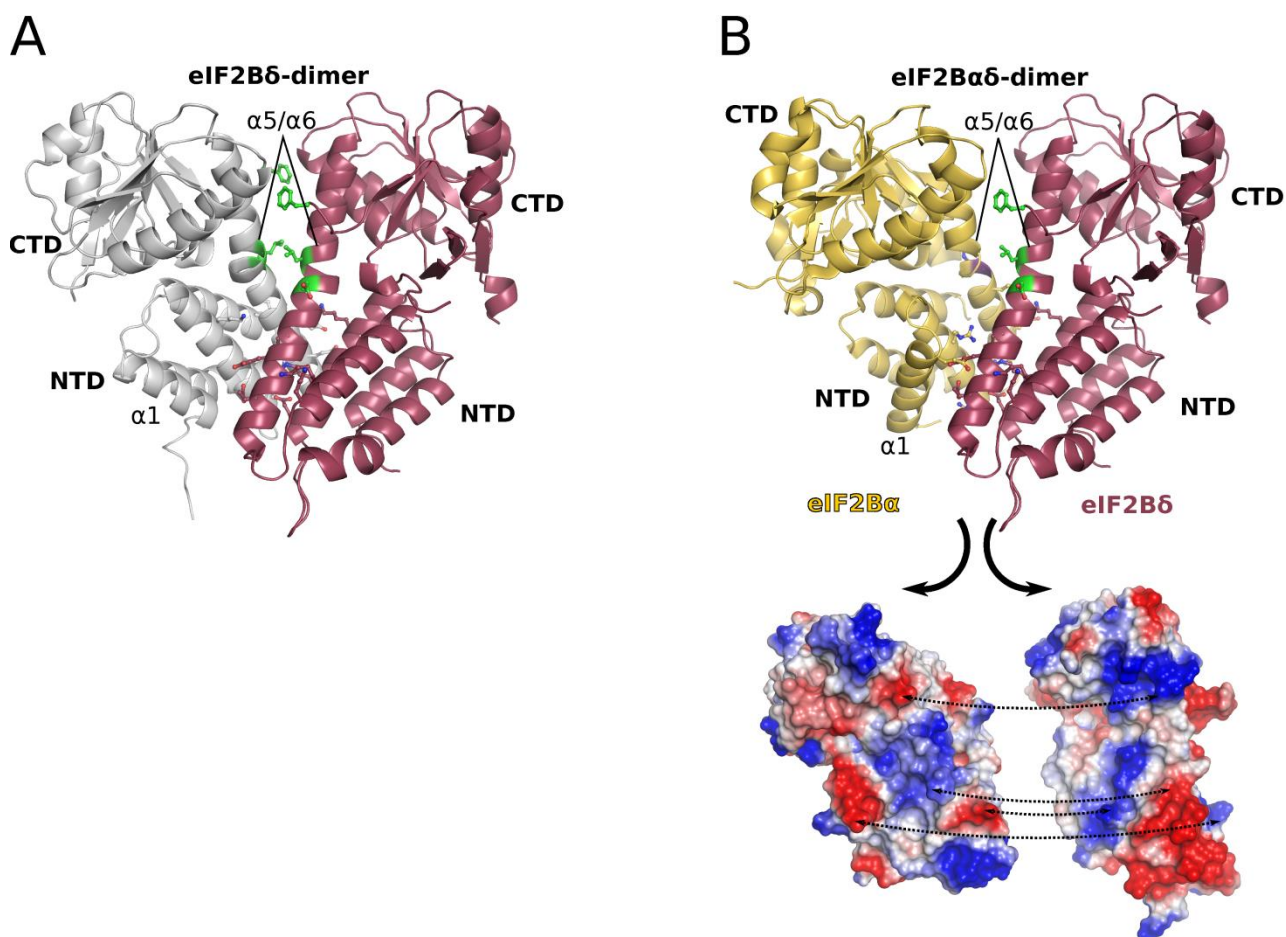


Figure 5. Model for the heterodimer between eIF2B α and eIF2B δ . **A)** The ctelF2B δ homodimer observed in the asymmetric unit of the crystal structure (see also Fig. 2). In both molecules, the interface is mainly formed by helices $\alpha 2$, $\alpha 5$ and $\alpha 6$, which are oriented nearly orthogonal between the two protomers. The most intimate contacts are formed in the area of the kink-region between helices $\alpha 5$ and $\alpha 6$, where the green residues indicate positions of Gcn⁻ mutations. The contact between the two ctelF2B δ molecules is mediated mainly by polar interactions between complementary charged surfaces (charged residues are shown as sticks). **B)** Model for the eIF2B α -eIF2B δ heterodimer, in which the grey copy of eIF2B δ from A) is exchanged for a homology model of ctelF2B α (golden; based on the hselF2B α structure, generated by the Phyre2 modeling server). The lower panel shows the direct view onto the potential binding interfaces of eIF2B α (left) and eIF2B δ (right) in surface charge presentation, with dashed arrows indicating the areas that contact each other in the model shown in the upper panel (red, negative; blue, positive).

Formation of the ctelF2B $\alpha\beta\delta$ complex depends on the presence of all three subunits. Mixing ctelF2B α with either ctelF2B β (full-length or $\Delta 123-148$) or with ctelF2B δ alone did not result in complex formation between the respective proteins, as indicated by the elution profiles of the SEC (Fig. 6A/B). In the case of the ctelF2B α -ctelF2B δ mixture it cannot be excluded that a hetero-dimer is formed that migrates at approximately the same volume as the respective homo-dimers; however, the elution profile is in good agreement with what would be expected for an interference

of the individual runs (blue line in Fig. 6B), and the amount of monomeric *ctelF2B δ* seems to be unchanged between the presence or absence of *ctelF2B α* . Thus, neither *ctelF2B β* nor *ctelF2B δ* seem to interact with *ctelF2B α* individually. By contrast, mixing *ctelF2B β* with *ctelF2B δ* in the absence of *ctelF2B α* results in the complete precipitation of both proteins, leaving in solution only the protein that had been added in excess over the other. Indirectly, this indicates that *eIF2B β* and *δ* interact with each other independently of *eIF2B α* and form a 1:1 complex with low solubility.

Finally, we tried to *in vitro* reconstitute the entire *ctelF2B $\alpha\beta\delta$* regulatory subcomplex by first mixing *eIF2B β* with a ~2-fold molar excess of *eIF2B α* , followed by the addition of *eIF2B δ* in ~1.5-fold excess over the β -subunit. This time, no precipitation occurred and the analytical SEC run clearly shows the formation of a new peak, eluting at a volume of 10.31 ml (Fig. 6C), which corresponds to an apparent molecular weight of ~320 kDa. SDS-PAGE analysis of the peak fractions demonstrates that they contain all three subunits in approximately a 1:1:1 ratio (Fig. 6C, right panel). The calculated molecular mass of a hetero-trimer of the three subunits is ~135 kDa, which is significantly smaller than the size of the observed complex in solution as indicated by SEC. Instead, the obtained results would be in better agreement with a hexamer of *eIF2B α* , β , and δ in a 2:2:2 ratio (*eIF2B $\alpha_2\beta_2\delta_2$*), which would add up to a complex of ~270 kDa. Importantly, this putative *eIF2B $\alpha_2\beta_2\delta_2$* complex also contained small amounts of the upper degradation product of *eIF2B δ* (35 kDa), which contains the crystallized fragment *eIF2B δ (148-443)* (Fig. 6C), while the second smaller degradation product elutes separately from the complex peak at a higher volume. Moreover, the construct *eIF2B β (Δ 123-148)*, used for structure determination (see above), formed the *eIF2B $\alpha\beta\delta$* complex like the wild-type protein.

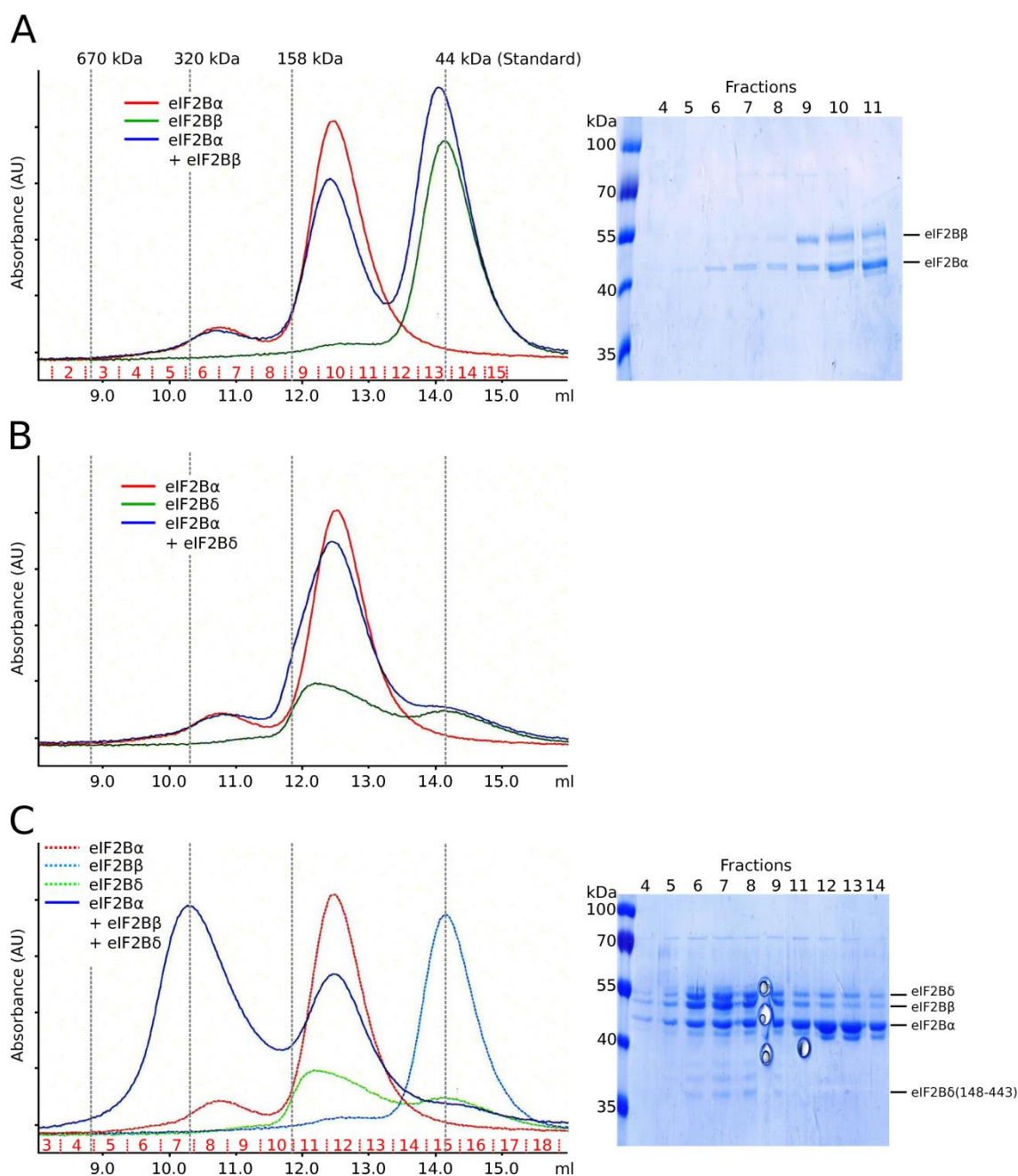


Figure 6. Reconstitution of the eIF2B regulatory subcomplex from *C. thermophilum* by analytical size exclusion chromatography. **A)** Chromatograms for *ctelF2B α* (red curve), *ctelF2B β* (green curve) and the mixture of *ctelF2B α* and *ctelF2B β* (blue curve). While *ctelF2B α* elutes as an apparent dimer at ~12.5 ml, corresponding to a size of ~95 kDa, *ctelF2B β* elutes at 14.2 ml, corresponding to an apparent molecular weight of ~40 kDa, as expected for a monomer. No shift in the elution volume is observed for either peak when both subunits are mixed, indicating that no complex formation takes place (as confirmed by the SDS-PAGE). **B)** Chromatograms for *ctelF2B α* (red curve), *ctelF2B δ* (green curve) and the mixture of *ctelF2B α* and *ctelF2B δ* (blue curve). *ctelF2B δ* elutes in two peaks at 12.1 ml and 14.1 ml, respectively, corresponding to apparent molecular weights of ~120 and ~40 kDa, respectively. No shift in the elution volume is observed for either peak when both subunits are mixed, indicating that no complex formation takes place. **C)** When all three regulatory subunits are mixed, a new peak emerges at an elution volume of 10.31 ml (blue line), which corresponds to an apparent molecular weight of ~320 kDa. SDS-PAGE analysis of the peak fractions (right panel) demonstrates that they contain all three subunits in approximately a 1:1:1 ratio.

4.3 Discussion

In comparison to most known GEFs of Ras-related G proteins, eIF2B, the GEF for eIF2, is an unusually large and complicated protein complex composed of five non-identical subunits. Despite considerable efforts over the last decades, little is known about the actual architecture of this large protein complex, the arrangement of the individual subunits relative to each other, and the way in which they bind their substrate eIF2. Previously available high-resolution structural information for the eIF2B complex was limited to the isolated ~20 kDa C-terminal catalytic domain of eIF2B ϵ and the eIF2B α regulatory subunit from *H. sapiens* [74, 139]. Thus, the lack of detailed structural information for the individual eIF2B subunits, as well as for their mutual interactions is one of the key problems that currently hamper the interpretation of available mutational and genetic data to obtain a detailed picture of the molecular mechanisms that underlie eIF2 binding by eIF2B, nucleotide exchange and its regulation under stress conditions.

The motivation for this present work was to provide insight into the architecture of the eIF2B regulatory subcomplex in its molecular details. For this purpose, the orthologs of the three subunits eIF2B α , - β , and - δ from the thermophilic fungus *Chaetomium thermophilum* were recombinantly expressed and purified in their respective full-length forms that were active in *in vitro* reconstitution experiments for the regulatory subcomplex (Fig. 6). Initial trials to crystallize the entire regulatory subcomplex were not successful. However, it was possible to improve the crystallizability of the isolated cteIF2B β by deleting a non-conserved predicted loop region within the N-terminal domain, resulting in the first high-resolution crystal structure of an eIF2B β ortholog (eIF2B β (Δ 123-148)) (Fig. 1). Moreover, by using a spontaneously occurring degradation product containing only the conserved C-terminal part of eIF2B δ , we solved the first crystal structure of an eIF2B δ ortholog (eIF2B δ (148-443)) (Fig. 2). Importantly, both constructs were found to be incorporated into the eIF2B $\alpha\beta\delta$ regulatory subcomplex with wild-type eIF2B α , indicating that the missing regions are not critical for its formation.

Together with the structure of *H. sapiens* eIF2B α , the newly determined structures provide a vantage point for further structural studies on the architecture of the regulatory subcomplex. In line with predictions on the basis of sequence homology [136], both crystal structures confirmed the structural homology between the three eIF2B regulatory subunits, with an all-helical N-

terminal domain and a C-terminal Rossmann-like α/β domain. One of the most striking observations from the crystal structures of eIF2B β and eIF2B δ is the fact that they constitute the first examples from this protein family that do not stably homodimerize *via* the usual interface in the C-terminal domain. Hence, the same interface used for homodimerization in eIF2B α , archaeal eIF2B-like proteins, 5M1PIs and RBPIs [138] would be available in eIF2B β and eIF2B δ for heterodimerization either with each other or with eIF2B α . The latter option is unlikely, since eIF2B α from *C. thermophilum* (Fig. 6) as well as from yeast forms stable homodimers in solution using this interface [138] and does not form stable complexes with the isolated eIF2B β or eIF2B δ (Fig. 6A/B). By contrast, the analytical SEC experiments revealed that eIF2B β forms a monomer and eIF2B δ is present as a mixture of monomers and homodimers in solution, which would allow the formation of heterodimers between both proteins. Consistently, eIF2B β or eIF2B δ interact with each other, most likely forming a tight 1:1 complex in solution that, however, was not soluble under the used experimental conditions. Heterodimerization between eIF2B β and eIF2B δ *via* the usual homodimerization interface has been suggested previously [138] and would be consistent with the complementary surface charge distribution on both *C. thermophilum* proteins (Fig. 4B/C). Moreover, phylogenetic analyses suggest a common clade for these two proteins within the family of eIF2B regulatory subunits [140], which indicates that they could constitute a derived homodimer that originates in a duplication event of their ancestral gene and a subsequent derivatization of the two lines without losing their ability to interact. The specific interaction between eIF2B β and eIF2B δ is further supported by previous studies that demonstrated co-depletion of eIF2B δ together with the genetic depletion of eIF2B β in *S. cerevisiae*, indicating that the latter is required to stabilize eIF2B δ in the cellular context [77].

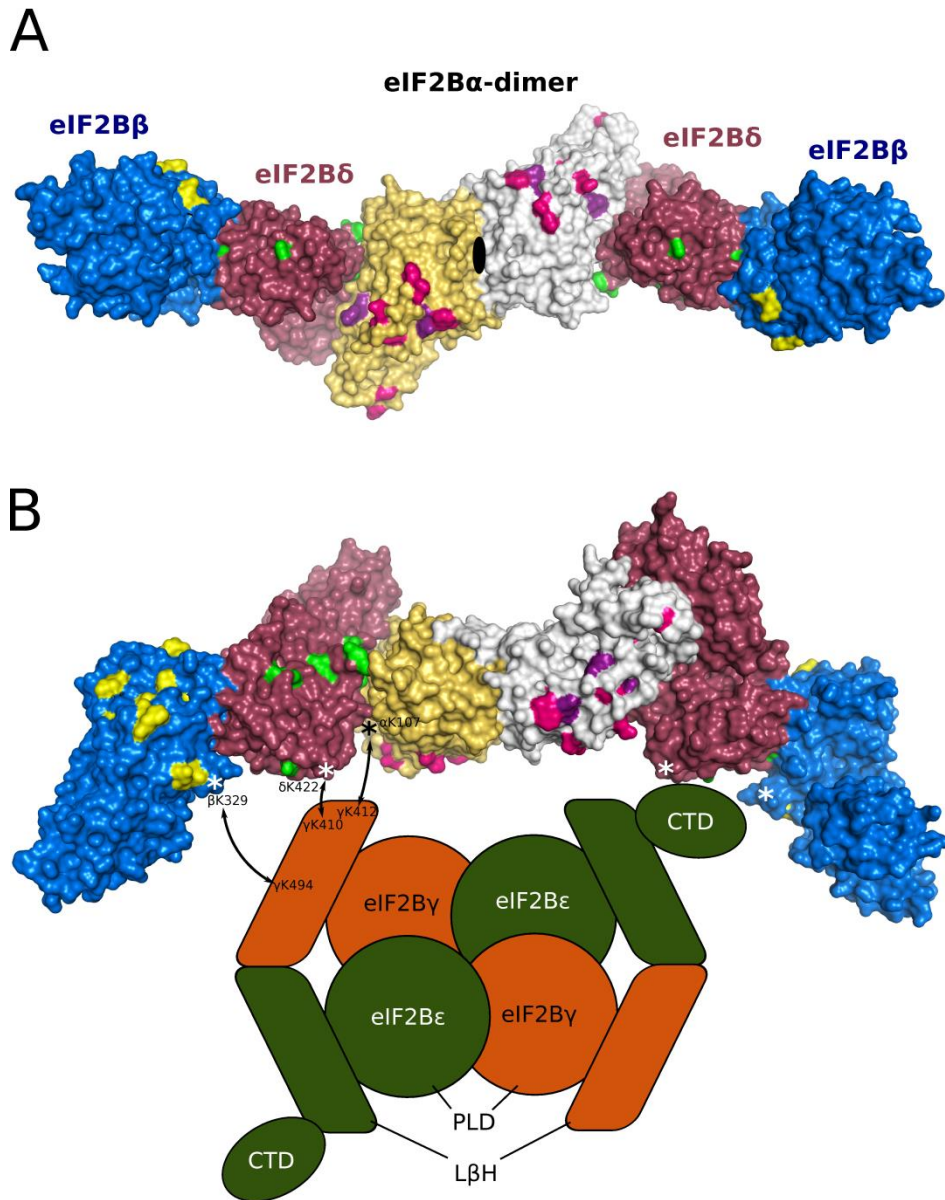


Figure 7. Structural model for the eIF2B regulatory subcomplex. A) According to the model, the regulatory eIF2B subcomplex consists of one central eIF2B α_2 homodimer (gold and grey surfaces) which mediates the interactions between two eIF2B $\beta\delta$ heterodimers (blue and red surfaces) through direct contact to the δ -subunit (as in Fig. 5B). Pink, green and yellow surfaces indicate positions of Gcn⁻ mutations in eIF2B α , eIF2B β and eIF2B δ , respectively [123, 135, 142, 143]. The complex has a two-fold symmetry axis through the dimerization interface of the eIF2B α_2 dimer (indicated by the black ellipsis). **B)** The resulting half-moon structure of the regulatory subcomplex suggest that the eIF2B $\gamma_2\epsilon_2$ catalytic subcomplex (presented as by Gordiyenko *et al.* [73]) becomes bound between the two eIF2B $\beta\delta$ heterodimers and thus in the vicinity of the previously identified Gcn⁻ mutations. The asterisks mark positions of lysine residues that were found to be crosslinked to specific positions on the eIF2B $\gamma_2\epsilon_2$ complex (indicated by black arrows) [73]. eIF2B γ and eIF2B ϵ each consist of a pyrophosphorylase-like domain (PLD) and a left-handed β -helix (L β H) domain, to which the additional catalytic C-terminal domain (CTD) is attached only in the ϵ -subunit.

An interesting question that arises from our own and previous data is that of the topology/connectivity within the eIF2B $\alpha\beta\delta$ regulatory subcomplex. In line with recent biochemical and mass-spectrometry data [72, 138], the analytical SEC experiments shown in Fig. 6 suggest that the regulatory subcomplex is not a heterotrimer as previously thought but in fact a dimer of heterotrimers, forming an eIF2B $\alpha_2(\beta\delta)_2$ complex. The necessity to allow further binding of two additional eIF2B $\gamma\epsilon$ subcomplexes assembled as a symmetrical $\gamma_2\epsilon_2$ complex [73], as well as the problem to avoid aggregation between eIF2B complexes favors an arrangement of the two eIF2B $\alpha\beta\delta$ trimers in a way that allows their superposition by a simple rotational symmetry operation. Within this complex, neither eIF2B β , nor eIF2B δ are individually sufficient to interact with eIF2B α but require the structural context of the eIF2B $\beta\delta$ complex to allow the formation of the hexamer. This suggests that the eIF2B $\beta\delta$ complex either forms a combined interaction surface for the α -subunit or that one subunit induces conformational changes within the other that render it active for interactions with eIF2B α . In both cases, the assumption that eIF2B α_2 and eIF2B $\beta\delta$ each dimerize *via* the usual interface of the C-terminal domain (Fig. 4) makes it necessary to search for an alternative interface to mediate the association between the two dimers.

One interesting candidate for such an interaction is the interface between the two eIF2B δ protomers within the asymmetric unit of the crystal structure (Fig. 5). This interface along helices α_5 and α_6 is sufficiently large ($\sim 7600 \text{ \AA}^2$ of combined buried surface area) to be physiologically relevant. Interestingly, yeast eIF2B α and eIF2B δ , but not eIF2B β , both contain sites of Gcn $^-$ and Gcd $^-$ mutants in the kink-region between helices α_5 and α_6 that forms the area for the most intimate contact within the eIF2B δ dimer interface (Fig. 5B). Thus, an appealing option would be that each of the two eIF2B $\beta\delta$ dimers associates with one copy of eIF2B α in the eIF2B α_2 homodimer through the δ -subunit and *via* an interface formed by helices α_5 and α_6 in both proteins (Fig. 7A). As an increased kink between helices α_5 and α_6 in eIF2B δ would allow a more intimate contact to its interaction partner eIF2B α , it is conceivable that eIF2B β -binding might stabilize the C-terminal helix in eIF2B δ (which is disordered in the crystal structure of eIF2B δ and stabilizes the large angles between α_5 and α_6 in eIF2B α and eIF2B β (Fig. 3A-C)), thereby providing a possible explanation for the apparent cooperativity in their binding to eIF2B α . In this scenario, the inability of the Gcn $^-$ mutants in the kink-regions to respond to eIF2 α phosphorylation would thus be due to the

destabilization or even loss of eIF2B α , the primary sensor of eIF2 α (S51-P), from the eIF2B complex by interrupting the contact to eIF2B δ .

In the resulting model, eIF2B α would play a critical role by mediating hexamer formation in the regulatory subcomplex (Fig. 7), consistent with previous studies that demonstrated that eIF2B α promotes decamer formation between two eIF2B $\beta\delta\gamma\epsilon$ complexes [72]. It should be noted however that data presented by Gordiyenko *et al.*[73] suggest that decamer formation is mediated between two eIF2B $\gamma\epsilon$ dimers, whereas the two regulatory subcomplexes, each comprising eIF2B $\alpha\beta\delta$ in a 1:1:1 stoichiometry would not contact each other directly [73]. This is ostensibly at odds with the data by Wortham *et al.*[72] and our own observations and would require the dissociation of the conserved stable eIF2B α_2 dimer upon complex formation. Although the studies by Wortham *et al.*[72] and by Gordiyenko *et al.*[73] were done with proteins from different species (mammals and yeast, respectively), it is in our opinion unlikely that the observed differences are due to species-specific modes of decamerization, particularly as our own data for the fungus *C. thermophilum* support the data from the mammalian system. To reconcile both data sets it is in our opinion conceivable that decamerization is in fact mediated by the eIF2B α_2 homodimer, as well as the eIF2B($\gamma\epsilon$) $_2$ tetramer, with each $\gamma\epsilon$ dimer binding independently to a regulatory subcomplex formed by one copy of eIF2B α and the eIF2B $\beta\delta$ heterodimer (Fig. 7B). This possibility would explain why Wortham and coworkers [72] found that the disruption of the eIF2B α dimer by mutagenesis does not abolish eIF2B α -dependent decamerization [72], while the data by Gordiyenko *et al.* [73] indicate that the presence of eIF2B α stabilizes eIF2B($\beta\delta$) $_2$ ($\gamma\epsilon$) $_2$ formation [73]. The resulting half-moon shape of the eIF2B α_2 ($\beta\delta$) $_2$ model would be consistent with an eIF2B($\gamma\epsilon$) $_2$ tetramer assembled on the inner side (Fig. 7B). Moreover, most identified Gcn⁻ mutations would as well map to the inner side of the model. Finally, Gordiyenko and coworkers [73] found that K107 in yeast eIF2B α and K422 in yeast eIF2B δ crosslink to K412 and K410 in the left-handed β -helix (L β H) domain of eIF2B γ , respectively. As K107 in eIF2B α and K422 in eIF2B δ occupy adjacent positions within our structural model (~ 17 Å apart) and are both orientated toward the inner side of the half-moon, these data add further support to the structural model presented in Fig. 7.

4.4 Materials and Methods

Cloning

The coding sequences of eIF2B subunits α , β and δ were amplified by PCR as individual exons from *Chaetomium thermophilum* genomic DNA and introduced into the expression vector according to the InFusion protocol (Clontech). The coding sequence for full-length eIF2B α was introduced into pET22b vector cleaved with the restriction enzymes NcoI and XhoI. The coding sequences for full-length eIF2B β and δ were introduced into the pGEX-6P1 vector cleaved with BamHI and XhoI. The InFusion mixture was transformed into XL1-Blue *E. coli* cells (Stratagene) and plated out on LB agar plates containing appropriate antibiotics. Several colonies of each plate were picked and subjected to a test PCR to identify positive clones. Positive colonies were grown over night in LB medium supplemented with antibiotics and the plasmid was purified with the Qiaprep Spin Miniprep Kit (Qiagen) according to the manufacturer's instructions. The sequences of the selected constructs were verified by DNA sequencing.

The construct encoding eIF2B β Δ 123-148 was generated by deletion of the corresponding codons from the original plasmid (wild-type eIF2B β in pGEX-6P1) according to the QuickChange technique (Stratagene) using appropriate mutagenesis primers. The plasmid was prepared and verified by sequencing as described above.

Protein expression and purification

Expression: All three constructs were expressed in *E. coli* BL21(DE3) Rosetta II cells (Novagene). Cells containing the respective plasmid were grown in 2xYT medium (supplemented with antibiotics) at 37 °C with shaking at 220 rpm until they reached an OD₆₀₀ of ~0.8. Subsequently the cell cultures were transferred to 16 °C, and the expression was induced after 20 min by the addition of isopropyl- β -D-thiogalactopyranosid (IPTG) to 0.5 mM final concentration. The cells were harvested after 16 hours at 16 °C.

Purification of eIF2B α : Cells containing C-terminally His-tagged eIF2B α were resuspended in L-100-His buffer (20 mM Hepes (pH 7.5), 100 mM KCl, 10% glycerol, 15 mM imidazole, 2 mM β -mercaptoethanol) containing a mixture of protease inhibitors including aprotinin, leupeptin, pepstatin (ALP), and PMSF. Cell lysis was performed in a microfluidizer (Microfluidics, USA), and

cell debris was removed by centrifugation for 30 min at 30,000 xg. The supernatant was loaded onto a HisTrap column (GE Healthcare) equilibrated in L-100-His buffer. The column was then washed with 2 column volumes of L-100-His buffer and bound protein was eluted with a linear gradient into elution buffer (L-100-His buffer with 350 mM imidazole). Fractions containing the target protein were pooled, concentrated to a volume of 5 ml and applied to a Superdex S-200 gelfiltration column (GE Healthcare) equilibrated in G-100 buffer (10 mM Hepes (pH 7.5), 100 mM KCl, 10% glycerol and 2 mM DTT). The pure protein was concentrated to 20 mg/ml, flash-frozen in liquid nitrogen and stored at -80 °C.

Purification of eIF2B β , eIF2B β (Δ 123-148) and eIF2B δ : All three constructs were expressed as N-terminally GST-tagged fusion proteins. Cell lysis was performed as described for eIF2B α with the difference that L-500 buffer (20 mM Hepes (pH 7.5), 500 mM KCl, 10% glycerol, 4 mM β -mercaptoethanol) was used to resuspend the cells. After removal of cell debris by centrifugation, the supernatant was applied to a GSTrap column (GE Healthcare) equilibrated in L-500 buffer. After washing the column with 4 column volumes of L-500 buffer, the bound fusion protein was eluted with 30 mM reduced glutathione in L-500 buffer. Fractions containing the target protein were pooled and desalted on a HiPrep Desalting column (GE Healthcare) equilibrated in desalting buffer (10 mM Hepes (pH 7.5), 200 mM KCl, 10% glycerol, 4 mM β -mercaptoethanol). The pooled protein was incubated over night at 4 °C with Prescission protease in a 1:100 weight ratio of protease to target protein to remove the GST-tag. In order to remove the GST-tagged protease, cleaved GST and uncleaved fusion protein the sample was applied to a second GSTrap column equilibrated in desalting buffer. The flow-through was pooled and concentrated to 5 ml before loading onto a Superdex S-200 gelfiltration column equilibrated in G-100 buffer. eIF2B β and eIF2B β (Δ 123-148), which eluted as pure protein in a single peak, were concentrated to 15-20 mg/ml and stored at -80 °C. eIF2B δ usually suffered strong degradation resulting in the cleavage of the full-length protein into two fragments migrating at ~36 kDa and ~20 kDa, respectively, on the SDS-PAGE. As a consequence, eIF2B δ eluted in two major peaks from the S-200 column containing either the full-length protein or the 36-kDa fragment. Both fragments were pooled independently, concentrated to 10-15 mg/ml and stored at -80 °C.

Protein crystallization and structure determination

eIF2B β . Initial crystallization trials for full-length eIF2B β were performed by sitting-drop vapor diffusion with commercially available standard screens. No crystals were obtained at any of the tested protein concentrations (between 6 and 15 mg/ml) or temperatures (4 and 20°C). In order to improve the crystallizability of the protein, we decided to remove residues 123 to 148 from the peptide-chain by deletion of the corresponding coding sequence from the expression vector. According to multiple sequence alignments of *C. thermophilum* eIF2B β with its homologs from other species, these residues are not conserved and seem to correspond to a loop region between two conserved α -helices that is idiosyncratic to *cteIF2B β* . Thus, we reasoned that its removal would have no negative impact on the overall structure of the protein, which is supported by the fact that it still forms a complex with eIF2B subunits α and δ (see below). In initial crystallization trials with the construct eIF2B $\beta\Delta$ 123-148, crystals were obtained after 5 days at 20 °C in a condition containing 100 mM HEPES (pH 7.5) and 1.0 M tri-sodium citrate. After optimization, diffraction quality crystals were obtained with 9.5 mg/ml protein at 20 °C in 100 mM HEPES (pH 6.8) and 1.33 M tri-sodium citrate. X-ray diffraction data were collected at BL 14.1 (HZB, BESSY, Berlin) [113]. The phase problem was solved by molecular replacement using the program PHASER [115] and the atomic coordinates of the N-terminal domain of the *Bacillus subtilis* 5-methylthioribose 1-phosphate isomerase (PDB: 2YVK) and the C-terminal domain of *Homo sapiens* eIF2B α (PDB: 3ECS) as independent search models. The structure was refined in trigonal space group R3 at a resolution of 2.54 Å using the program PHENIX [117]. Missing regions of the peptide chain were built manually in Coot [116]. The final model contains two molecules per asymmetric unit (see Table 1 for details of data collection and refinement).

eIF2B δ . Initial crystallization trials for eIF2B δ were performed by sitting-drop vapor diffusion with commercially available standard screens. With the truncated version of eIF2B δ (35 kDa fragment) initial crystals grew with 10 and 12 mg/ml protein at 20 °C in a condition containing 100 mM MES (pH 6.0) and 1.0 M (NH₄)₂SO₄. After optimization, diffraction quality crystals were obtained in 100 mM MES (pH 6.2) and 0.8 M (NH₄)₂SO₄. X-ray diffraction data were collected at BL 14.1 (HZB, BESSY, Berlin) [113]. The phase problem was solved by molecular replacement using PHASER [115]. As independent search models we used the atomic coordinates of α -helices 2-4

(residues 27-93) of the N-terminal domain of *Homo sapiens* eIF2B α (PDB: 3ECS), and residues 116-295 of its C-terminal domain. The structure was refined in primitive orthorhombic space group $P2_12_12_1$ at a resolution of 2.54 Å using the program PHENIX [117]. The final model contains two molecules per asymmetric unit (see Table 1 for details of data collection and refinement).

Interaction studies by analytical size exclusion chromatography

Complex formation between eIF2B α , - β and - δ was studied by size exclusion chromatography on an analytical Superdex S-200 (10/300) column (GE Healthcare). For the individual standard runs for the subunits, 50 μ g protein in a total volume of 300 μ l was loaded onto the column equilibrated in running buffer (100 mM KCl, 20 mM Tris/HCl (pH 7.5) and 2 mM DTT). For the analysis of binary complex formation between two subunits, 50 μ g of each protein were mixed in 300 μ l running buffer and incubated for 5 min at 20 °C before loading onto the column. In case of the eIF2B β -eIF2B δ mixture, the simultaneous presence of both proteins resulted in their complete precipitation until only the subunit added in excess over the other was still in solution. To study complex formation between all three subunits, eIF2B β (50 μ g) was first mixed with a ~2-fold excess of eIF2B α (100 μ g), followed by the addition of eIF2B δ in ~1.5-fold excess over the β -subunit (80 μ g). The mixture was incubated for 5 min at 20 °C in 300 μ l running buffer before loading onto the column. The runs were monitored at absorption wavelengths of 280 and 254 nm.

Chapter 5 • The domain release mechanism of eIF5B

This manuscript has originally been published in *The EMBO Journal*

eIF5B employs a novel domain release mechanism to catalyze ribosomal subunit joining

Bernhard Kuhle^{1,§} and Ralf Ficner¹

¹ Abteilung für Molekulare Strukturbiologie, Institut für Mikrobiologie und Genetik, Göttinger Zentrum für Molekulare Biowissenschaften, Georg-August-Universität Göttingen, D-37077 Göttingen, Germany

[§] To whom correspondence should be addressed: bkuhle@gwdg.de

Keywords: crystal structure; molecular machines; GTPase; ribosome; subunit joining; translation initiation

Received 6 November 2013 | Revised 6 February 2014 | Accepted 20 February 2014 | Published online 31 March 2014

The EMBO Journal (2014) 33: 1177–1191 (DOI 10.1002/emboj.201387344)

Author contributions:

BK: Conceived the study and designed the experiments; prepared and crystallized proteins, collected X-ray data and solved the structures; performed ITC experiments; created figures; analyzed data and wrote the manuscript. RF: analyzed data and helped to draft the manuscript.

Abstract

eIF5B is a eukaryal translational GTPase that catalyzes ribosomal subunit joining to form elongation competent ribosomes. Despite its central role in protein synthesis, the mechanistic details that govern the function of eIF5B or its archeal and bacterial (IF2) orthologs remained unclear. Here, we present six high resolution crystal structures of eIF5B in its apo, GDP- and GTP-bound form that, together with an analysis of the thermodynamics of nucleotide binding, provide a detailed picture of the entire nucleotide cycle performed by eIF5B. Our data show that GTP binding induces significant conformational changes in the two conserved switch regions of the G domain, resulting in the reorganization of the GTPase center. These rearrangements are accompanied by the rotation of domain II relative to the G domain and release of domain III from its stable contacts to switch 2, causing an increased intrinsic flexibility in the free GTP-bound eIF5B. Based on these data, we propose a novel domain release mechanism for eIF5B/IF2 activation that explains how eIF5B and IF2 fulfill their catalytic role during ribosomal subunit joining.

5.1 Introduction

Translation is the fundamental cellular process in which the ribosome synthesizes proteins according to genetically encoded information. Among the individual steps, translation initiation is the most complex and most divergent in the three domains of life, which is highlighted by the different number of initiation factors (IFs) employed by eukaryal (~12 eIFs) or bacterial cells (three IFs) to accomplish the same goals during ribosome assembly [9]. The major differences between eukaryal and bacterial translation initiation concern the formation of the 48S/30S pre-initiation complex (pre-IC) where the small 40S/30S ribosomal subunit is assembled at the AUG start codon of an mRNA with the charged initiator-tRNA (Met-tRNA_i^{Met}/fMet-tRNA^{fMet}) in its P site [9]. This is followed by the formation of the elongation competent 80S/70S ribosome, which is achieved by the joining of the large 60S/50S ribosomal subunit, catalyzed by the orthologous GTPases eIF5B, aIF5B and IF2 in eukarya, archaea and bacteria, respectively [15, 144, 145].

Together with the elongation factors EF-Tu and EF-G the initiation factors eIF5B, aIF5B and IF2 form the set of canonical translational GTPases (trGTPases) that are ubiquitous in extant

cellular life. This suggests that the function of eIF5B and its orthologs was fixed at an early stage of cellular evolution before the onset of speciation, reflecting the importance of subunit joining as the final control step in the initiation pathway. Up to now, however, the structural dynamics between the active and inactive factor that govern the process of subunit joining, and the degree of their conservation across the three domains of life remain unclear.

Earlier crystal structures of aIF5B and IF2 revealed similar architectures for both proteins with an N-terminal GTP binding (G) domain and a β -barrel domain II as structural core, followed by domains III and IV [82-84]. IF2 and eIF5B contain an additional N-domain, which displays little conservation in sequence and length and was shown to be dispensable for the function of yeast eIF5B [85].

Like all trGTPases eIF5B and its orthologs belong to the family of guanine nucleotide-binding (G) proteins [24]. Consequently, their mechanism has to be viewed as a specific variation of the classical concept of G proteins as molecular switches that alternate between an inactive GDP- and a structurally distinct active GTP-bound state. The transition between the two states is defined by conformational changes in two dynamic elements of the G domain, termed switch 1 and switch 2, which specifically interact with the γ -phosphate of the GTP molecule [23]. Only in the GTP-bound state the G protein interacts tightly and productively with effector molecules. Accordingly, the functional cycle of the G protein ends when it is 'switched off' by GTP hydrolysis and the following structural transition to the inactive GDP-bound state [23, 24].

For eIF5B it was demonstrated that it interacts with the ribosomal subunits and catalyzes 80S ribosome formation in a GTP-dependent manner [145, 146]. It was further shown that subunit joining occurs catalytically in the presence of GTP but only stoichiometrically with the nonhydrolyzable GTP analog GDPNP. This indicates that GTP hydrolysis is required for the release of the factor from the 80S ribosome, in line with the observation that GDPNP but not GTP slows down the dissociation of eIF5B from 80S ribosomes and inhibits the peptidyl-transfer reaction [85, 145]. Similarly, it was found that IF2 promotes subunit joining much more efficiently in the presence of GTP and GDPNP than with GDP, and that GTP hydrolysis is required for the dissociation of the factor and subsequent peptide-bond formation [147-149]. Based on this evidence, it was

suggested that eIF5B and IF2 employ a similar mechanism to promote subunit joining [147] which is compatible with the classical concept of G protein function.

However, this assumption stands in sharp contrast to other structural and biochemical data. It was found that GDP- and GTP-bound IF2 catalyze subunit joining nearly equally well, and that GTP hydrolysis is not required for the release of IF2 from the ribosome [150, 151]. Based on these observations, it was proposed that IF2 functions differently from eIF5B and as a non-classical GTPase with apparently no role for GTP hydrolysis [27, 82, 150], raising the question why the catalytic machinery required for GTP binding and hydrolysis is universally conserved in IF2.

So far available structure-based models for eIF5B/IF2 function do not provide explanations for these contradictory results. The ‘articulated lever model’ for eIF5B/IF2 function, which is based on crystal structures of aIF5B, assumes that a GTP-induced ~ 2 Å shift in switch 2 is amplified by an *en bloc* rearrangement of domains II to IV into a ~ 5 Å movement of domain IV [84]. According to this model, neither switch 1 nor switch 2 undergoes the conformational changes or form the direct contacts to the γ -phosphate that are typical for the classical molecular switch. However, low resolution cryo-EM reconstructions of bacterial and eukaryal 70S/80S ICs revealed conformations of IF2 and eIF5B that are incompatible with the articulated lever model [91, 152]. In order to reconcile the contradictory experimental data with the classical concept of molecular switching it was suggested that eIF5B and IF2 follow a mechanism of ‘conditional switching’, in which GTP binding alone is insufficient to activate eIF5B/IF2 but requires the ribosome as a cofactor that shifts the equilibrium between an inactive and an active GTP-bound form toward the latter [153, 154]. More recently it was proposed that IF2 does not have an ‘effector domain’ like other trGTPases and therefore behaves different from eIF5B and not as a classical GTPase [82], which, however, leaves open the question how the nucleotide status of the G domain is communicated into domains III and IV.

For aIF5B as well as IF2, crystal structures have previously been solved in the GDPNP- and GTP-bound state, respectively [83, 84]. However, in both cases the G domain remained in the apo/GDP conformation despite the presence of the γ -phosphate. Thus, the knowledge of eIF5B and IF2 function is limited by the fact that up to now no high resolution structural information is available for their GTP-bound forms that is in agreement with the classical concept of molecular

switching. Though of paramount importance to the understanding of eIF5B/IF2 function, it is therefore not known what distinguishes the active from the inactive state of the G domain and how these differences modulate the affinity of the overall eIF5B/IF2 to ribosomal effector complexes or influence the mechanism of ribosome induced GTP hydrolysis.

Here we present thermodynamic data and high resolution structures of eIF5B that provide a detailed picture of its entire nucleotide cycle. We determined six crystal structures of eIF5B from *Saccharomyces cerevisiae* and *Chaetomium thermophilum* containing the G domain and domains II-IV or substructures thereof in the apo, GDP- and GTP-bound states. These structures unambiguously demonstrate that the G domain of free eIF5B follows the classical switch mechanism involving large structural rearrangements of the two switch regions. The GTP-induced changes result in the formation of a catalytic GTPase center similar to that in EF-Tu suggesting a possible scenario for ribosome dependent GTPase activation in eIF5B. Most importantly, the various structures in combination with an analysis of the thermodynamics of nucleotide binding suggest a mechanism for eIF5B activation in which the local switch within the G domain is propagated into the rest of the factor through the release of domain III, resulting in an increase of intrinsic flexibility that is necessary for efficient subunit joining. Based on these observations, we propose a domain release mechanism for eIF5B activation, which represents a novel variation from the classical paradigm of G proteins and suggests a unified picture of subunit joining by α -eIF5B and IF2.

5.2 Results

Overall structure and domain arrangement in apo eIF5B

Six different crystal structures of eIF5B from *Chaetomium thermophilum* (Ct) and *Saccharomyces cerevisiae* (Sc) were solved either in the apo form or cocrystallized with GDP or GTP. All structures were solved by means of molecular replacement. A summary of structures, crystallographic details and data statistics is presented in Table I and Fig. S1.

The topology of the individual domains as well as the overall domain arrangement of apo eIF5B is similar to that of the archeal ortholog aIF5B [84] (Fig. 1). Domains I-III form the core structure that is assembled as triangle around switch 2 of domain I (G domain). Domains I and II

Table 1. Crystallization, X-ray data collection and refinement statistics

Organism	<i>C. thermophilum</i>				<i>S. cerevisiae</i>	
Construct (purified)	eIF5B(517C)	eIF5B(517C)	eIF5B(517-970)	eIF5B(517-970)	eIF5B(399-852)	eIF5B(399-852)
Construct in structure	eIF5B(517C) apo	eIF5B(870C)	eIF5B(520-970)-GDP	eIF5B(517-860)-GTP	eIF5B(401-852) apo	eIF5B(401-852)-GDP
Crystallization						
Condition	100 mM MES (pH 6.8), 12% PEG 20000, 10 mM Na-lactate	100 mM MES (pH 6.8), 12% PEG 20000, 10 mM Na-lactate	15% PEG 8000 and 0.5 M Li ₂ SO ₄	100 mM Hepes (pH 7), 13% PEG 4000 and 100 mM NaOAc	20% ethylene glycol, 5% PEG 3350 and 20 mM MgCl ₂	8% PEG 8000 and 0.37 M Li ₂ SO ₄
Temperature (°C)	4	4	20	20	4	10
Data Collection						
Space Group	P3 ₂ 21	P3 ₂ 21	P2 ₁ 2 ₁ 2 ₁	P2 ₁	P41	P2 ₁ 2 ₁ 2 ₁
Unit Cell	a = b = 111.5 Å c = 115.2 Å	a = b = 98.2 Å c = 97.4 Å	a = 66.9 Å b = 72.9 Å c = 199.2 Å	a = 55.4 Å b = 114.8 Å c = 65.9 Å	a = b = 118.0 Å c = 77.5 Å	a = 73.6 Å b = 119.5 Å c = 120.7 Å;
	α = β = 90° γ = 120°	α = β = 90° γ = 120°	α = β = γ = 90°	α = 90° β = 102.3° γ = 90°	α = β = γ = 90°	α = β = γ = 90°
Molecules/asym. unit	1	1	2	2	2	2
Resolution (Å)	2.75 (2.85-2.75)	3.2 (3.3-3.2)	2.12 (2.21-2.12)	1.87 (1.97-1.87)	1.83 (1.93-1.83)	3.02 (3.12-3.02)
Observed reflections	168769 (15898)	59836 (5506)	288203 (38832)	251805 (36887)	426259 (62736)	108724 (10591)
Unique reflections	22063 (2217)	9288 (800)	56555 (7213)	66297 (9605)	93360 (13677)	21521 (1972)
Completeness (%)	99.9 (100)	99.8 (100)	99.7 (99.9)	99.8 (99.8)	99.8 (99.9)	99.2 (99.5)
<I>/σ	32.66 (3.29)	32.12 (4.31)	17.79 (2.97)	20.53 (2.38)	21.05 (3.11)	23.3 (3.52)
R _{sym} (%)	3.7 (58.9)	3.4 (57.4)	5.6 (63.1)	4.4 (62.0)	3.9 (52.5)	5.3 (60.6)
Refinement						
R _{work} (%)	19.3	19.0	21.9	16.7	16.8	24.9
R _{free} (%)	23.8	22.0	25.2	20.6	19.4	28.7
Rmsd from Standard Stereochemistry						
Bond length (Å)	0.005	0.003	0.005	0.019	0.008	0.004
Bond angles (°)	0.82	0.66	0.95	1.75	1.17	0.99
Ramachandran Plot Statistics						
Most favored (%)	98.0	98.0	98.8	98.3	98.5	97.0
Allowed regions (%)	2.0	2.0	1.2	1.7	1.5	3.0
Disallowed regions (%)	0	0	0	0	0	0

Values in parentheses refer to the highest resolution shell.

R_{work} and R_{free} factors are calculated using the formula $R = \frac{\sum_{hkl} |F(obs)_{hkl}| - |F(calc)_{hkl}|}{\sum_{hkl} |F(obs)_{hkl}|}$, where F(obs)_{hkl} and F(calc)_{hkl} are observed and measured structure factors, respectively. R_{work} and R_{free} differ in the set of reflections they are calculated from: R_{free} is calculated for the test set, whereas R_{work} is calculated for the working set.

are tightly associated through hydrophobic contact areas composed of β2 (part of switch 1), β3 and β4 in the G domain as well as β9, β10 and β16 in domain II (Fig. 1). The orientation of domain II relative to the G domain is nearly identical in Ct-eIF5B and Sc-eIF5B and similar to that found in IF2, EF-G or GDPNP-bound EF-Tu [48, 83, 155].

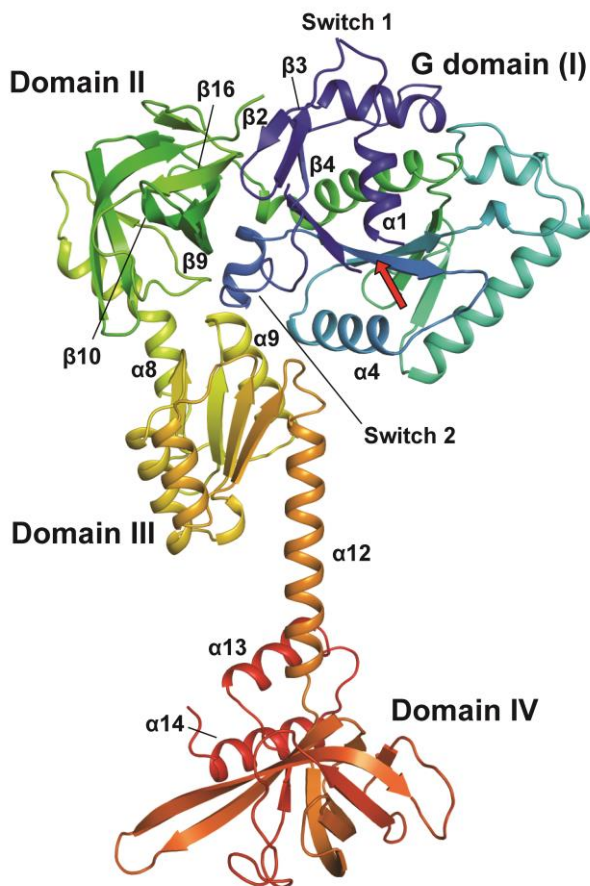


Figure 1. Front view of the overall structure of *C. thermophilum* eIF5B(517C) in the apo form. The C_{α} trace is shown in rainbow coloring from the N- (blue) to the C-terminus (red). The functional core of eIF5B is composed of the G domain (I) with the nucleotide binding site (arrow), domain II, domain III and domain IV.

Stable interactions of domain III with other domains are restricted to the area surrounding the N-terminal half of helix $\alpha 9$ (Fig. 1 and 3A/B). Van der Waals contacts are formed with domain II and the linker-helix $\alpha 8$ with a buried surface area of $\sim 700 \text{ \AA}^2$. Helix $\alpha 9$ also interacts with switch 2 as the only stable contact partner for domain III within the G domain. Further contacts are formed between the N-terminus of helix $\alpha 12$ and $\alpha 4$; however, these do not seem to be functionally relevant, as they differ between the various apo structures. Consequently, the orientation of domain III relative to the G domain differs considerably in Sc-eIF5B, Ct-eIF5B and aIF5B, which amounts to a displacement of the C-terminus of $\alpha 12$ by 12-22 \AA between the three apo structures (Fig. S2A). In a direct superposition of domain III from aIF5B, Ct-eIF5B(517C) and Ct-eIF5B(870C) the C-terminal ends of $\alpha 12$ lie only 3-3.5 \AA apart. However, domain IV adopts significantly different orientations relative to $\alpha 12$ and domain III, indicating a high degree of flexibility (Fig. S2B).

Conformational changes in the G domain of eIF5B upon GTP binding

GTP is bound by eIF5B in the way common for G proteins involving five conserved sequence motifs termed G1-G5 [24] (Fig. 2 and S3). The base is in contact with the $^{530}\text{NKID}^{533}$ (G4) and $^{598}\text{SAX}^{600}$ (G5) motifs (unless stated otherwise, *S. cerevisiae* sequence numbering will be used throughout) and

the phosphates of the nucleotide are stabilized by main- and side-chain interactions with the P loop (G1).

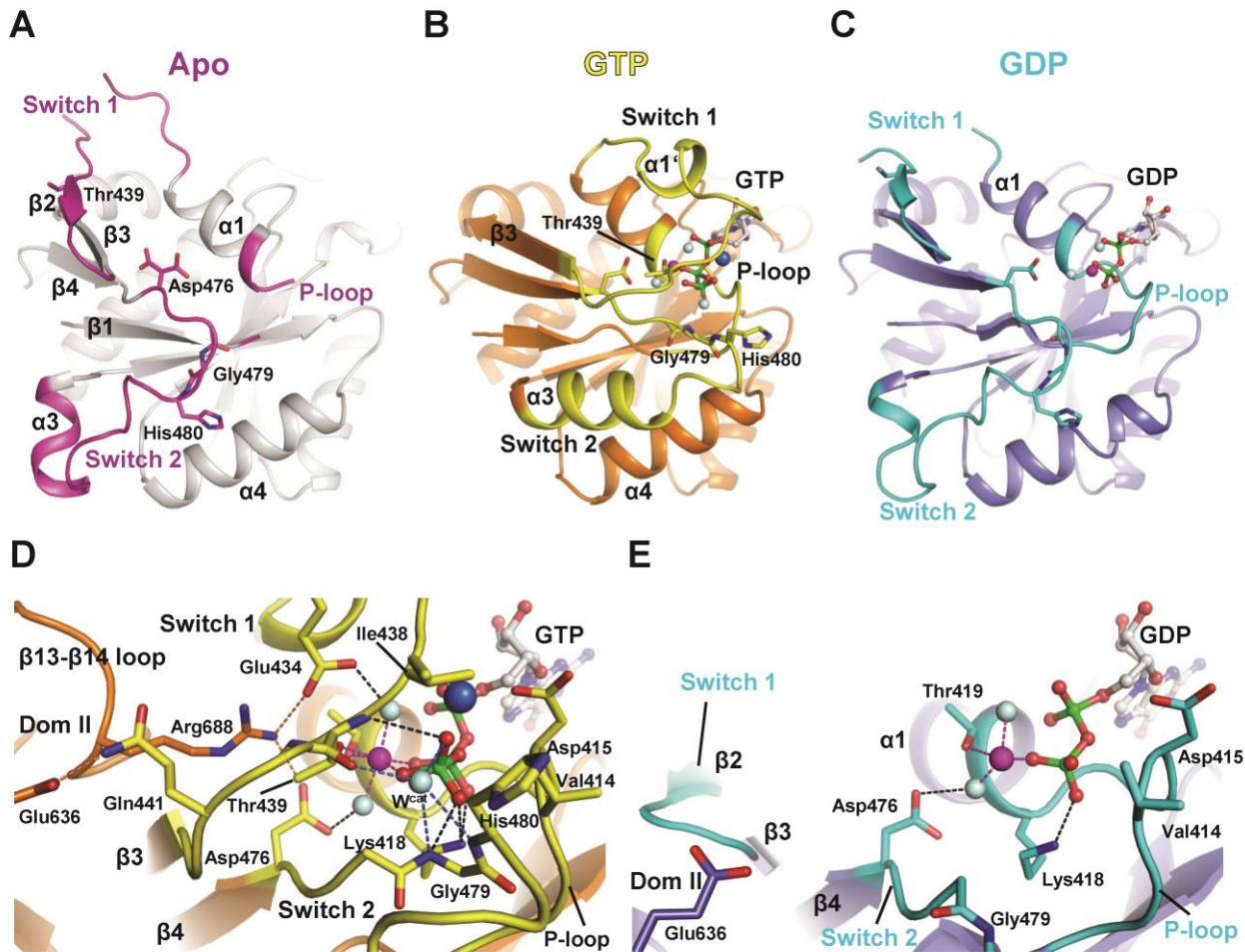


Figure 2. The nucleotide-dependent conformational switch in the G domain of eIF5B. **A-C)** Structural transition of the G domain from its apo form (**A**) to the GTP- (**B**) and the GDP-bound (**C**) states. P-loop, switch 1 and switch 2 are colored pink in the apo state, yellow in the GTP-bound state and cyan in the GDP-bound state. Thr439, Asp476, Gly479 and His480 (*S. cerevisiae* numbering) are shown as sticks; the Mg^{2+} ion, Na^+ ion and water molecules are shown as spheres in magenta, blue and grey, respectively; nucleotides are shown as balls and sticks. **D, E)** Network of interactions in the nucleotide binding pocket of the GTP- (**D**) and GDP-bound (**E**) factor. Direct interactions are indicated by dashed lines.

The most severe conformational changes are observed for the two switch regions which contain the $^{437}GIT^{439}$ (G2) and $^{476}DTPG^{479}$ (G3) motifs that function as sensors for the presence of the γ -phosphate (Fig. 2). In the apo state most of switch 1 (residues 427-443) forms an unstructured loop, which points away from the nucleotide binding pocket. Only within its last third

the inactive switch 1 forms a short β strand ($\beta 2$) oriented antiparallel to $\beta 3$ as part of the interface with domain II. Upon GTP binding, switch 1 flips over by $\sim 180^\circ$ using Gln427 and Gly443 as hinges (Fig. 2A/B and S4A). As a result its N-terminal part is oriented antiparallel to helix $\alpha 1$ toward the nucleotide binding pocket where it forms a one-turn α -helix ($\alpha 1'$) above the α -phosphate, followed by a turn toward the β - and γ -phosphates that continues into $\beta 3$. The critical Thr439 is displaced from its position in $\beta 2$ of the apo state by nearly 20 Å to form direct contacts to the Mg^{2+} ion and the γ -phosphate. In this new position switch 1 has almost no contacts outside the nucleotide binding pocket with the exceptions of a salt bridge between Glu434 and Arg688 of the $\beta 13$ - $\beta 14$ loop and a hydrogen bond of Gln441 to the conserved Glu636 in domain II (Fig. 2D).

Switch 2 (476-492) undergoes a substantial rearrangement as well. In the apo state the G3 motif in switch 2 runs parallel to $\beta 4$ as far as Gly479, where the peptide backbone makes a sharp turn of $>90^\circ$ and continues through the inter-domain cleft formed by domains I-III toward the back of the protein (Fig. 2A and 3B). Here switch 2 turns a second time toward the dorsal side of the G domain forming the two-turn helix $\alpha 3$. In this conformation switch 2 makes van der Waals contacts to domain II but mainly interacts with domain III: The backbone CO of Ser484 accepts a hydrogen bond from Gly763, Arg487 forms a hydrogen bond and salt bridges to Glu766 and Asp770, and Arg489 forms a strong salt bridge to Asp740 (Fig. 3A/B).

Upon GTP binding Asp476 moves 3.1 Å toward the γ -phosphate and forms a hydrogen bond to one of the water molecules coordinating the Mg^{2+} ion (Fig. 2B/D and S4B). The universally conserved Gly479 of switch 2 moves ~ 8 Å toward the γ -phosphate; concomitantly, the peptide bond between Pro478 and Gly479 flips by $\sim 160^\circ$. In its new position Gly479 interacts directly with the γ -phosphate and the putative catalytic water molecule (W^{cat}). The movement of the G3 motif has a profound impact on the rest of switch 2: His480 moves by 12 Å and forms part of a loop at the front of the G domain that is stabilized by Arg487 (Fig. S4B). In its new position His480 lies next to Val414 (P loop) with the imidazole moiety pointing outward, away from W^{cat} (Fig. 2D). The rest of switch 2 (484-493) forms the extended helix $\alpha 3$ next to $\alpha 4$, with some residues up to 15 Å relocated from their original position in apo eIF5B; the axis through $\alpha 3$ is thereby rotated by more than 90° (Fig. S4A). In order to achieve this conformational change in switch 2 all its interactions to domain III in the apo state are necessarily broken (Fig. 3A/B).

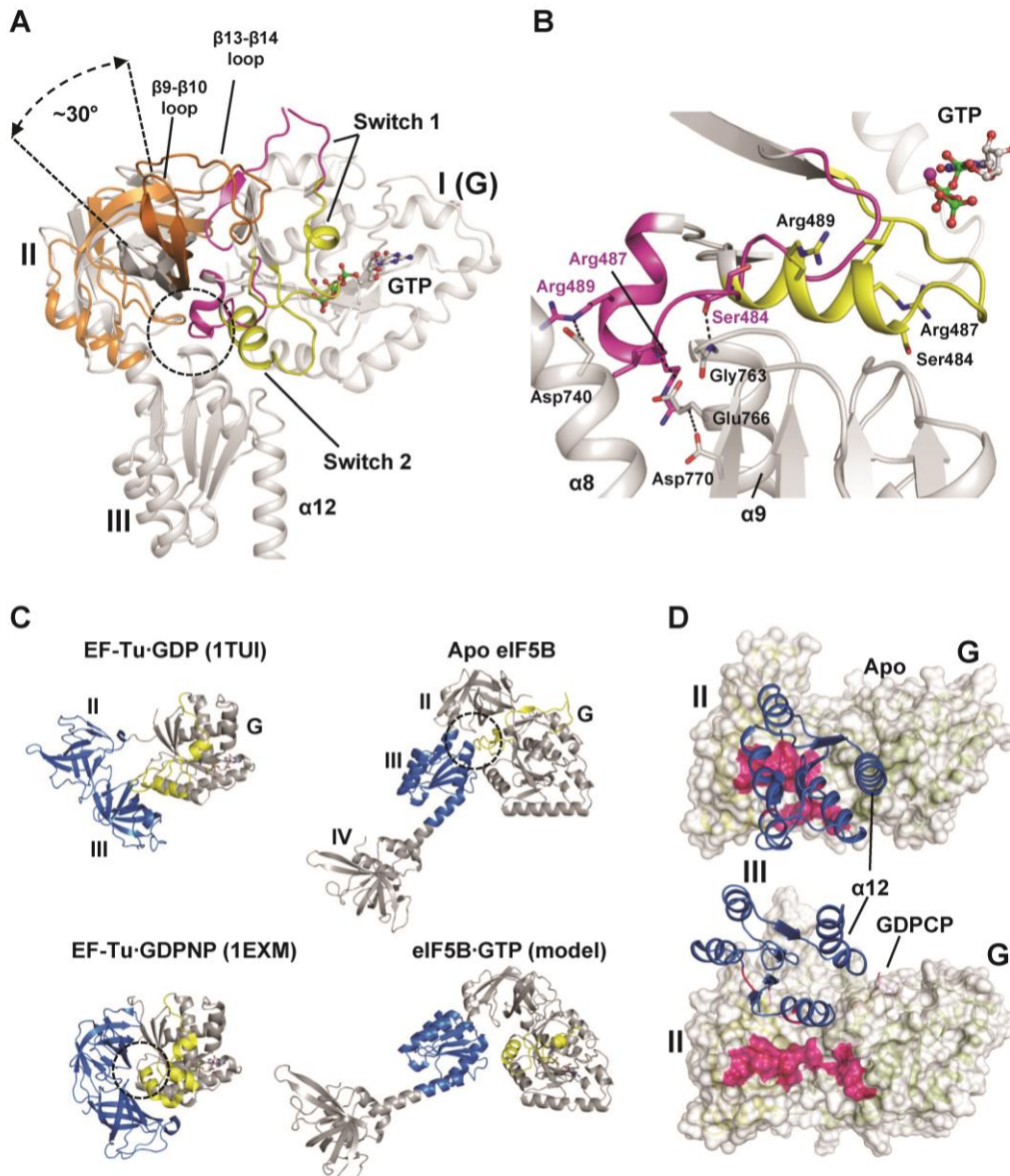


Figure 3. Nucleotide-dependent conformational changes in eIF5B. A) G domain-based superposition of domains I (G), II and III from Ct-eIF5B in the apo and GTP-bound state. Both G domains are shown in grey; otherwise the same color code as in Fig. 2. The GTP-induced rearrangements result in the loss of interactions between switch 2 and helices $\alpha 8$ and $\alpha 9$ (circle) and ultimately in the release of domain III from the G domain. Domain II rotates by $\sim 30^\circ$ relative to the G domain and is stabilized in its new orientation by the newly formed contact between $\beta 13\text{-}\beta 14$ loop and domain I. **B)** In apo eIF5B the inactive switch 2 (pink) forms stable contacts to helices $\alpha 8$ and $\alpha 9$ of domain III which are broken upon the GTP-induced transition of switch 2 to its active state (yellow). **C)** Comparison of the molecular switch mechanisms in EF-Tu (left) and eIF5B (right). Both trGTPases are shown in their inactive apo or GDP-bound (top) and GTP-bound (bottom) states, respectively. Functionally relevant interactions between the switch regions (yellow) of the G domain and downstream functional domains (blue) are indicated by dashed circles. **D)** The contact surface (pink) found between domain III (blue) and domains I and II in apo eIF5B (top) is entirely lost in ribosome-bound eIF5B-GDPCP (bottom; PDB: 4BVX [91]), where domains III and IV become stabilized between SRL and Met-tRNA_i^{Met} (not shown).

Switch 1 and switch 2 are stabilized in their active GTP-bound conformations through a network of interactions surrounding the Mg^{2+} ion and γ -phosphate (Fig. 2D). The Mg^{2+} ion is coordinated by six oxygen ligands with octahedral coordination geometry; two of the ligands are water molecules, two come from the β - and γ -phosphates and two are provided by the side chains of Thr419 and Thr439. The γ -phosphate is further stabilized by Lys418 (P loop), Thr439 and Gly479. W^{cat} lies 2.8 Å from the outward pointing γ -phosphate oxygen in position for an in-line attack on the γ -phosphate, stabilized by the backbone amides of Gly479 and His480 and the backbone CO of Thr439. Next to the γ -phosphate an additional strong electron density was observed, which was assigned to a Na^+ ion. Its pentagonal coordination shell with the typical bond lengths of 2.3-2.5 Å [156] is constituted by two oxygens from the α - and γ -phosphates, the β - γ -bridging oxygen, the carboxylate of Asp415 (P loop) and the CO from Gly437 in switch 1. Together, P loop, switch 1 and switch 2 form a closed ~ 10 Å deep pocket that accommodates the Mg^{2+} and Na^+ ions as well as all three phosphates with the γ -phosphate and W^{cat} at its bottom. His480 and bulk solvent are excluded from this pocket by a gate formed by Val414 and Ile438.

A comparison with the structure of EF-Tu·GDPNP [157] shows a strikingly high degree of similarity between the catalytic centers in GTP/GDPNP-bound EF-Tu and eIF5B with nearly identical positions for all conserved residues with a pair-wise C_{α} rmsd of 1.1 Å over 99 residues as well as for W^{cat} and the Mg^{2+} ion (Fig. 4A and S5A). However, the position occupied by the Na^+ ion in eIF5B is vacant in the EF-Tu·GDPNP structure and a perfect agreement between eIF5B and EF-Tu is restricted to residues that are directly involved in nucleotide binding or implicated in GTPase activity. Switch 1 in eIF5B lacks the second helix (A'') that serves factor specific functions in EF-Tu [48].

Domain rearrangements in eIF5B upon GTP binding

Upon GTP binding domain II performs two main movements that result from the activation of the G domain (Fig. 3A): on the one hand the dorsal portion of domain II tilts inward, following the movement of $\beta 3$ and $\beta 4$ that was induced by the 3.1 Å shift of Asp476 toward the Mg^{2+} ion (Fig. S4); on the other hand domain II rotates by $\sim 30^\circ$ causing the front portion to move upward and the ventral side to move parallel to switch 2 toward the front. The rotated orientation of domain II

is stabilized by a newly formed interaction of the β 13- β 14 loop (residues 684-689) with the G domain, which takes over the position next to β 3 that was originally occupied by β 2 and left vacant after the GTP-induced rearrangement of switch 1 (Fig. 2 and 3A).

As described above, all residues of switch 2 that are involved in contacts with domains II and III in the apo structure are rearranged and move by an average of ~ 14 Å upon GTP binding (Fig. 3B and S4). Since switch 2 is the main contact area for domain III in the G domain either a completely new set of interactions has to be formed or the interaction of domain III to the G domain is entirely lost. As domain III is not present in the structure of Ct-eIF5B-GTP, direct information about its position in free eIF5B-GTP is not available. However, our ITC experiments described below point toward a scenario in which domain III is released from the G domain without forming stable new contacts with the reorganized G domain in the free form of eIF5B-GTP (see below).

Conformational changes in eIF5B during the transition from the GTP- to the GDP-bound state

Subsequent to GTP hydrolysis and release of P_i most conformational rearrangements that followed GTP binding are reversed in eIF5B-GDP (Fig. 2). Switch 1 flips back to its original position, thereby displacing the β 13- β 14 loop. Switch 2 loses part of its α -helical structure and retracts toward the back of the protein to adopt a conformation nearly identical to that found in the apo form (Fig. S4). However, Asp476 in the G3 motif of Ct-eIF5B-GDP remains in its activated position in contact with the Mg^{2+} ion. Likewise, Thr477 and Pro478 retain their activated positions, whereas Gly479 is rotated back. As a consequence, the entire switch 2 is still shifted ~ 3 Å relative to its apo position but already forms the interactions to domains II and III found in apo eIF5B (Fig. S4). Accordingly, α 9 and therewith domain III are shifted 3-4 Å relative to their apo state position. Finally, also the ventral side of domain II is still shifted forward, however, no upward movement of its frontal face occurs, indicating that the loss of interactions between domains I and III is a prerequisite for this domain rearrangement (Fig. S4C).

In summary, the transition from the GTP to the GDP state allows domain III to reassociate with the core domains of eIF5B and reverses the rotation of domain II. Interestingly, binding of GDP and Mg^{2+} seems to be able to partially activate switch 2 (including the peptide flip of Gly479), which induces conformational strain on the switch 2-domain III interactions.

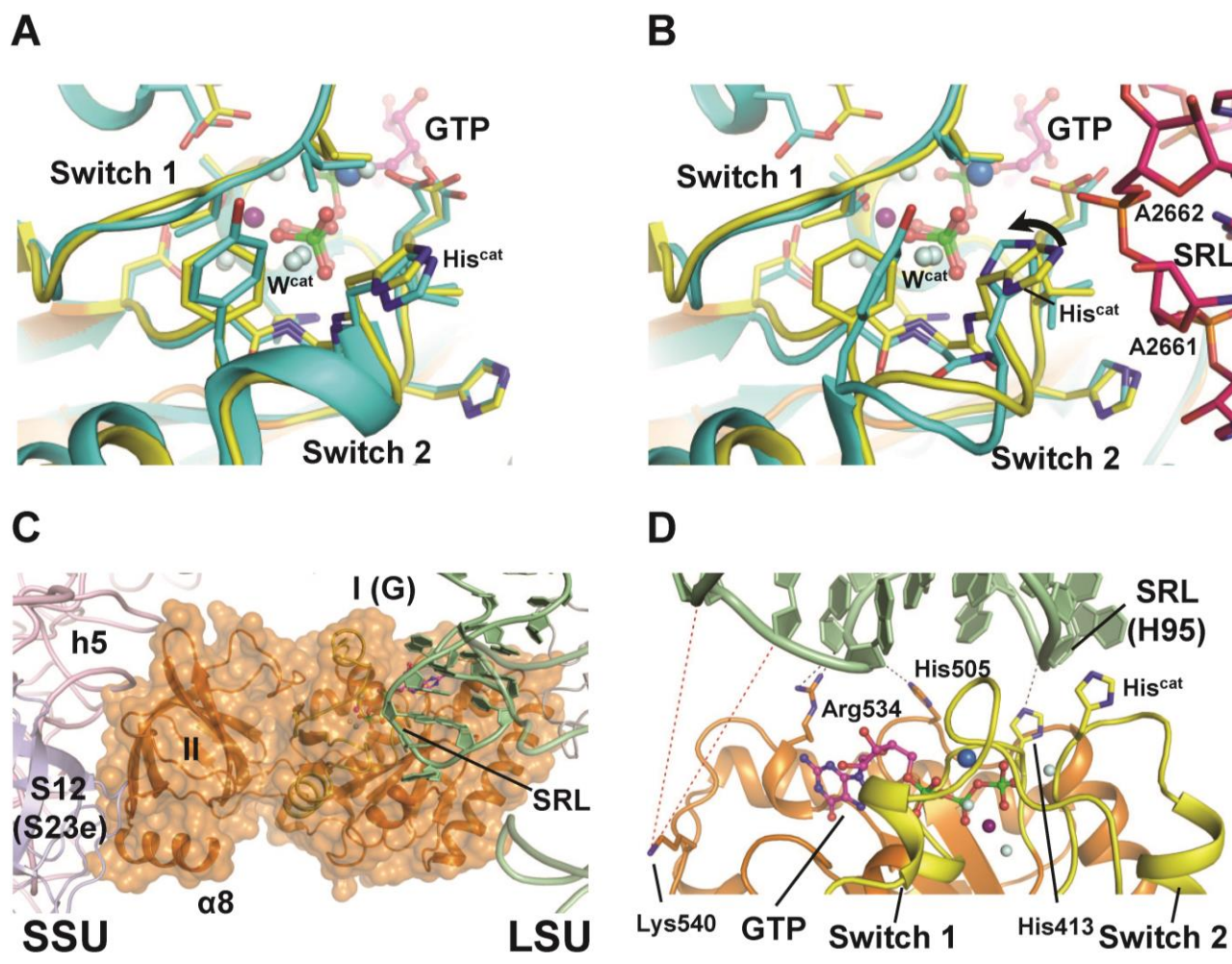


Figure 4. Structural model of eIF5B-GTP on the ribosome. **A**) Superposition of the catalytic centers of eIF5B-GTP (yellow) and free EF-Tu-GDPNP (cyan; PDB: 1EXM). Conserved residues are shown as sticks; GDPNP is omitted for clarity. **B**) Superposition of the catalytic centers of eIF5B-GTP (yellow) and ribosome-bound EF-Tu-GDPCP (PDB: 2XQD, 2XQE) with the sarcin-ricin loop (SRL) in pink. Structural alterations relative to free eIF5B-GTP and EF-Tu-GDPNP are limited to His^{cat} of EF-Tu, which is reoriented (arrow) into its active position between A2662 and W^{cat}. **C**) Model of domains I and II of eIF5B (orange) on the ribosome, based on the superposition with EF-Tu-GDPCP. Similar to eIF5B-GDPCP in the cryo-EM model of the 80S IC (see Fig. S5B) the G domain is associated with the SRL of the large subunit (LSU; green), while domain II interacts with the body of the small subunit (SSU; light pink). **D**) Putative interactions between the G domain and the SRL/H95 (green). Direct interactions are indicated by black dashed lines; red dashed lines indicate the positions in H95 that are cleaved by Fe(II)-BABE introduced in the position of Lys540 [90]. His505 lies only 3.5 Å from H95, explaining why the H505Y mutation results in a reduced affinity for the ribosome and GTPase deficiency in eIF5B [85] (see also Table S1). The conserved Arg534 likely contributes to the interactions with H95.

Thermodynamics of the interactions between eIF5B and guanine nucleotides

In order to gain further insight into the domain rearrangements during the nucleotide cycle of eIF5B we performed ITC experiments to determine the thermodynamic parameters of eIF5B binding to GTP and GDP in the temperature interval of 5-30 °C (a summary of the data is given in Tables II and III; Fig. 5 and S6).

To probe the conformational changes in eIF5B upon GTP binding and to test the particular influence of domain III we performed ITC experiments with two different constructs, one comprising domains I-IV (Ct-eIF5B(517C)), the other comprising only domains I and II (Ct-eIF5B(517-858)). In both cases, GTP binding was driven by favorable negative changes in binding enthalpy ($\Delta H = -9.34$ kcal/mol for domains I-IV and -18.8 kcal \cdot mol $^{-1}$ for domains I-II at 30 °C) and opposed by unfavorable entropic contributions (Table II).

For both constructs, ΔH plotted against the temperature results in a straight line with negative slope (Fig. 5A) representing the change in heat capacity (ΔC_p) which can be used as estimate for the change in solvent accessible surface area (ΔASA) upon complex formation (see Materials and Methods). For Ct-eIF5B(517C) a ΔC_p of -155 cal \cdot mol $^{-1}\cdot$ K $^{-1}$ is calculated, corresponding to 344 to 646 Å 2 of surface area that become buried upon GTP binding (Table III). In contrast, GTP binding to Ct-eIF5B(517-858), the construct lacking domains III and IV, gives a ΔC_p of -553 cal \cdot mol $^{-1}\cdot$ K $^{-1}$, corresponding to a GTP-dependent surface burial of 1229 to 2304 Å 2 , in agreement with the ~ 1800 Å 2 that become buried by switch 1 and the $\beta 13$ - $\beta 14$ loop in domains I and II according to the crystal structures (Table III). Thus, the presence of domains III and IV contributes to the overall ΔC_p of -155 cal \cdot mol $^{-1}\cdot$ K $^{-1}$ in Ct-eIF5B(517C) \cdot GTP with $+398$ cal \cdot mol $^{-1}\cdot$ K $^{-1}$ to compensate the contribution of -553 cal \cdot mol $^{-1}\cdot$ K $^{-1}$ by domains I and II alone. This corresponds to a ΔASA of 884 to 1658 Å 2 that are *exposed* upon GTP binding simultaneously to the *burial* of ~ 1800 Å 2 (or 1229 to 2304 Å 2) in domains I and II. The only reasonable candidates that can account for this compensatory effect are the surface areas buried between domain III and the G domain (~ 1150 Å 2) and domain II (~ 700 Å 2), respectively, in apo eIF5B (Fig. 5B). Thus, these data indicate that domain III is released from most or all its contacts with the G domain and domain II in response to the GTP-induced rearrangement of switch 2.

Table 2. Thermodynamic parameters of eIF5B binding to GDP and GTP at different temperatures and in presence or absence of Mg²⁺ ions.

Construct	Ligand	MgCl ₂ [mM]	T [°C]	K _d [μM]	ΔH [cal/mol]	ΔG [kcal/mol]	TΔS [kcal/mol]
Ct-eIF5B(517C)							
	GDP	2.5	5	2.09	-6286	-7.23	1.0
	GDP	2.5	10	1.92	-5057	-7.4	2.3
	GDP	2.5	15	2.61	-5240	-7.36	2.0
	GDP	2.5	20	2.9	-5520	-7.43	1.9
	GDP	2.5	25	3.3	-6058	-7.48	1.4
	GDP	2.5	30	3.45	-6650	-7.58	0.9
	GDP	0	5	0.8	-1855	-7.76	5.9
	GDP	0	10	1.0	-2385	-7.77	5.4
	GDP	0	15	1.14	-2805	-7.84	5.0
	GDP	0	25	1.96	-3912	-7.79	3.9
	GTP	2.5	5	4.21	-5346	-6.84	1.5
	GTP	2.5	10	4.83	-6192	-6.89	0.7
	GTP	2.5	15	5.68	-7033	-6.92	0.12
	GTP	2.5	20	6.02	-7423	-7.0	-0.6
	GTP	2.5	25	6.20	-8426	-7.1	-1.3
	GTP	2.5	30	7.04	-9344	-7.03	-2.2
Ct-eIF5B(517-858)							
	GTP	2.5	5	1.34	-4860	-7.47	2.6
	GTP	2.5	10	1.58	-7822	-7.52	-0.3
	GTP	2.5	20	2.12	-12985	-7.61	-5.4
	GTP	2.5	30	4.07	-18810	-7.48	-11.3

All measurements were performed two to four times; for GTP binding to both constructs and for GDP binding in the presence of Mg²⁺ the experiments were done with two independent purifications of the respective construct; for GDP binding in the absence of Mg²⁺ the experiments were done with protein from one purification.

K_d, dissociation equilibrium constant; calculated as 1/K_a.

K_a, association equilibrium constant; standard deviation did not exceed ±15%.

ΔH, standard enthalpy change; standard deviation did not exceed ±10%.

ΔG, Gibbs energy; calculated from equation $\Delta G = -RT \ln K_a$.

TΔS, standard entropy change; calculated from equation $\Delta G = \Delta H - T\Delta S$.

GDP binding to Ct-eIF5B(517C) was driven by favorable contributions of both, binding enthalpy and entropy (ΔH = -6.65 kcal/mol and TΔS = 0.9 kcal/mol at 30 °C) (Table II). In contrast to GTP binding, the temperature dependency of ΔH was not linear for GDP binding; instead the data between 10 and 30 °C fit better to a second order polynomial function, indicating a strong temperature dependency of ΔC_p (Fig. 5A). This suggests that the amount of contact surface within the formed complex changes over the used temperature range. At higher temperatures (30 °C)

Table 3. Changes in heat capacity and solvent accessible surface area for eIF5B binding to GDP and GTP

Construct	Ligand	ΔC_p [cal/mol·K]	ΔASA_{min} [Å ²]	ΔASA_{max} [Å ²]	ΔASA_{calc} [Å ²]
Ct-eIF5B(517C)	GDP _{+Mg}	-140 ± 23 ^a	-311	-583	-400 ^c
	GDP _{-Mg}	-102 ± 5 ^b	-227	-425	
	GTP _{+Mg}	-155 ± 8 ^b	-344	-646	
Ct-eIF5B(517-858)	GTP _{+Mg}	-553 ± 11 ^b	-1229	-2304	-1800 ^c

ΔC_p , heat capacity change; obtained from $\Delta H/dT$

ΔASA_{min} and ΔASA_{max} , changes in solvent accessible surface areas assuming that all changes were conferred by either apolar or 70% apolar and 30% polar surfaces, respectively

^a Calculated for 30 °C from the first derivative of the second order polynomial fit to ΔH measured at five different temperatures between 10 and 30 °C.

^b Obtained from the slope of the linear fit to ΔH measured at different temperatures between 5 and 30 °C.

^c Calculated from the crystal structures of GDP- and GTP-bound eIF5B relative to the apo state.

GDP binding results in a ΔC_p of $-140 \text{ cal}\cdot\text{mol}^{-1}\cdot\text{K}^{-1}$, corresponding to a surface burial of 311 to 583 Å² (Table III), which agrees well with a ΔASA of $\sim 400 \text{ Å}^2$ for GDP binding according to the crystal structures. However, the negative value for ΔC_p decreases with lower temperatures. Below 10 °C the second order polynomial behavior of ΔH breaks down and ΔC_p changes sign, indicating a net *exposure* of ASA upon GDP binding. Here, three observations based on the eIF5B·GDP structures are of particular interest: i) GDP/Mg²⁺ is able to partially activate switch 2 and to induce conformational strain on its interactions to domains II and III (Fig. S4), ii) domain III contacts switch 2 primarily through ionic interactions (Fig. 3B) which are destabilized at low temperatures [158, 159], and iii) domain III is released from the G domain in molecule B of Sc-eIF5B·GDP for which crystals were obtained at 10 °C (Table I; Fig. S1E and S7A). Since switch 1 and the $\beta 13$ - $\beta 14$ loop remain flexible in this structure, the release of domain III upon GDP binding results in a positive ΔASA corresponding to a positive contribution to ΔC_p as observed in the ITC experiments. The non-linear behavior of ΔC_p above 10 °C would thus indicate that domain III always has the propensity to be released in eIF5B·GDP due to the partial activation of switch 2 in the presence of Mg²⁺, however, with a reduced tendency to do so with increasing temperatures at which the ionic interactions to the G domain become increasingly stable [158, 159]. In line with this interpretation,

we found that the temperature dependency of ΔH does not break down at low temperatures when the ITC experiments are repeated with GDP in the absence of Mg^{2+} (Fig. 5A). Instead, ΔH plotted against the temperature results in a straight line with a slope (ΔC_p) of $-102 \text{ cal}\cdot\text{mol}^{-1}\cdot\text{K}^{-1}$, which is comparable to that for the eIF5B·GDP complex in the presence of Mg^{2+} at higher temperatures (Table III).

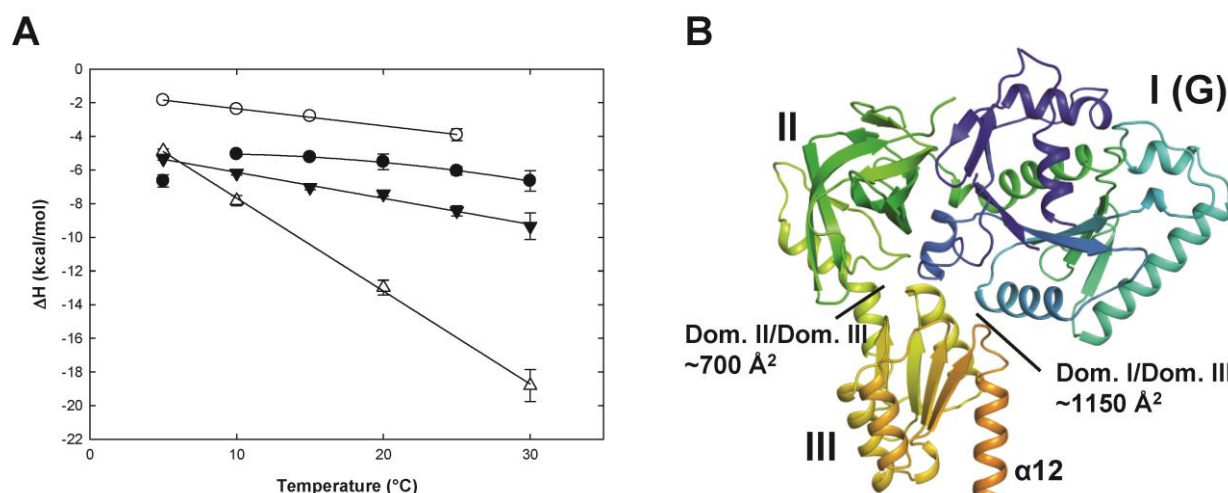


Figure 5. eIF5B interactions with guanine nucleotides measured by ITC. **A)** Heat capacity changes upon eIF5B interaction with GDP or GTP. Temperature dependency of binding enthalpy changes (ΔH) upon Ct-eIF5B(517C) interactions with GDP in the presence (●) or absence (○) of $MgCl_2$ and of Ct-eIF5B(517C) (▼) and Ct-eIF5B(517-852) (△) with GTP in the presence of $MgCl_2$. Standard deviations are given by error bars (in some cases not visible because they are smaller than the symbol size). **B)** Domains I-III of apo Ct-eIF5B. Indicated are the contact areas of domain III to domains I and II, respectively.

Taken together, these data support the idea that the conserved Asp476 in the G3 motif plays a critical role in the reorganization of switch 2 in response to nucleotide binding and indicate a direct connection between the Mg^{2+} ion and the temperature dependency of ΔC_p in the eIF5B·GDP complex. The fact that GTP binding in contrast to GDP binding shows no temperature dependency of ΔC_p indicates that the interactions of domain III to domains I and II in apo eIF5B are broken upon GTP binding regardless of the temperature at which the reaction takes place. However, here the

positive contribution to ΔC_p is compensated by the large negative contribution due to the burial of ASA in the GTP-bound G domain.

5.3 Discussion

The molecular switch between the GDP- and GTP-bound states of eIF5B: the domain release mechanism

The structural and thermodynamic data presented here provide the first detailed picture of the entire nucleotide cycle of eIF5B. The structures of eIF5B in its apo, GTP- and GDP-bound states reveal that its G domain follows the classical molecular switch mechanism, oscillating between an inactive (apo and GDP-bound) and a structurally distinct active GTP-bound form (Fig. 2). The GTP-induced transition from the inactive to the active conformation of the G domain is characterized by marked rearrangements in the two switch regions, which allow the conserved Thr439 of switch 1 and Gly479 of switch 2 to directly contact the γ -phosphate and W^{cat} , resulting in the formation of the catalytic GTPase center (Fig. 2B/D). This observation is in line with previous findings that the mutagenesis of Thr439 or Gly479 to Ala results in severe functional defects in eIF5B, including GTPase deficiency [85, 160] (see also Table S1). In switch 2 the initial signal of GTP binding experiences a considerable amplification along its way through the inter-domain cleft toward the back of the protein with a movement of 3 Å at Asp476, 8 Å in Gly479, 12 Å in His480 and finally ~14 Å in Arg487 and Arg489, which form the primary contact surface for domain III in apo eIF5B (Fig. 3A/B and S4A/B). As a result, domain III is released from the activated G domain, accompanied by the counter-clockwise rotation of domain II with respect to the G domain (Fig. 3A). As indicated by the ITC data, domain III remains released in free eIF5B·GTP and does not form stable new contacts to the reorganized switch regions. Thus, the signal of GTP binding is amplified from a relatively small conformational change in the nucleotide binding pocket into the release of domain III and thereby ultimately translated into a gain of conformational freedom and higher structural flexibility of domains III and IV relative to domains I and II.

This mechanism for the activation of eIF5B in solution contradicts earlier assumptions that GTP alone is insufficient to induce the conformational switch in free eIF5B in the absence of the ribosome as auxiliary cofactor, which forms the basis for the hypothesis that eIF5B follows a

mechanism of conditional switching [153]. Moreover, the domain release mechanism is in stark contrast to the previously proposed non-classical articulated lever model for eIF5B/IF2 function, in which the GTP-induced conformational changes in the G domain are limited to a ~ 2 Å shift in switch 2. This causes a rigid body movement of domains III and IV and a displacement of the latter by ~ 5 Å as ultimate result of eIF5B activation [84, 144]. In contrast to the release mechanism, this involves neither a conformational change in switch 1 or switch 2 to form the canonical catalytic GTPase center nor does it require the loss or the formation of contacts between G domain and domains II and III at any stage of the activation process (Fig. S8). The articulated lever model therefore does not explain why switch 1 and switch 2 are universally conserved among eIF5B orthologs and why the mutagenesis of conserved residues in both motifs results in severe functional defects in eIF5B [85, 161, 162].

eIF5B combines the classical GTP operated switch mechanism in the G domain with a novel mechanism of activation for a trGTPase

TrGTPases such as eIF5B and EF-Tu are multidomain proteins which consist of a universally conserved structural core composed of the G domain and domain II that is supplemented with additional functional domains related to the respective role of the GTPase during translation. The activation of trGTPases by GTP is therefore not merely restricted to the G domain but involves a reorganization of the overall domain arrangement, induced by a modulation of the interactions between G domain and the downstream functional domains.

This principle was first established for the elongation factor EF-Tu. Here, the GTP-induced transition from the inactive apo form to the GTP-bound state depends on the rearrangement of the switch regions in the G domain that follows the canonical switch mechanism of Ras-like GTPases [163]. As a consequence, domain II, which is separated from the G domain in inactive EF-Tu, stably associates with the reorganized G domain involving the newly formed surface of the activated switch 2 [163] (Fig. 3C). Only in this more compact GTP-conformation EF-Tu is able to form a stable ternary complex with aminoacyl-tRNA – involving also the reorganized switch 1 – for delivery of the latter to the ribosome [48, 164-167]. Thus, the *presence* of the defined

active conformation of switch 1 and 2 functions as the critical signal and thereby is a necessity for the overall activation of EF-Tu (Fig. 3C).

The same basic principle of activation also applies to eIF5B. The G domain follows the classical molecular switch mechanism (Fig. 2) and the signal of G domain activation is propagated into domains II-IV through the reorganization of the switch regions. However, the mechanism by which this signal transduction is achieved appears to be different from that in EF-Tu and so far unprecedented in trGTPases: in eIF5B the GTP-induced *absence* of the *inactive* conformation of switch 2 and the resulting release of domain III seems to be the decisive signal that renders eIF5B·GTP activated for productive interactions with the ribosome (Fig. 3). This does not imply that the GTP-bound conformation of the G domain is irrelevant for eIF5B function but is most likely required for tight interactions of the G domain with the large ribosomal subunit and GTPase activity (Fig. 4) as well as to prevent the reassociation of domain III before GTP hydrolysis. Instead, this means that the defined GTP-conformation is not as critical for productive interactions between eIF5B and its effector molecules as it is for EF-Tu.

This scenario is in line with earlier biochemical studies that identified mutations in the G domain and domain III that are able to partially activate eIF5B by destabilizing the interactions between domain III and switch 2 in inactive eIF5B. The mutation of Gly479 in switch 2 to Ala was found to reduce GTP binding and to impair subunit joining and ribosome dependent GTP hydrolysis [160]. Our structural analysis shows that this Gly residue undergoes a peptide flip of $\sim 160^\circ$ during the transition of switch 2 from its inactive to the active state (Fig. 4B), a conformational change that is energetically not allowed for any other residue. G479A would thus stabilize the inactive switch 2 preventing the formation of the GTPase center and the release of domain III, ultimately causing the inability of the mutant to promote subunit joining and to hydrolyze GTP. A444V and D740R were identified as two independent intragenic suppressor mutants for G479A that restore nucleotide binding, GTP hydrolysis and subunit joining activities in eIF5B [160]. Interestingly, Asp740 is located in domain III ~ 30 Å apart from the nucleotide binding pocket and forms a direct salt bridge to the conserved Arg489 of the *inactive* switch 2 which moves ~ 15 Å upon GTP binding (Fig. 3B and S7B/C). Consequently, D740R would result in a steric and electrostatic repulsion of the inactive switch 2 and thereby a destabilization of the domain III-switch 2 contact in apo eIF5B.

A444V is located at the N-terminus of strand $\beta 3$ close to Asp476 in the G3 motif and most likely causes the constitutive reduction of the energy barrier that has to be overcome by GDP and GTP to move Asp476 into a GTP-like position thereby facilitating the distortion of the interactions between switch 2 and domain III [160] (Fig. S7C). Particularly interesting is that A444V does not only restore GTP dependency in eIF5B but even allows GDP to activate eIF5B for stable interactions with the ribosome [160]. This demonstrates that the full GTP-conformation in the G domain is not an absolute requirement for stable interactions between eIF5B and the ribosome. Instead, it seems to be critical that the suppressor mutations overcome the increased energy barrier introduced by G479A by destabilizing the inactive conformation and thereby the contact between switch 2 and domain III either directly in the case of D740R or indirectly in the case of A444V (see also Table S1).

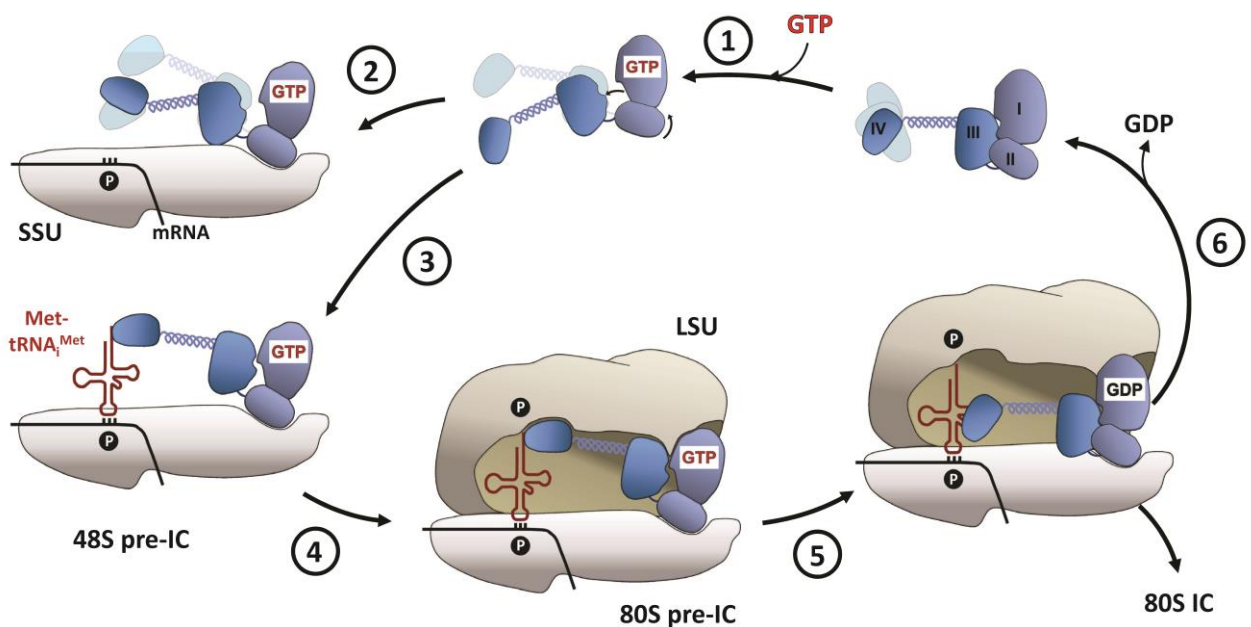


Figure 6. Schematic model of the nucleotide cycle of eIF5B during subunit joining. eIF5B with domains I (G) to IV is shown in blue. (1) GTP binding activates eIF5B by release of domain III and rotation of domain II relative to the G domain. **(2)** Binding of eIF5B-GTP to the small subunit (SSU) in the absence of Met-tRNA^{Met} results in a nonproductive complex in which eIF5B is not able to stimulate subunit joining. **(3)** In the correctly preassembled 48S pre-IC the subunit joining competent conformation of eIF5B-GTP is stabilized by the P site-bound initiator-tRNA, **(4)** resulting in the recruitment of the large ribosomal subunit (LSU). **(5)** Formation of the 80S pre-IC triggers GTP hydrolysis in eIF5B, which reverts back into its inactive conformation, **(6)** followed by the dissociation of eIF5B-GDP from the elongation competent 80S ribosome.

Implications of the domain release mechanism for ribosomal subunit joining

eIF5B interacts with the ribosomal subunits and catalyzes subunit joining in a GTP-dependent manner [145, 146]. This indicates that eIF5B undergoes a structural transition from the inactive apo-conformation to a GTP-bound state that allows productive interactions with its ribosomal effector complexes. However, it was shown in kinetic experiments that even in its GTP-bound state, eIF5B is unable to catalyze subunit joining unless the Met-tRNA_i^{Met} has been positioned in the P site of the 40S subunit [146]. This seemingly paradoxical situation is compatible with the domain release mechanism of eIF5B activation. On the one hand the GTP-induced release of domain III allows domain II to stably interact with the 18S rRNA (without steric hindrance by domain III as discussed below; see also Fig. S5C). On the other hand the conformational freedom of domains III and IV relative to each other (Fig. S2B), relative to domains I and II, as well as to the 40S subunit, prevent eIF5B from *self-supporting* a conformation that allows efficient subunit docking on the 40S·eIF1A complex without Met-tRNA_i^{Met} (Fig. 6). Consequently, for the domain release model a distinction has to be drawn between the activated state of eIF5B·GTP in solution and its subunit joining competent conformation on the 48S pre-IC, which is only one of the many possible conformations accessible to the free eIF5B·GTP, and which requires the reduction of conformational freedom of domains III and IV and their stabilization in the correct orientation. This proposed dependency of eIF5B·GTP on the ribosomal effector complex resembles the hypothesis of conditional switching for eIF5B [153]. However, the critical conceptual difference is that eIF5B does not require the ribosome as cofactor to induce the GTP-dependent conformational switch, but instead depends on the ribosomal effector complex to stabilize the sole conformation of GTP-bound eIF5B (among the many possible) capable to promote the association of the 60S subunit. The recent cryo-EM structures of eIF5B on the 80S ribosome demonstrate that this stability is primarily provided by the methionylated 3'-CCA end of Met-tRNA_i^{Met} [91]. In agreement with the domain release mechanism, the cryo-EM structures show that the activation of the G domain by GDPCP is sufficient to induce the release of domain III from switch 2 and domain II, but insufficient to stabilize domains III and IV in a defined conformation, as they remain disordered in the absence of amino-acylated tRNA. Only through the interactions between domain IV and the amino-acylated tRNA, domain III and IV become stabilized in their subunit joining competent conformation, in

which domain III is released from all its contacts to the G domain and domain II that are also found in the apo state of eIF5B and is reoriented relative to domain I and II by $\sim 65^\circ$ (Fig. 3D and S5C) [91].

Taken together, according to the presented domain release mechanism the preparation of eIF5B for the catalysis of subunit joining involves a two-step process: i) activation of the G domain by GTP binding, resulting in the release of domain III and an increased intrinsic flexibility that allows productive binding to the effector complexes and ii) stabilization of eIF5B·GTP in the subunit joining competent conformation by the 48S pre-IC through a reduction of conformational entropy within the factor (Fig. 6). According to this scenario, eIF5B requires GTP as well as the correctly assembled 40S·Met-tRNA_i^{Met} effector complex for its function. Thus, the domain release mechanism seems evolved to ensure the formation of productive 80S ICs by discriminating against pre-ICs that do not contain Met-tRNA_i^{Met}.

Ribosome induced GTP hydrolysis by eIF5B

Crystal structures of EF-G·GDPCP and EF-Tu·GDPCP on the ribosome suggest a common mechanism of GTPase activation for both elongation factors [168, 169]. According to the current model, the G domain of the translation factor binds to the sarcin-ricin loop (SRL) of the 50S ribosomal subunit and the GTPase activity is triggered as His^{cat} (His84 in EF-Tu) rotates inward, where it is stabilized by hydrogen bond interactions with the phosphate of A2662 (SRL) and W^{cat} which becomes subsequently activated for the in-line attack on the γ -phosphate [168].

Our own structural investigations show that the catalytic centers in eIF5B·GTP and free EF-Tu·GDPNP exhibit nearly identical positions for residues implicated in ribosome binding and GTP hydrolysis (Fig. 4). In line with the recent cryo-EM model of ribosome bound eIF5B [91], this suggests that domains I and II of eIF5B bind the 80S ribosome in the same way as the bacterial elongation factor (Fig. 4 and S5A/B). As for His84 in free EF-Tu·GDPNP, the imidazole moiety of His480 (His^{cat}) in eIF5B points outward and therefore requires rearrangement in order to contact W^{cat} (Fig. 4B). In combination with earlier studies that highlight the importance of His480 for GTP hydrolysis [161, 162], these observations strongly suggest that the ribosome dependent GTPase

activation of initiation factor eIF5B follows the same basic mechanism as employed for the elongation factors EF-Tu and EF-G.

Dissociation of eIF5B·GDP from the 80S ribosome

In accordance with the function of G proteins as molecular switches, the formation of the elongation competent 80S ribosome by eIF5B·GTP results in GTP hydrolysis and P_i release, followed by the dissociation of eIF5B·GDP [145, 161]. Thus, the reduced affinity for the ribosome and dissociation of eIF5B depends on its structural transition from the GTP-bound state to the inactive GDP-bound conformation.

Our data show that upon transition from the GTP- to the GDP-bound state the G domain of eIF5B switches back into its inactive conformation (Fig. 2 and S4A). As a result, domain III is retrieved to interact with switch 2 and domain II, causing the latter to rotate clockwise relative to the G domain (Fig. 3A and S4C). This reorientation relative to each other necessarily disrupts the interactions of the G domain and domain II with the 60S and 40S subunits, respectively, which were formed by eIF5B·GTP in the rotated state (the rotation is also observable in the cryo-EM structure of eIF5B in the 80S IC [91]). Under the assumption that the interactions between domain II and the 18S rRNA are the last to be broken (as they do not directly depend on the presence of GTP as do those of the G domain with the SRL), domain III moves away from the SRL and domain IV moves away from the peptidyl-transferase center (PTC) toward the 40S subunit and helix H38 (60S) (Fig. S5C). This position of eIF5B·GDP is not stable as domains III and IV would clash with the ribosomal protein S23e and eIF1A, respectively, and the G domain is rotated into the SRL. As a result, eIF5B would have to retreat from the factor binding site toward h6 of the 40S subunit as seen in the cryo-EM structure of IF2·GDP on the 70S ribosome [170], followed by its dissociation (Fig. 6).

IF2 might function according to the domain release mechanism

Despite a large body of experimental data for IF2, its precise mode of function during subunit joining in bacteria is still unclear [27, 82, 147, 150, 151]. For the reasons discussed below it is in our opinion reasonable to assume that the domain release mechanism also applies to IF2. Nearly all

residues involved in the contacts between switch 2 and domain III in eIF5B, particularly also those in the N-terminus of helix $\alpha 9$, are highly conserved in a/eIF5B/IF2 orthologs (Fig. S3). In structures of the IF2 G domain switch 2 is usually flexible with only partial helical character [82, 83, 171] and would thus be easily accessible for interactions with domain III. Moreover, from the high degree of structural and sequence homology it can be inferred that the G domain of IF2, like in eIF5B, follows the classical switch mechanism, resulting in the formation of the canonical active site. The transition of IF2 between the GDP- and GTP-bound states would therefore result in the release of domain III and an increase in the overall flexibility of the factor, and the reduction of flexibility and retraction of domain III upon GTP hydrolysis. Indeed this becomes apparent in cryo-EM structures of bacterial initiation complexes, where domain III is associated with domains I and II in IF2-GDP whereas the GTP/GDPNP-bound forms adopt an elongated shape to contact the P site-bound fMet-tRNA^{fMet} [152, 170, 172, 173].

The assumption that the domain release mechanism applies to IF2 seems to be contradicted by two recent structural studies [82, 83]. The only so far available high resolution structure of GTP-bound IF2 appears to indicate that its G domain does not follow the classical switch mechanism as switch 1 remains virtually unchanged upon GTP binding and switch 2 undergoes only a small local rearrangement without forming a contact to the γ -phosphate [83]. However, it is important to note that this IF2-GTP structure was obtained by soaking GTP into crystals of apo IF2, in which both switch regions are fixed by extensive contacts to symmetry related molecules. A reorganization of the G domain that would allow the G2 and G3 motifs to contact the GTP molecule in the classical way is thus most likely prevented by crystal contacts and not due to a non-classical behavior of IF2. The recent crystal structure of *T. thermophilus* IF2(3-467) in the apo and GDP-bound state as well seems to argue against the domain release mechanism for IF2 as domain III has no direct contact to either of the switch regions [82]. The authors propose that the increased length of helix $\alpha 8$ (the linker between domains II and III) compared to $\alpha 8$ in aIF5B accounts for the inability of domain III to contact switch 2 [82]. However, the lengths of helix $\alpha 8$ and the following flexible linker to domain III are actually compatible with a direct contact between the N-terminal half of helix $\alpha 9$ and switch 2 as observed in apo a/eIF5B (Fig. 3A/B). Instead, the crystal packing shows that the position occupied by domain III in a/eIF5B is occupied by symmetry related molecules in the IF2

crystals. Crystallization would therefore be selective for the state in which domain III is released, irrespective of its fraction among the IF2 molecules in solution. As we show by means of ITC and observe in the Sc-eIF5B-GDP structure (Fig. S1E and S7A), domain III in eIF5B has the ability to dissociate from the G domain even in the absence of GTP. This, we suggest, also applies to IF2.

As for eIF5B, the domain release model can explain why IF2 requires GTP for efficient interactions with ribosomal complexes and the fMet-tRNA^{fMet} in the context of the 30S pre-IC [147, 174], why IF2·GTP is unable to promote subunit docking in the absence of the initiator-tRNA [175] and finally, why even GDP is able to partially activate IF2 for ribosome binding and subunit joining in *in vitro* studies despite its inability to stabilize the GTP-conformation of the G domain. With the critical conceptual difference that in the domain release mechanism the GTP-dependent conformational switch in IF2 precedes and is therefore not a consequence of its interaction with the ribosome, this hypothesis of a common mechanism for eIF5B and IF2 is in agreement with previous proposals of a stepwise activation mechanism for IF2 by GTP and the 30S·fMet-tRNA^{fMet} complex made on the basis of biochemical experiments [147, 154].

5.4 Materials and Methods

Protein preparation, crystallization and structure determination

The N-terminally His-tagged versions of eIF5B from *C. thermophilum* (Ct-eIF5B(517-1116), -(517-970) and -(517-858)) and *S. cerevisiae* (Sc-eIF5B(399-852)) were expressed in *E. coli* and purified using standard procedures. Crystals used for structure determination were obtained by sitting-drop vapor diffusion using standard screens either in the presence or absence of GDP or GTP (for details see Table I and supplementary text).

X-ray diffraction data were collected using synchrotron radiation. For all structures, the phase problem was solved by molecular replacement using the program PHASER [115]. Structures were refined to reasonable R-values and stereochemistry using the program PHENIX [117]. Data collection and refinement statistics are summarized in Table I. See supplementary text for details.

Isothermal Titration Calorimetry

The thermodynamic parameters of Ct-eIF5B binding to GDP or GTP were measured using a MicroCal VP-ITC instrument (GE Healthcare). Experiments were carried out essentially as described previously [176]. The obtained values for enthalpy changes (ΔH) at different temperatures were used to estimate the change in heat capacity (ΔC_p) for the various protein-nucleotide complexes. These ΔC_p values were then used to estimate the conformational changes occurring in Ct-eIF5B upon GDP or GTP binding, using the empirically determined relation $\Delta C_p = \Delta c_{ap} \cdot \Delta ASA_{ap} + \Delta c_p \cdot \Delta ASA_p$ (where Δc_{ap} and Δc_p are the area coefficients in $\text{cal} \cdot \text{K}^{-1} \cdot (\text{mole} \cdot \text{\AA}^2)^{-1}$ for contributions of apolar or polar side chains to the change in solvent accessible surface area (ΔASA), respectively) [177]. For more details see supplementary text.

Coordinates

Coordinates have been deposited in the PDB: Apo Ct-eIF5B(517C) (4N3N); Ct-eIF5B(870C) (4N3G); Ct-eIF5B(517-970)·GDP (4NCL); Ct-eIF5B(517-858)·GTP (4NCN); Apo Sc-eIF5B(399-852) (4N3S); Sc-eIF5B(399-852)·GDP (4NCF).

Supplementary Information

The Supplementary Information includes extended Materials and Methods, eight figures and one table and is available at The EMBO Journal Online.

Acknowledgments

We thank the beam line scientists at BESSY (Berlin) and EMBL/DESY (Hamburg) as well as P. Neumann for support during X-ray diffraction data collection, M. Franke for technical assistance and L. K. Dörfel and A. Dickmanns for critical reading of the manuscript.

Author Contributions

Author contributions: BK designed the experiments, prepared and crystallized proteins, collected X-ray data, solved structures, performed ITC experiments, created figures. BK and RF analyzed the data and wrote the manuscript.

Conflict of interest

The authors declare that they have no conflict of interest.

5.5 Supplementary information

Supplementary Materials and Methods

Protein preparation and crystallization

The plasmid for the expression of N-terminally His-tagged *C. thermophilum* (Ct-)eIF5B(517C) (comprising residues 517-1116 that form the G domain, domain II, III and IV) was transformed into *E. coli* BL21 (DE3) cells (Stratagene) by heat shock. Transformed cells were grown in 1 l cultures of 2YT medium at 37 °C to an OD₆₀₀ of 0.6-0.8, followed by the induction of protein expression with 0.5 mM isopropyl-β-D-thiogalactopyranoside (IPTG). Cells were grown for an additional 18 h at 16 °C before harvesting. The harvested cells were resuspended in buffer A (40 mM Hepes (pH 7.5), 500 mM KCl, 10% glycerol, 30 mM imidazole, 2 mM β-mercaptoethanol), lysed using a Microfluidizer (Microfluidics) and clarified by ultracentrifugation. The supernatant was loaded onto two HisTrap columns (GE Healthcare), equilibrated in buffer A. After the elution of bound proteins with a linear gradient of imidazole (30-300 mM), eIF5B-containing fractions were pooled and desalted in buffer B (20 mM Hepes (pH 7.5), 200 mM KCl, 10% glycerol, 30 mM imidazole and 2 mM β-mercaptoethanol) for subsequent TEV-protease cleavage at 4 °C over night to remove the His-Tag. Uncleaved protein was removed by a second HisTrap in buffer B and the flow-through was pooled and concentrated for the final size exclusion chromatography step on a Superdex 200 column (GE Healthcare), equilibrated in buffer C (10 mM Hepes (pH 7.5), 50 mM KCl, 3 mM MgCl₂ and 1 mM DTT). The purified eIF5B was finally pooled and concentrated to 15-20 mg/ml. Other versions of Ct-eIF5B containing residues 517-970 or 517-858 and of *S. cerevisiae* (Sc-) eIF5B containing residues 399-852 were purified according to the same protocol.

For ITC experiments truncated versions of Ct-eIF5B were purified according to the above protocol with the difference that ITC buffer (see below) was used in the size exclusion chromatography step. The concentration of the protein was determined by absorbance at 280 nm (with extinction coefficients for the different Ct-eIF5B constructs: $\epsilon_{517C} = 30370 \text{ M}^{-1}\text{cm}^{-1}$, $\epsilon_{517-970} = 20400 \text{ M}^{-1}\text{cm}^{-1}$ and $\epsilon_{517-852} = 14440 \text{ M}^{-1}\text{cm}^{-1}$). The protein was >95 % pure as judged by SDS-PAGE and free of nucleotides as determined by HPLC.

Crystals of Ct-eIF5B(517C) without nucleotide were obtained after two days at 4 °C *via* sitting-drop vapor diffusion against 100 mM MES (pH 6.8), 12% PEG 20000 and 10 mM Na-lactate. The crystals grow in primitive hexagonal space group P3₂21 with one molecule per asymmetric unit (unit cell: a = b = 111.47 Å, c = 115.21 Å, $\alpha = \beta = 90^\circ$, $\gamma = 120^\circ$; diffraction limit = 2.75 Å).

Despite extensive trials we were not able to obtain crystals of the Ct-eIF5B(517C) construct in the GDP- or GTP-bound forms. However in the presence of GTP another type of crystals was obtained after 5 days at 4 °C under the above conditions. These crystals grew in the primitive hexagonal space group $P3_121$ (unit cell: $a = b = 98.23 \text{ \AA}$, $c = 97.42 \text{ \AA}$, $\alpha = \beta = 90^\circ$, $\gamma = 120^\circ$; diffraction limit = 3.2 \AA) with one molecule per asymmetric unit comprising only domains III and IV of Ct-eIF5B (residues 870-1116).

Crystals of Ct-eIF5B(517-970) in the presence of 2 mM GDP grew within 4 days at room temperature against 15% PEG 8000 and 0.5 M Li_2SO_4 in primitive orthorhombic space group $P2_12_12_1$ with two protein-GDP complexes per asymmetric unit (unit cell: $a = 66.9 \text{ \AA}$, $b = 72.96 \text{ \AA}$, $c = 199.23 \text{ \AA}$, $\alpha = \beta = \gamma = 90^\circ$; diffraction limit = 2.1 \AA).

Crystals of Ct-eIF5B(517-970) in the presence of 2 mM GTP grew over night at room temperature against 100 mM Hepes (pH 7), 13% PEG 4000 and 100 mM sodium acetate in primitive monoclinic space group $P2_1$ with two protein-GTP complexes per asymmetric unit (unit cell: $a = 55.4 \text{ \AA}$, $b = 114.83 \text{ \AA}$, $c = 65.85 \text{ \AA}$, $\alpha = 90^\circ$, $\beta = 102.3^\circ$, $\gamma = 90^\circ$; diffraction limit = 1.87 \AA).

Crystals of the nucleotide free form of Sc-eIF5B(399-852) grew after 2 days at 4 °C against 20% ethylene glycol, 5% PEG 3350 and 20 mM MgCl_2 in primitive tetragonal space group $P41$ with two molecules per asymmetric unit (unit cell: $a = b = 118.01 \text{ \AA}$, $c = 77.51 \text{ \AA}$, $\alpha = \beta = \gamma = 90^\circ$; diffraction limit = 1.83 \AA). The data were twinned with a twin fraction of 18% (twin law $h, -k, -l$).

Finally, crystals of the GDP-bound form of Sc-eIF5B(399-852) could be obtained over night at 10 °C against 8% PEG 8000 and 0.37 M Li_2SO_4 in primitive orthorhombic space group $P2_12_12_1$ with two protein-GDP complexes per asymmetric unit (unit cell: $a = 73.56 \text{ \AA}$, $b = 119.46 \text{ \AA}$, $c = 120.73 \text{ \AA}$, $\alpha = \beta = \gamma = 90^\circ$; diffraction limit = 3.02 \AA).

X-ray data collection, structure determination and refinement

For the structure of Ct-eIF5B-GTP X-ray diffraction data were collected at BL 14.1 (HZB, BESSY, Berlin) [113]. All other structures were solved using X-ray diffraction data collected at P13 beamline (EMBL, PETRA III, Hamburg). The structure of free Ct-eIF5B(517C) was solved by molecular replacement using the program PHASER [115] using the atomic coordinates of the archeal ortholog of eIF5B from *M. thermoautotrophicum* (PDB: 1G7R) with the individual domains as independent search models. The structure was refined using the program PHENIX [117]. The other structures were solved by means of molecular replacement using the individual domains of the newly determined structure as search model as described below (Data collection and refinement statistics are summarized in Table I).

The second structure obtained from Ct-eIF5B(517C), this time in the presence of GTP, was solved using domains I to IV of Ct-eIF5B(517C) as independent search models. A solution was found only for domains III and IV and the final model after refinement comprises residues 870 to 1116 (domains III and IV). A Coomassie Blue-stained SDS-PAGE gel of dissolved crystals confirmed that domains I and II are missing, probably due to a proteolytic event during crystallization.

The structures of Ct-eIF5B(517-970) in the GDP- and GTP-bound state and of free Sc-eIF5B(399-852) were solved using domains I to III of Ct-eIF5B(517C) as independent search models. The resulting models of Ct-eIF5B(517-970) in complex with either GDP or GTP contains two copies of Ct-eIF5B(517-970), each bound to a Mg^{2+} ion and GDP or GTP, respectively. In the final model of Ct-eIF5B(517-970)·GTP residues 517-859 are resolved in the electron density, however the entire domain III (residues 860-970) is missing, probably due to a proteolytic event during crystallization as indicated by a Coomassie Blue-stained SDS-PAGE gel of dissolved crystals. The final model of the nucleotide-free form of Sc-eIF5B(399-852) contains two copies of Sc-eIF5B(399-852).

Finally, the structure of Sc-eIF5B·GDP was solved using domains I to III of free Sc-eIF5B(399-852) as independent search models. The final model contains two Sc-eIF5B·GDP complexes in the asymmetric unit.

Isothermal Titration Calorimetry

The thermodynamic parameters of eIF5B binding to GDP or GTP were measured by means of ITC using a MicroCal VP-ITC instrument (GE Healthcare). Experiments were carried out in ITC buffer (30 mM Hepes pH 7.5, 100 mM KCl, 10% glycerol, 4 mM β -mercaptoethanol, 0.01% tween20, 2.5 mM $MgCl_2$) at six different temperatures (5, 10, 15, 20, 25 and 30 °C). 14- μ l aliquots of 200-400 μ M ligand were injected into the 1.42 ml cell containing 10-30 μ M eIF5B. The heat of dilution was measured by injecting the ligand into the buffer solution without protein; the values were then subtracted from the heat of the individual binding reactions to obtain the effective heat of binding. The final titration curves were fitted using the 'Origin' based MicroCal software, assuming one binding site per protein molecule. For each isotherm the binding stoichiometry (N), enthalpy changes (ΔH) and the association constants (K_a), were obtained by a nonlinear regression fitting procedure. These directly measured values were then used to estimate the Gibbs energy (ΔG) from the relation $\Delta G = -R \cdot T \cdot \ln K_a$ and the entropy changes (ΔS) through $\Delta G = \Delta H - T \cdot \Delta S$.

To investigate the influence of the Mg^{2+} ion on the binding of GDP to eIF5B, experiments were repeated in a modified ITC buffer, containing 0.25 mM EDTA instead of $MgCl_2$ (Mg^{2+} was omitted also from the buffers used during purification).

In order to estimate the change in heat capacity (ΔC_p) upon complex formation, the measured ΔH values were plotted against the temperature [178, 179]. Depending on whether a linear or non-linear temperature dependency was applicable for ΔH , the data were fitted either to a linear or a second-order polynomial function. In the first case, the slope of the fitted line directly represents the ΔC_p of the binding reaction, whereas in the second case the ΔC_p for a given temperature can be calculated from the first derivative of the polynomial function.

ΔC_p can be used as an estimate for the change in solvent-accessible surface area (ΔASA) upon complex formation as it was found to be proportional to the size of the area which is either exposed to or excluded from the aqueous environment during the binding event [176, 177, 180-183]. ΔC_p and ΔASA are connected by the empirically determined relation $\Delta C_p = \Delta c_{ap} \cdot \Delta ASA_{ap} + \Delta c_p$

$\cdot\Delta ASA_p$ where Δc_{ap} and Δc_p are the area coefficients in $\text{cal}\cdot\text{K}^{-1}\cdot(\text{mole}\cdot\text{\AA}^2)^{-1}$ for the contributions of apolar or polar side chains to ΔASA , respectively [177]. Studies on the dissolution of model compounds and protein unfolding suggest a negative contribution due to the burial of apolar surfaces (ΔASA_{ap}) and a positive contribution upon burial of polar surfaces (ΔASA_p) with values for Δc_{ap} and Δc_p of 0.45 and -0.26, respectively [177, 182, 184]. Since binding of guanine nucleotides can be expected to involve both, apolar and polar residues, a treatment of the obtained Δc_p values solely based on nonpolar contributions according to Connelly et al. (1992) would be insufficient. At the same time, the differential treatment by calculating the individual contributions of apolar and polar groups to the total surface area often proved to be inaccurate, especially in cases where the interactions did not conform to a rigid-body binding model [185-188]. We therefore use two values for the area coefficients to estimate the total surface area upon ligand binding: $\Delta c_{\max} = 0.24$ ($= 0.7\cdot\Delta c_{ap} + 0.3 \cdot \Delta c_p$) as the upper limit case, assuming ~70% apolar and ~30% polar groups contributing to the total ΔASA (calculated from the crystal structures of Ct-eIF5B in its apo, GDP and GTP forms using the program AREAIMOL from the CCP4 Program Suite 6.3.0) and $\Delta c_{\min} = 0.45$ as the lower limit case in which all involved residues are apolar.

Supplementary Images

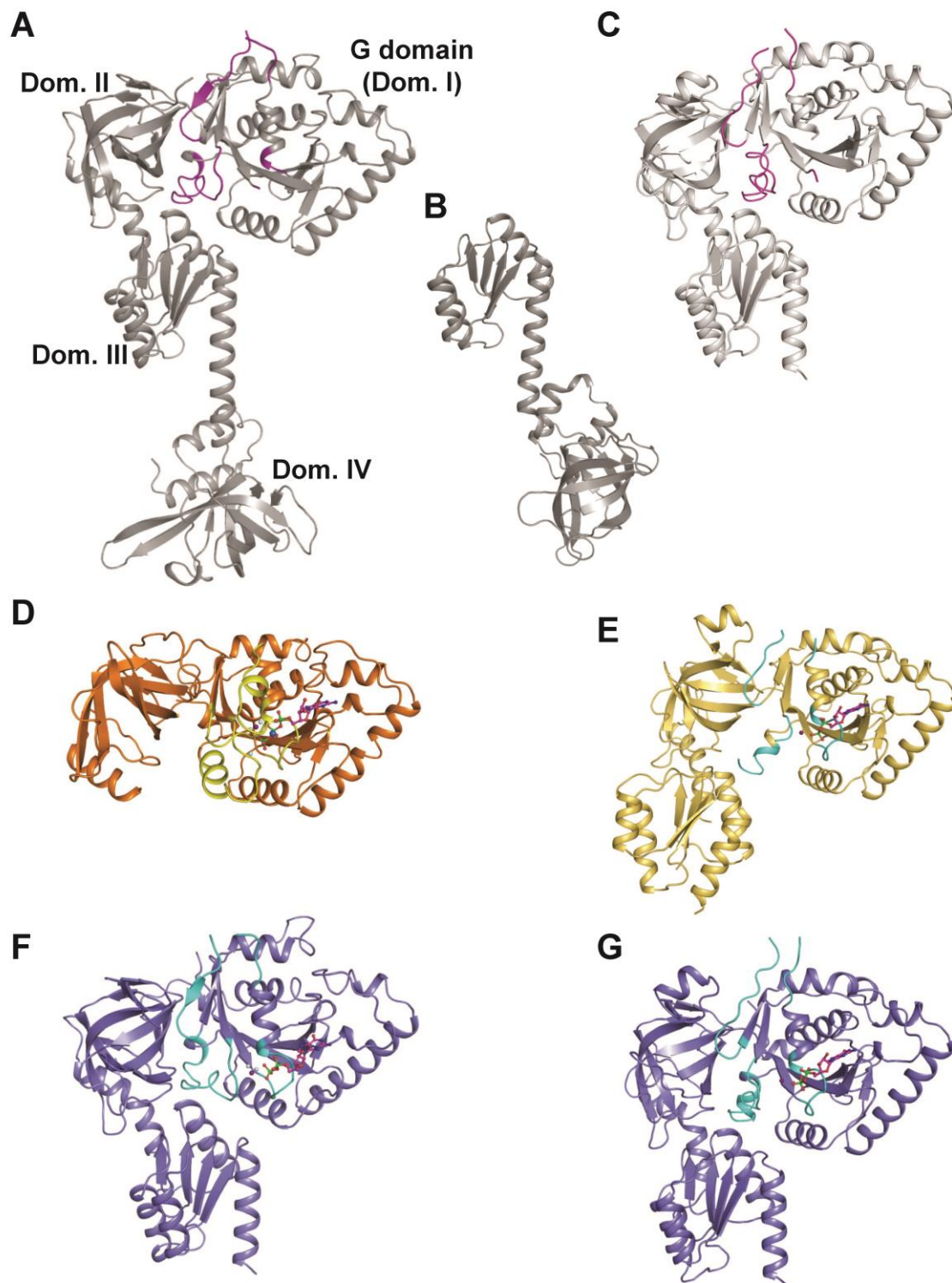


Figure S1. Structures of eIF5B from *C. thermophilum* and *S. cerevisiae*. **A)** Structure of apo Ct-eIF5B(517C) containing residues 517-1116 comprising the G domain (domain I) and domains II, III and IV. The P-loop, switch 1 and 2 are colored pink. **B)** Structure of Ct-eIF5B(870C) with residues 870-1116, comprising domains

III and IV. **C)** Structure of apo Sc-eIF5B(401-852) comprising the G domain, domain II and domain III. Switch 1 and switch 2 are shown in pink. **D)** Structure of Ct-eIF5B(517-859) in the GTP-bound state comprising G domain and domain II. The switch regions and the P-loop are shown in yellow; the Mg^{2+} ion, Na^+ ion and water molecules are shown as spheres in magenta, blue, and grey, respectively; GTP is shown as balls and sticks. **E)** Molecule B in the asymmetric unit of the Sc-eIF5B·GDP structure containing residues 401-852, comprising G domain and domains II and III. P-loop and the switch regions are colored cyan; the GDP molecule is shown as balls and sticks. **F)** Structure of Ct-eIF5B(520-970)·GDP comprising G domain, domain II and domain III. P-loop and switch regions are colored cyan, the GDP molecule is shown as balls and sticks. **G)** Molecule A in the asymmetric unit of the Sc-eIF5B·GDP structure containing residues 401-852, comprising the G domain, domain II and domain III. Same color code as in **F**).

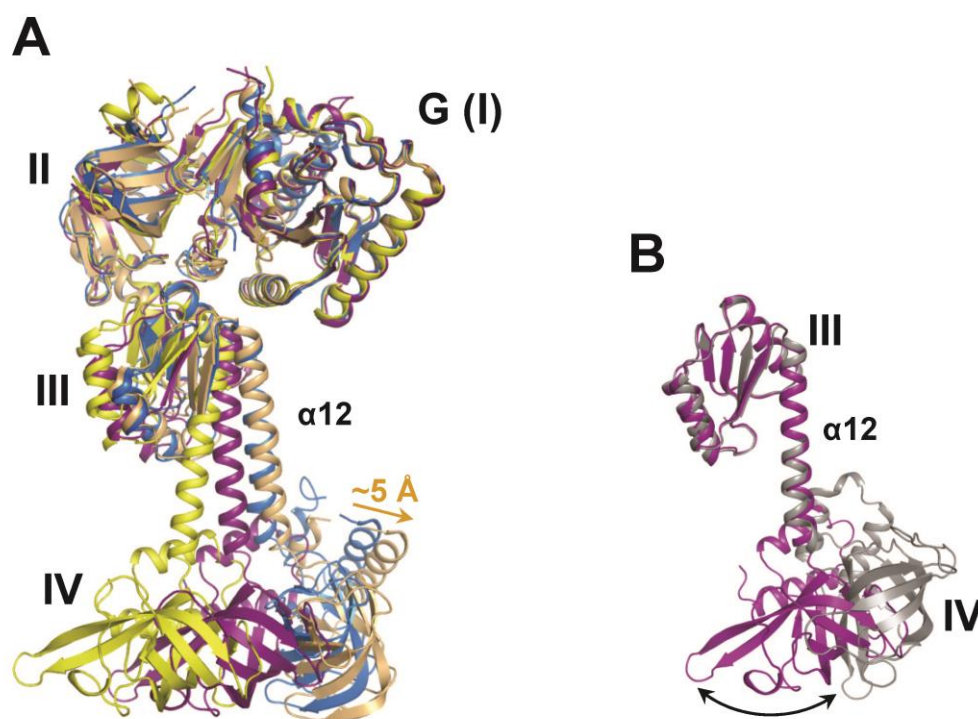


Figure S2.A) G domain based superposition of the apo structures of eIF5B from *C.thermophilum* (purple), *S.cerevisiae* (yellow) and aIF5B from *M. thermoautotrophicum* (blue; PDB: 1G7R), showing the conformational flexibility of domain III relative to domain I in the absence of a bound nucleotide. The C-terminus of helix $\alpha 12$ in apo aIF5B lies 12 and 22 Å apart from that in Ct-eIF5B and Sc-eIF5B, respectively. The GDPNP-bound form of aIF5B is also shown (wheat; PDB: 1G7T), highlighting the relatively changes observed in the archeal ortholog upon binding of the GDPNP (see also Fig. S8). As the structure of the *S. cerevisiae* ortholog does not contain the second half of helix $\alpha 12$ and domain IV, domains III and IV of the Ct-eIF5B structure were superimposed onto domain III of the Sc-eIF5B structure. **B)** Superposition of domains III and IV of the apo Ct-eIF5B(517C) structure (purple) with the structure of Ct-eIF5B(870C) (grey), based on domain III. Domain III and the following helix $\alpha 12$ are nearly identical in both structures; in contrast, the orientation of domain IV relative to domain III differs significantly, indicating a high degree of conformational flexibility in the linker between helix $\alpha 12$ and domain IV.

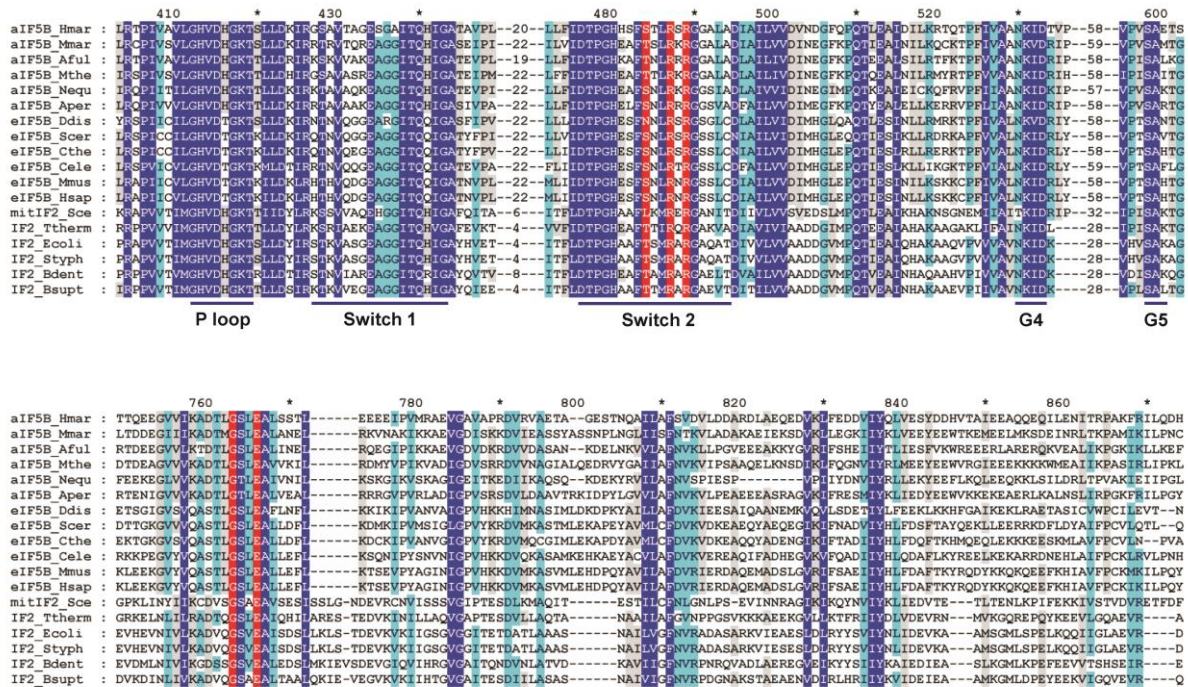


Figure S3. Sequence alignment of the G domains (upper panel) and domains III (lower panel) from different aIF5B, eIF5B and IF2 homologues. Highly conserved residues are highlighted in blue; conserved residues that are directly involved in the stable contacts between switch 2 and domain III in inactive (apo and GDP-bound) eIF5B are highlighted in red. P-loop (G1 motif), switch 1 (with the G2 motif containing Thr439), switch 2 (with the G3 motif “DTPG”) and motifs G4 and G5 in the G domain are indicated. The numbering above the sequences is according to the eIF5B homologue from *Saccharomyces cerevisiae*. Residues within the G domain that are implicated in nucleotide binding and the GTP-dependent molecular switch in eIF5B are universally conserved among all three orthologs. Domain III is significantly less well conserved than the G domain; however, the N-terminal part of helix α 9 (residues 763-768 in eIF5B) is highly conserved, particularly in those residues involved in the interactions with switch 2. Species names are abbreviated as follows: Hmar, *Haloarculamarismortui*; Mmar, *Methanococcusmaripaludis*; Aful, *Archaeoglobusfulgidus*; Mthe, *Methanothermobacterthermoautotrophicum*; Nequi, *Nanoarchaeumequitans*; Aper, *Aeropyrumpernix*; Ddis, *Dictyosteliumdiscoideum*; Scer, *Saccharomycescerevisiae*; Cter, *Chaetomiumthermophilum*; Cele, *Caenorhabditiselegans*; Mmus, *Musmusculus*; Hsap, *Homo sapiens*; Ttherm, *Thermusthermophilus*; Ecoli, *Escherichiacoli*; Styph, *Salmonellatyphimurium*; Bdent, *Bifidobacteriumdentium*; Bsupt, *Bacillussubtilis*; mitIF2_Sce, mitochondrial IF2 from *S. cerevisiae*.

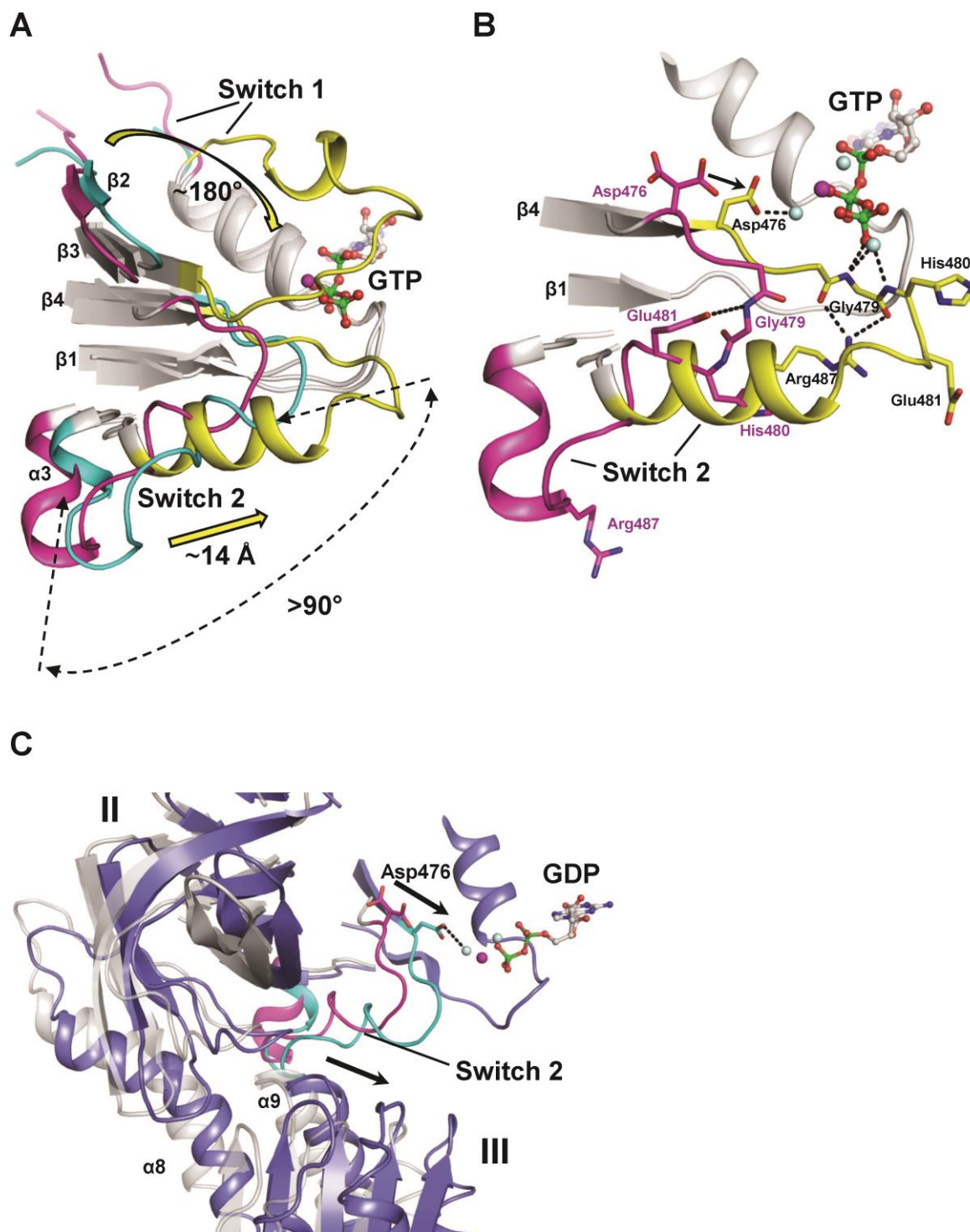


Figure S4. Nucleotide-dependent conformational changes in switch 1 and switch 2 of eIF5B. **A)** Overview of the GTP-induced conformational changes in the G domain. P loop, switch 1 and switch 2 are colored pink for apo eIF5B, cyan for eIF5B-GDP and yellow for eIF5B-GTP; the Mg^{2+} ion is shown as sphere in magenta; GTP is shown in balls and sticks; GDP is omitted for clarity. In the apo state switch 1 points away from the nucleotide binding pocket and is partially disordered. Switch 2 adopts a loop conformation with most residues positioned at the backside of the G domain (left). Upon GTP binding the switch regions become

reorganized (yellow arrows) to form the catalytic center around the GTP- γ -phosphate. Switch 1 flips over by $\sim 180^\circ$ relative to its position in the apo state and the residues forming strand $\beta 2$ are repositioned to form part of the coordination sphere for the Mg^{2+} ion. Switch 2 moves up to 15 Å in some residues, resulting in an extended helix $\alpha 3$, which is reoriented relative to $\alpha 3$ in the apo state by more than 90° . The transition from the GTP- to GDP-bound state reverses these changes and results in conformations of switch 1 and 2 like for the apo form, however, with switch 2 shifted ~ 3 Å towards the nucleotide binding pocket. **B)** Details of the transition between apo and GTP-bound forms of switch 2. The color code is the same as in A); water molecules are shown as grey spheres; hydrogen bonds indicated as dashed lines. Upon GTP binding Asp476 moves ~ 3 Å towards the GTP molecule (arrow). Gly479 moves towards the γ -phosphate (meanwhile the peptide bond to the preceding Pro478 flips by $\sim 160^\circ$) resulting in a reorganization of the rest of switch 2 including His480 (His^{cat}) and Arg487, which is involved in interactions with domain III in the apo and GDP-bound states of the factor (see also Fig. 3A/B). **C)** As shown in A), switch 2 in Ct-eIF5B-GDP (blue with switch 2 in cyan) remains ~ 3 Å closer to the nucleotide binding pocket than in the apo form (grey with switch 2 in pink) but forms the same contacts to domains II and III as found in apo eIF5B. As a consequence, also domain III and the ventral side of domain II are shifted in the same direction as switch 2 (arrows).

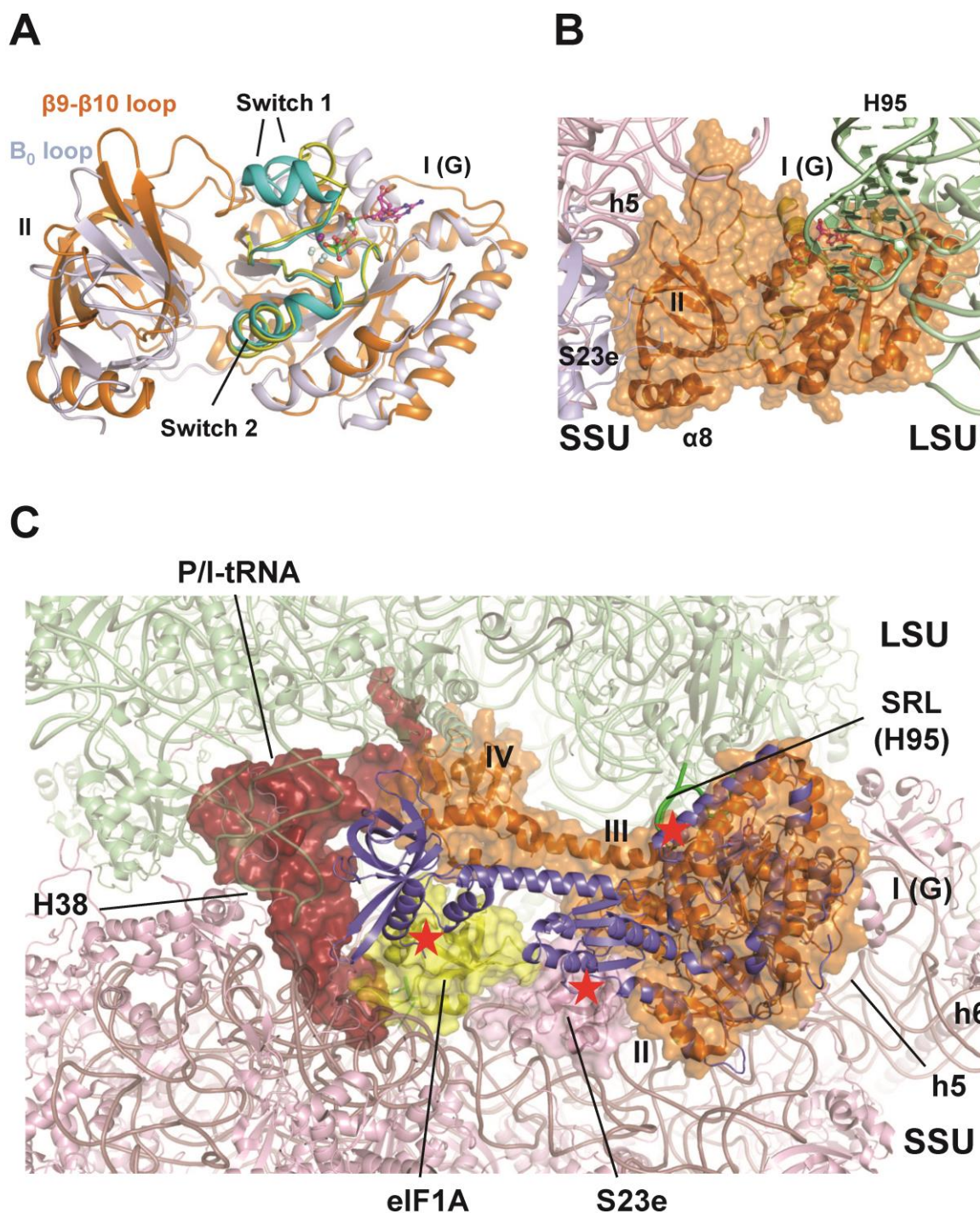


Figure S5. A) Superposition of eIF5B-GTP (orange with P loop, switch 1 and switch 2 in yellow) and free EF-Tu-GDPNP (light blue with P loop, switch 1 and switch 2 in cyan; PDB code: 1EXM), based on their respective catalytic centers. Domains I and II from eIF5B and EF-Tu show the same overall dimensions and exhibit very similar arrangements in regions involved in nucleotide binding (switch 1 and switch 2) or in interactions with the small ribosomal subunit (e.g. the $\beta 9$ - $\beta 10$ loop in eIF5B and the B₀ loop in EF-Tu). **B)** Cryo-EM model of domains I and II of eIF5B-GDPCP (orange) on the 80S ribosome [91]. The large ribosomal subunit (LSU) is shown in green; the small ribosomal subunit (SSU) is shown in light pink. **C)** Comparison of eIF5B-GDPCP in

the 80S IC (orange; [91]) with inactive eIF5B (blue). The structure of inactive eIF5B was modeled by superposition of its domain II onto domain II of eIF5B-GDPCP. According to this model, GTP hydrolysis and subsequent P_i release causes domain IV to move away from the acceptor end of the tRNA (dark red) as domain III associates with domains I and II. Simultaneously, the G domain rotates with respect to domain II by $\sim 30^\circ$ towards the SRL. These movements result in clashes (red stars) of domains I, III and IV with the SRL, ribosomal protein S23e and A site-bound eIF1A (yellow; modeled according to the structure of eIF1 and eIF1A on the 40S subunit (PDB: 4BPE)), respectively, which reduce the affinity of eIF5B-GDP to the ribosome and facilitate its dissociation.

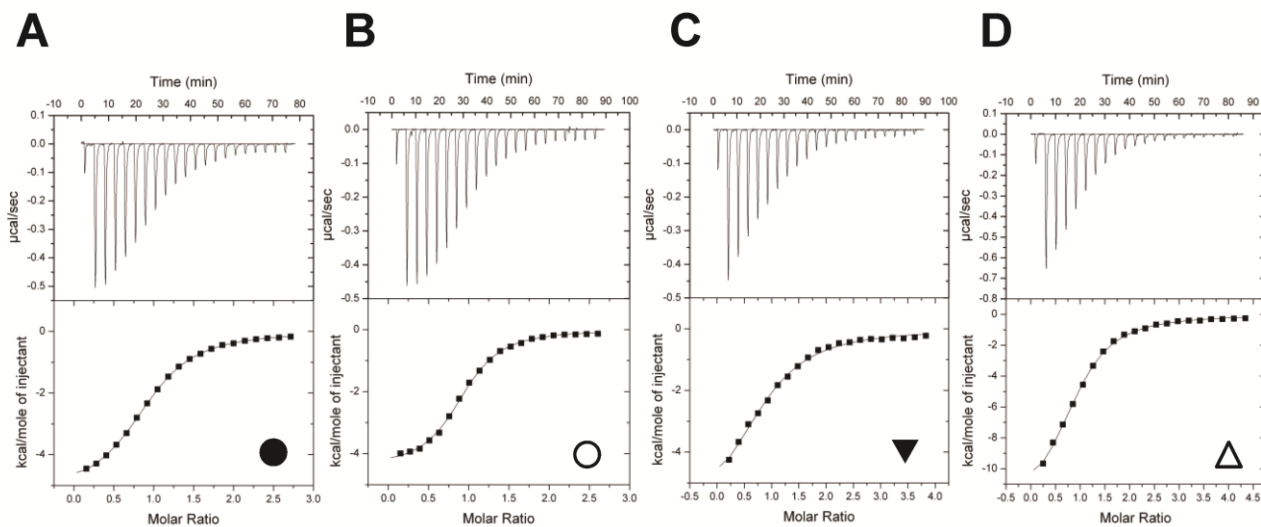


Figure S6. A-D) Titration curves (upper panels) and binding isotherms (lower panels) of eIF5B interactions with GDP or GTP. **A)** Ct-eIF5B(517C) with GDP at 20 °C in the presence of $MgCl_2$; **B)** Ct-eIF5B(517C) with GDP at 25 °C in the absence of $MgCl_2$; **C)** Ct-eIF5B(517C) with GTP at 20 °C in the presence of $MgCl_2$; **D)** Ct-eIF5B(517-852) with GTP at 20 °C in the presence of $MgCl_2$.

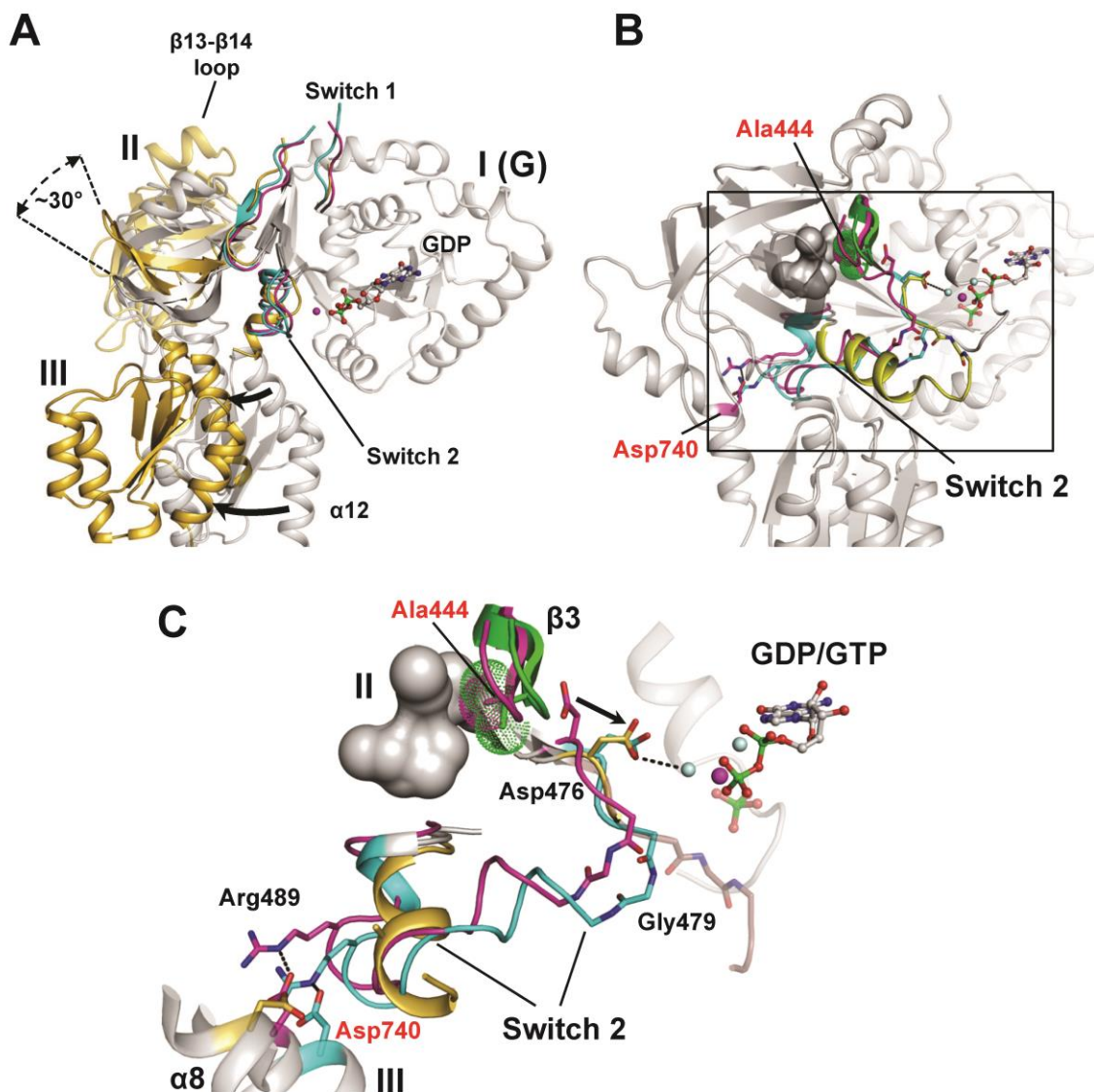


Figure S7. A) G domain-based superposition of eIF5B domains I-III from *S. cerevisiae* in its apo and GDP-bound states. The G domain is colored grey; the switch regions are colored pink for the apo state, cyan for molecule A of Sc-eIF5B-GDP and dark yellow for molecule B of Sc-eIF5B-GDP. While domains II and III of molecule A in the Sc-eIF5B-GDP structure superimpose well with domains II and III of the apo form (grey), domain III in molecule B (dark yellow) is moved away from the G domain (arrows) and has no contact to the partially disordered switch 2. Domain II of molecule B is in its rotated state with the $\beta 9\text{-}\beta 10$ loop moved upwards; switch 1 and the $\beta 13\text{-}\beta 14$ loop remain in their respective inactive conformations. **B)** Overview of apo eIF5B with the locations of Ala444 and Asp740 relative to the nucleotide binding pocket and switch 2. Switch 2 is shown in its apo (pink), GDP- (cyan) and GTP-bound forms (yellow). **C)** Detail of the area indicated in B) (box). Switch 2 is shown in four different states: i) The inactive apo state (pink), in which Asp476 and Gly479 point away from the nucleotide binding pocket and Arg489 forms a salt bridge to Asp740 of domain III. ii) The partially activated GDP state in Ct-eIF5B-GDP (cyan), in which Asp476 interacts with the Mg^{2+} ion. Gly479 has undergone the peptide flip relative to the apo state. iii) The partially activated GDP state in molecule B of Sc-eIF5B-GDP (dark yellow). Asp476 interacts with the Mg^{2+} ion; switch 2 is shifted towards the GDP molecule and has lost its contacts to domain III (see also Fig. S5A). iv) The G3 motif

of the activated switch 2 in Ct-eIF5B-GTP (brown; the rest of switch 2 is not shown). Gly479 has undergone the peptide flip relative to the apo state and contacts the γ -phosphate. Mutagenesis of Gly479 to Ala most likely prevents the peptide flip and thereby stabilizes the inactive conformation of switch 2. Mutagenesis of Asp740 to Arg would result in the steric and electrostatic repulsion of switch 2 in its inactive conformation. Mutagenesis of Ala444 to Val would result in a steric clash with domain II (grey surface), most likely causing strand β 3 to move towards Asp476 (green model). To avoid a clash with the repositioned strand β 3 Asp476 would have to retreat towards the nucleotide binding pocket, thereby facilitating the partial or full activation of switch 2 by GDP as well as GTP.

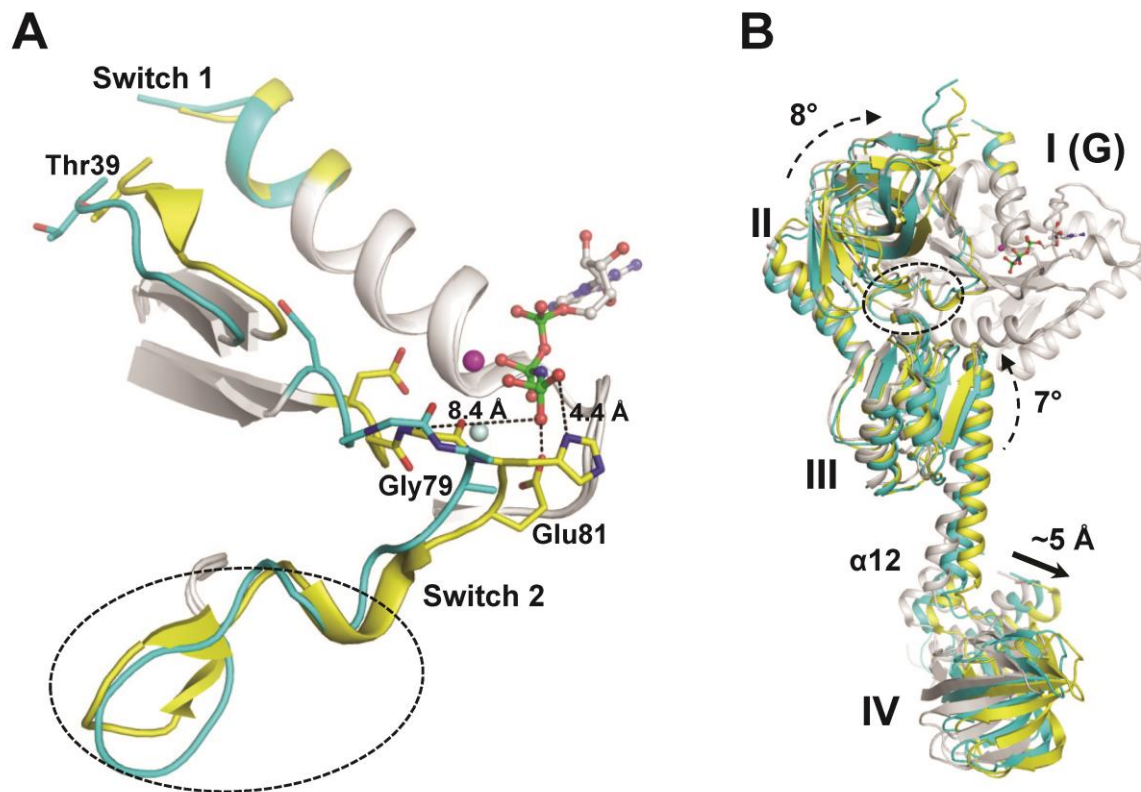


Figure S8. The articulated lever model for eIF5B/IF2 activation [84, 144]. **A)** Superposition of switch 1 and switch 2 from GDP- (cyan) and GDPNP-bound (yellow) aIF5B from *M. thermoautotrophicum* (PDB: 1G7S, 1G7T). The structural transition from the GDP-bound state to the GDPNP-bound form is limited to the N-terminal half of switch 2, which moves ~ 2 Å towards the nucleotide binding pocket, while switch 1 remains unaltered. Neither Thr39 in the G2 motif nor Gly79 in G3 form a direct contact to the γ -phosphate; the only potential interaction occurs between Glu81 and the γ -phosphate. The region of switch 2 forming the contacts to domain III (dashed circle) remains virtually unchanged. Compare also to Fig. S4. **B)** The GDPNP-induced shift in switch 2 is thought to cause a concerted rearrangement of domains II and III (dashed arrows), resulting in a ~ 5 Å shift of domain IV (arrow). The interaction interface between switch 2 and domains II and III (dashed circle) remains nearly unchanged. The switch regions are colored as in A); domains II-IV are colored grey for apo aIF5B (PDB: 1G7R), cyan for aIF5B-GDP and yellow for aIF5B-GDPNP. Compare also to Fig. S2A.

Chapter 6 • Recognition of amino-acylated initiator tRNA by eIF5B in the 80S IC

This manuscript has been accepted for publication in BMC Structural Biology

Structural insight into the recognition of amino-acylated initiator tRNA by eIF5B in the 80S initiation complex

Bernhard Kuhle^{1,§} and Ralf Ficner¹

¹ Abteilung für Molekulare Strukturbiologie, Institut für Mikrobiologie und Genetik, Göttinger Zentrum für Molekulare Biowissenschaften, Georg-August-Universität Göttingen, D-37077 Göttingen, Germany

[§]To whom correspondence should be addressed: bkuhle@gwdg.de

Author contributions:

BK: designed the study, analyzed structures and cryo-EM density, performed the structural modeling and sequence alignments, analyzed and interpreted the data and wrote the manuscript. RF analyzed the data and helped to draft the manuscript.

Background

From bacteria to eukarya, the specific recognition of the amino-acylated initiator tRNA by the universally conserved translational GTPase eIF5B/IF2 is one of the most central interactions in the process of translation initiation. However, the molecular details, particularly also in the context of ribosomal initiation complexes, are only partially understood.

Results

A reinterpretation of the 6.6 Å resolution cryo-electron microscopy (cryo-EM) structure of the eukaryal 80S initiation complex using the recently published crystal structure of eIF5B reveals that domain IV of eIF5B forms extensive interaction interfaces with the Met-tRNA_i, which, in contrast to the previous model, directly involve the methionylated 3' CCA-end of the acceptor stem. These contacts are mediated by a conserved surface area, which is homologous to the surface areas mediating the interactions between IF2 and fMet-tRNA^{fMet} as well as between domain II of EF-Tu and amino-acylated elongator tRNAs.

Conclusions

The reported observations provide novel direct structural insight into the specific recognition of the methionylated acceptor stem by eIF5B domain IV and demonstrate its universality among eIF5B/IF2 orthologs in the three domains of life.

6.1 Background

The process of translation initiation results in the formation of an elongation-competent ribosome with the start codon of an mRNA in its P site, base paired to the amino-acylated initiator tRNA. In bacteria and eukarya this process follows significantly different mechanisms, highlighted by different numbers of auxiliary protein factors (initiation factors or IFs) that are employed by bacterial (three IFs) or eukaryal cells (at least 12 eIFs) for correct ribosome assembly [9]. Only two of these factors, α /eIF1A/IF1 and the translational GTPase α /eIF5B/IF2, are universally conserved in the three domains of life [81]. In bacteria, IF2 plays a critical role throughout the initiation pathway. In the early stages, IF2 binds to the 30S subunit in a GTP-dependent manner and stimulates the recruitment of the N-formylmethionylated initiator tRNA (fMet-tRNA^{fMet}) to the P site of the 30S ribosomal subunit to form the 30S pre-initiation complex (pre-IC). Finally, IF2·GTP

catalyzes the joining of the 50S ribosomal subunit to form the elongation-competent ribosome [15, 189]. Speed and accuracy of both processes depend of the specific recognition of the α NH-blocked methionine esterified to the 3' CCA-end of tRNA^{fMet} [190-193]. Biochemical studies showed that all determinants required for this interaction are located in domain IV of IF2, which consists of a six-stranded β barrel [194-197]. Domain IV of IF2 exhibits a marked structural homology to domain II of EF-Tu that, together with the G domain, forms the universally conserved structural core among translational GTPases [198] and in EF-Tu constitutes part of the binding pocket for the aminoacylated acceptor arm of elongator tRNAs [48, 163, 197]. Based on this observation it was suggested that IF2 domain IV and EF-Tu domain II use similar interfaces for their interactions with the tRNA [197]. This assumption is at least partially corroborated by mutational and NMR spectroscopy analyses [196]. Cryo-EM structures of bacterial 30S pre-ICs and 70S IC containing GTP/GDPNP-bound IF2 show how this interaction mutually stabilizes fMet-tRNA^{fMet} and IF2 in conformations that allow the efficient association of the 50S subunit [152, 172]. However, none of these structures were determined at sufficiently high resolution to give any detailed insight into the interaction that would allow a correlation with the biochemical data.

In contrast to bacterial IF2, the role of a/eIF5B in eukarya and archaea seems to be confined to the GTP-dependent promotion of subunit joining, the last step of the initiation process [145, 161, 199]. The recruitment of the charged initiator tRNA (Met-tRNA_i) to the small ribosomal subunit is carried out by the heterotrimeric a/eIF2, a specialized EF-Tu paralog that has no counterpart in bacteria [200]. Accordingly, a/eIF5B·GTP binds to the small ribosomal subunit already containing the P site-bound Met-tRNA_i, which invokes the question whether a/eIF5B still has to interact with Met-tRNA_i to promote joining of the large ribosomal subunit, and whether this interaction would involve a specific recognition of the methionylated acceptor end, similar to the recognition of the fMet-tRNA^{fMet} by IF2. Genetic, biochemical and structural studies point toward essentially the same mechanisms for eIF5B and IF2 catalyzed subunit joining [84, 91, 145, 154, 199, 201]. Crystal structures of aIF5B and eIF5B revealed a six-stranded β barrel fold for domain IV, homologous to domain IV in IF2 [84, 201]. Indirect biochemical assays showed that a/eIF5B binds Met-tRNA_i in solution, however, with very low affinity and specificity for the methionyl moiety in case of eIF5B [84, 202]. NMR studies revealed a weak but specific interaction between methionine-

ethyl ester (mimicking the ester bond between tRNA and the methionyl moiety) and eIF5B domain IV in the area corresponding to the surface on IF2 that is affected by N-formylmethionine binding [86]. Finally, the recently determined 6.6 Å resolution cryo-EM structure of the yeast 80S IC (EM-Databank: EMD-2422) demonstrates that, like IF2 in the corresponding bacterial 70S complex [152], eIF5B and the P site-bound Met-tRNA_i stabilize each other in their subunit joining-competent conformations through the direct contact between domain IV and acceptor stem [91]. Surprisingly however, according to the structural model this contact does not involve the methionylated 3' CCA-end of the tRNA [91]. Instead, the CCA-end points away from domain IV, placing the methionyl moiety ~23 Å from the protein. Thus, this model is clearly at odds with the observations from biochemical studies [86, 202] and fails to explain why deacylation of the initiator tRNA results in the loss of its ability to stabilize eIF5B [91].

Here, we provide an analysis and reinterpretation for the cryo-EM density of the yeast 80S IC [91] for domain IV and its contact to the initiator tRNA. We show that the original structural model for this region, based on the fit of the archaeal aIF5B ortholog, is only partially consistent with the available density. Fitting of the recently determined structure of eIF5B domain IV from *C. thermophilum*, which shows a significantly higher degree of sequence similarity to the *S. cerevisiae* ortholog, allows a reinterpretation of the 6.6 Å resolution density. The resulting model demonstrates a direct contact between the methionylated CCA-end of the tRNA and a conserved surface area of domain IV that directly corresponds to the binding sites for the tRNA acceptor arm on domain IV of IF2 or domain II of EF-Tu [48, 196, 197]. Thus, we show that the high-quality cryo-EM density of the 80S complex not only provides the first direct structural indications for the EF-Tu-like interactions between eIF5B/IF2 domain IV and the initiator tRNA but also for their universality among a/eIF5B/IF2 orthologs in the three domains of life. Finally, we use our observations to propose a possible scenario for the evolution of the translational β barrel fold in eIF5B/IF2 and EF-Tu and its interactions with tRNAs.

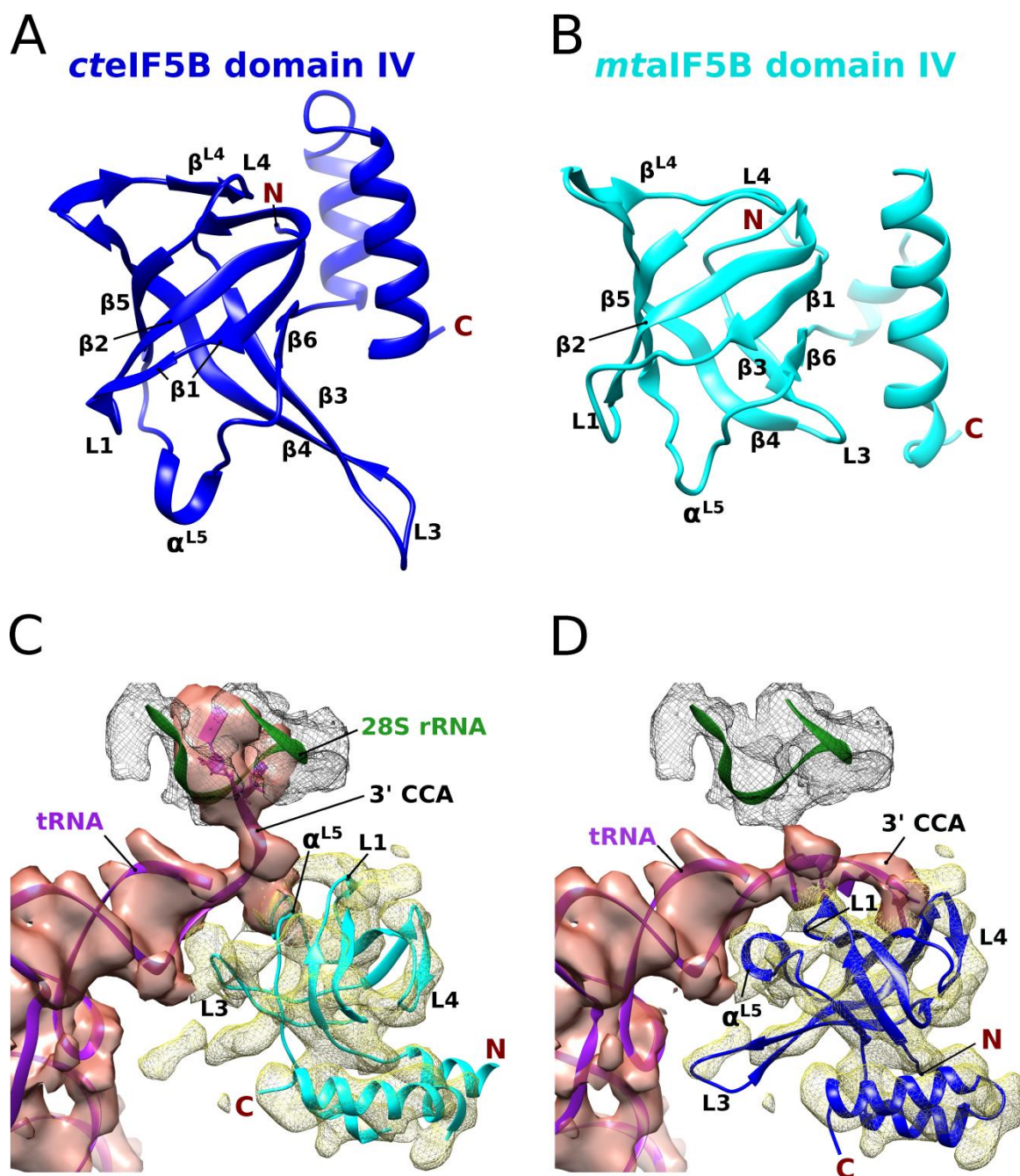


Figure 1. Model for the interactions between eIF5B domain IV and Met-tRNA_i in the 80S IC. **A)** Crystal structure of *cteIF5B* domain IV (PDB: 4N3G). The most marked differences to domain IV of aIF5B from the archaeon *M. thermoautotrophicum* (PDB: 1G7T) **(B)** are found in the lengths of the β 3- β 4 hairpin and loop L5 as well as in the arrangement of the two C-terminal α helices. **(C)** Original model for the interactions between domain IV (cyan) and Met-tRNA_i (purple), fitted into the cryo-EM density of the 80S IC (EMD-2422) [91]. **(D)** New model for the interactions between domain IV (blue) and Met-tRNA_i (purple), based on the rigid-body fitting of the crystal structure of domain IV from *cteIF5B*. The 3' CCA-end now forms a direct contact with the surface of domain IV, and α^{L5} occupies a position in the major groove of the acceptor stem.

6.2 Results and Discussion

Model of eIF5B domain IV and the acceptor end of Met-tRNA_i in the 80S IC.

Recently, we were able to solve two structures of eIF5B domain IV from the fungus *C. thermophilum* [201]. It consists of six antiparallel β strands (β 1- β 6) forming a closed β barrel that is followed by two α helices (Figure 1A). At its top and bottom, the β barrel is closed by an additional short β strand (β^{L4}) and a one-turn α helix (α^{L5}), respectively. Despite relatively low sequence similarity, it is structurally very similar to domain IV of aIF5B from the archaeon *M. thermoautotrophicum* (rmsd of 2.2 Å for C $_{\alpha}$ atoms with ~20% identity and ~30% similarity). However, in the *ct*eIF5B ortholog the β hairpin formed by β strands 3 and 4 and the loop following strand β 5 (L5) contain 9 and 5 additional amino acids, respectively (Figure 1A/B). Further differences can be found in the organization of the two C-terminal α helices that are rotated by ~25° with respect to the β barrel.

Compared to the archaeal ortholog, domain IV from *ct*eIF5B shows a relatively high sequence similarity to the yeast ortholog (19% identity and 30% similarity for *mt*aIF5B compared to 49% identity and 65% similarity for *ct*eIF5B) including the β 3- β 4 hairpin, L5 and the two C-terminal α helices. Based on this observation, we assumed that the *ct*eIF5B structure allows a better fit to the recently determined cryo-EM density of the yeast 80S IC with initiator tRNA and eIF5B-GDPCP than obtained with the *mt*aIF5B structure [91] (Figure 1C). Rigid-body fitting of *ct*eIF5B domain IV (cross-correlation coefficient (CCC) of 73%) results in an improved correlation between structural model and density (Figure 1D): In contrast to the original fit of *mt*aIF5B [91], no clashes occur between the ribosomal RNA and *ct*eIF5B domain IV, as the loop between β strands 1 and 2 (L1) is moved away from C2284-U2286 and now lies next to the acceptor stem of the tRNA. Compared to the original model [91] the β barrel is rotated by ~30°, causing the conserved helix α^{L5} at the bottom of the β barrel to displace the β 3- β 4 hairpin in the major groove of the initiator tRNA acceptor stem. In turn, the long, poorly conserved β 3- β 4 hairpin now occupies previously unexplained density close to the C-terminus of the last α helix and forms apparently no direct contacts to the tRNA (Figure 1D).

An interesting consequence of this reorganization of domain IV is the emergence of a well defined but unexplained density packed alongside the β barrel, directly opposite to the C-terminal

α helices (Figure 1D). This density starts next to the very C-terminus of β strand 4 and the following loop (L4) and runs across strands β 5, β 2 and finally β 1 where it directly leads into the continuous density of the phosphate backbone of the initiator tRNA at A73. Interestingly, this same position (A73) also marks the starting point for the distortion of the following 3' CCA-end in the original model that is markedly different from its canonical conformation [91]. For the following reasons, it is unlikely that this original model gives the correct conformation for the tRNA acceptor arm in the 80S pre-IC: First, C75 and A76 clash extensively with the ribosomal RNA between G2615 and C2625 (Figure 1C). Second, the CCA-end is oriented away from eIF5B domain IV, resulting in a distance of ~ 23 Å between the ribose of A76 (which carries the methionyl moiety) and the nearest parts of domain IV. This is clearly inconsistent with the observation that deacylation of the tRNA results in the loss of its contact to eIF5B in the 80S complex [91] and is at odds with the expected direct contact between the methionyl moiety and domain IV [86, 199, 202]. Remodeling of the 3' CCA-end into the vacant density next to the β barrel of eIF5B avoids the clashes with the rRNA and, moreover, allows a direct recognition of the aminoacyl group by the protein by placing the 3' end of the tRNA directly on top of the conserved Ala1056 of strand β 5 (Figure 1D). It is important to note, that there is no alternative density present that could accommodate the entire CCA-end without causing a sterical conflict with the rRNA. Independent support for this new placement of the CCA-end is provided by the just recently published lower resolution (8-9 Å) cryo-EM model of the mammalian 80S pre-IC with eIF5B bound on HCV-IRES RNA, which suggests a direct contact between the acceptor end of the Met-tRNA_i and domain IV of eIF5B [203].

As reported previously for *mta*eIF5B [84], the β barrel of eIF5B is structurally homologous to domain IV (C2 domain) of bacterial IF2 [197] and domain II of EF-Tu homologs, despite an overall low sequence similarity (Figure 2 and 3). Using site directed mutagenesis and NMR spectroscopy, it was shown that IF2 interacts with the α NH-formylmethionylated CCA-end of fMet-tRNA^{fMet} through a surface of domain IV that overlaps with that used by EF-Tu domain II to interact with the acceptor end of elongator tRNAs [48, 163, 196, 197]. The superposition of domain IV of *cte*eIF5B with domain IV of IF2 from *Bacillus stearothermophilus*[197] and domain II of EF-Tu from *Thermus aquaticus* in complex with Phe-tRNA^{Phe}[48] reveals that these surface areas coincide perfectly with those occupied by the CCA-end in our cryo-EM density-based model (Figure 2). Consistently, a

structure-based sequence alignment reveals the highest degree of sequence conservation between the eIF5B orthologs and EF-Tu domain II in those residues implicated in tRNA binding in IF2 and EF-Tu (Figure 3).

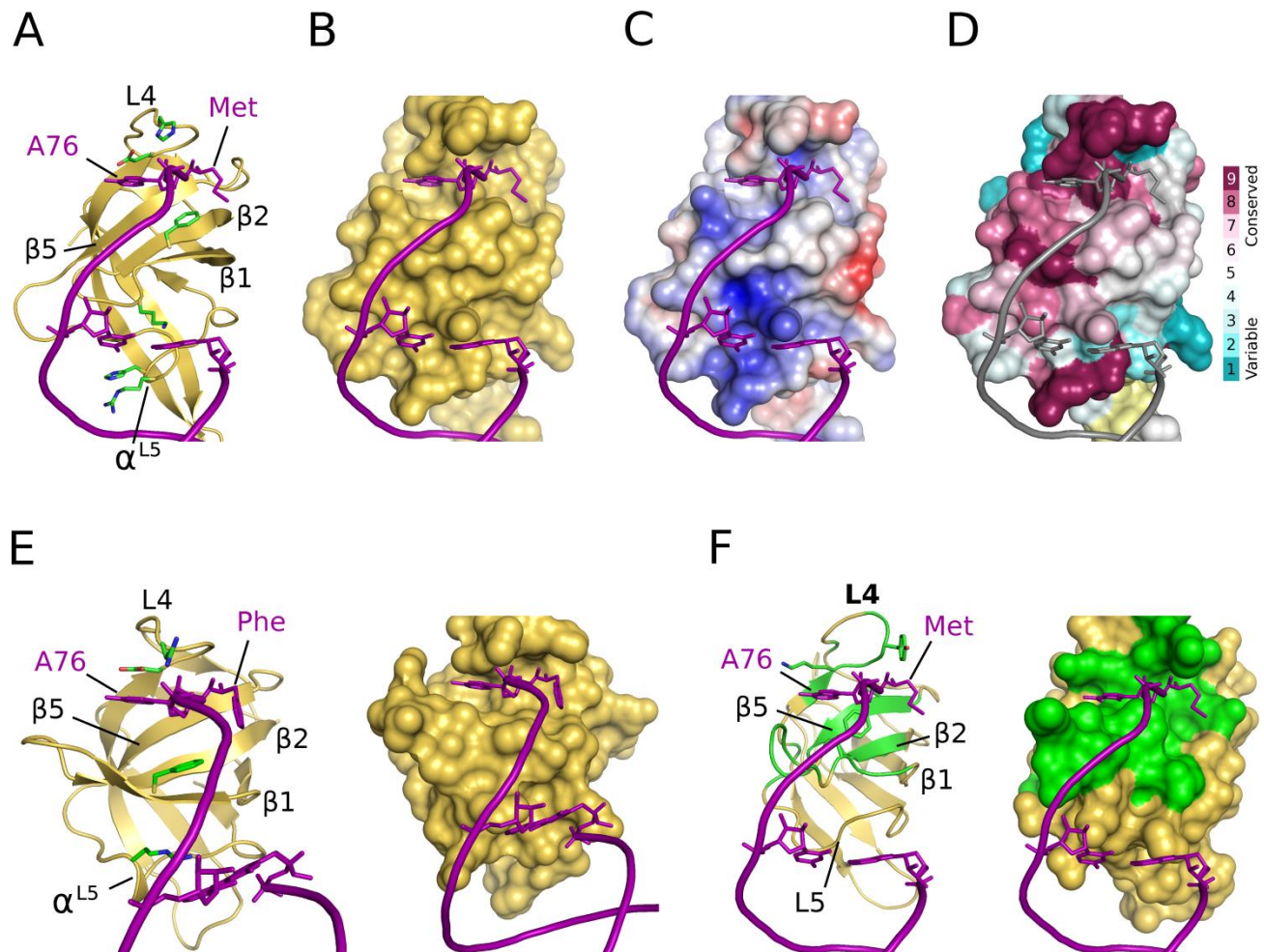


Figure 2. The interaction interface between the acceptor stem of Met-tRNA_i and domain IV of eIF5B. Interactions between Met-tRNA_i (purple) and eIF5B domain IV (**A-D**), Phe-tRNA^{Phe} and domain II of EF-Tu (PDB: 1TTT) (**E**) and fMet-tRNA^{fMet} and IF2 domain IV (**F**). **A**) Domain IV of eIF5B in ribbon presentation (yellow) with residues potentially involved in interactions with the tRNA as green sticks. **B**) Surface presentation of domain IV, revealing the two well defined pockets below loop L4 that are also visible on the surfaces of EF-Tu domain II (**E**, right) and IF2 domain IV (**F**, right), and might accommodate A76 and the methionyl moiety of the 3' CCA-end. **C**) Electrostatic surface potential of domain IV. **D**) Conservation of residues lying in the proposed interaction interface to the acceptor stem. **E**) Position of the acceptor stem of Phe-tRNA^{Phe} (purple) on the surface of domain II of EF-Tu (yellow; PDB: 1TTT). **F**) Model of domain IV of IF2 (PDB: 1D1N) and the initiator tRNA positioned as in **A**). The green surfaces indicate residues of IF2 that were shown to interact with fMet-tRNA^{fMet}[196, 197].

The analysis of the surface area in *ct*eIF5B reveals two pockets next to the modeled 3' end of the tRNA (Figure 2 and 4). The first formed by Val999, Gly1037, Glu1039 and the aliphatic part of Lys1058, corresponding to the EF-Tu residues Val237, Gly269, Glu271 and Leu289, respectively, which accommodate the base of A76 in Phe-tRNA^{Phe} [48]. A similar pocket is found on the surface of IF2, whose residues are directly affected by fMet-tRNA^{fMet} binding [196, 197]. The second pocket is separated from the first by the methyl group of Ala1056 (corresponding to the conserved Gly287 in EF-Tu and Gly715 in *bs*IF2) and is formed on the one side by the hydrophobic Val989, Ala990, Phe992, Gly1001 and Ala1054 and on the other by the peptide backbone of Glu1039 to His1042. The position of this pocket corresponds to the localization of the aminoacyl groups in ternary complexes of EF-Tu, and residues of this area were found to interact specifically with N-formylmethionine in IF2 [196] and methionine-ethyl ester in eIF5B [86]. Consistently, this second pocket is compatible with the binding of a methionyl moiety in size as well as electrostatic surface properties (Figure 2 and 4). Notably, in both available crystal structures of *ct*eIF5B domain IV, this pocket is occupied by a large additional electron density. Due to the absence of alternatives in the crystallization condition (100 mM MES, 12% PEG 20000, 10 mM Na-lactate; ethylene glycol was used for cryo protection), this density was originally assigned to a lactate molecule [201]. However, refinement with the lactate molecule still results in positive difference electron density. A simulated annealing omit map for this area gives a density too large for a lactate (Figure 4B). Thus, the density would be compatible with the size of a methionine or other similarly large amino-acids whose α -carboxylate and α -amino groups form hydrogen bonds to the amide proton of Asp1041 and the main chain CO of Ala1054, respectively, corresponding to His273 and Asn285 that form similar contacts to the aminoacyl group in ternary complexes of EF-Tu [48, 204] (Figure 4D). However, the resolution of the structures (2.75 and 3.02 Å) necessarily does not allow an unambiguous assignment of the densities to a certain ligand, and a possible origin for a putative amino acid in this position remains elusive, as the weak binding between IF2 and fMet or eIF5B and methionine-ethyl ester [86, 196] makes a co-purification unlikely. The critical point, however, is the observation that the described pocket is evidently suited to accommodate organic molecules of a size similar to that of methionine and could thus accommodate the methionyl moiety of the Met-tRNA_i in a way analogous to domains II in EF-Tu and aIF2 γ (Figure 4).

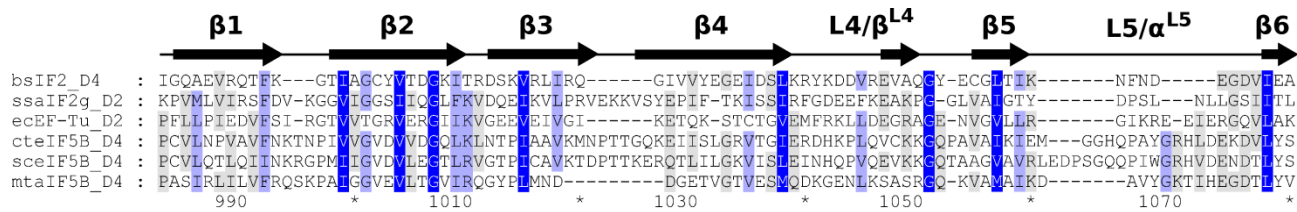


Figure 3. Partial structure-based sequence alignment of the β barrel fold of domain IV (D4). The aligned sequences are from *B. stearothermophilus* IF2, *M. thermoautotrophicum* aIF5B, *C. thermophilum* eIF5B and *S. cerevisiae* eIF5B with domain II (D2) from *E. coli* EF-Tu and *S. solfataricus* aIF2 γ (GenBank: CAA27987, AAB84765, EGS21143, AAC04996, CAA40370, AAK40740, respectively). Highly conserved residues are highlighted in dark blue, conserved residues in light blue and similar residues in grey. Sequence numbering and secondary structure elements correspond to the *cteIF5B* structure (PDB: 4N3G). As there is no structure of *sceIF5B* available so far, its sequence was aligned directly with that of *cteIF5B*.

In ternary complexes of EF-Tu, the binding site for the 3' CCA-end on domain II is complemented by the conserved Phe229 in strand $\beta 1$ that stacks against C4 and C5 of the A76 ribose and by Arg274 (sometimes Gln or Lys) in the flexible loop following strand $\beta 4$ that interacts with the phosphate of A76 [48, 204] (Figure 4C). The density assigned to the CCA-end of the Met-tRNA_i suggests similar interactions for the conserved Phe992 (in few cases Tyr or Ile) and His1042 in *cteIF5B* (Figure 4A). According to the model, the rest of the acceptor stem of the tRNA adopts a slightly different orientation relative to the β barrel than observed for aa-tRNA bound to EF-Tu. In good agreement with the predictions made for IF2 [196], C75 and C74 seem to be rotated $\sim 20^\circ$ toward the L1 loop (Figure 2). Interestingly, the orientation of the β barrel would allow several positively charged residues to interact directly with the acceptor stem. Lys994 in the L1 loop could contact the initiator tRNA specific A1:U72 base pair. The conserved Arg1070 and His1071 in helix α^{L5} , positioned in a well defined density in the cryo-EM map (Figure 1D), are within contact distance to the phosphate backbone at G68 and C69 in the major groove. Notably, EF-Tu domain II contains a corresponding short helix α^{L5} in which the conserved Arg295 as well forms a contact to the acceptor arm of the bound tRNA [48, 204] (Figure 2E). Based on the comparison with EF-Tu it was previously assumed that a similar contact might be formed between Lys725 and Glu726 of *bsIF2* and fMet-tRNA^{fMet}. However, such an interaction could not be observed by NMR spectroscopy in solution [196]. It is therefore conceivable that these interactions are formed only in the context of the ribosomal pre-IC, where the tRNA is stabilized in a specific orientation relative to domain IV of eIF5B/IF2.

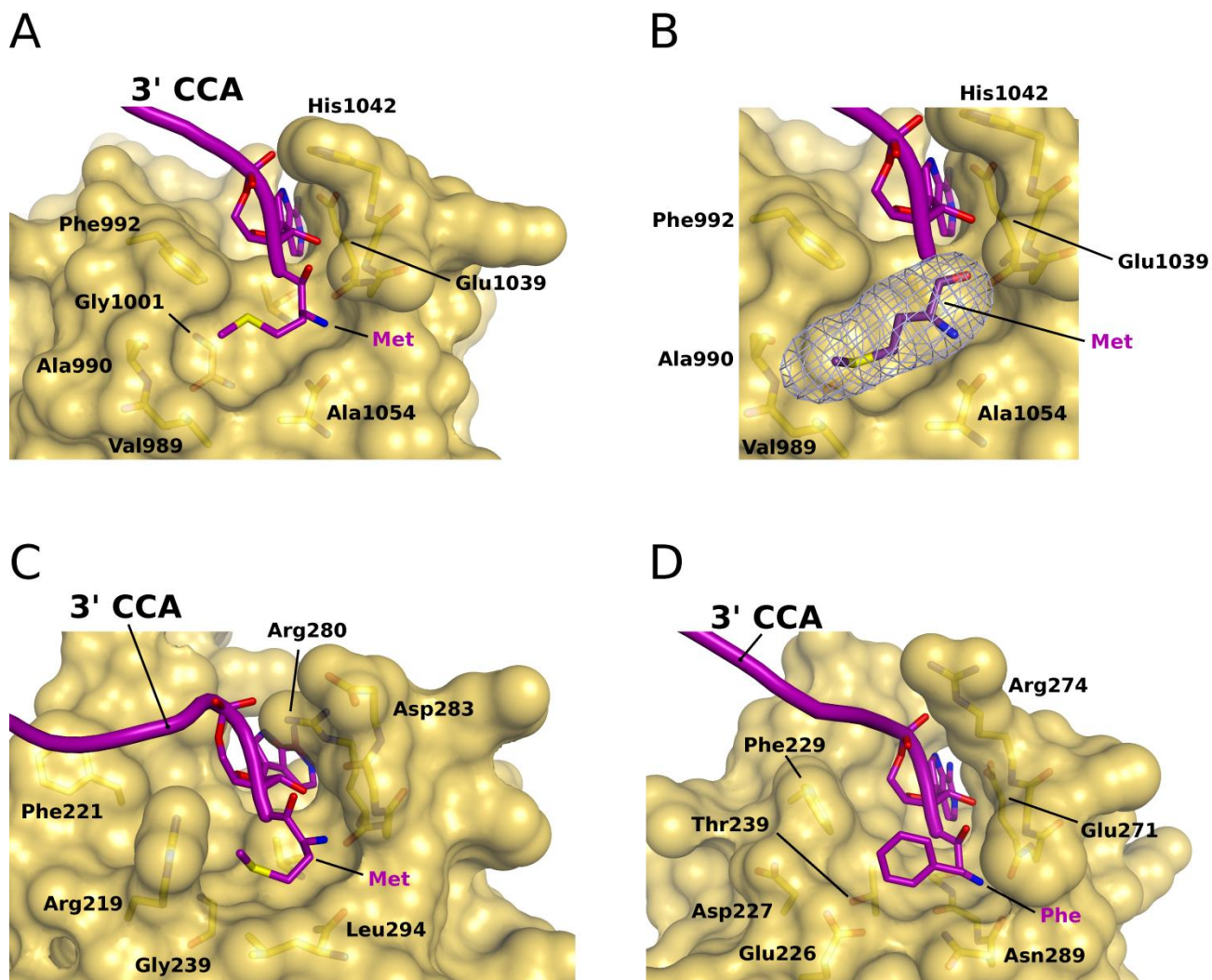


Figure 4. Recognition of the methionylated 3' CCA-end by eIF5B domain IV. **A)** CCA arm, A76 and the methionyl moiety of Met-tRNA_i modeled into the two surface pockets on eIF5B domain IV according to the cryo-EM density. Residues implicated in the interactions with the 3' end are indicated. **B)** Simulated annealing f_o-f_c omit map for the putative methionyl-binding pocket in eIF5B domain IV (blue mesh; contoured at 3σ). **C)** Met-tRNA_i bound to aIF2 γ (PDB: 3V11). **D)** Phe-tRNA^{phe} bound to EF-Tu (PDB: 1TTT).

Biological relevance of this domain IV-tRNA interaction lies in the mutual stabilization of initiator tRNA and eIF5B in conformations that allow efficient recruitment of the large ribosomal subunit and insertion of the acceptor arm into the peptidyl-transferase center (PTC). In the 80S complex domain IV stabilizes the tRNA in a non-canonical P/I orientation [91] that according to our model places the 3' end ~ 20 Å from the PTC without inducing a major distortion of the CCA-end from its canonical conformation (Figure 5). The following GTP hydrolysis and dissociation of eIF5B would thus allow the acceptor stem to rotate into the PTC while the overall tRNA relaxes into its

canonical P site conformation. Through the specificity of domain IV for the methionylated acceptor arm, which might be more pronounced in the context of the preassembled 40S·Met-tRNA_i complex than in solution [202], this interaction would mark a final checkpoint in the initiation process that allows subunit joining only on correctly assembled 48S pre-ICs with a charged initiator tRNA bound in the P site [146, 201].

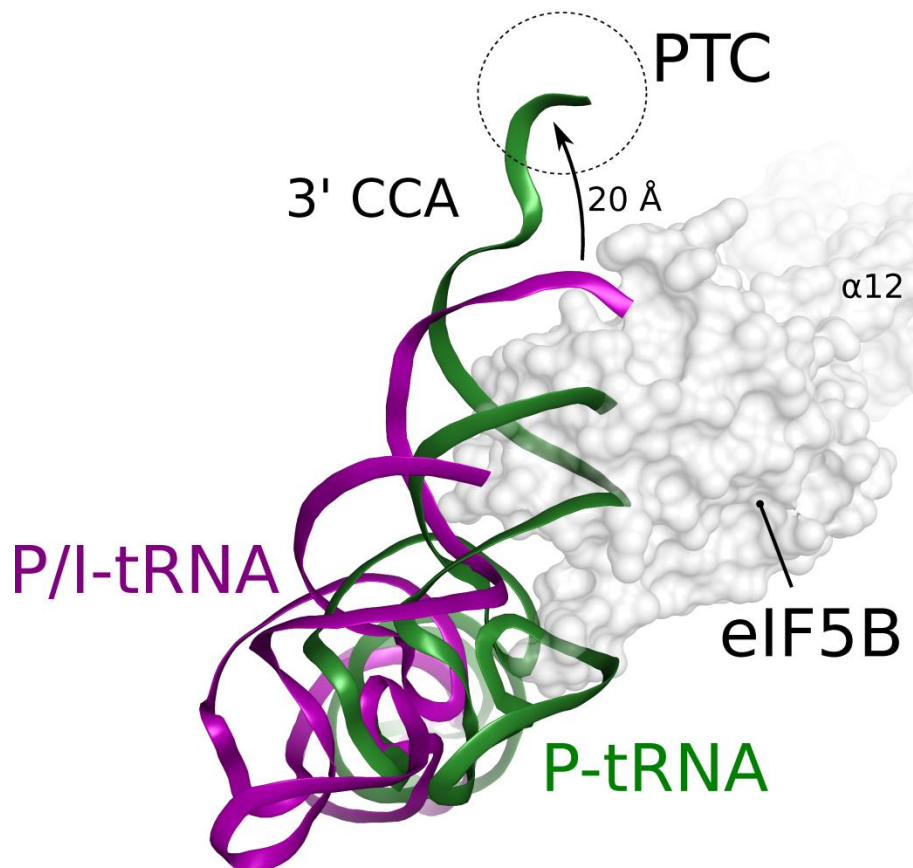


Figure 5. Conformational rearrangement of Met-tRNA_i on the initiation complex. eIF5B stabilizes the initiator tRNA (purple) in a non-canonical P/I conformation [91] with the 3' CCA-end outside of the PTC. Upon GTP hydrolysis in eIF5B and the release of the 3' CCA-end from its contacts to domain IV, the initiator tRNA rearranges into the canonical P site conformation, involving a 20 Å repositioning of the 3' end into the PTC.

Implications for the evolution of the translational β barrel fold

As reported previously, domain IV of IF2 and the structurally homologous domain II of EF-Tu use similar surface areas to interact with amino-acylated tRNAs [196, 197] (Figure 2E/F). The structure of the ternary complex of aIF2 shows the same interface for the interactions between domain II of

aIF2 γ (a paralog of EF-Tu) and the Met-tRNA_i[42] (Figure 4C). Our observations provide structural evidence that this also applies to domain IV of eIF5B. This common binding interface for the 3' CCA-end on the translational β barrel fold is centered on β strands 1, 2 and 5 and framed by the flexible loops L1 and L4 (Figure 2 and 4). In all cases additional interactions are made by the short capping α -helix that provides positively charged residues for contacts to the phosphate backbone of the acceptor stem, while at the same time allowing substantially different overall orientations of the tRNA relative to the β barrel, irrespective of an identical polarity of the bound CCA-end (Figure 6). Despite the low average sequence identity over the various β barrel folds (Figure 3), the significant structural and functional parallels in their interactions with amino-acylated tRNAs clearly point toward a common evolutionary origin. As eIF5B/IF2 and EF-Tu are both universally conserved in the three domains of life, their divergence and thus the origin for their respective tRNA-binding domains most likely lies long before the onset of speciation; this raises the interesting question of potential homologies to other ancient RNA-binding protein folds.

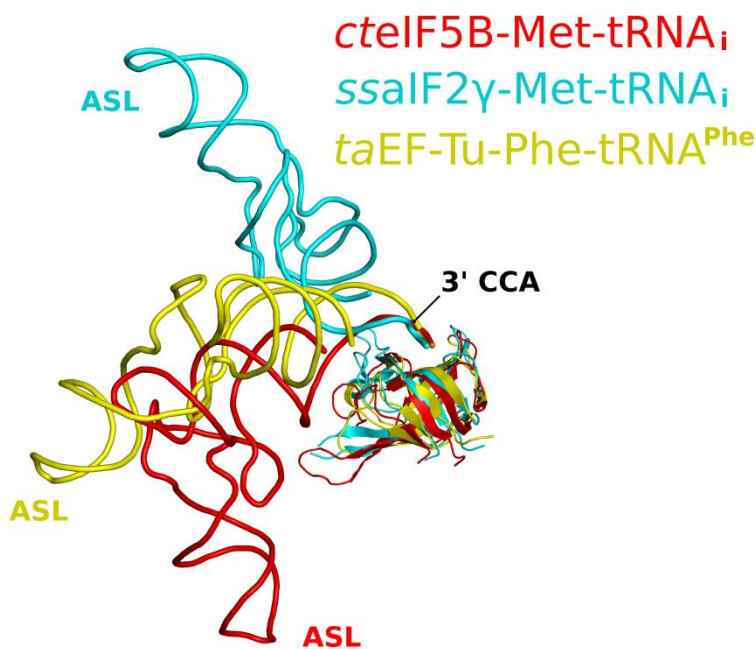


Figure 6. Comparison of the interactions between eIF5B, EF-Tu and aIF2 with tRNA. Despite the same polarity and similar interfaces for the interactions between the translational β barrel fold and the single-stranded 3' CCA-end, the tRNAs adopt significantly different overall orientations relative to the protein in ribosome-bound eIF5B (red) or the ternary complexes of *S. solfataricus* aIF2 (cyan; PDB: 3V11) and *T. aquaticus* EF-Tu (yellow; PDB: 1TTT). ASL is anticodon stem loop.

A central question for the problem of cellular evolution is the appearance of the basic protein-folding types and of domains as functional building blocks for proteins. Folded proteins adopt only a limited number of folding structures; however, whether these folds emerged by

divergent evolution from a single ancestor or independently by convergent evolution from different lineages is unclear. In this context, it is interesting that the characteristic features of tRNA binding by the translational β barrel fold show significant parallels to those between OB-fold domains and single-stranded nucleic acids (Figure 7). The OB-fold is a five-stranded mixed β barrel, capped on one end by an α -helix [205]. Most known OB-fold domains are involved in interactions with single-stranded RNA or DNA [206]. Despite very low sequence similarity among its members, the OB-fold superfamily is thought to be an ancient domain structure that derived by divergent evolution from a common ancestral protein – an assumption that is based on the common features of their fold-related ligand-binding interface [206, 207]. Despite a different overall topology of the OB-fold (Figure 7C/D) and a different classification in the SCOP (Structural Classification of Proteins) database, this interface, composed of $\beta 1$ -L1- $\beta 2$ - $\beta 3$ -L3/ α^{L3} - $\beta 4$ -L4 (Figure 7B), shows an intriguing structural and functional correspondence to the identically arranged but differently connected building blocks of $\beta 1$ -L1- $\beta 2$ and $\beta 4$ -L4- $\beta 5$ -L5/ α^{L5} - $\beta 6$ in the translational β barrel fold that are responsible for its interactions with tRNA (Figure 7A).

These similarities might merely be a functional analogy between both protein families that arose by convergent evolution from two distinct starting points. However, by the argument of a common descent based on a fold-related ligand-binding interface, the evident similarities might as well be indicative of a common evolutionary origin for the two equally ancient protein folds. For this hypothesis, two previously proposed theories are of particular interest: i) The emergence of domain folds by polyphyletic evolution from self-assembling short peptide ancestors, whose remnants (in sequence, structure or function) still exist in extant proteins [208]; and ii) the theory of a chemoautotrophic origin of life on volcanic iron-sulfur surfaces, according to which protein domains emerged from functional peptides that used metal ions as folding determinants or formed surface-bonded β -sheets that finally detached from the stabilizing surfaces (e.g. to form β -barrel domains) in the course of progressing cellularization [209-211]. In both theories, the transition from the peptide- to the independently folding protein-domain proceeds concomitant to the refinement of the genetic machinery that allows the synthesis of increasingly long polypeptides with sufficiently high fidelity [208, 210, 211].

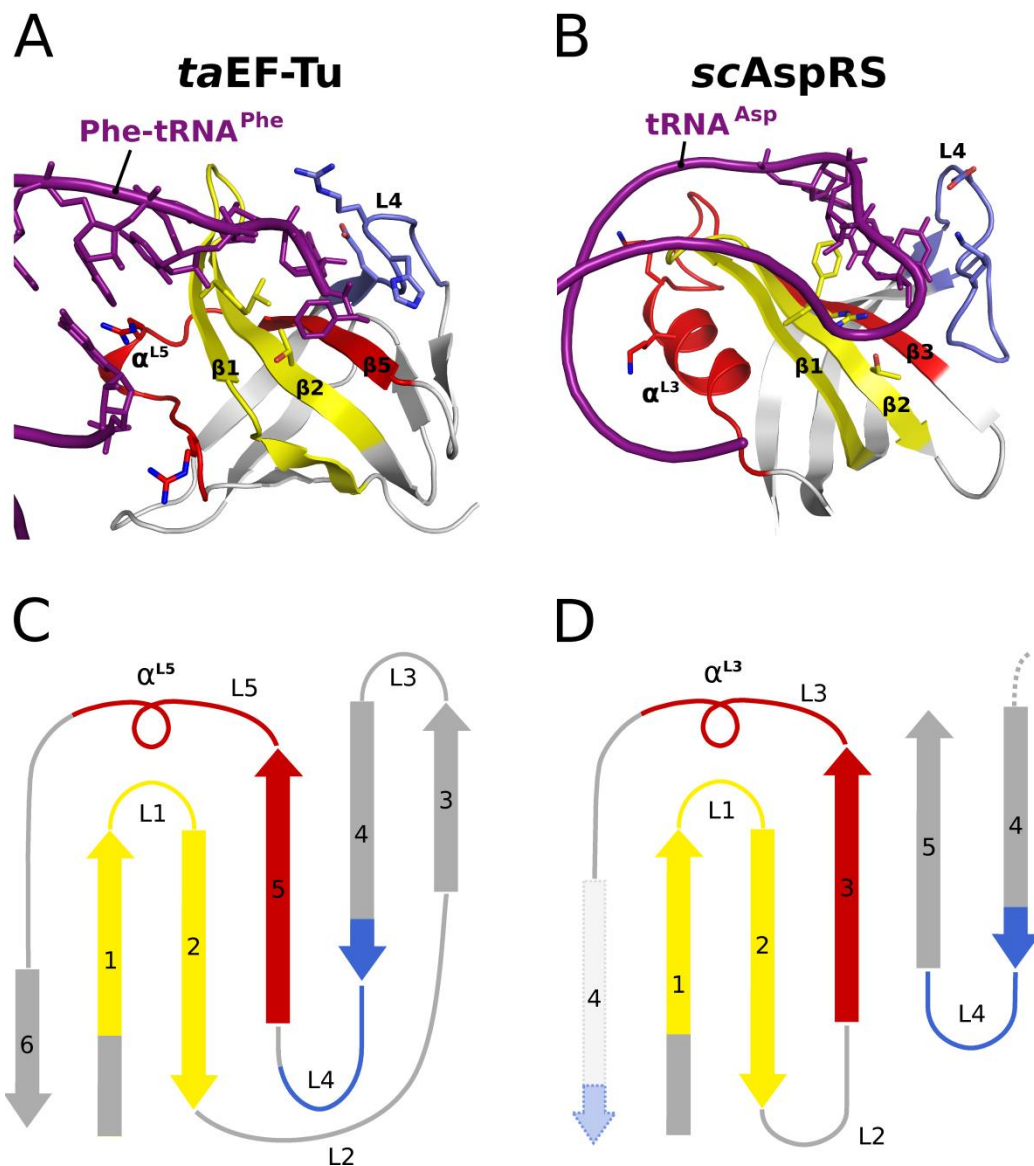


Figure 7. Translational β barrel fold and OB-fold share the same fold related ligand-binding interface. **A and C) The interaction interface between the 3' CCA-end of the tRNA and the translational β barrel (here Phe-tRNA^{Phe} (purple) bound to *T. aquaticus* EF-Tu domain II (PDB: 1TTT)) centers on β strands 1, 2 and 5 and is augmented by loops L1, L4 and L5, containing helix α^{L5} . **B and D)** A related ligand-binding interface is found in single-stranded nucleic acid binding OB-folds (here the anticodon binding domain of the aspartyl-tRNA synthetase (PDB: 1ASZ) from *S. cerevisiae*[212]). Similar to the interactions observed for EF-Tu and despite a different topology, the bases of the anticodon stem loop (purple) point toward the surface of the β barrel, centered on β strands 1, 2 and 3, while the flexible loops L1, L4 and L3 with α^{L3} form additional contacts to the phosphate backbone.**

In light of these hypotheses, we suggest a possible common polyphyletic origin of both fold-related RNA binding interfaces discussed above. At the earliest stages of cellular evolution, when the fidelity of the primordial translation apparatus allowed the synthesis only of short peptides,

nucleic acid-peptide interactions most likely played an essential role, particularly for the genetic machinery. In this context, it would be conceivable that the common ligand-binding interface in the ancient lineages of OB-fold proteins and translational GTPases has arisen as an ancient structural entity formed by individually synthesized peptides, associating with single-stranded nucleic acids as folding determinants, similar to metallo-peptides as precursors for metallo-proteins [209-211]; during the gradual replacement of peptides by their fusion into independently folding proteins, this would ensure the conservation of the nucleic acid-binding interface, while at the same time allowing a substantially different connectivity of the individual building blocks in the emerging protein families.

Conclusions

In this study, we used the recently reported medium resolution cryo-EM density of the yeast 80S IC [91] and high resolution crystal structures of eIF5B from *C. thermophilum* to propose a new model for the interactions between eIF5B domain IV and the Met-tRNA_i in the context of the ribosome (Figure 1). According to this model, domain IV forms direct interactions with the phosphate backbone in the major groove of the acceptor arm, the initiator tRNA specific A1:U72 base pair and – most importantly – with the methionylated 3' CCA-end. The relevance of these findings lies in the novel insight into the specific recognition of the amino-acylated initiator tRNA by eIF5B/IF2 in the context of pre-initiation complexes, which, as a final checkpoint for ribosomal subunit joining, is one of the central interactions in the process translation initiation. Finally, the identified binding interface between eIF5B and Met-tRNA_i directly corresponds to that reported earlier for the interaction between the homologous domains in IF2, EF-Tu and aIF2 γ with their respective tRNA ligands [48, 197] and exhibits a striking structural and functional similarity to the fold-related ligand-binding interface of OB-fold domains, possibly reflecting a common evolutionary origin of the two ancient domain folds.

6.3 Methods

Model building

Rigid-body fitting of *ctelF5B* domain IV (residues 382-1116; PDB codes 4N3N and 4N3G) was performed using UCSF Chimera [213]. Despite entirely different sets of crystal contacts for domain IV in the two X-ray structures they are very similar to each other (rmsd of 0.34), indicating a high degree of structural rigidity. Thus, although domain IV might undergo minor conformational changes upon interacting with ribosome and tRNA, particularly in the loop regions, we decided not to include any flexible fitting procedures to avoid overfitting of the model. Manual rebuilding of the acceptor stem of the Met-tRNA_i between bases G70 and A76 into the density next to domain IV was done in COOT [116]. Figures were prepared using UCSF Chimera [213] or Pymol (<http://www.pymol.org>).

We would like to mention here that in our hands the isolated domain IV of the *mtalF5B* crystal structure (PDB: 1G7R) is fitted to the cryo-EM density in the same way as the *ctelF5B* structure (with a CCC of 67%), supporting the newly proposed fit shown in Figure 1D. However, the *mtalF5B* domain IV of the cryo-EM based model (PDB: 4BYX) is fitted as presented in [91] with a CCC of 78.7% (Figure 1C), most likely as the result of a combination of rigid-body and flexible fitting procedures [91], which gave rise to rmsds of 5.8 Å and 7.5 Å (over 106 C_α atoms) relative to the crystal structures of *mtelF5B* and *ctelF5B*, respectively, while the two crystal structures themselves differ only by an rmsd of 2.2 Å. Thus, the higher CCC for the cryo-EM-based model is most likely due to its distortion from the original rigid structure of *mtalF5B* and is therefore not comparable to the CCC values obtained for our rigid-body fit.

Sequence alignments

Multiple sequence alignments were done using the iterative alignment program MUSCLE [214]. Structural sequence alignments were done using the DALI server [215].

Author contributions

BK designed the study, analyzed structures and cryo-EM density, performed the structural modeling and sequence alignments, analyzed and interpreted the data and wrote the manuscript. RF analyzed the data and helped to draft the manuscript. All authors read and approved the final manuscript.

Acknowledgments

We thank L. K. Dörfel for critical reading of the manuscript.

List of abbreviations

IF, initiation factor; eIF, eukaryal initiation factor; aIF, archaeal initiation factor; cryo-EM, cryo-electron microscopy; pre-IC, pre-initiation complex; EMD, EM-Databank; EF-Tu, elongation factor-Tu; *ct*, *Chaetomium thermophilum*; *mt*, *Methanococcus thermoautotrophicum*; *sc*, *Saccharomyces cerevisiae*; *bs*, *Bacillus stearothermophilus*; PDB, protein data bank; CCC, cross-correlation coefficient; SCOP, Structural Classification of Proteins; OB-fold, oligo-nucleotide/oligo-saccharide binding fold; rmsd, root mean square deviation; PTC, peptidyl-transferase center; ASL, anticodon stem loop.

Competing interests

The authors declare that they have no competing interests.

Chapter 7 • A monovalent cation as cofactor in translational GTPases

This manuscript has originally been published in *The EMBO Journal*

A Monovalent Cation Acts as Structural and Catalytic Cofactor in Translational GTPases

Bernhard Kuhle^{1,§} and Ralf Ficner¹

¹ Abteilung für Molekulare Strukturbiologie, Institut für Mikrobiologie und Genetik, Göttinger Zentrum für Molekulare Biowissenschaften, Georg-August-Universität Göttingen, D-37077 Göttingen, Germany

[§] To whom correspondence should be addressed: bkuhle@gwdg.de

Keywords: translation, catalytic mechanism, monovalent cation, crystal structure, GTPase

Received 18 March 2014 | Revised 1 July 2014 | Accepted 14 August 2014

Author contributions:

BK: Conceived the study and designed the experiments; prepared and crystallized proteins, collected X-ray data and solved the structures; performed ITC and fluorescence experiments; created figures; analyzed data and wrote the manuscript. RF: analyzed the data and helped to draft the manuscript.

Abstract

Translational GTPases are universally conserved GTP hydrolyzing enzymes, critical for fidelity and speed of ribosomal protein biosynthesis. Despite their central roles, the mechanisms of GTP-dependent conformational switching and GTP-hydrolysis that govern the function of trGTPases remain poorly understood. Here, we provide biochemical and high-resolution structural evidence that eIF5B and aEF1A/EF-Tu bound to GTP or GTP γ S coordinate a monovalent cation (M^+) in their active site. Our data reveal that M^+ ions form constitutive components of the catalytic machinery in trGTPases acting as structural cofactor to stabilize the GTP-bound 'on' state. Additionally, the M^+ ion provides a positive charge into the active site analogous to the arginine-finger in the Ras-RasGAP system indicating a similar role as catalytic element that stabilizes the transition state of the hydrolysis reaction. In sequence and structure, the coordination shell for the M^+ ion is, with exception of eIF2 γ , highly conserved among trGTPases from bacteria to human. We therefore propose a universal mechanism of M^+ -dependent conformational switching and GTP-hydrolysis among trGTPases with important consequences for the interpretation of available biochemical and structural data.

7.1 Introduction

Translation – the ribosome-catalyzed synthesis of biologically functional polypeptides according to genetically encoded information – is one of the most fundamental and complex biochemical processes in extant cellular life. In all stages of protein biosynthesis the ribosome depends on a set of auxiliary guanine nucleotide binding (G) proteins (termed translational GTPases or trGTPases) that include initiation factor 2 (IF2), which catalyzes ribosomal subunit joining and formation of the elongation-competent ribosome, elongation factor Tu (EF-Tu), which delivers aminoacyl-tRNA (aa-tRNA) to the ribosomal A site, as well as elongation factor G (EF-G) that catalyzes the translocation of the mRNA-tRNA complex on the ribosome [8, 9]. Despite the differences in their respective functions, trGTPases from bacteria to eukarya share a common evolutionarily conserved structural core composed of the G domain and domain II, which is supplemented with additional factor specific domains. The G domain forms the functional center in all trGTPases that couples GTP

binding and hydrolysis to the specific biological function of the translation factor [9]. This present work focuses on so far unresolved aspects of the universal molecular mechanisms that govern the functional cycle of the G domain in trGTPases and that are therefore central to the understanding of the process of translation as well as its evolution.

In sequence and architecture the G domain in trGTPases is related to small Ras-like G proteins and thus belongs to the superfamily of P-loop GTPases [24]. According to the classical view, G proteins are thought to act as molecular switches that oscillate between a GDP-bound 'off' state and a structurally distinct GTP-bound 'on' state [23, 24]. The exchange of GDP for GTP is accompanied by conformational changes in two conserved dynamic elements termed switch 1 and switch 2 that form specific interactions with the GTP- γ -phosphate. Conversion back to the GDP-bound state requires the hydrolysis of GTP and release of inorganic phosphate (P_i), allowing switch 1 and 2 to relax back into their inactive conformations. These structural changes ensure that only the GTP-bound form of a G protein is able to interact productively with effector molecules to carry out its biological function [23].

Despite its importance for the understanding of the translation process, the mechanism of GDP/GTP-dependent conformational switching has remained obscure for nearly all trGTPases. Over the years, high resolution structures have become available for various trGTPases in their apo states as well as in complex with GDP and the nonhydrolyzable GTP analogs GDPNP or GDPCP (β - γ -imidoguanosine 5'-triphosphate and β - γ -methyleneguanosine 5'-triphosphate, respectively). Surprisingly, however, from these structures a highly heterogeneous picture emerged for the mechanisms of conformational switching in the G domains of trGTPases that is at odds with their evolutionary and structural homology: While only EF-Tu exhibited clearly distinct GDP- and GDPNP-bound conformations in agreement with the classical concept [38, 163], EF-G, aIF5B and eRF3 adopted virtually identical structures in their respective GDP- and GDPNP/GDPCP-bound forms, invoking suggestions about non classical mechanisms in these G proteins [84, 216, 217]. SelB, finally, seemed to constitute an intermediate case with switch 2 undergoing conformational changes upon GDPNP binding, while switch 1 remained mainly flexible similar to the GDP-bound state [218]. In order to reconcile the structural data with the classical model of GTPase function it was proposed that some of these apparently non-classical trGTPases follow a mechanism of

'conditional switching' [153]. According to this concept, the GTP alone is insufficient to induce the GTP-conformation in the G domain but requires the ribosome as additional cofactor for the efficient conformational switch to the 'on' state. However, biochemical experiments as well as a recent crystal structure of eIF5B bound to GTP indicate that EF-G, SelB and eIF5B in fact do undergo significant structural rearrangements in the presence of true GTP instead of GDPNP or GDPCP, indicating that they conform to the classical model without the requirement of the ribosome or aa-tRNA for the conformational switch [183, 219, 220]. These observations are paralleled by a large body of biochemical data indicating that GDPNP is not an authentic GTP analog for nearly all trGTPases [153, 183, 221-224] and that the use of nonhydrolyzable analogs in structural experiments most likely accounts for the apparent deviation from the classical switch mechanism [153]. Hence, it seems evident that the stable conformational switch is dependent on critical contributions by the GTP molecule that are, however, not provided by the structurally similar GDPNP/GDPCP. It is therefore a central conceptual assumption of this present work that the identification of this so far unknown contribution by the GTP molecule provides a key to a more unified view on the GDP/GTP cycle in trGTPases, in agreement with their common evolutionary descent.

Another central and yet unresolved problem in the functional cycle of trGTPases is the molecular mechanism of ribosome-induced GTP hydrolysis. Similar to other Ras-like G proteins, trGTPases possess a low intrinsic GTPase activity which is accelerated by several orders of magnitude upon productive binding to the ribosome [27, 225]. In analogy to the systems of the GTPase activating protein (RasGAP) of Ras or the regulators of G protein signaling (RGS) of G α proteins, it was shown that the ribosome stimulates rapid GTP hydrolysis in trGTPases by the precise positioning of an invariant histidine (His^{cat}) in switch 2 (corresponding to Gln61 in Ras) in its catalytically active conformation [168, 169]. However, the actual origin of the catalytic effect in the activated system has remained controversial [168, 226-229]. That is, it remained unclear how the nucleophilic water (W^{cat}) is activated for its attack on the γ -phosphate and how the subsequent stabilization of the transition state (TS) is achieved. In the Ras system RasGAPs further stimulate GTP hydrolysis by supplying an additional catalytic residue, the 'arginine-finger', into the active site, which is responsible for a ~2000-fold acceleration of the GTPase reaction by direct

electrostatic stabilization of developing negative charges in the TS [106]. Analogous catalytic elements provided *in cis* or *in trans* have been identified in P-loop GTPases from G α proteins to MnmE, dynamin and the signal recognition particle [25, 230-232]. However, up to now, trGTPases seemed to be an exception among Ras-related G proteins, as the search for an arginine-finger or an analogous catalytic element has been unsuccessful [233-236].

Here, we discuss the unresolved questions concerning the GTP-induced conformational switch and GTP hydrolysis in trGTPases in light of the novel assumption that trGTPases utilize a monovalent cation (M^+ ion) as structural and catalytic cofactor. We show that eIF5B (eukaryal IF2 ortholog) as well as aEF1A (archaeal EF-Tu ortholog) coordinate an M^+ ion in their active sites in the same position as known M^+ -dependent GTPases, thus placing a positive charge analogous to the guanidino group of the arginine-finger in the Ras-RasGAP complex. The coordination shell for the M^+ ion is, with the notable exception of eIF2 γ , universally conserved among trGTPases from bacteria to humans and directly involves the oxygen atom of GTP that is replaced in GDPNP and GDPCP but not in the slowly hydrolyzable GTP γ S. In combination with mutational, biochemical and isothermal titration calorimetry (ITC) data, these findings provide the conceptual framework and a significant explanatory power for the interpretation of a large body of previously unexplained observations for trGTPases, resulting in the conclusions that i) the M^+ ion acts as structural cofactor that stabilizes the 'on' state of the G domain and thus contributes to the conformational switch in trGTPases; ii) GDPNP and GDPCP are unable to coordinate the M^+ ion and thereby destabilize the GTP-conformation; iii) GTP γ S is able to coordinate the M^+ ion and thus a suitable GTP analog for trGTPases; iv) the M^+ ion participates in the GTP hydrolysis reaction, most likely by stabilizing its TS; v) with few exceptions M^+ -dependency is universal among canonical trGTPases.

7.2 Results

GTP-bound eIF5B coordinates an M^+ ion in its catalytic center

Recently we reported the crystal structure of GTP-bound eIF5B from *C. thermophilum*, solved at 1.9 Å resolution (protein data bank (PDB): 4NCN) [220]. This structure revealed a Na^+ ion next to the GTP- γ -phosphate in a catalytically relevant position of the active site, which has so far never been reported for a trGTPase (Fig. 1A and E1A). In line with previously reported values [156], this

Na⁺ ion is penta-coordinated with coordination distances between 2.3 and 2.5 Å by two oxygens from the α- and γ-phosphates, the β-γ-bridging oxygen, the carboxylate group of Asp533 in the P-loop (which we denote Asp^{MC} for aspartate involved in monovalent cation-binding) and the backbone CO from Gly555 in switch 1 (Gly^{MC}). The latter is part of a short peptide backbone excursion of switch 1 (formed by Gly554 and Gly555) which approaches the Na⁺ ion opposite to the β-γ-bridging oxygen and is denoted 'MC-loop' (Fig. 1).

GTPγS but not GDPNP supports crystallization of eIF5B in its GTP-bound conformation.

The position of the M⁺ ion in eIF5B·GTP suggests that it provides a direct contribution to the stabilization of the GTP-bound switch 1 by forming a stable link to the GTP molecule (Fig. 1A). To test the relevance of this contribution, crystallization trials were performed with the construct *ct*eIF5B(517-858) in the presence of GTP, GDPNP and GTPγS. If the M⁺ is relevant for the conformational switch in eIF5B, GTP and GTPγS but not GDPNP, in which the β-γ-bridging oxygen is replaced by an NH-group (Fig. 2A), should readily stabilize the GTP-conformation and allow crystallization of *ct*eIF5B(517-858) in an optimization screen for the original crystallization condition (0.1 M HEPES/NaOH (pH 7); 13% PEG 4000; 0.1 M NaOAc) (see Expanded View for details).

In line with our assumption, eIF5B(517-858)·GTP and eIF5B(517-858)·GTPγS readily crystallized, while no crystals grew in the presence of GDPNP. The structure of eIF5B(517-858)·GTP, solved at 1.55 Å resolution, is very similar to that reported previously [220] (see Table 1 for details of data collection and refinement). The electron densities for both Na⁺ ions in the asymmetric unit are well defined with occupancies of 100%.

The structure of eIF5B(517-858)·GTPγS was solved at 1.53 Å resolution, exhibiting an overall structure and nucleotide binding virtually identical to that of the GTP-bound form (Fig. E1B/D). The sulfur atom of the γ-phosphate points outward and thus replaces the non-bridging oxygen atom that is involved in the coordination of the M⁺ ion in eIF5B·GTP. Nonetheless, both eIF5B·GTPγS complexes in the asymmetric unit contain the Na⁺ ion in the pentameric coordination shell with coordination distances of 2.2-2.6 Å to the four oxygen ligands from the GTP molecule, Asp^{MC} and Gly^{MC}, and 2.83 Å to the sulfur atom (in agreement with the theoretical distance of 2.8 Å,

calculated from the van der Waals radius of sulfur (1.8 Å) and the effective ion radius of Na⁺ (1.0 Å for coordination number 5) [237, 238]).

Table 1. Crystallization, X-ray data collection and refinement statistics for structures of wild-type eIF5B(517-858)

	eIF5B(517-858)·GTP·Na ⁺	eIF5B(517-858)·GTPγS·Na ⁺	eIF5B(517-858)·GTPγS·K ⁺
Crystallization			
Condition	100 mM HEPES (pH 7.25), 12% PEG 4000, 100 mM NaOAc	100 mM HEPES (pH 7), 13% PEG 4000, 125 mM NaOAc	11% PEG 8000, 6% glycerol, 50 mM KCl
Temperature (°C)	20	20	20
Data Collection			
Space Group	P2 ₁	P2 ₁	P4 ₁ 2 ₁ 2
Unit Cell	a = 55.6 Å b = 116.5 Å c = 66.2 Å α = β = 90° β = 101.1°	a = 55.6 Å b = 115.9 Å c = 66.1 Å α = β = 90° β = 101.4°	a = 116.1 Å b = 116.1 Å c = 120.3 Å α = β = γ = 90°
Molecules/asym. unit	2	2	2
Resolution (Å)	1.55 (1.64-1.55)	1.53 (1.63-1.53)	2.28 (2.42-2.28)
Observed reflections	405616 (64352)	510862 (86738)	307464 (49685)
Unique reflections	118431 (18849)	121606 (20942)	38004 (6021)
Completeness (%)	98.8 (97.7)	98.5 (98.4)	99.9 (99.7)
<I>/σ	15.5 (2.3)	18.8 (2.8)	19.3 (3.8)
R _{sym} (%)	4.6 (50.5)	3.7 (49.6)	6.3 (54.2)
CC(1/2) (%)	99.9 (75.1)	99.9 (82.2)	99.9 (99.1)
Refinement			
R _{work} (%)	15.7	16.3	20.0
R _{free} (%)	18.4	18.8	23.9
Rmsd from Standard Stereochemistry			
Bond length (Å)	0.019	0.02	0.005
Bond angles (°)	1.8	1.9	1.0
Ramachandran Plot Statistics			
Most favored (%)	98.9	98.1	98.5
Allowed regions (%)	1.1	1.9	1.5
Disallowed regions (%)	0	0	0

Values in parentheses refer to the highest resolution shell.

R_{work} and R_{free} factors are calculated using the formula $R = \frac{\sum_{hkl} ||F(obs)_{hkl}| - |F(calc)_{hkl}||}{\sum_{hkl} |F(obs)_{hkl}|}$, where F(obs)_{hkl} and F(calc)_{hkl} are observed and measured structure factors, respectively. R_{work} and R_{free} differ in the set of reflections they are calculated from: R_{free} is calculated for the test set, whereas R_{work} is calculated for the working set.

These results demonstrate that GTPγS is a suitable structural GTP analog that is able to coordinate the M⁺ ion and to stabilize the GTP-conformation in eIF5B. In contrast, GDPNP seems

unable to stabilize efficiently the same conformation (and thus to provide the same surfaces for crystal contacts) as GTP, resulting in the inability of the eIF5B-GDPNP complex to crystallize under the same conditions as eIF5B-GTP. The likely explanation for this observation is that, while GTP and GTP γ S provide all the ligands required for the coordination of the Na⁺ ion and thus allow the stable association of switch 1, GDPNP is unable to provide the M⁺ ion as structural cofactor due to the replacement of the β - γ -bridging oxygen of GTP with a β - γ -bridging imido (NH) group (Fig. 2A).

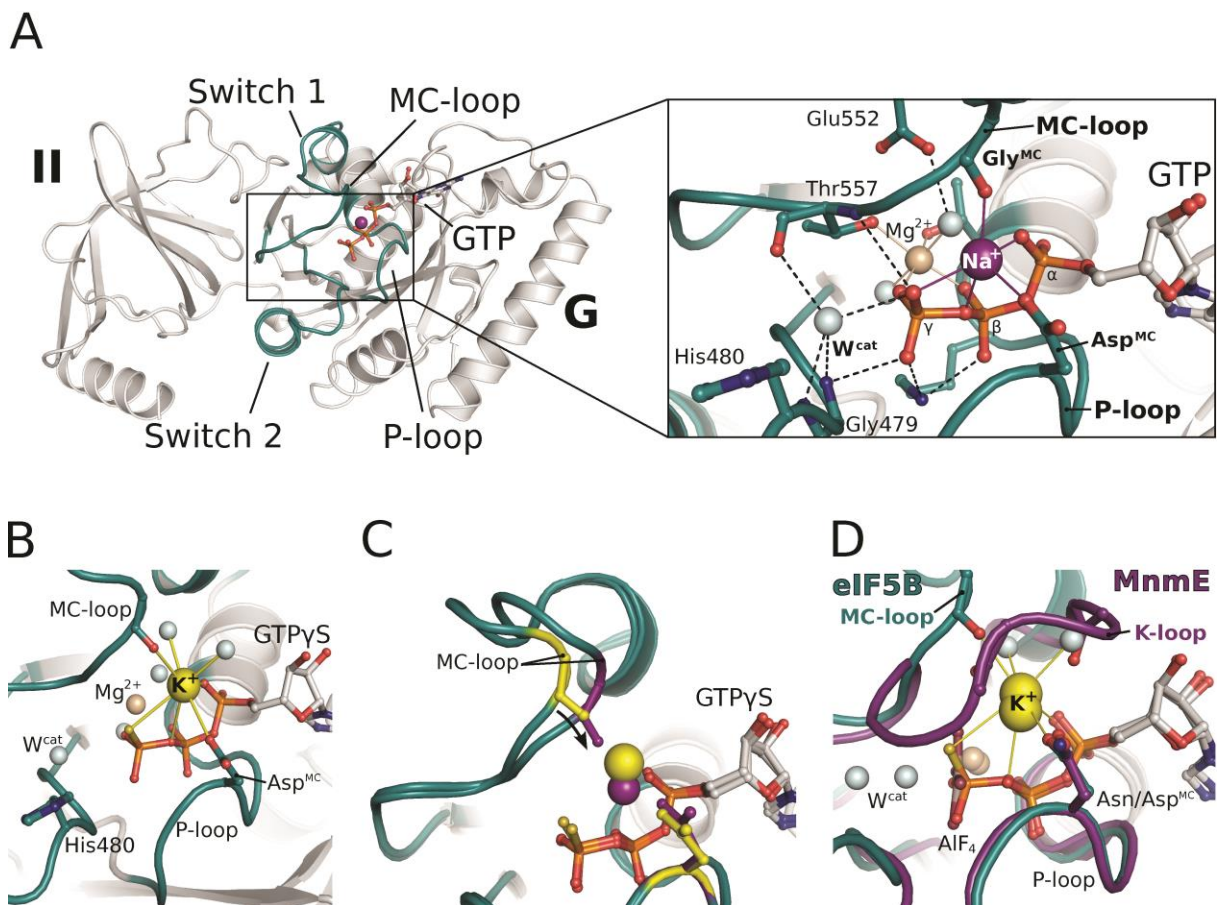


Figure 1. GTP-bound eIF5B coordinates an M⁺ ion in its GTPase center. **A)** Overview of G domain and domain II of GTP-bound eIF5B with a Na⁺ ion (purple sphere) in the active site. P-loop and switch regions are shown in cyan; GTP is shown as balls and sticks. The Na⁺ ion is bound by a pentameric coordination sphere (inset; indicated by purple lines) formed by GTP, Asp^{MC} and Gly^{MC}. Mg²⁺ and water molecules are shown as spheres in light brown and grey, respectively; the catalytic histidine (His480) and highly conserved residues that interact with GTP or the cations are indicated; hydrogen bonds are shown as dashed lines. **B)** The active site of eIF5B-GTP γ S with a K⁺ ion (yellow sphere) bound in a heptameric coordination sphere. **C)** Superposition of eIF5B-GTP γ S structures with either Na⁺ (purple sphere) or K⁺ (yellow sphere) bound in the active site. Due to the shorter coordination distances to the Na⁺ ion, Asp^{MC} and Gly^{MC} (purple sticks) are drawn closer to the GTP molecule than in the K⁺-structure (yellow sticks). **D)** Superposition of eIF5B-GTP γ S-K⁺ and MnME (purple; PDB: 2GJ8) bound to GDP, AlF₄ and K⁺.

GTP γ S but not GDPNP is able to substitute for GTP to induce the conformational switch of eIF5B in solution.

GTP binding to apo eIF5B induces a substantial rearrangement of the switch regions, involving a $\sim 180^\circ$ flip of switch 1 and the burial of $\sim 1800 \text{ \AA}^2$ of solvent accessible surface area (ASA) within G domain and domain II, accompanied by significant changes in heat capacity ($\Delta C_p = -553 \text{ cal}\cdot\text{mol}^{-1}\cdot\text{K}^{-1}$) [220]. Our structural data argue for a scenario in which the M^+ ion provides a direct contribution as structural cofactor to stabilize the 'on' state of eIF5B. In order to test this assumption for free eIF5B we probed the conformational changes in *ctelF5B(517-858)* upon binding of GDP, GTP γ S or GDPNP using ITC under conditions reported earlier for GTP binding [220] (Table E1, Fig. 2B and E2).

The affinities of GDP, GTP γ S and GDPNP to *ctelF5B(517-858)* were measured at different temperatures between 10 and 30 °C. At 30 °C GDP binds to *ctelF5B(517-858)* with an equilibrium dissociation constant (K_d) of 10.4 μM , 2.5-fold weaker than GTP (4.1 μM). GDPNP binds with a K_d of 20.8 μM (at 30 °C), ~ 5 -fold weaker than GTP. GTP γ S has an about 4-fold higher affinity to *ctelF5B(517-858)* (0.92 μM at 30 °C) than GTP. Comparable values were reported from fluorescence experiments with mammalian eIF5B and mant-nucleotides [239].

The interactions of *ctelF5B(517-858)* with GTP γ S, GDPNP and GDP result in significant exothermic heat effects ($\Delta H = -15.8, -9.7$ and $-11.5 \text{ kcal}\cdot\text{mol}^{-1}$, respectively, at 30 °C). As for GTP, their binding is driven by favorable changes in binding enthalpy and opposed by unfavorable entropic contributions ($T\Delta S = -7.4, -3.2$ and $-4.6 \text{ kcal}\cdot\text{mol}^{-1}$ for GTP γ S, GDPNP and GDP at 30 °C, respectively) (Table E1).

In the temperature range between 10 and 30 °C ΔH is temperature dependent. When ΔH was plotted against the temperature, straight lines were obtained with the slopes representing the changes in heat capacity (ΔC_p) upon complex formation (Table 2 and Fig. 2B) [179]. GTP γ S causes a ΔC_p of $-539 \text{ cal}\cdot\text{mol}^{-1}\cdot\text{K}^{-1}$, very similar to the value observed for GTP ($-553 \text{ cal}\cdot\text{mol}^{-1}\cdot\text{K}^{-1}$) [220]. Significantly smaller changes in heat capacity were obtained for GDPNP and GDP binding ($\Delta C_p = -197 \text{ cal}\cdot\text{mol}^{-1}\cdot\text{K}^{-1}$ and $-228 \text{ cal}\cdot\text{mol}^{-1}\cdot\text{K}^{-1}$, respectively). ΔC_p can be used as an estimate for the change in solvent accessible surface area (ΔASA) upon complex formation. The burial of surface area was shown to be associated with a negative change in heat capacity, with ΔC_p being proportional to the size of the surface area involved in the ligand binding process [177, 180, 240].

According to this correlation, GTP γ S binding induces major structural rearrangements in *ctelF5B*(517-858) similar to those observed for GTP binding (Table 2), suggesting nearly identical structures for *ctelF5B*(517-858)·GTP and *ctelF5B*(517-858)·GTP γ S in solution. In contrast, GDPNP induces significantly smaller changes which are similar to those for GDP (Table 2), indicating a GDP-like conformation for the *ctelF5B*(517-858)·GDPNP complex. These results are in line with the observations from the crystal structures of GTP-, GTP γ S- and GDP-bound eIF5B and GDPNP-bound aIF5B [84], as well as the assumption of a specific inability of GDPNP to efficiently stabilize the conformational switch of the G domain by repulsion of the M⁺ ion (Fig. 2A).

Table 2. Changes in heat capacity and solvent accessible surface area for *ctelF5B*(517-858) binding to GTP, GTP γ S, GDPNP and GDP

Ligand	ΔC_p [cal mol ⁻¹ ·K ⁻¹]	ΔASA_{min} [Å ²] (with $\Delta c_{min} = 0.45$)	ΔASA_{max} [Å ²] (with $\Delta c_{max} = 0.24$)
GTP	-553 ± 11 ^a	1229	2304
GTP γ S	-539 ± 30 ^b	1198	2254
GDPNP	-197 ± 26 ^b	438	820
GDP	-228 ± 10 ^b	507	950

ΔC_p , heat capacity change; obtained from $\Delta H/dT$

Δc_{min} and Δc_{max} , area coefficients in cal·K⁻¹·(mol·Å²)⁻¹ for calculation of ΔASA .

ΔASA_{min} and ΔASA_{max} , changes in solvent accessible surface areas assuming that all changes were conferred by either apolar or 70% apolar and 30% polar surfaces, respectively.

^a Obtained from [220].

^b Obtained from the slope of the linear fit to ΔH measured at different temperatures between 10 and 30 °C.

The structure of eIF5B bound to GTP γ S and potassium.

Most M⁺-dependent enzymes show a preference for potassium (K⁺) over other M⁺ ions as cofactor. A preference for K⁺ is known also for the translation apparatus in general and the function of trGTPases in particular [241-244]. We therefore assumed that K⁺ is able to substitute for Na⁺ as cofactor in the GTP-bound form of eIF5B. Consistently, we were able to obtain crystals of eIF5B(517-858)·GTP γ S in space group P4₁2₁2 that grew within two weeks at 20 °C under a condition containing 50 mM KCl (Table 1). The structure was solved at 2.28 Å resolution and contains two eIF5B·GTP γ S complexes in the asymmetric unit. The two water molecules in the coordination shell of the Mg²⁺ ion and W^{cat} are weakly defined in the electron density, with the latter lying 3.1-3.2 Å from the outward pointing sulfur atom of GTP γ S. On the other side of the

sulfur atom, opposite to W^{cat} , a strong electron density peak was observed that was assigned to a K^+ ion with a coordination shell nearly identical to that of the Na^+ ion in eIF5B·GTP γ S (Fig. 1B and E1C). However, additional weak densities were observed on the solvent exposed side of the cation, suggesting that two water molecules contribute to a heptameric coordination shell. As expected for a K^+ ion [156], the coordination distances to most oxygen ligands lie between 2.7 and 3.0 Å and are thus clearly different from those observed for the Na^+ ions. The distance to the β - γ -bridging oxygen is slightly increased (~ 3.47 Å), most likely due to the large sulfur atom that coordinates the K^+ ion at a distance of 3.2 Å (in good agreement with the theoretical distance of 3.26 Å, calculated from the van der Waals radius of sulfur (1.8 Å) and effective ion radius of K^+ (1.46 Å for coordination number 7) [237, 238]).

Despite the different crystallization conditions and a different set of crystal contacts, the overall structure of eIF5B·GTP γ S bound to K^+ is nearly identical to that of eIF5B·GTP/GTP γ S bound to Na^+ with the switch regions stabilized in their typical GTP-conformation. Significant differences are limited to Gly^{MC} and the MC-loop of switch 1 which is moved ~ 2 Å away from the guanine nucleotide, owing to the increased coordination distances to the K^+ ion (Fig. 1C). This demonstrates that the position of the MC-loop in switch 1 is directly influenced by the species of the M^+ ions coordinated next to the nucleotide, indicating a direct contribution of the M^+ ion to the stabilization of the activated switch 1 conformation.

eIF5B coordinates the M^+ ion in the same position as known M^+ -dependent GTPases.

Superposition of the eIF5B·GTP/GTP γ S structures with MnmE and dynamin reveals that the K^+ and Na^+ ions in eIF5B are coordinated in the same position as the catalytic K^+ and Na^+ ions in the presence of GDP·AlF_x in the two known M^+ -dependent GTPases [231, 232] (Fig. 1D and E1E). Asp^{MC} replaces an identically positioned and conserved Asn or Ser, and the backbone CO of Gly^{MC} replaces two backbone COs from the 'K-loop' in switch 1 which circles around the position of the MC-loop of eIF5B. The contacts formed between the K^+ and Na^+ ions and GTP in eIF5B are virtually identical to those of the K^+ ion in MnmE or the Na^+ ion in dynamin with the transition state mimic GDP·AlF_x, where a β -phosphate oxygen of GDP represents the former β - γ -bridging oxygen and the outward pointing non-bridging γ -phosphate oxygen is mimicked by a fluoride ion.

The structural elements required for M^+ coordination in eIF5B are highly conserved among trGTPases

The G domains of trGTPases are highly conserved in sequence and structure. In order to investigate whether M^+ ion binding may be a common characteristic among trGTPases we analyzed sequences and available structures with regard to key features involved in M^+ ion binding in eIF5B. The key determinants for M^+ ion binding are Asp^{MC} in the P-loop and Gly^{MC} in the MC-loop of switch 1. Sequence analysis reveals that both residues, Asp^{MC} and Gly^{MC}, are universally conserved among orthologs of eIF5B, EF-Tu, SelB, aIF2 γ , eRF3, EF-G, RF3 and LepA from bacteria to human (Fig. 3A). The only notable exception among trGTPases is eIF2 γ , where Asp^{MC} and Gly^{MC} are replaced by Ala and Asn, respectively.

Structurally, the P-loop is well conserved among trGTPases. In contrast, switch 1 shows a high degree of variability in sequence and structure, which is, however, limited to regions lying N-terminally of the MC-loop. In a superposition of eIF5B·GTP with EF-Tu·GDPNP or the ribosome-bound EF-G·GDPCP (Fig. 3B/C), the nucleotide binding motifs occupy virtually identical positions including all residues directly involved in the coordination of the nucleotide and Mg²⁺ ion. Importantly, the structural homology extends to Asp^{MC} as well as Gly^{MC}, the latter of which invariably forms part of the characteristic MC-loop excursion of switch 1 at the end of helix A'' in EF-Tu and EF-G, placing its carbonyl group in the correct position to coordinate the cation.

GTP-bound aEF1A coordinates an M^+ ion in its catalytic center

Most known structures of trGTPases that were reported to be in the GTP-conformation do not contain GTP but GDPNP or GDPCP that contain either an NH or a CH₂ group in lieu of the β - γ bridging oxygen. Both prevent the coordination of the M^+ ion as observed in structures of known M^+ -dependent GTPases [245, 246] (Fig. 2A and E4). We therefore searched the PDB for structures of trGTPases that were cocrystallized with GTP and found two structures, both of the archaeal EF-Tu ortholog aEF1A either in complex with pelota (PDB: 3AGJ) or with release factor RF1 (PDB: 3VMF).

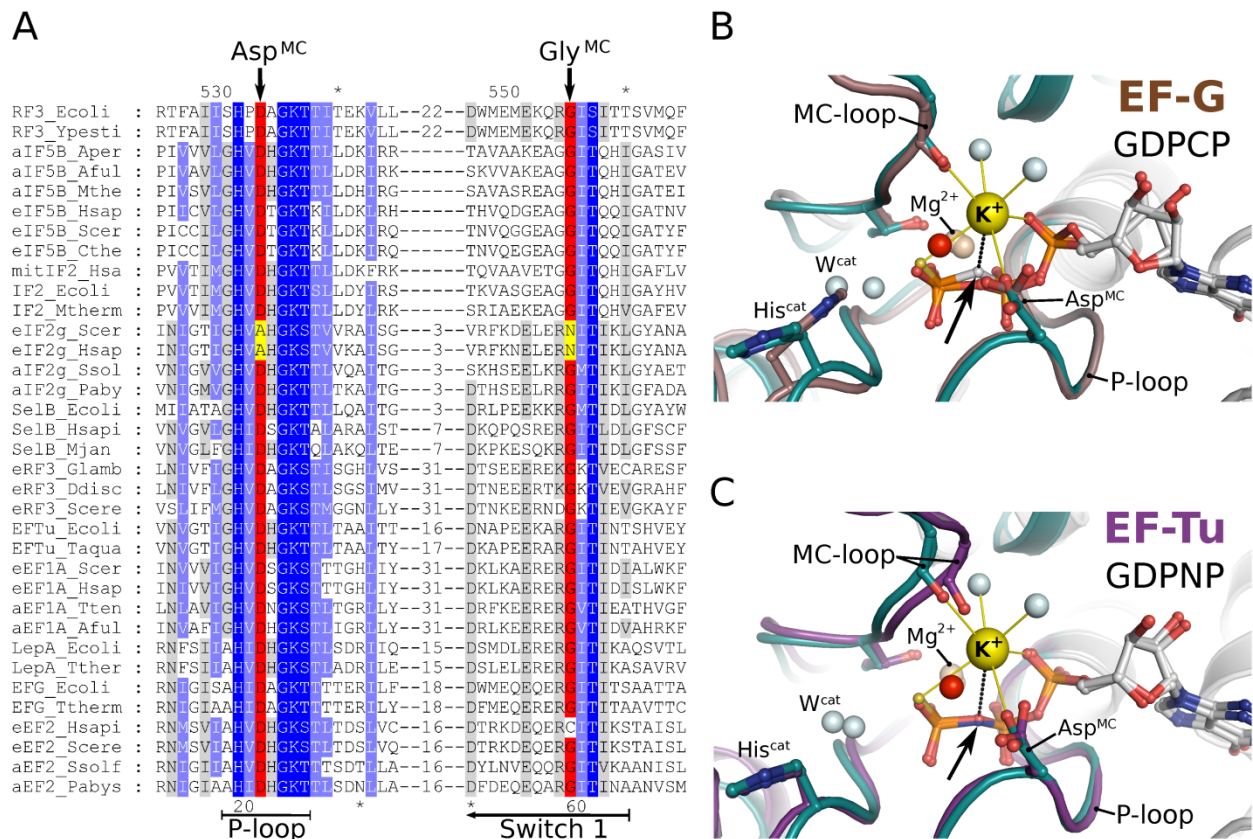


Figure 3. Structural elements required for M^+ -coordination in eIF5B are universally conserved among trGTPases. **A)** Excerpt of a multiple sequence alignment of different trGTPases (orthologs of RF3, eIF5B, eIF2 γ , SelB, eRF3, EF-Tu, LepA, EF-G) showing P-loop and switch 1. The upper and lower numbering corresponds to *C. thermophilum* eIF5B (Cthe) and *E. coli* EF-Tu (Ecoli), respectively. Highly conserved residues are highlighted in dark blue, conserved residues in light blue. Asp^{MC} and Gly^{MC} are highlighted in red, residues in eIF2 γ that replace Asp^{MC} and Gly^{MC} are highlighted in yellow. **B)** Superposition of eIF5B-GTP γ S \cdot K⁺ (colored as in Fig. 1) with ribosome-bound EF-G-GDPCP (brown; PDB: 4JUW). Ribosome-bound EF-G provides all structural elements to bind the M^+ ion; however, its coordination is prevented by the CH₂ group of GDPCP in lieu of the β - γ -bridging oxygen (arrow). A water molecule (red sphere) is bound next to the M^+ -binding site instead. **C)** Similarly, EF-Tu-GDPNP (purple; PDB: 2C78) provides all structural elements to bind the M^+ ion; however, its coordination is prevented by the NH group of GDPNP (arrow). A water molecule (red sphere) is bound next to the M^+ binding site instead.

Crystals of the aEF1A/pelota complex contained four aEF1A molecules (chains A, C, E, G) per asymmetric unit, each bound to GTP. The structure had been determined at 2.3 Å resolution [247]. Each of the aEF1A molecules contains a water molecule modeled in the position occupied by the M^+ ion in eIF5B-GTP. Accordingly, the supposed water molecules are coordinated by five hydrogen bond acceptors with the sphere formed by the outward pointing α - and γ -phosphate oxygens and the β - γ -bridging oxygen of GTP, Asp16 in the P-loop (Asp^{MC}) and the CO of Gly69 (Gly^{MC}) in switch

1. The MC-loop lies at the end of helix A'' in switch 1 and adopts the same conformation found in eIF5B (Fig. 1A and 4A/B). The coordination distances of the supposed water molecules lie between 2.2 and 2.7 Å with an overall average of 2.45 Å. Thus, the coordination pattern as well as the distances is in better agreement with those expected for a Na⁺ ion than for water [156]. Reevaluation of the experimental X-ray diffraction data (downloaded from the PDB (3AGJ)) revealed positive difference electron density for the supposed water molecules in aEF1A molecules C and E in the asymmetric unit, indicating a higher density of electrons in these positions than provided by H₂O (Fig. E3A). Replacement of the four water molecules by Na⁺ and subsequent refinement results in occupancies of 92 and 94% for the Na⁺ ions in molecules A and G, respectively, and 100% in molecules C and E. Since the crystals used for structure analysis were grown in the presence of NaCl [247], these observations indicate that the supposed water molecules next to Asp16 of aEF1A are most likely Na⁺ ions (Fig. 4A and E3C).

The structure of the aEF1A/aRF1 complex was solved at 2.3 Å resolution and contains one copy of GTP-bound aEF1A per asymmetric unit [248]. This structure as well has been built with a water molecule in the pentameric coordination sphere described above. Its contact distances lie between 2.6 and 3.1 Å (2.7 to 3.0 Å after reevaluation of the experimental data, downloaded from the PDB (3VMF)) which are typical for the coordination of a K⁺ ion [156]. However, the electron density in this position does not correspond to K⁺. This observation is supported by the fact that the crystallization condition did not contain K⁺ but instead 200 mM of NH₄⁺ ions [248]. NH₄⁺ has a similar ion radius as K⁺ (1.46 Å and 1.38 Å, respectively) and was shown to substitute for the latter structurally and functionally in the K⁺-dependent GTPase MnmE [231]. Thus, the properties of the observed coordination point toward an NH₄⁺ ion lying in the same position as the K⁺ and Na⁺ ions in eIF5B-GTP and the aEF1A-GTP/pelota complex (Fig. 4B and E3D).

The intrinsic GTPase activity of eIF5B depends on monovalent cations

The position of the observed M⁺ ion in eIF5B suggests a direct involvement in the catalysis of GTP hydrolysis in analogy to MnmE and dynamin. To test this possibility, we monitored the intrinsic GTPase activity of either wild-type eIF5B(517-858) or various Asp^{MC} mutants (D533A, D533R and D533N) under different salt conditions (Fig. 2C-F and Table 3).

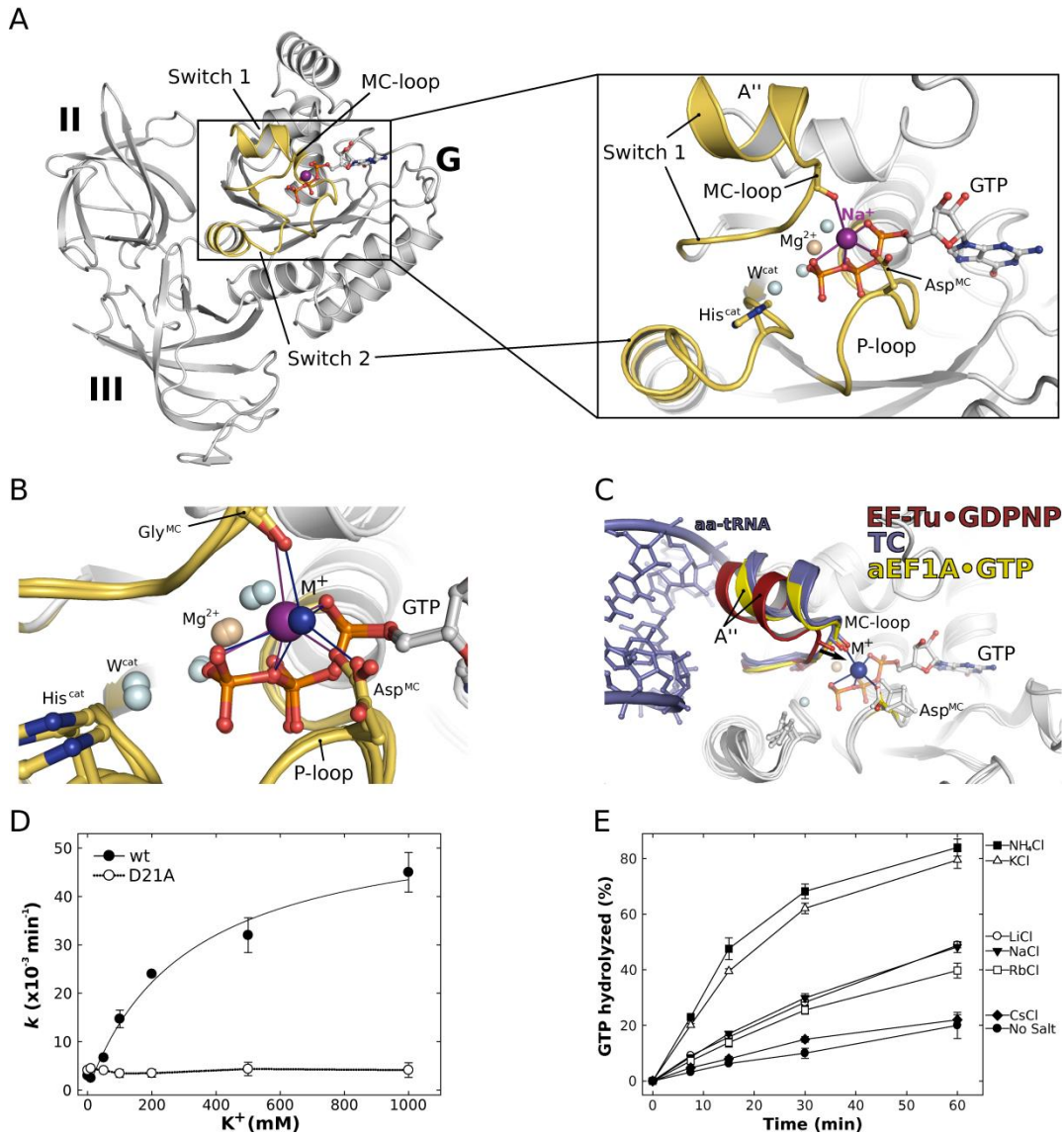


Figure 4. The GTP-bound EF-Tu ortholog aEF1A coordinates an M⁺ ion in its GTPase center. **A**) Overview of domains I (G) to III of GTP-bound aEF1A with a Na⁺ ion (purple sphere) in the active site. P-loop and switch regions are shown in yellow. The inset shows a detailed view on the active site with the coordination sphere of the Na⁺ ion (indicated by purple lines) formed by GTP, Asp^{MC} and Gly^{MC} in the MC-loop. **B**) Superposition of GTP-bound aEF1A with either a Na⁺ (purple sphere) or NH₄⁺ ion (blue sphere) in the active site. Both ions are coordinated by the identical sphere, however, with different coordination distances. **C**) Superposition of EF-Tu·GDPNP (switch 1 in red; PDB: 1EXM) with EF-Tu·GDPNP in the ternary complex (TC) with aa-tRNA (blue; PDBs: 1TTT, 1OB2) and aEF1A·GTP·M⁺ (M⁺ in blue; switch 1 in yellow). The M⁺ ion stabilizes a conformation of helix A'' that is required for stable TC formation. **D**) Dependency of the intrinsic GTPase activity of *E. coli* EF-Tu wild-type (●) or the D21A mutant (○) on the concentration of K⁺ ions, determined in the presence of 0-1 M KCl under single turnover conditions (20 μM GTP-bound EF-Tu) at 30 °C and subsequent analysis by HPLC. **E**) Intrinsic GTPase activity of *E. coli* EF-Tu determined in the presence of 200 mM of the indicated salts under single turnover conditions. The order in which the combinations are given on the right corresponds to the relative rates of GTP hydrolysis. Experiments were repeated two to three times; standard deviations are given by error bars (in some cases not visible because they are smaller than the symbol size).

First, we tested whether GTPase stimulation in eIF5B depends on the species of the available M^+ ion (at 200 mM) (Fig. 2C). The experiments revealed that the GTPase activity is stimulated most in the presence of Na^+ and K^+ , followed by Rb^+ , Li^+ and finally Cs^+ and NH_4^+ with the lowest degree of activation. Importantly, this dependency was lost for the eIF5B mutant carrying Ala in lieu of Asp^{MC}. In the presence of 200 mM K^+ or Na^+ , wild-type eIF5B catalyzed GTP hydrolysis at rates of 0.023 and 0.027 min^{-1} , respectively. The Ala mutant of Asp^{MC} exhibited significantly reduced rates of 0.0018 min^{-1} in K^+ or Na^+ , corresponding to a 13- to 15-fold reduction of the intrinsic GTPase activity. Similar results were obtained for the substitution of Asp^{MC} by Arg (D533R) (Table 3). By contrast, an Asn mutant retained the ability to catalyze GTP hydrolysis nearly at wild-type rates (Fig. 2D), in line with the assumption that an Asn but not an Ala or Arg residue would retain the ability to coordinate the M^+ ion. This is corroborated by crystal structures of the respective mutants in complex with GTP (or GTPyS), which reveal that D533N contains the M^+ ion in its active site, whereas the cation is not present in D533R and D533A and exchanged for a water molecule in the latter (Fig. E5). Moreover, fluorescence measurements with mant-labeled GTP show that all three mutants bind the nucleotide with a K_d comparable to that of the wild-type protein, speaking against the possibility that the observed effects on the GTPase activity are due to reduced affinities to the substrate (Fig. E5E-H).

Next, we studied the effect of increasing Na^+/K^+ ion concentrations (Fig. 2E/F). In the absence of M^+ ions ($\sim 600 \mu M Na^+$ were added with the GTP), eIF5B hydrolyzed GTP with a rate of 0.002 min^{-1} . This rate successively increased with increasing concentrations of K^+ or Na^+ ions, resulting in an 11- to 12-fold rate enhancement at 200 mM salt (Table 3). By contrast, the rate of GTP hydrolysis in the D533A mutant was found to be insensitive to the salt concentration with invariably low rates in the absence or presence of M^+ ions, whereas D533R exhibited a slightly increased GTPase activity in the absence of M^+ ions (0.005 min^{-1}), which successively decreased with increasing salt concentrations (Fig. 2F).

The intrinsic GTPase activity of EF-Tu depends on monovalent cations

The GTPase center of bacterial EF-Tu is virtually identical to that of its archaeal ortholog and therefore most likely coordinates an identically positioned M^+ ion in its GTP-bound form (Fig. E3B).

To test the generality of our assumption of M^+ -dependency in trGTPases, we studied the influence of M^+ ions on the intrinsic GTPase activity of *E. coli* EF-Tu by monitoring GTP hydrolysis at different K^+ -concentrations (Fig. 4D). As observed for eIF5B, the rate of GTP hydrolysis successively increased with increasing concentrations of K^+ , corresponding to a nearly 10-fold rate enhancement for the intrinsic GTPase reaction at 200 mM (Table 3). This dependency is lost when Asp21 (Asp^{MC}) in EF-Tu is mutated to Ala (D21A), consistent with a role of Asp^{MC} as key ligand for the coordination of an M^+ ion in EF-Tu at physiological salt concentration as observed for GTP-bound aEF1A (see above; Fig. 4A/B).

Table 3. Intrinsic GTPase activities of wt and mutant *ctelF5B*(517-858) and *ecEF-Tu*.

Protein	Construct	KCl (mM)	$k(\text{min}^{-1})$	Fold reduction compared to wild-type at 200 mM KCl
<i>ctelF5B</i>^a	wt	200	0.023 ± 0.0015	
	wt	0	0.0021 ± 0.001	11
	D533A	200	0.0018 ± 0.0005	13
	D533A	0	0.0016 ± 0.0008	14
	D533N	200	0.017 ± 0.002	1.4
	D533R	200	0.0028 ± 0.0007	8
<i>ecEF-Tu</i>^b	wt	200	0.026 ± 0.0005	
	wt	0	0.003 ± 0.0002	9
	D21A	200	0.0035 ± 0.0008	7
	D21A	0	0.0041 ± 0.0001	6

Measurements were performed two to three times.

k , rate of GTP hydrolysis under the used experimental conditions.

^a, Measured under multiple turnover conditions at 35 °C.

^b, Measured under single turnover conditions at 30 °C.

In order to identify the preferences of EF-Tu for GTPase stimulation, we analyzed the effect of different alkali salts (Li^+ , Na^+ , K^+ , Rb^+ , Cs^+) or NH_4^+ (each at 200 mM) on the intrinsic hydrolysis rates (Fig. 4E). The strongest stimulating effect was observed for NH_4^+ and K^+ . Na^+ , Li^+ and Rb^+ ions showed only a slight activation; virtually no effect was observed for the large Cs^+ ion. Importantly, none of the tested M^+ ion species show a significant stimulating effect on the D21A mutant of EF-Tu, which, moreover, shows no preference for NH_4^+ or K^+ as observed for the wild-type protein (Fig. E6).

7.3 Discussion

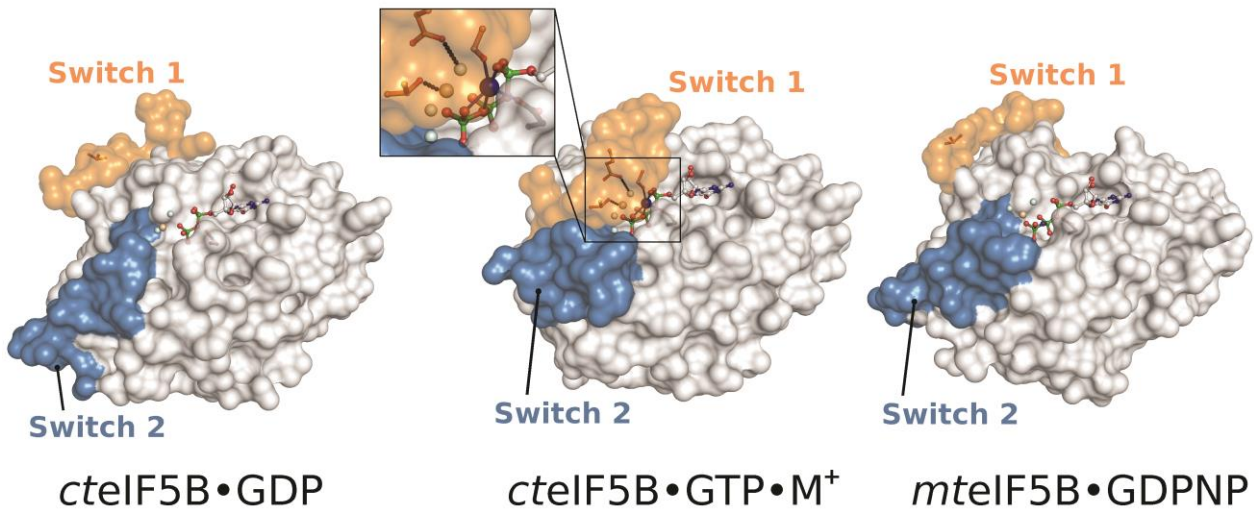
M⁺-dependent conformational switching of eIF5B

Elucidation of the structural dynamics – that is the conformational switch – of the G domain in response to GDP/GTP exchange and GTP hydrolysis is one of the central problems to understand the functional cycle of GTPases. Here we identified a monovalent cation (Na⁺/K⁺) as structural cofactor in the active site of GTP-bound eIF5B, which stabilizes the GTP-dependent reorganization of its G domain (Fig. 1 and 5). The M⁺ ion is bound in a highly conserved coordination shell formed by two non-bridging α - and γ -phosphate oxygens and the β - γ -bridging oxygen of the GTP molecule, Asp^{MC} in the P-loop and Gly^{MC} in the MC-loop of switch 1. P-loop and GTP molecule thus form a stable socket for the M⁺ ion, which in turn constitutes an anchor point for the reorganized switch 1 in the ‘on’ state. Structural and thermodynamic data demonstrate that GTPyS is a faithful replacement for GTP that coordinates the M⁺ ion and is thus able to stabilize the GTP-bound ‘on’ state of eIF5B (Fig. 1 and E4A). In contrast, replacement of GTP with GDPNP disrupts the coordination shell, resulting in the inability of the analog to stabilize the GTP-conformation in eIF5B through the M⁺ ion (Fig. 2A/B and 5A). As a consequence, the equilibrium between ‘on’ state and GDP-like ‘off’ state is shifted toward the latter in eIF5B·GDPNP allowing the GDPNP-bound factor to crystallize in the GDP-conformation, as observed for aIF5B·GDPNP from *M. thermoautotrophicum* [84] (Fig. 5A and E4A).

This interpretation is supported by the parallels between our observations and previous reports on M⁺-dependent GTPases, distantly related to trGTPases. In MnME an identically positioned K⁺ ion (Fig. 1D) is required for the rearrangement of switch 1 and subsequent dimerization [231]. K⁺-dependent dimerization in MnME was found to be induced by GTP and GTPyS, while GDPNP and GDPCP failed to support the stable switching of the G domain in biochemical as well as structural experiments [231, 249]. Similarly, GDPCP was found to be unable to induce stable G domain dimerization in dynamin or the conformational switch in EngA GD2, with structural changes limited to a shift of switch 2 [232, 246, 250]. Moreover, FeoB was crystallized in the presence of GDP-AlF_x with switch 1 stabilized in the ‘on’ state by a K⁺ ion [245], whereas the GDPNP-bound structures either remained in the ‘off’ state (2WIC) or did switch to the ‘on’ state containing either a water molecule or nothing at all in place of the M⁺ ion (3B1X; 3LX5). These

findings support the idea that GDPNP and GDPCP are incompatible with the coordination of an M^+ ion and thereby destabilize the GTP-conformation of M^+ -dependent GTPases as observed for a/eIF5B.

A



B

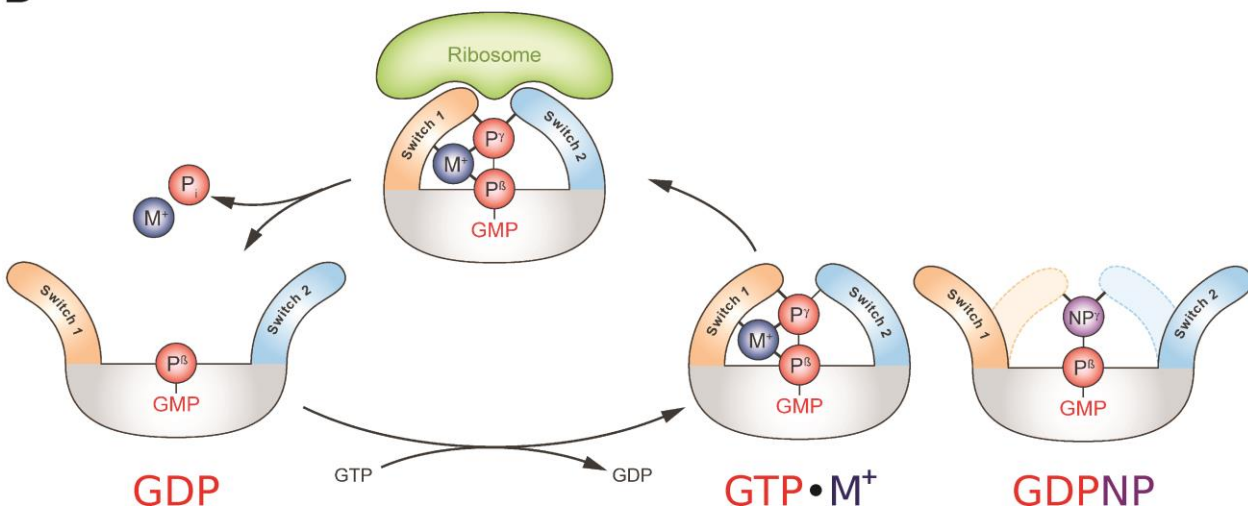


Figure 5. The mechanism of M^+ -dependent conformational switching in trGTPases. A) The nucleotide-dependent conformational switch in the G domain of a/eIF5B. In eIF5B-GDP, switch 1 and 2 are oriented away from the nucleotide binding pocket. Upon exchange of GDP for GTP, the switch regions undergo a large conformational rearrangement that results in direct contacts with the γ -phosphate. Here, the M^+ ion (blue sphere) provides a direct contribution to the stabilization of switch 1 (inset). This contribution is missing in aIF5B-GDPNP (PDB: 1G7T), allowing it to crystallize in the GDP-like 'off' state conformation. **B)** Schematic presentation of the M^+ -dependent conformational switch mechanism in trGTPases.

Based on the presented data, we propose an M^+ -dependent conformational switch mechanism for eIF5B in solution (Fig. 5) similar to that in MnME [231], where the M^+ ion in tandem with Mg^{2+} acts as structural cofactor that supports binding of the GTP molecule and helps to reorganize and close the active site around the substrate. The M^+ ion would thus form a constitutive component in the preorganized active site, required to stabilize the 'on' state conformation of the trGTPase for productive interactions with the ribosome.

Universality of M^+ -dependent conformational switching among trGTPases

Like for eIF5B, the mechanism of nucleotide-dependent conformational switching has remained obscure for most other trGTPases. Crystal structures of isolated EF-G and eRF3 reveal essentially identical conformations for their respective apo, GDP- and GDPNP-bound forms [216, 217] (Fig. E4). In SelB, the canonical GDPNP-induced structural rearrangements are limited to switch 2, while switch 1 is only partially reorganized and remains mainly flexible [218] (Fig. E4C). In the crystal structure, GDPNP is bound by SelB in the canonical way and provides the Mg^{2+} ion as well as its coordinating water molecules that usually contribute to the association of switch 1. However, although Thr46 (Thr557 in *ctelF5B*) interacts with Mg^{2+} in the canonical way, the preceding residues starting with Ile45 and Gly44 (Gly^{MC} in *ctelF5B*) remain flexible together with the rest of switch 1 [218]. This observation cannot be explained by the loss of the hydrogen bond between the β - γ -bridging atom of the nucleotide and the backbone NH of the P-loop, but can be readily explained by the loss of the M^+ ion as structural cofactor, required to stabilize Gly44 (Gly^{MC}) and thereby the rest of switch 1 in the 'on' state. This is corroborated by ITC experiments with SelB, showing that GDP and GDPNP binding result in similar structures for SelB·GDP and SelB·GDPNP, whereas GTP and GTPyS induce substantial structural rearrangements [183]. Similarly, ITC experiments with EF-G indicate large differences between the GTP-bound and apo conformation [219]. In both cases, these results were interpreted as the GTP-induced burial of surface areas by switch 1 and 2 that, however, do not become apparent from the crystal structures.

The parallels to the observations discussed above for a/eIF5B are obvious. It is moreover evident from sequence comparison that nearly all trGTPases, including EF-Tu, EF-G, SelB, and eRF3 contain the highly conserved Asp^{MC} and Gly^{MC} and would thus be able to provide the coordination

shell for the M^+ ion (Fig. 3). The loss of the M^+ ion as structural cofactor between nucleotide and switch 1 due to the use of GDPNP or GDPCP therefore provides a general explanation for the observations for EF-G, SelB and eRF3, as well as other previously reported discrepancies in the behavior of trGTPases toward GTP or its nonhydrolyzable analogs [166, 183, 221-224]. The common evolutionary origin of trGTPases and their functional homology during the translation process argue in favor of a systematic origin rather than individual reasons why GDPNP and GDPCP but not GTP γ S are generally unable to substitute for GTP. In light of the above presented observations, we therefore propose that with few exceptions (eIF2 γ) trGTPases utilize M^+ ions as structural cofactor and that the mechanism of M^+ -dependent conformational switching as suggested for eIF5B (Fig. 5B) is universal among canonical trGTPases.

This proposed commonality of M^+ -dependency is corroborated by the example of elongation factor Tu (EF-Tu). In line with our prediction on the basis of sequence and structural homology to eIF5B, we found that the active site of the archaeal EF-Tu ortholog aEF1A bound to GTP as well contains an M^+ ion (Na^+/NH_4^+), bound by an identical coordination shell as observed for eIF5B·GTP (Fig. 4 and E3). Likewise, M^+ ion binding was demonstrated for free EF-Tu by the finding that its intrinsic GTPase activity is accelerated by M^+ ions in a manner dependent on Asp21 (Asp^{MC}), in line with its role as key ligand for M^+ ion coordination (Fig. 4D/E). The usage of M^+ ions as structural cofactor in EF-Tu provides a simple explanation why ternary complexes (TC) of EF-Tu with aa-tRNA formed in the presence of GDPNP exhibit decreased stability compared to those formed with GTP [166, 224] due to the loss of the M^+ -dependent allosteric stabilization of the GTP-conformation required for aa-tRNA binding. This is highlighted by the comparison of EF-Tu·GDPNP with the structures of EF-Tu·GDPNP·aa-tRNA complexes and aEF1A·GTP, which indicates that the M^+ ion specifically stabilizes a conformation of switch 1 in which helix A'' is drawn toward the GTP molecule, which seems necessary for stable TC formation (Fig. 4C). Hence, in the absence of the M^+ ion, the aa-tRNA itself has to overcome the entropic penalty to arrange switch 1 in the correct conformation that would otherwise be paid by the M^+ ion in the correctly assembled active site with GTP.

The M^+ ion as catalytic element in the GTPase reaction of trGTPases

Apart from the GTP-induced conformational switch, the mechanism of GTP hydrolysis is another unresolved problem in the universal functional cycle of trGTPases. Although it has been established that the precise ribosome-induced positioning of the invariant His^{cat} from the inactive ground state to the catalytically active conformation is critical for GTP hydrolysis [168], it remained obscure how the ribosome-bound trGTPase stabilizes the transition state (TS) of the hydrolysis reaction in the absence of an arginine-finger.

As demonstrated above, trGTPases coordinate an M^+ ion next to the GTP- γ -phosphate in a conserved coordination shell, where it forms a structurally relevant component of the catalytic center (Fig. 1 and 4). The M^+ ion thus adds another positive charge to the preorganized active site of trGTPases that together with the invariant lysine of the P-loop and the Mg^{2+} ion forms a triangle of positively charged moieties around the β - γ -bridging oxygen of the GTP molecule (Fig. 6A). Following the ribosome-induced activation of His^{cat} (which leaves the coordination shell for the M^+ ion intact (Fig. 3B) [168]), the M^+ ion would thus be in a suitable position to neutralize negative charges of the TS in the γ -phosphate as well as the designated leaving group (GDP) (Fig. 6A/B). This suggests that the M^+ ion might function as the so far elusive catalytic element in trGTPases that acts in the second step of the ribosome-dependent GTPase reaction and contributes to rapid GTP hydrolysis by providing electrostatic stabilization for the TS, in analogy to the arginine-finger in the Ras-RasGAP system (Fig. 6) or the M^+ ion in MnME (Fig. 1D).

Structurally, this role for the M^+ ion in trGTPases is supported by the superposition of GTP-bound eIF5B and aEF1A with MnME, dynamin or the Ras-RasGAP complex where the catalytic M^+ ions and the guanidino group are located in virtually identical positions (Fig. 1D, 6C and E1E) [106, 231, 232]. For Asp^{MC} this indicates a role of vital importance in the universal functional cycle of trGTPases as key ligand for the M^+ ion that provides an explanation for its invariant conservation (Fig. 3A). Consistently, we found that the loss of Asp^{MC} in the D533A mutant results in M^+ -independency of the intrinsic GTPase activity in eIF5B, whereas the M^+ -dependency of the wild-type protein is retained in the D533N mutant. The marked effect of Asp^{MC} mutations in eIF5B, which directly correlates with the ability of the substituted residue to coordinate M^+ ions, clearly argues in favor of a direct contribution by the M^+ ion to the GTPase reaction.

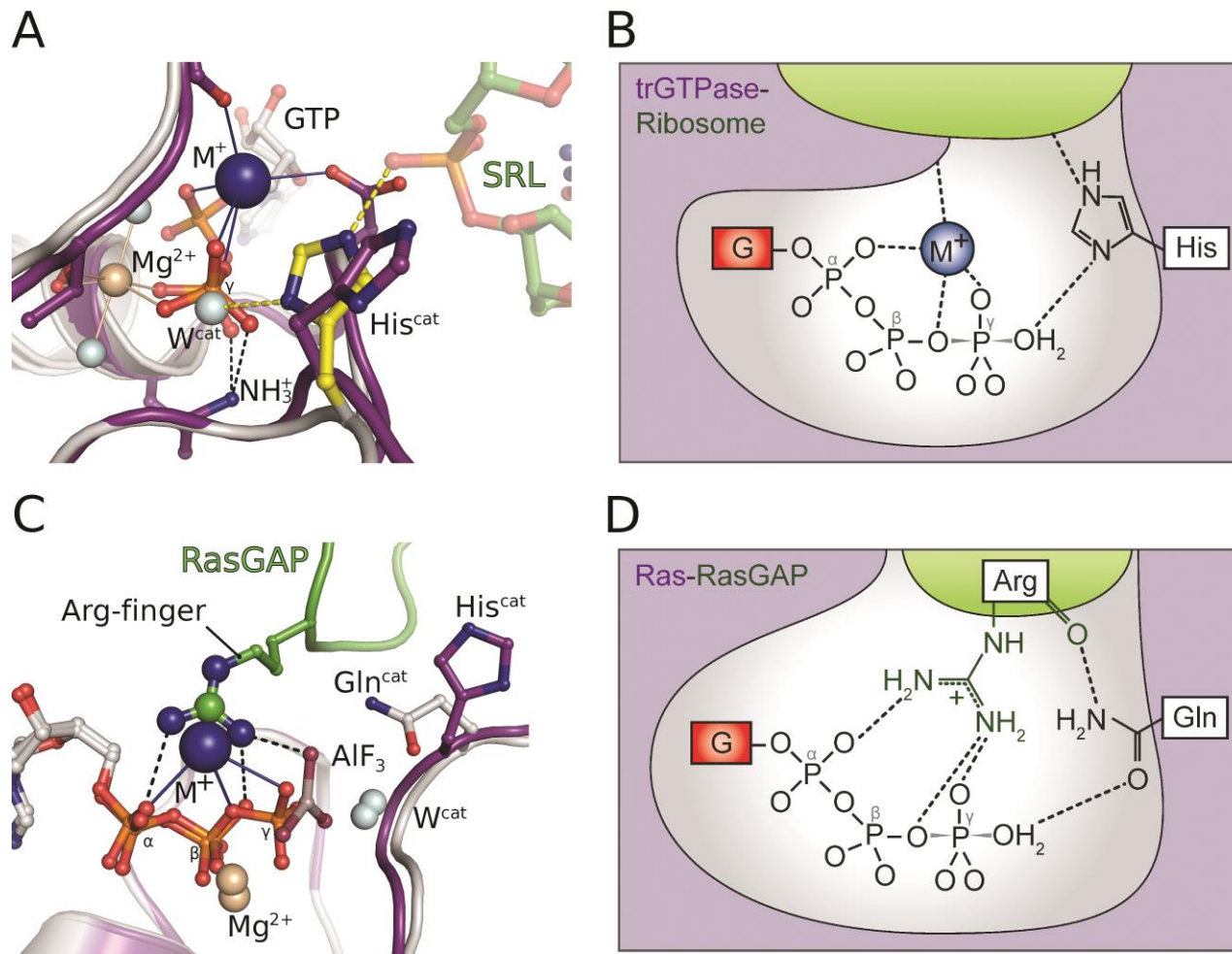


Figure 6. The M^+ ion as catalytic element in the GTP hydrolysis reaction. **A)** Model of aEF1A-GTP- M^+ on the ribosome (the sarcin-ricin loop (SRL) is shown as green sticks), based on a superposition with ribosome-bound EF-Tu (grey; PDB: 2XQD). Upon productive interactions with the SRL, the imidazole moiety of His^{cat} is reoriented from its inactive ground state (purple) to the active position (yellow) in which it forms a hydrogen bond to W^{cat}[168]. The invariant P-loop lysine, the Mg²⁺ ion (light brown sphere) and the M^+ ion (blue sphere) form a triangle of positively charged moieties around the β - γ -bridging oxygen. The M^+ ion is thus suitably positioned to stabilize negative charges that develop in the TS of the hydrolysis reaction. **B)** Schematic presentation of the active site of a ribosome-bound trGTPase with GTP in the transition state of the hydrolysis reaction stabilized by the M^+ ion (blue). TrGTPase and ribosome are colored in purple and green, respectively; negative charges, the P-loop lysine and the Mg²⁺ ion are omitted for clarity. For simplicity, His^{cat} is shown in its neutral form, although it might be double protonated in its activated state [226-229]. **C and D)** The M^+ ion in eIF5B and aEF1A (purple) is coordinated in a position analogous to the arginine-finger in the complex of Ras (grey) and RasGAP (green) (Fig. B and D are modified from [25, 233]).

Further evidence is provided by experiments with bacterial EF-Tu. In agreement with earlier observations from Parmeggiani and coworkers [244] we found the intrinsic GTPase activity of EF-Tu to depend on the concentration as well as the species of M^+ ions, with a preference for K^+ and NH_4^+ (Fig. 4D/E and E6). As for eIF5B, the reduced activity in the absence of M^+ ions and the loss of M^+ -

dependency in the D21A (Asp^{MC}) mutant argues for a direct effect on GTP hydrolysis. Moreover, kinetic experiments indicated that mutations of Asp21 in *E. coli* EF-Tu result in a significant reduction of the GTPase activity in the EF-Tu·GTP·aa-tRNA complex in the presence of the correct codon on the ribosome (C. Maracci and M.V. Rodnina, personal communication). This observation as well is consistent with a role of Asp^{MC} as key ligand for a catalytic M⁺ ion in EF-Tu, involved in ribosome-dependent GTP hydrolysis. Moreover, the ribosome-dependent GTPase activity of EF-Tu, EF-G as well as IF2 was reported to depend on M⁺ ions [149, 243, 244]. However, in all these cases the GTPase activity reaches maximum values between 20 and 100 mM M⁺ ions, most likely reflecting compensating effects of the salt concentration e.g. on the stability and/or conformation of the ribosomal complexes and their interactions with trGTPases [251] that necessarily obscure a direct effect of M⁺ ions on the GTPase reaction. Importantly, similar observations are known from dynamins, where the stimulating effect of M⁺ ions on GTP hydrolysis is compensated at increasing salt concentrations due to an inhibition of oligomerization and consequently dimerization-dependent GTPase activation [246, 252, 253].

The question, whether trGTPases are specific for K⁺ ions under physiological conditions cannot be unambiguously answered at present. The structural and biochemical analyses indicate that eIF5B and EF-Tu/aEF1A have slightly different specificities in their usage of M⁺ ions *in vitro*. However, given the general preference of the translation apparatus for K⁺ or ions with similar ionic radii [149, 241-244], the similarly strong stimulation of the GTPase activity in eIF5B and EF-Tu by K⁺, and the usually high cellular K⁺/Na⁺ ratio, we assume that K⁺ is preferred by trGTPases under physiological conditions.

An interesting case that provides further indirect evidence for M⁺-dependency among trGTPases is the γ -subunit of eukaryal initiation factor 2 (eIF2 γ). Notably, eIF2 γ is the only trGTPase for which a specific GAP (eIF5) has been identified that was reported to provide an arginine-finger as catalytic element to promote GTP hydrolysis in eIF2 [53, 254]. The coordination sphere for the M⁺ ion would therefore not be required in eIF2 γ . Consistently, eIF2 γ is the only trGTPase that contains neither an Asp^{MC} nor Gly^{MC} (Fig. 3A). Instead, Asp^{MC} is replaced by Ala, which might be necessary to allow the introduction of the bulky guanidino group into the active site instead of the

M⁺ ion. Importantly, the archaeal ortholog, aIF2 γ , contains Asp^{MC} and Gly^{MC} and no GAP is known indicating that aIF2 γ in contrast to eIF2 γ may be M⁺-dependent.

Implications for the evolution of trGTPases

At the center of this work stands the conclusion that trGTPases belong to the group of M⁺-dependent G proteins. This establishes trGTPases as a functionally distinct subfamily among GTPases in which the ribosome, as an RGS-like GAP, stabilizes the active conformation of the catalytic machinery of the GTPase [168] which includes an M⁺ ion as an additional *trans*-acting catalytic element, constitutively bound in the active site. Conceptually, this places trGTPases between the classical GAP- or RGS-activated GTPases and GTPases activated by homodimerization (GADs) (e.g. MnmE and dynamin), which, like trGTPases, directly couple the GTPase reaction to their biological function in the cell [230].

The proposed universality of M⁺-dependency among canonical trGTPases is particularly interesting from the evolutionary perspective, as it points toward a common origin in an ancestral M⁺-dependent trGTPase. At the same time, usage of M⁺ ions as structural and catalytic cofactor constitutes a functional link to other known M⁺-dependent GTPases that – like trGTPases – usually belong to particularly ancient lineages of the TRAFAC class, associated with basic cellular functions such as tRNA modification or ribosome assembly [22, 255]. It is therefore conceivable that M⁺-dependency might represent the primordial form of catalysis of GTP hydrolysis in GTPases of the TRAFAC class that antedates the convergent occurrence of arginine-finger-dependent catalysis.

7.4 Materials and Methods

Protein purification, crystallization and structure determination

C. thermophilum eIF5B constructs containing residues 517-858 (cteIF5B(517-858)) were purified as previously described [220]. *E. coli* EF-Tu was prepared essentially as described in [256]. *E. coli* EF-Ts was prepared using standard procedures (see Expanded View for details).

Crystallization trials were performed by sitting-drop vapor diffusion method using either self-made optimization screens for the original crystallization condition for cteIF5B·GTP (0.1 M HEPES/NaOH (pH 7); 13% PEG 4000; 0.1 M NaOAc) [220] or standard screens in the presence of

Mg²⁺ and varying concentrations of guanine nucleotides. Crystals of *ctelF5B(517-858)*·GTP used for structure determination grew over night at 20 °C in 100 mM HEPES (pH 7.25), 12% PEG 4000 and 100 mM NaOAc with 10 mg/ml of protein in the presence of 2 mM GTP. Crystals of *ctelF5B(517-858)* bound to GTPγS grew over night at 20 °C under similar conditions (100 mM HEPES (pH 7), 13% PEG 4000 and 125 mM NaOAc) with 12 mg/ml protein and 2 mM GTPγS. The crystals for both proteins grew in space group P2₁.

Crystals of *ctelF5B(517-858)*·GTPγS with a potassium ion bound in the active site were obtained after two weeks at 20 °C in 11% PEG 8000, 6% glycerol, and 50 mM KCl. The best diffracting crystals grew when using 10 mg/ml protein in the presence of 2 mM GTPγS. The crystals grew in space group P4₁2₁2.

Crystals of the Asp^{MC} mutant *ctelF5B(517-858)D533N* were obtained with 8 mg/ml protein and 3 mM GTP at 20 °C in a condition containing 100 mM HEPES (pH 7), 13% PEG 4000 and 125 mM NaOAc. As for the wild-type protein crystals that were obtained under similar conditions, the crystals of *ctelF5B(517-858)D533N* belonged to space group P2₁. Initially, no crystals were obtained for the mutants D533A and D533R. However, high-quality crystals for both mutants could finally be obtained by repeated microseeding experiments (see Expanded View for details). Crystals of *ctelF5B(517-858)D533A* (with 15 mg/ml protein and 6 mM GTPγS) grew in space group P2₁ in a condition containing 0.1 M HEPES/NaOH (pH 7.3), 15% PEG 4000, and 150 mM NaOAc. Crystals of *ctelF5B(517-858)D533R* (with 15 mg/ml protein and 4 mM GTPγS) grew in space group P4₁2₁2 in a condition containing 100 mM MES (pH 6.7), 13% PEG 8000, 225 mM NaOAc.

X-ray diffraction data were collected using synchrotron radiation. For all structures, the phase problem was solved by molecular replacement using the program PHASER [115]. Structures were refined to reasonable R-values and stereochemistry using the program PHENIX [117]. Data collection and refinement statistics for the structures of wild-type *eIF5B(517-858)* and for the three Asp^{MC} mutants are summarized in Tables 1 and E2, respectively. See Expanded View for details.

Isothermal Titration Calorimetry

The thermodynamic parameters of *eIF5B* binding to GDP or GDPNP were measured using a MicroCal VP-ITC instrument (GE Healthcare). Experiments were carried out as previously described

[220] in ITC buffer (30 mM HEPES/KOH (pH 7.5), 100 mM KCl, 10% glycerol, 4 mM β -mercaptoethanol, 0.01% tween 20, 2.5 mM $MgCl_2$) at different temperatures (10, 15, 20, 25 or 30°C). 14- μ l aliquots of 200-400 μ M ligand were injected into the 1.42 ml cell containing 10-30 μ M *ct*eIF5B(517-858). The heat of dilution was measured by injecting the ligand into the buffer solution without protein; the values were then subtracted from the heat of the individual binding reactions to obtain the effective heat of binding. The final titration curves were fitted using the 'Origin' based MicroCal software, assuming one binding site per protein molecule. For each isotherm the binding stoichiometry (N), enthalpy changes (ΔH) and the association constants (K_a), were obtained by a nonlinear regression fitting procedure. These directly measured values were used to estimate the Gibbs energy (ΔG) from the relation $\Delta G = -R \cdot T \cdot \ln K_a$ and the entropy changes (ΔS) through $\Delta G = \Delta H - T \cdot \Delta S$.

In order to estimate the change in heat capacity (ΔC_p) upon complex formation between eIF5B and guanine nucleotides, the measured ΔH values were plotted against the temperature, where the slope of the fitted line directly represents the ΔC_p of the binding reaction [178, 179]. See Expanded View for details about the correlation between ΔC_p and the change in solvent accessible surface area (ΔASA).

Analysis of the GTPase reaction of eIF5B and EF-Tu by HPLC

The intrinsic GTP hydrolysis of *C. thermophilum*eIF5B(517-858) and *E. coli* EF-Tu was analyzed by HPLC (GE Healthcare). Nucleotides were separated on a NUCLEOSIL 4000 PEI (Macherey Nagel) in 10 mM Tris/HCl (pH 8.0) with a linear gradient from 0-1 M NaCl. For EF-Tu, the reactions were followed under single-turnover conditions, for which 25 μ M EF-Tu·GTP was incubated at 30 °C in 25 mM Tris/HCl (pH 7.5), 7 mM $MgCl_2$, 2 mM DTT and alkali salts at different concentrations. At various time points, 50 μ l aliquots were taken and incubated at 96 °C for 2 min to stop the reaction. Denatured protein was removed by centrifugation and the supernatant applied to the HPLC.

For eIF5B, the reactions were followed under multiple-turnover conditions, for which 25 μ M nucleotide-free eIF5B was incubated with 300 μ M GTP at 35 °C in 25 mM Tris/HCl (pH 7.5), 3 mM

MgCl₂, 2 mM DTT and alkali salts at different concentrations. 50 µl aliquots were taken at various time points and treated as described above.

Multiple sequence alignments

Multiple sequence alignments were done using the iterative alignment program MUSCLE [214].

Coordinates

Coordinates and structure factors have been deposited in the PDB: 4TMW(*ct5B(517-858)*·GTP·Na⁺); 4TMV (*ct5B(517-858)*·GTPγS·Na⁺); 4TMZ (*ct5B(517-858)*·GTPγS·K⁺); 4TMT (*ct5B(517-858)*D533A·GTPγS); 4TMX (*ct5B(517-858)*D533N·GTP·Na⁺); 4TN1 (*ct5B(517-858)*D533R·GTPγS).

Expanded View

Expanded View information is available at The EMBO Journal Online and includes six figures, two tables and extended Materials and Methods.

Acknowledgments

We thank the beam line scientists at EMBL/DESY (Hamburg) and ESRF (Grenoble) as well as P. Neumann for support during X-ray diffraction data collection and L. Hsu for help with figures. We are also grateful to L. K. Dörfel and A. Dickmanns for critical reading of the manuscript as well as C. Maracci and M.V. Rodnina for comments on the manuscript and for sharing data before publication.

Author Contributions

Author contributions: BK designed the experiments, prepared and crystallized proteins, collected X-ray data, solved structures, performed GTPase and ITC experiments, created figures. BK and RF analyzed the data and wrote the manuscript.

Conflict of interest

The authors declare that they have no conflict of interest.

7.5 Expanded View

Expanded View Materials and Methods

Protein purification

The purification of *Chaetomium thermophilum* eIF5B(517-858) was done as previously described [220]. The plasmid for the expression of N-terminally His-tagged cteIF5B(517-858) (comprising G domain and domain II) was transformed into *E. coli* BL21(DE3) cells (Stratagene) by heat shock. Transformed cells were grown in 1 l cultures of 2YT medium at 37 °C to an OD₆₀₀ of 0.6-0.8, followed by the induction of protein expression with 0.5 mM isopropyl-β-D-thiogalactopyranoside (IPTG). Cells were grown for an additional 18 h at 16 °C before harvesting. Harvested cells were resuspended in buffer A (40 mM HEPES/KOH (pH 7.5), 500 mM KCl, 10% glycerol, 30 mM imidazole, 2 mM β-mercaptoethanol), lysed using a Microfluidizer (Microfluidics) and clarified by 30 min ultracentrifugation at 30,000 xg. The supernatant was loaded onto two HisTrap columns (GE Healthcare), equilibrated in buffer A. After the elution of bound proteins with a linear gradient of imidazole (30-300 mM), eIF5B-containing fractions were pooled and desalted in buffer B (20 mM HEPES/KOH (pH 7.5), 200 mM KCl, 10% glycerol, 30 mM imidazole and 2 mM β-mercaptoethanol) for subsequent TEV-protease cleavage at 4 °C over night to remove the His-Tag. Uncleaved protein was removed by a second HisTrap in buffer B and the flow-through was pooled and concentrated for the final size exclusion chromatography step on a Superdex 200 column (GE Healthcare), equilibrated in buffer C (10 mM HEPES/KOH (pH 7.5), 50 mM KCl, 3 mM MgCl₂ and 1 mM DTT). The absence of copurified guanine nucleotides was confirmed by HPLC. The purified apo eIF5B was pooled, concentrated to 15-20 mg/ml, and finally stored at -80 °C.

Mutant constructs of cteIF5B, in which Asp533 (Asp^{MC}) was substituted by alanine (D533A), asparagine (D533N) or arginine (D533R), respectively, were generated by site-directed mutagenesis according to the QuikChange protocol (Stratagene, Instruction Manual, 2006). All mutants were expressed and purified according to the above described protocol for wild-type cteIF5B(517-858) [220].

For ITC experiments cteIF5B(517-858) was purified according to the above protocol with the difference that ITC buffer (30 mM HEPES/KOH (pH 7.5), 100 mM KCl, 10% glycerol, 4 mM β-mercaptoethanol, 0.01% tween 20, 2.5 mM MgCl₂) was used in the final gelfiltration step.

For GTPase activity assays under different salt conditions, purified cteIF5B(517-858) (wild-type or mutant) was desalted in the desired buffer (Tris/HCl (pH 7.5), 3 mM MgCl₂, 2 mM DTT and alkali salts at different concentrations) prior to the experiment (see below).

E. coli EF-Ts was expressed with an N-terminal His-tag in *E. coli*BL21(DE3)pLysS cells (Stratagene). Transformed cells were grown in 1 l cultures of LB medium at 37 °C to an OD₆₀₀ of ~0.8, followed by the induction of protein expression with 0.5 mM IPTG. Cells were grown for an additional 4 h at 37 °C before harvesting. Purification of EF-Ts (including the removal of the His-tag) was performed according to the protocol described above for cteIF5B(517-858), with the difference that a

Superdex 75 column (GE Healthcare), equilibrated in a buffer containing 25 mM Tris (pH 7.5), 30 mM KCl, 70 mM NH₄Cl and 7 mM MgCl₂, was used in the final size exclusion chromatography step. Purified protein was flash-frozen in liquid nitrogen and stored at -80 °C.

E. coli EF-Tu was prepared essentially as described previously [256]. The final gel filtration buffer contained 20 mM Tris/HCl (pH 7.5), 50 mM KCl, 7 mM MgCl₂ and 2 mM DTT. GTP-bound EF-Tu was prepared by incubating 100 μM purified EF-Tu with 3 mM GTP, 3 mM phosphoenolpyruvate (Roche), 0.05 mg/ml pyruvate kinase (Roche) and 0.04 μM EF-Ts for 1 h at 37 °C. To remove excess GTP and phosphoenolpyruvate, GTP-bound EF-Tu was desalted on a HiTrap Desalting column (GE Healthcare) at 4 °C in the desired buffer (25 mM Tris/HCl (pH 7.5 at 25 °C), 7 mM MgCl₂, 2 mM DTT and alkali salts at different concentrations).

Crystallization and structure determination

The first crystallization trials with *ctefF5B*(517-858) were performed in an optimization screen for the condition under which the original crystals of GTP-bound *ctefF5B*(517-860) had been obtained using a fragment comprising residues 517-970 (0.1 M HEPES/NaOH (pH 7); 13% PEG 4000; 0.1 M NaOAc) [220]. 8, 10 or 12 mg/ml of protein were mixed with GTP, GTPγS or GDPNP at final concentrations of 1, 2 or 3 mM (up to 10 mM for GDPNP in the presence of 10 mM MgCl₂) of the respective guanine nucleotides. Crystallization was performed at 4 and 20 °C by vapor diffusion using a 1:1 or 2:1 ratio of protein to reservoir solution. For *ctefF5B*(517-858)·GDPNP no crystals were obtained under any of the tested conditions. Crystals of *ctefF5B*(517-858)·GTP and *ctefF5B*(517-858)·GTPγS grew over night in most conditions, irrespective of the temperature or used guanine nucleotide concentration. In both cases the best diffracting crystals that were finally used for structure determination grew at 20 °C in primitive monoclinic space group P2₁.

To find a crystallization condition for *ctefF5B*(517-858) in the presence of potassium, crystallization trials with 10 mg/ml protein were performed in the presence of 2 mM GTPγS using standard screens. Diffraction quality crystals were obtained after two weeks at 20 °C in a condition containing 11% PEG 8000, 6% glycerol, and 50 mM KCl. The crystals used for structure determination grew in space group P4₁2₁2 and contained two protein-GTPγS complexes per asymmetric unit.

Initial crystallization trials for the Asp^{MC} mutants of *ctefF5B*(517-858) (D533A, D533N and D533R) were performed with 8 mg/ml protein in the presence of 3 mM GTP or GTPγS using fine-screens around the two conditions described above. Only for the D533N mutant high quality crystals in space group P2₁ grew over night that could be directly used to determine the structure of *ctefF5B*(517-858)D533N bound to GTP and a Na⁺ ion. No crystals were initially obtained for the other mutants D533A and D533R. We then performed microseeding experiments for both mutants, in which crystals of the wild-type protein were destroyed and used as crystallization nuclei to induce crystallization. At protein concentrations of 15 mg/ml and 6 mM guanine nucleotide, this resulted in the formation of thin needle clusters for D533A in conditions containing

0.1 M HEPES/NaOH (pH 7.3), 15% PEG 4000, and 150 mM NaOAc. These were then used in an additional round of microseeding, finally yielding large enough crystals for structure determination. As the wild-type protein, the D533A mutant crystallized in space group $P2_1$ and the structure was finally solved at a resolution of 1.58 Å. In contrast to D533A, no crystals were obtained for D533R in the initial microseeding experiments but only small spherulite-like aggregates which could not be used as seeds. We therefore performed new crystallization trials for the D533R mutant in various commercially available grid screens, in combination with microseeding. This yielded thin, plate-shaped crystals in a condition containing 100 mM MES (pH 6.5), 11% PEG 8000, and 150 mM NaOAc. Using these crystals as microseeds in an optimized screen, we were finally able to obtain *ctelF5B*(517-858)D533R crystals in the presence of GTPγS suited for structure determination. Despite the fact that the D533R mutant crystals were obtained in the presence of Na⁺ ions, they grew in space group $P4_12_12$ as did those obtained in the presence of K⁺. The structure of *ctelF5B*(517-858)D533R could finally be solved at a resolution of 2.75 Å.

Based on the observations for the *ctelF5B* mutants, additional crystallization trials were performed with wild-type *ctelF5B*(517-858) in the presence of GDPNP and microseeds. In the fine-screens, microseeding resulted in the formation of large spherulites, which, however, did not yield any crystals when used as seeds themselves.

For the structures of wild-type *ctelF5B*(517-858) bound to GTP or GTPγS and Na⁺, X-ray diffraction data were collected at P13 beamline at PETRA III (EMBL, Hamburg). For the structures of wild-type *ctelF5B*(517-858) bound to GTPγS and K⁺ and all Asp^{MC} mutants, X-ray diffraction data used for structure determination were collected at beamline ID23-1 at ESRF (Grenoble). For all structures, the phase problem was solved by molecular replacement using the program PHASER [115] with the original structure of *ctelF5B*·GTP as search model. Structures were refined to reasonable R-values and stereochemistry using the program PHENIX [117]. Data collection and refinement statistics are summarized in Table 1 and Table E2.

Structure factors and coordinates for the two aEF1A structures were obtained from the protein data bank (PDB: 3AGJ, 3VMF). The structures were refined using the program PHENIX [117]. Manual model rebuilding was performed against electron density maps in Coot [116]. Figures were prepared using Pymol (<http://www.pymol.org>).

Isothermal Titration Calorimetry

The thermodynamic parameters of eIF5B binding to GDP or GDPNP were measured using a MicroCal VP-ITC instrument (GE Healthcare). Experiments were carried out as previously described [220] in ITC buffer at different temperatures (10, 15, 20, 25 or 30°C). 14-μl aliquots of 200-400 μM ligand were injected into the 1.42 ml cell containing 10-30 μM *ctelF5B*(517-858). The heat of dilution was measured by injecting the ligand into the buffer solution without protein; the values were then subtracted from the heat of the individual binding reactions to obtain the effective heat of binding. The final titration curves were fitted using the 'Origin' based MicroCal software,

assuming one binding site per protein molecule. For each isotherm the binding stoichiometry (N), enthalpy changes (ΔH) and the association constants (K_a), were obtained by a nonlinear regression fitting procedure. These directly measured values were used to estimate the Gibbs energy (ΔG) from the relation $\Delta G = -R \cdot T \cdot \ln K_a$ and the entropy changes (ΔS) through $\Delta G = \Delta H - T \cdot \Delta S$.

In order to estimate the change in heat capacity (ΔC_p) upon complex formation, the measured ΔH values were plotted against the temperature [178, 179]. The slope of the fitted line directly represents the ΔC_p of the binding reaction. ΔC_p can be used as an estimate for the change in solvent accessible surface area (ΔASA) upon complex formation as it was found to be proportional to the size of the area which is either exposed to (associated with a positive value for ΔC_p) or removed from (negative value for ΔC_p) the aqueous environment during the binding event [177, 180-182]. ΔC_p and ΔASA are connected by the empirically determined relation $\Delta C_p = \Delta c_{ap} \cdot \Delta ASA_{ap} + \Delta c_p \cdot \Delta ASA_p$ where Δc_{ap} (0.45) and Δc_p (-0.26) are the area coefficients in $\text{cal} \cdot \text{K}^{-1} \cdot (\text{mol} \cdot \text{\AA}^2)^{-1}$ for the contributions of apolar or polar side chains to ΔASA , respectively [177, 182, 184]. As previously described [220], we use two values for the area coefficients to estimate the change in surface area upon ligand binding: $\Delta c_{max} = 0.24 (= 0.7 \cdot \Delta c_{ap} + 0.3 \cdot \Delta c_p)$ as the upper limit case and $\Delta c_{min} = 0.45$ as the lower limit case in which all involved residues are apolar.

Analysis of the GTPase reaction of eIF5B and EF-Tu by HPLC

The intrinsic GTP hydrolysis of *C. thermophilum* eIF5B(517-858) and *E. coli* EF-Tu was analyzed by HPLC (GE Healthcare). Nucleotides were separated on a NUCLEOSIL 4000 PEI (Macherey Nagel) in 10 mM Tris/HCl (pH 8.0) with a linear gradient from 0-1 M NaCl. For EF-Tu, the reactions were followed under single-turnover conditions, for which 25 μM EF-Tu·GTP was incubated at 30 °C in 25 mM Tris/HCl (pH 7.5), 7 mM MgCl_2 , 2 mM DTT and alkali salts at different concentrations. At various time points, 50 μl aliquots were taken and incubated at 96 °C for 2 min to stop the reaction. Denatured protein was removed by centrifugation and the supernatant applied to the HPLC.

For eIF5B, the reactions were followed under multiple-turnover conditions, for which 25 μM nucleotide-free eIF5B was incubated with 300 μM GTP at 35 °C in 25 mM Tris/HCl (pH 7.5), 3 mM MgCl_2 , 2 mM DTT and alkali salts at different concentrations. 50 μl aliquots were taken at various time points and treated as described above.

Steady-state fluorescence measurements

Fluorescence measurements were carried out on a Fluoromax-3 spectrophotometer (Jobin Yvon Inc.) using a 1 ml quartz cuvette with magnet stirrer. Titrations of eIF5B constructs with mant-GTP were performed at 20 °C in buffer containing 25 mM Tris/HCl (pH 7.5), 200 mM KCl, 3 mM MgCl_2 and 2 mM DTT. Binding of mant-GTP to eIF5B constructs was monitored by tryptophan Foerster Resonance Energy Transfer (FRET) using an excitation wavelength of 290 nm and an emission wavelength of 440 nm. In order to estimate the equilibrium dissociation constant (K_d) between

Chapter 7

eIF5B constructs and mant-GTP, 2 μM of the protein was titrated with increasing amounts of the mant-nucleotide (dilution was less than 1%). The resulting signal was corrected for the contribution of unbound nucleotide by titrating mant-GTP into buffer and subsequently subtracting these values from the signals obtained with protein. The titration data were analyzed using a quadratic binding model:

$$F = F_0 + \Delta F_{\max} \frac{(X + Y + K_d) - \sqrt{(X + Y + K_d)^2 - 4XY}}{2X}$$

where F is the fluorescence signal of the mant-nucleotide in the presence of eIF5B, F_0 is the initial fluorescence signal, ΔF_{\max} is the maximum fluorescence signal, X is the total concentration of eIF5B, Y is the total concentration of the added mant-nucleotide and K_d is the equilibrium dissociation constant.

Expanded View Figures

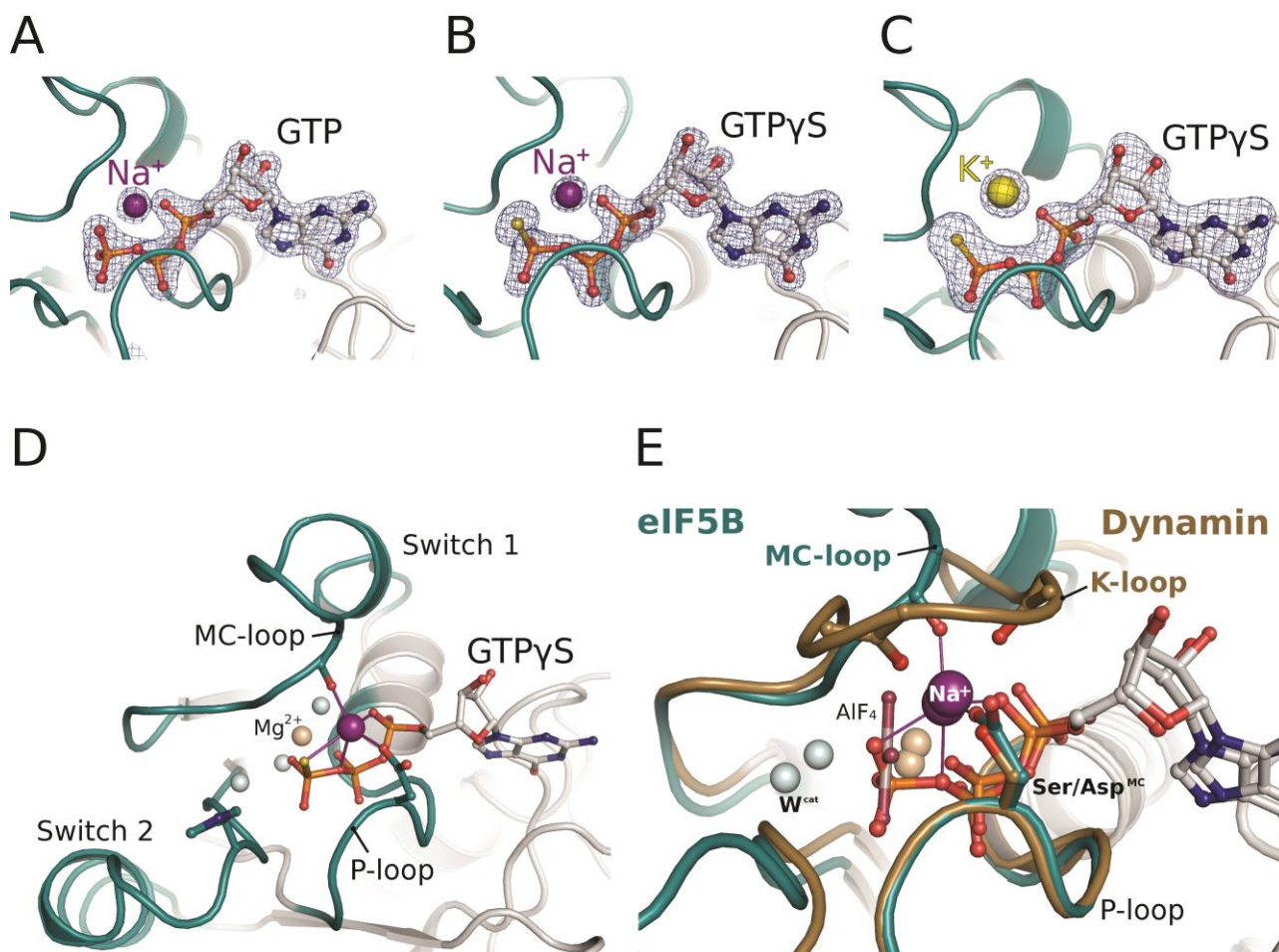


Figure E1. The GTPase center of eIF5B bound to GTP or GTP γ S. A-C) $F_o - F_c$ omit maps for GTP and Na⁺ (A), GTP γ S and Na⁺ (B) or GTP γ S and K⁺ (C) bound to eIF5B (contoured at 3σ). P-loop, switch 1 and switch 2 are colored in cyan. The electron density maps for GTP γ S clearly indicate that the sulfur atom of the γ -phosphate is oriented outward and interacts with the respective M⁺ ion. **D**) Overview of the active site of eIF5B bound to GTP γ S and Na⁺ (purple sphere). The pentameric coordination sphere is indicated by purple lines. GTP, Asp^{MC}, Gly^{MC} and His^{cat} are shown as balls and sticks; P-loop, switch 1 and switch 2 are colored in cyan; the Mg²⁺ ion and water molecules are shown as spheres in light brown and grey, respectively. **E**) Superposition of eIF5B-GTP-Na⁺ (coloring as in D) and dynamin (brown) bound to GDP, AlF₄ and Na⁺ (PDB: 2X2E). The M⁺ ions are coordinated by both proteins in nearly identical positions, despite differences in the ligands forming the coordination shell: Asp^{MC} is replaced by a Ser residue and two backbone oxygens from the K-loop replace Gly^{MC} from the MC-loop.

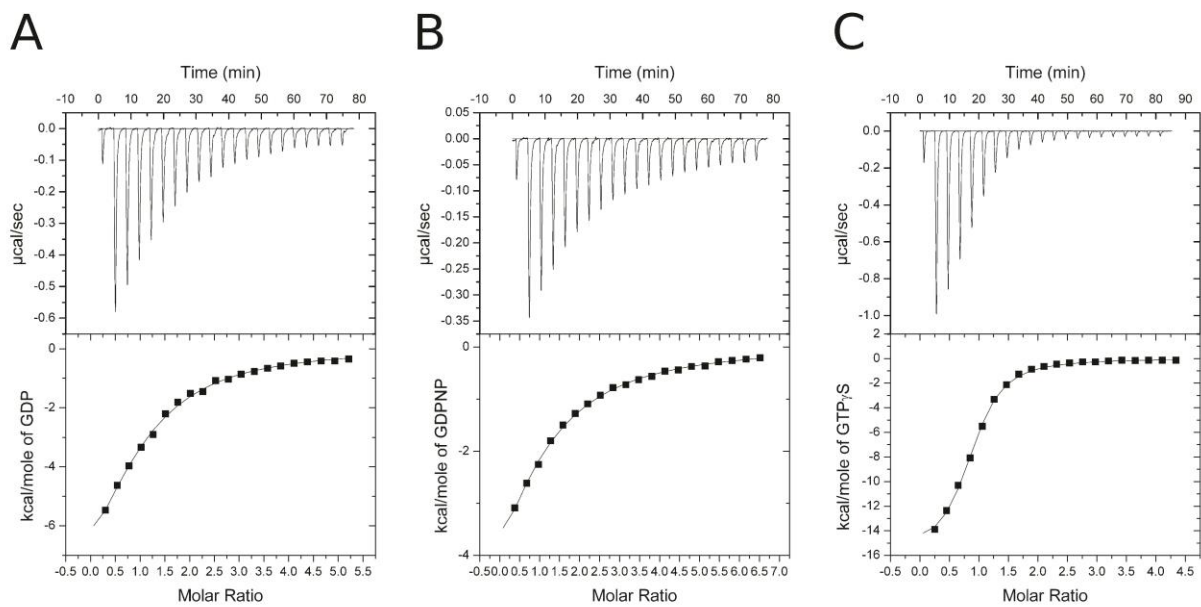


Figure E2. A-C) Titration curves (upper panels) and binding isotherms (lower panels) of eIF5B(517-858) interactions with GDP (A), GDPNP (B) or GTP γ S (C) at 30 °C.

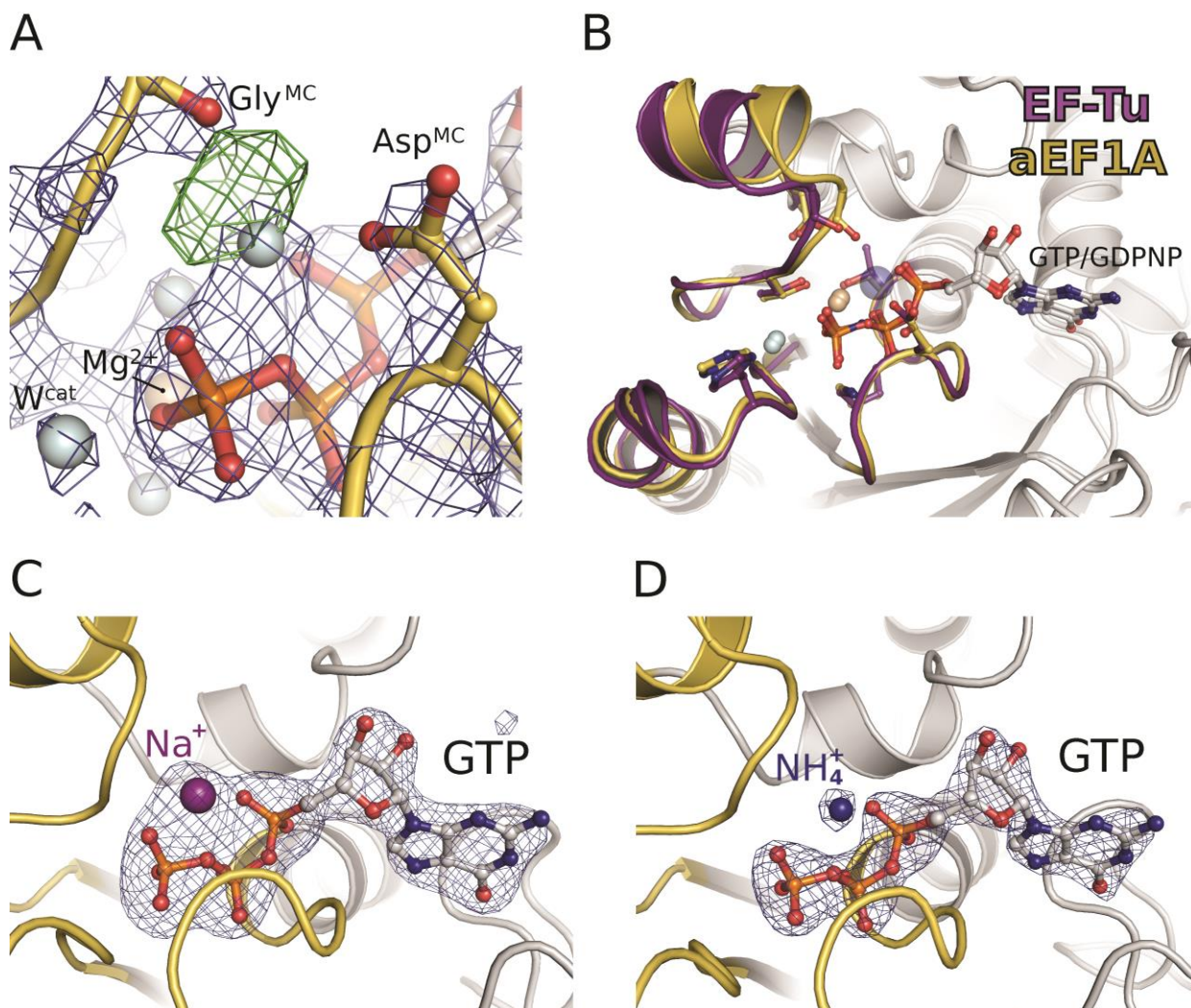


Figure E3. Analysis of M^+ ion coordination in structures of GTP-bound aEF1A. **A)** $2mF_o-DF_c$ map (blue mesh) and mF_o-DF_c difference map (green mesh) for GTP and its surrounding in aEF1A molecule E of the aEF1A/Pelota complex (PDB: 3AGJ) (contoured at 3σ). The coloring is the same as in Fig. 4. In the original structure a water molecule is modeled into the pentameric coordination sphere between Asp^{MC} and Gly^{MC} and the phosphates of the GTP molecule with coordination distances of ~ 2.45 Å. Despite its solvent exposed position, the electron density for this water molecule is significantly stronger than that for the catalytic water (W^{cat}) or the water molecules coordinating the Mg^{2+} ion in the center of the active site. The positive difference electron density for the supposed water molecule (green mesh) indicates a higher density of electrons in this position than provided by H_2O . **B)** The GTPase center in EF-Tu in its GDPNP conformation is virtually identical to that of aEF1A-GTP. With the exception of the β - γ -bridging oxygen of GTP EF-Tu-GDPNP provides all structural elements that are involved in M^+ coordination in the archaeal ortholog. The M^+ ion is indicated as semi-transparent blue sphere. Some universally conserved residues involved in GTP/GDPNP binding or GTP hydrolysis are shown as sticks. **C and D)** F_o-F_c omit maps for GTP and Na^+ (C), or GTP and NH_4^+ (D) bound to aEF1A (contoured at 3σ). P-loop and switch regions are colored yellow.

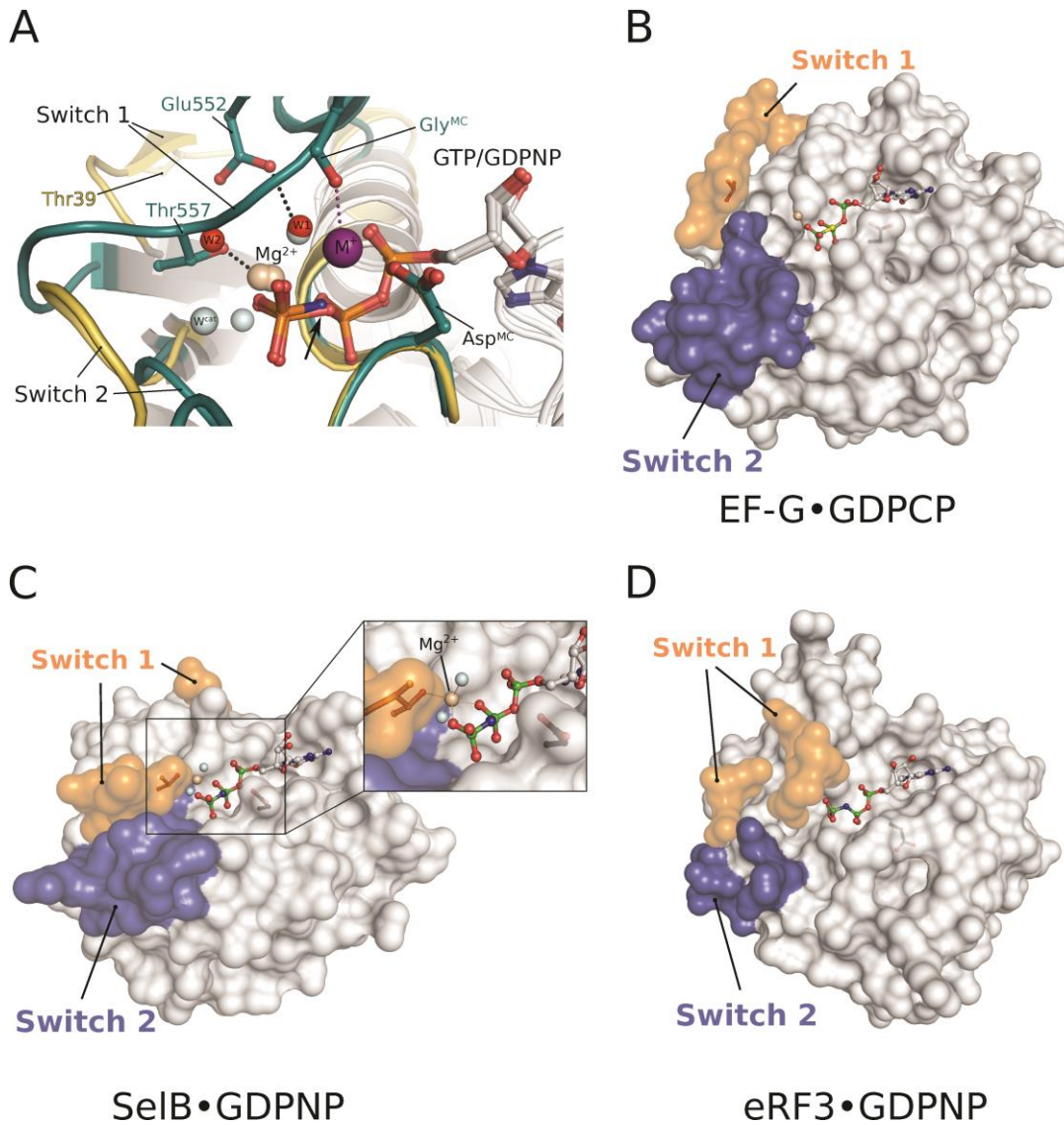


Figure E4. GDPNP and GDPCP prevent the coordination of the M^+ ion, which results in their inability to stably induce the conformational switch in trGTPases. **A)** Detailed view on the nucleotide binding pocket in a superposition of eIF5B-GTP (P-loop and switch regions in cyan) and aIF5B-GDPNP (P-loop and switch regions in yellow). GDPNP provides the γ -phosphate oxygens, the Mg^{2+} ion (light brown sphere) and its water ligands (red sphere; W1) in the identical positions as GTP for interactions with switch 2 and the stable association of switch 1 through Glu552 and Thr557 (*C. thermophilum* numbering). However, in contrast to the GTP-structure switch 1 and switch 2 remain in their GDP-like conformation in GDPNP-bound aIF5B and the position of Thr39 (corresponding to Thr557) is instead occupied by an additional water molecule (red sphere; W2). The only significant difference between GTP and GDPNP is the inability of the latter to coordinate the M^+ ion (purple sphere), resulting in the loss of its contribution as structural cofactor to stabilize the GTP-conformation of switch 1 through the interaction with Gly^{MC} (purple dashed line). (It is important to note that in the originally downloaded structure file for aIF5B-GDPNP (PDB: 1G7T), W1 (red sphere) is interpreted as the Mg^{2+} ion, whereas a water (number 844) was modeled in the position which is here indicated as Mg^{2+} ion (light brown sphere). Our reinterpretation is based on the coordination geometry as well as the coordination distances for these two positions (coordination distances between 2.1 and 2.4 Å

for water 844 and between 2.6 and 3.4 Å for the supposed Mg^{2+} ion). This reinterpretation is consistent with previously reported values for the coordination of Mg^{2+} ions [257]. As the structure factors are not deposited in the PDB, we were unable to examine whether our reinterpretation is consistent with the experimental data). **B)** Surface presentation of the G domain in free EF-G-GDPCP (PDB: 2J7K). As for aIF5B-GDPNP, switch 1 (orange) and switch 2 (blue) remain in their 'off' state conformation despite the presence of the GTP analog. Like in the case of GDPNP, the coordination of the M^{+} ion is prevented by the β - γ -bridging CH_2 group instead of the required oxygen ligand. **C)** In SelB-GDPNP switch 2 (blue) interacts with the γ -phosphate in the canonical way. Switch 1 as well undergoes a conformational change, resulting in the canonical direct contact between Thr46 (corresponding to Thr557 in *ctelF5B*) and the Mg^{2+} ion (inset). However, despite the stabilization of Thr46, the preceding regions including the residues corresponding to the MC-loop in eIF5B and aEF1A remain flexible and are not defined in the electron density, most likely due to the loss of the M^{+} ion as stable interaction partner. **D)** Surface presentation of GDPNP-bound eRF3. As in the cases of aIF5B and EF-G, both switch regions remain in their 'off' state conformation.

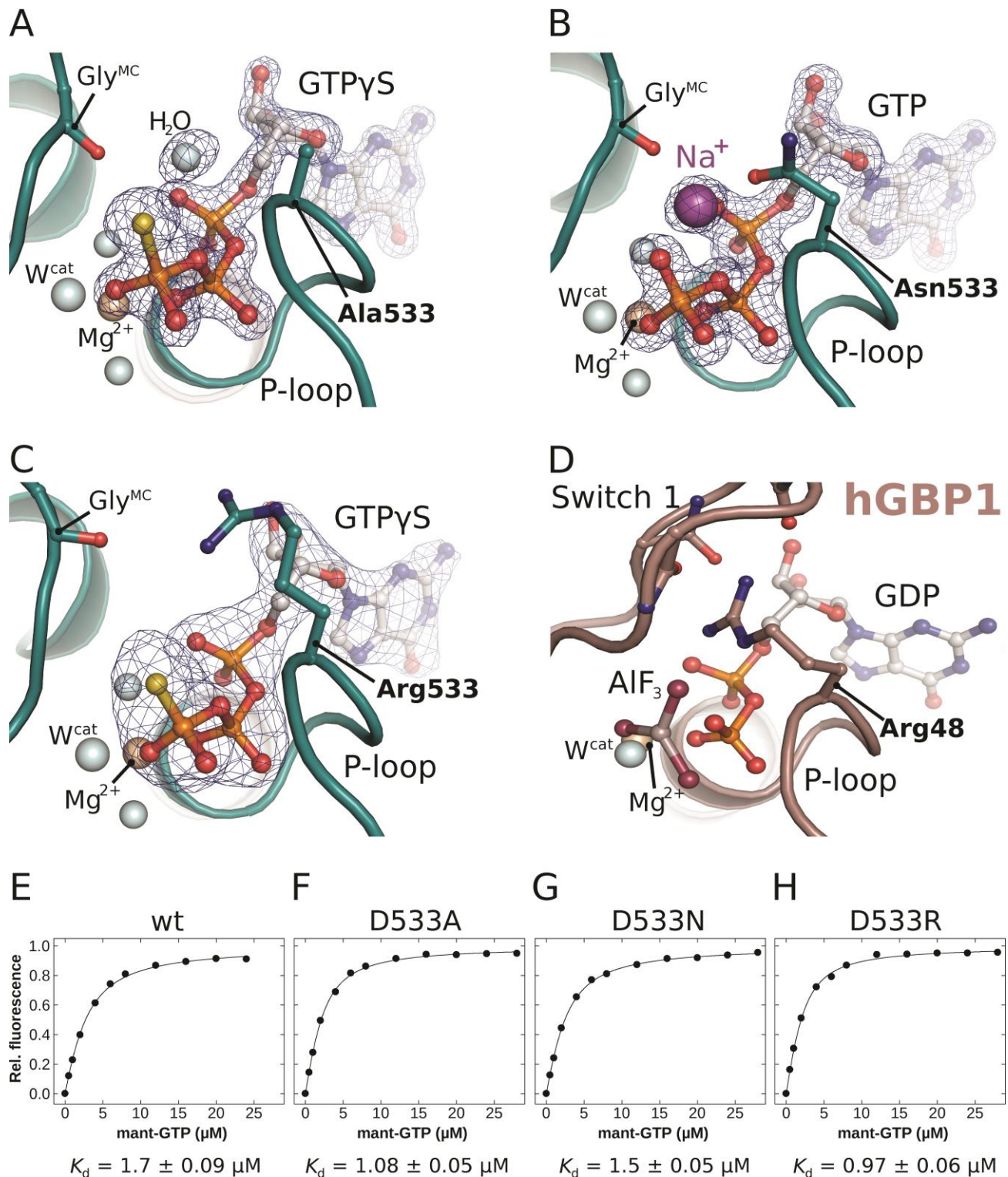


Figure E5. Crystal structures of eIF5B Asp^{MC} (D533) mutants bound to GTP or GTP γ S. The coloring is the same as in Figure E1. **A)** Nucleotide binding pocket of eIF5B-D533A bound to GTP γ S. Due to the replacement of Asp^{MC} by Ala, one of the key ligands and thus the pentagonal coordination sphere for the M⁺ ion is lost. Accordingly, a water molecule (H₂O) is now asymmetrically coordinated by four ligands provided by Gly^{MC} in the P-loop and the GTP γ S molecule instead of the M⁺ ion. The coordination distances lie between 2.8 Å (to

the α -phosphate) and 3.2 Å (to Gly^{MC}) to the oxygen ligands and ~3.3 Å to the sulfur atom. These distances to the oxygen ligands are significantly too large for a Na⁺ ion (~2.42 Å [156]). The F_o-F_c omit map is shown for GTP γ S and the water molecule, contoured at 3σ . **B**) The nucleotide binding pocket of eIF5B-D533N bound to GTP and Na⁺. Unlike the D533A mutant, Asn in lieu of Asp^{MC} still provides the oxygen ligand required for the coordination of the M⁺ ion, analogous to the P-loop Asn in MnmE (see Figure 1D). Consistently, the crystal structure of eIF5B-D533N was found to coordinate a Na⁺ ion virtually identically to the wild-type protein (see Figure 1A). The coordination distances in the pentameric coordination shell lie between 2.22 Å (to Gly^{MC}) and 2.45 Å (to the α -phosphate), consistent with the expected values for a Na⁺ ion [156]. The F_o-F_c omit map is shown for GTP and the Na⁺ ion, contoured at 3σ . **C**) The nucleotide binding pocket of eIF5B-D533R bound to GTP γ S. In both eIF5B molecules of the asymmetric unit, the side chain of Arg533 is oriented toward the nucleotide and forms a hydrogen bond to Gly^{MC} (in one of the eIF5B molecules, Arg533 adopts a second (alternative) conformation, in which the guanidino group is oriented away from the nucleotide (not shown)). As expected from the disruption of the coordination sphere, no M⁺ ion is bound in the active site. Moreover, no water molecule seems to be bound in lieu of the M⁺ ion as seen in the D533A mutant (A). Although the guanidino group in this structure does not form a direct contact to the phosphate moieties of GTP γ S, it is conceivable that – particularly at low salt concentrations – Arg533 may transiently adopt a conformation similar to that observed for Arg48, the *cis*-acting arginine-finger, in the GTPase hGBP1 (D) [258], to allow the observed slightly stimulating effect on the intrinsic GTPase activity (see Fig. 2F). The F_o-F_c omit map is shown for GTP γ S, contoured at 3σ . **D**) The nucleotide binding pocket of hGBP1 (with P-loop and switch 1 in brown) bound to the transition state mimic GDP/AlF₃ (PDB: 2B92). Several hydrogen bonds to switch 1 stabilize Arg48 in its active conformation, in which the guanidino group forms direct contacts to GDP and AlF₃. **E-H**) Steady-state fluorescence measurements for the affinity of wild-type eIF5B(517-858) and Asp^{MC} mutants to mant-GTP. Increasing amounts of mant-GTP were titrated to 2 μ M wild-type eIF5B (E) or the Asp^{MC} mutants D533A (F), D533N (G) and D533R (H) at 20 °C in buffer containing 25 mM Tris/HCl (pH 7.5), 200 mM KCl, 3 mM MgCl₂ and 2 mM DTT. Under these conditions, wild-type eIF5B(517-858) bound mant-GTP with a K_d of $1.7 \pm 0.09 \mu$ M. A similar value was obtained for the D533N mutant (K_d of $1.5 \pm 0.05 \mu$ M), while D533A and D533R showed slightly lower K_d values of $1.08 \pm 0.05 \mu$ M and $0.97 \pm 0.06 \mu$ M, respectively. The K_d value for each construct was calculated from three independent equilibrium titrations.

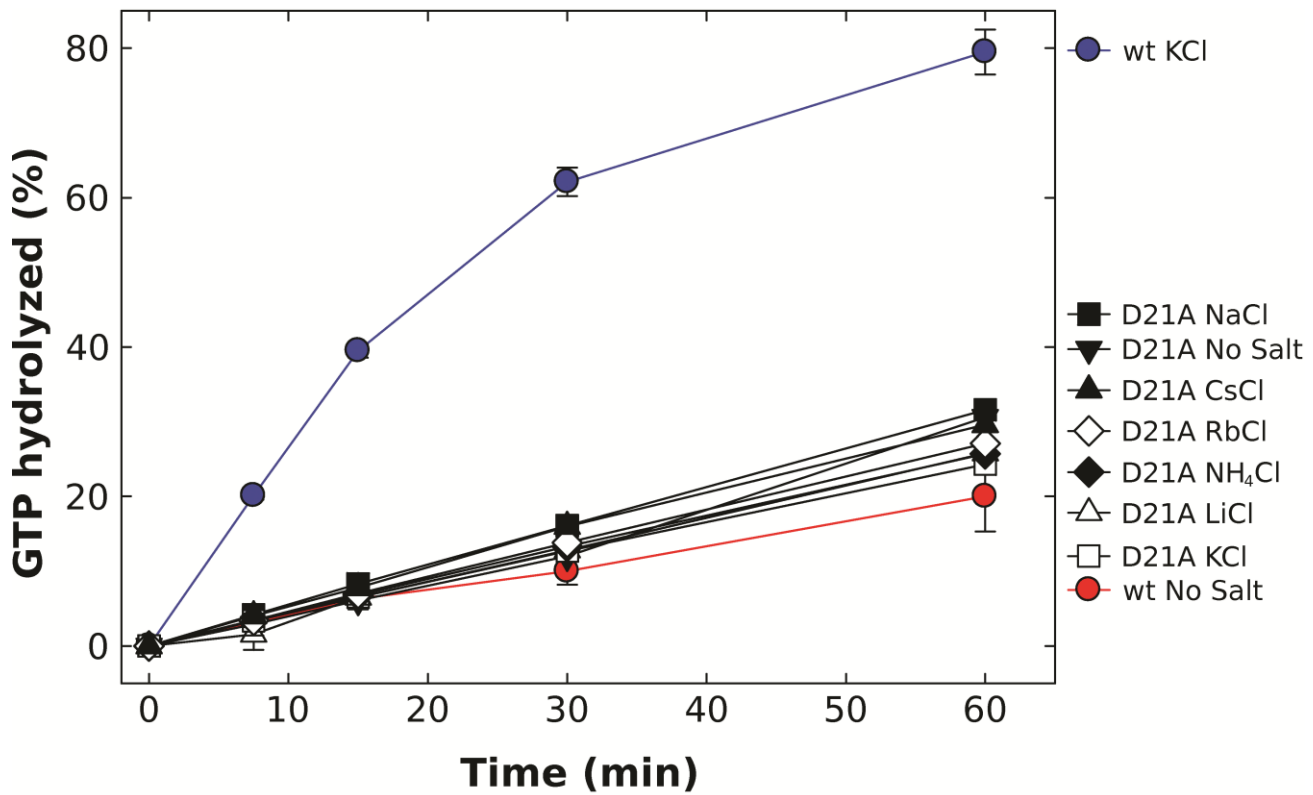


Figure E6. Comparison of the effect of different species of M^+ ions on the intrinsic GTPase activity of the *E. coli* EF-Tu D21A mutant (black and white) and wild-type EF-Tu (red and blue). The intrinsic GTPase activity was determined in the presence of 200 mM of the indicated salts under single turnover conditions. The order in which the combinations are given on the right corresponds to the relative rates of GTP hydrolysis. Experiments were repeated two to three times; standard deviations are given by error bars (in some cases not visible because they are smaller than the symbol size).

Expanded ViewTables

Table E1. Thermodynamic parameters of *ctelF5B*(517-858) binding to GTP γ S, GDPNP and GDP at different temperatures.

Ligand	T [°C]	K _d [μ M]	Δ H [kcal/mol]	Δ G [kcal/mol]	T Δ S [kcal/mol]
GTP γ S	10	0.58	-5.06	-8.06	3.0
GTP γ S	20	0.67	-9.67	-8.27	-1.4
GTP γ S	25	0.82	-12.93	-8.83	-4.1
GTP γ S	30	0.92	-15.81	-8.41	-7.4
GDPNP	10	10.67	-5.89	-6.44	0.55
GDPNP	15	12.3	-7.31	-6.48	-0.83
GDPNP	20	15.47	-8.09	-6.49	-1.6
GDPNP	25	15.0	-9.58	-6.68	-2.9
GDPNP	30	20.8	-9.67	-6.47	-3.2
GDP	10	3.37	-6.94	-7.09	0.15
GDP	20	5.85	-9.06	-7.76	-2.3
GDP	30	10.4	-11.51	-6.91	-4.6

Measurements were performed two to three times.

K_d, dissociation equilibrium constant; calculated as 1/K_a.

K_a, association equilibrium constant; standard deviation did not exceed $\pm 15\%$.

Δ H, standard enthalpy change; standard deviation did not exceed $\pm 15\%$.

Δ G, Gibbs energy; calculated from equation $\Delta G = -R \cdot T \cdot \ln K_a$.

T Δ S, standard entropy change; calculated from equation $\Delta G = \Delta H - T\Delta S$.

Table E2. Crystallization, X-ray data collection and refinement statistics for structures of eIF5B(517-858) mutants

	eIF5B(517-858)D533A-GTPyS	eIF5B(517-858)D533R-GTPyS	eIF5B(517-858)D533N-GTP·Na ⁺
Crystallization			
Condition	100 mM HEPES (pH 7.3), 15% PEG 4000, 150 mM NaOAc	100 mM MES (pH 6.7), 13% PEG 8000, 225 mM NaOAc	100 mM HEPES (pH 7), 13% PEG 4000, 125 mM NaOAc
Temperature (°C)	20	20	20
Data Collection			
Space Group	P2 ₁	P4 ₁ 2 ₁ 2	P2 ₁
Unit Cell	a = 55.6 Å b = 115.8 Å c = 65.9 Å α = 90° β = 102.3° γ = 90°	a = 115.7 Å b = 115.7 Å c = 119.8 Å α = 90° β = 90° γ = 90°	a = 55.4 Å b = 115.9 Å c = 66.1 Å α = 90° β = 101.4° γ = 90°
Molecules/asym. unit	2	2	2
Resolution (Å)	1.58 (1.68-1.58)	2.75 (2.92-2.75)	1.5 (1.59-1.5)
Observed reflections	374970 (60270)	154138 (23582)	542902 (84681)
Unique reflections	110416 (17665)	21704 (3403)	131458 (20989)
Completeness (%)	98.8 (98.0)	99.8 (99.1)	99.2 (98.2)
<I>/σ	17.7 (2.2)	19.35 (3.11)	24.4 (2.9)
R _{sym} (%)	3.9 (51.5)	7.8 (56.8)	3.0 (46.3)
CC(1/2) (%)	99.9 (73.9)	99.9 (86.1)	100 (82.8)
Refinement			
R _{work} (%)	16.9	20.6	15.5
R _{free} (%)	19.4	25.7	18.2
Rmsd from Standard Stereochemistry			
Bond length (Å)	0.012	0.005	0.014
Bond angles (°)	1.5	1.0	1.6
Ramachandran Plot Statistics			
Most favored (%)	98.7	98.2	98.5
Allowed regions (%)	1.3	1.8	1.5
Disallowed regions (%)	0	0	0

Values in parentheses refer to the highest resolution shell.

R_{work} and R_{free} factors are calculated using the formula $R = \frac{\sum_{hkl} |F(obs)_{hkl}| - |F(calc)_{hkl}|}{\sum_{hkl} |F(obs)_{hkl}|}$, where F(obs)_{hkl} and F(calc)_{hkl} are observed and measured structure factors, respectively. R_{work} and R_{free} differ in the set of reflections they are calculated from: R_{free} is calculated for the test set, whereas R_{work} is calculated for the working set.

Chapter 8 •Synopsis and outlook

Translation is an intriguing problem from two different perspectives: the mechanistic aspect of the translation apparatus as a biochemical process, and the evolutionary aspect of translation as the result of selective historical constellations. Necessarily, both aspects are inseparably connected with each other, with the accumulated mechanistic details being relicts of the former selective constellations under which the translation apparatus emerged. Hence, the problem to understand translation as an evolved mechanism, the relationship between the different stages of the translation process and the emergence of domain-specific variations cannot be derived from sequence-based phylogenetic analysis alone but must be based on an understanding of its structural and functional details, which, moreover, remain an intriguing problem in themselves. In turn, a full understanding of the mechanistic details and the underlying principles that govern translation in extant cells is not possible without simultaneously treating it as an evolutionary problem. This intersection is exemplified by translational GTPases, an ancient protein family with common evolutionary descent, whose members became involved in a variety of steps in the translation process.

The principle aim of this thesis was the structural and functional characterization of eIF2 and eIF5B, the two translational GTPases involved in eukaryal translation initiation, which, in comparison with their homologs from bacteria and archaea or from other stages of the translation process, provide two disparate examples for the intersection between mechanistic and evolutionary aspects of translation.

The first part of this thesis (chapters 2-4) was dedicated to the structural and functional characterization of the interactions between eIF2 and its effector proteins eIF5 and eIF2B ϵ , which

perform essential and opposing roles during the guanine-nucleotide cycle of eIF2. On the one hand, a refined model for the intricate interaction network in the eIF2·eIF5 complex could be derived using a combination of complementary structural and biochemical approaches, which included the first crystal structure of a complex between the eIF5-CTD and the eIF2 β -NTT. This model suggests that eIF5 uses three distinct binding interfaces with the eIF2 complex, two of which are formed by the eIF5-CTD that becomes clamped between the eIF2 β -NTT and eIF2 γ and the third formed between the eIF5-NTD and eIF2 γ , which might become relevant at overlapping stages of the initiation process (chapter 2). On the other hand, an analogous interaction model could be derived for the complex between eIF2 and the catalytic subdomain of its GEF eIF2B ϵ (chapter 3), which provided insight into the mechanism by which the isolated eIF2B ϵ (outside the structural context of the eIF2B holo-complex) binds its substrate to promote GDP release from eIF2 and its exchange against GTP. The comparison between the two proposed binding models for the interactions between eIF2 and its effector proteins finally gave rise to the hypothesis that the structurally similar C-terminal domains of eIF5 and eIF2B ϵ share a common evolutionary descent from an ancestral form which has already been engaged in eIF2 binding and the modulation of its nucleotide-binding properties (chapter 3).

Both binding models are currently based on a number of complementary biochemical and structural approaches used in this work as well as previous biochemical and genetic studies. However, several conclusions or suggestions presented in the two chapters only form the vantage point for further studies. In this context, interesting future aims would be the model-based introduction of additional Bpa-sites in the various proteins and the identification of additional crosslinking sites (e.g. the crosslinking target of eIF2B ϵ (524-712)N569Bpa on eIF2 α) or a structural confirmation of the proposal that the DWEAR-motif forms part of the C-terminal domain of eIF5 by solving a crystal structure with helix α 1 accommodated in the hydrophobic cleft as suggested in figure 5 of chapter 2. The ultimate goal, however, remains the structural analysis of the entire eIF2·eIF5 and eIF2·eIF2B ϵ complexes either in isolation or in the structural contexts of pre-ICs or the eIF2·eIF2B complex by means of X-ray crystallography or cryo-EM, in order to correlate biochemical and genetic data with structural information. Particularly interesting would be the

structure of a 43S pre-IC containing the TC as well as eIF5 to test the hypotheses presented in chapter 2 concerning the location and involvement of its C-terminal domain.

Chapter 4 presented the vantage point to solve the problem of eIF2B function with the *in vitro* reconstitution of the eIF2B $\alpha\beta\delta$ regulatory subcomplex and the determination of the first crystal structures of eIF2B β and eIF2B δ from the thermophilic fungus *C. thermophilum*. Unlike the usually used *S. cerevisiae* system, all three subunits can be purified recombinantly in large amounts and like in other known cases, the thermophilic origin of the source organism appears to result in structural properties of the proteins that are favorable for crystallization. It would thus be an interesting scheme for future studies to obtain a high-resolution structural model for the eIF2B regulatory subcomplex. Necessarily, the next step would be the reconstitution of the eIF2B holo-complex including eIF2B ϵ and eIF2B γ , which is, however, currently hampered by the insolubility of eIF2B γ when expressed recombinantly in *E. coli*.

The first two chapters of the second part of the thesis (chapters 5 and 6) were dedicated to the structural and functional characterization of eIF5B. Specific aspects of the findings for eIF5B subsequently served as the basis to develop the hypothesis of universal monovalent cation dependency among trGTPases, which was presented in chapter 7.

The initial question at hand was the specific function of eIF5B in the process of subunit joining and its relation to the functional characteristics of the archaeal and bacterial orthologs. The starting point for this study was the observation that previously proposed structural and functional models for eIF5B were incompatible with the classical concepts of G protein function, at odds with the universal conservation of the nucleotide-binding motifs within α /eIF5B/IF2 homologs and finally incompatible with most available biochemical and structural data. The structural and biochemical studies presented in chapter 5 revealed that the activation mechanism of the eIF5B G domain for ribosomal subunit joining indeed follows the classical paradigms of G protein function as molecular switches. Moreover, this mechanism was found to be coupled to a so far unprecedented mode of overall activation of eIF5B, called domain release mechanism, which provides eIF5B·GTP with the means to discriminate against erroneously assembled pre-ICs by the

requirement of stabilizing interactions with the unique P site bound initiator tRNA (chapters 6) to promote the formation of an elongation competent 80S IC (chapter 5).

Chapter 7 was finally dedicated to the hypothesis of M^+ ion-dependent conformational switching and GTP hydrolysis among trGTPases. This hypothesis is so far based on biochemical and structural studies on the canonical trGTPases eIF5B, aEF1A and EF-Tu, the common descent of trGTPases as reflected in the high degree of sequence and structural homology in their G domains, as well as the immense explanatory power of M^+ dependency for previously unresolved problems concerning the function of trGTPases. It is clear however that the claim of universality for this hypothesis, although in agreement with the available data, will have to be confirmed by structural and biochemical studies on the various trGTPases it has been proposed for. In this context, a number of additional projects were initiated in the course of this thesis, which included attempts to crystallize the GTP/GTP γ S-bound forms of *T. thermophilus* IF2 and EF-Tu, aIF2 γ and aEF2 from *S. solfataricus*, as well as eRF3 from *C. thermophilum* either in isolation or in a complex with eRF1 (data not shown). Up to now, none of the desired structures could be determined. However, for several of the projects crystallization conditions could be identified as promising starting points for future studies. Moreover, future work will have to comprise mutational analyses, in particular of the key P loop aspartate (Asp^{MC}) in terms of its influence on the intrinsic and ribosome-dependent GTPase activity of the various trGTPases. However, as for the work concerning eIF2 function, the ultimate goal would be to provide high-resolution structural evidence for M^+ coordination by a trGTPase in the context of the ribosome, which, due to the limitations of nonhydrolyzable GTP analogs as discussed in chapter 7, would require the usage of GDP in combination with transition state mimics such as fluoroaluminates or berylliumfluorides to trap the M^+ -bound state.

References

1. Wei, Z., et al., *Crystal structure of the C-terminal domain of S.cerevisiae eIF5*. J Mol Biol, 2006. **359**(1): p. 1-9.
2. Ramakrishnan, V., *Ribosome structure and the mechanism of translation*. Cell, 2002. **108**(4): p. 557-72.
3. Ban, N., et al., *The complete atomic structure of the large ribosomal subunit at 2.4 Å resolution*. Science, 2000. **289**(5481): p. 905-20.
4. Wimberly, B.T., et al., *Structure of the 30S ribosomal subunit*. Nature, 2000. **407**(6802): p. 327-39.
5. Ben-Shem, A., et al., *The structure of the eukaryotic ribosome at 3.0 Å resolution*. Science, 2011. **334**(6062): p. 1524-9.
6. Klinge, S., et al., *Atomic structures of the eukaryotic ribosome*. Trends Biochem Sci, 2012. **37**(5): p. 189-98.
7. Schmeing, T.M. and V. Ramakrishnan, *What recent ribosome structures have revealed about the mechanism of translation*. Nature, 2009. **461**(7268): p. 1234-42.
8. Voorhees, R.M. and V. Ramakrishnan, *Structural basis of the translational elongation cycle*. Annu Rev Biochem, 2013. **82**: p. 203-36.
9. Marintchev, A. and G. Wagner, *Translation initiation: structures, mechanisms and evolution*. Q Rev Biophys, 2004. **37**(3-4): p. 197-284.
10. Rodnina, M.V. and W. Wintermeyer, *Recent mechanistic insights into eukaryotic ribosomes*. Curr Opin Cell Biol, 2009. **21**(3): p. 435-43.
11. Dever, T.E. and R. Green, *The elongation, termination, and recycling phases of translation in eukaryotes*. Cold Spring Harb Perspect Biol, 2012. **4**(7): p. a013706.
12. Hinnebusch, A.G. and J.R. Lorsch, *The mechanism of eukaryotic translation initiation: new insights and challenges*. Cold Spring Harb Perspect Biol, 2012. **4**(10).
13. Kozak, M., *Initiation of translation in prokaryotes and eukaryotes*. Gene, 1999. **234**(2): p. 187-208.
14. Shine, J. and L. Dalgarno, *The 3'-terminal sequence of Escherichia coli 16S ribosomal RNA: complementarity to nonsense triplets and ribosome binding sites*. Proc Natl Acad Sci U S A, 1974. **71**(4): p. 1342-6.
15. Gualerzi, C.O., et al., *Initiation factors in the early events of mRNA translation in bacteria*. Cold Spring Harb Symp Quant Biol, 2001. **66**: p. 363-76.
16. Jackson, R.J., C.U. Hellen, and T.V. Pestova, *The mechanism of eukaryotic translation initiation and principles of its regulation*. Nat Rev Mol Cell Biol, 2010. **11**(2): p. 113-27.
17. Biou, V., F. Shu, and V. Ramakrishnan, *X-ray crystallography shows that translational initiation factor IF3 consists of two compact alpha/beta domains linked by an alpha-helix*. EMBO J, 1995. **14**(16): p. 4056-64.
18. Fletcher, C.M., et al., *Structure and interactions of the translation initiation factor eIF1*. EMBO J, 1999. **18**(9): p. 2631-7.
19. Weisser, M., et al., *The crystal structure of the eukaryotic 40S ribosomal subunit in complex with eIF1 and eIF1A*. Nat Struct Mol Biol, 2013. **20**(8): p. 1015-7.
20. Lomakin, I.B. and T.A. Steitz, *The initiation of mammalian protein synthesis and mRNA scanning mechanism*. Nature, 2013. **500**(7462): p. 307-11.

References

21. Nanda, J.S., et al., *Coordinated movements of eukaryotic translation initiation factors eIF1, eIF1A, and eIF5 trigger phosphate release from eIF2 in response to start codon recognition by the ribosomal preinitiation complex.* J Biol Chem, 2013. **288**(8): p. 5316-29.
22. Leipe, D.D., et al., *Classification and evolution of P-loop GTPases and related ATPases.* J Mol Biol, 2002. **317**(1): p. 41-72.
23. Vetter, I.R. and A. Wittinghofer, *The guanine nucleotide-binding switch in three dimensions.* Science, 2001. **294**(5545): p. 1299-304.
24. Bourne, H.R., D.A. Sanders, and F. McCormick, *The GTPase superfamily: conserved structure and molecular mechanism.* Nature, 1991. **349**(6305): p. 117-27.
25. Bos, J.L., H. Rehmann, and A. Wittinghofer, *GEFs and GAPs: critical elements in the control of small G proteins.* Cell, 2007. **129**(5): p. 865-77.
26. Margus, T., M. Remm, and T. Tenson, *Phylogenetic distribution of translational GTPases in bacteria.* BMC Genomics, 2007. **8**: p. 15.
27. Rodnina, M.V., et al., *GTPases mechanisms and functions of translation factors on the ribosome.* Biol Chem, 2000. **381**(5-6): p. 377-87.
28. Kyrpides, N.C. and C.R. Woese, *Archaeal translation initiation revisited: the initiation factor 2 and eukaryotic initiation factor 2B alpha-beta-delta subunit families.* Proc Natl Acad Sci U S A, 1998. **95**(7): p. 3726-30.
29. Yatime, L., et al., *Structure-function relationships of the intact aIF2alpha subunit from the archaeon Pyrococcus abyssi.* Biochemistry, 2005. **44**(24): p. 8749-56.
30. Ito, T., A. Marintchev, and G. Wagner, *Solution structure of human initiation factor eIF2alpha reveals homology to the elongation factor eEF1B.* Structure, 2004. **12**(9): p. 1693-704.
31. Schmitt, E., M. Naveau, and Y. Mechulam, *Eukaryotic and archaeal translation initiation factor 2: a heterotrimeric tRNA carrier.* FEBS Lett, 2010. **584**(2): p. 405-12.
32. Naveau, M., et al., *tRNA binding properties of eukaryotic translation initiation factor 2 from Encephalitozoon cuniculi.* Biochemistry, 2010. **49**(40): p. 8680-8.
33. Yatime, L., et al., *Structural switch of the gamma subunit in an archaeal aIF2 alpha gamma heterodimer.* Structure, 2006. **14**(1): p. 119-28.
34. Sokabe, M., et al., *Structure of archaeal translational initiation factor 2 betagamma-GDP reveals significant conformational change of the beta-subunit and switch 1 region.* Proc Natl Acad Sci U S A, 2006. **103**(35): p. 13016-21.
35. Asano, K., et al., *Conserved bipartite motifs in yeast eIF5 and eIF2Bepsilon, GTPase-activating and GDP-GTP exchange factors in translation initiation, mediate binding to their common substrate eIF2.* EMBO J, 1999. **18**(6): p. 1673-88.
36. Das, S., et al., *Specific interaction of eukaryotic translation initiation factor 5 (eIF5) with the beta-subunit of eIF2.* J Biol Chem, 1997. **272**(50): p. 31712-8.
37. Schmitt, E., S. Blanquet, and Y. Mechulam, *The large subunit of initiation factor aIF2 is a close structural homologue of elongation factors.* EMBO J, 2002. **21**(7): p. 1821-32.
38. Polekhina, G., et al., *Helix unwinding in the effector region of elongation factor EF-Tu-GDP.* Structure, 1996. **4**(10): p. 1141-51.
39. Abel, K., et al., *An alpha to beta conformational switch in EF-Tu.* Structure, 1996. **4**(10): p. 1153-9.
40. Erickson, F.L., et al., *Functional analysis of homologs of translation initiation factor 2gamma in yeast.* Mol Gen Genet, 1997. **253**(6): p. 711-9.
41. Naveau, M., et al., *Roles of yeast eIF2alpha and eIF2beta subunits in the binding of the initiator methionyl-tRNA.* Nucleic Acids Res, 2013. **41**(2): p. 1047-57.
42. Schmitt, E., et al., *Structure of the ternary initiation complex aIF2-GDPNP-methionylated initiator tRNA.* Nat Struct Mol Biol, 2012. **19**(4): p. 450-4.

43. Yatime, L., et al., *Structure of an archaeal heterotrimeric initiation factor 2 reveals a nucleotide state between the GTP and the GDP states*. Proc Natl Acad Sci U S A, 2007. **104**(47): p. 18445-50.
44. Kapp, L.D. and J.R. Lorsch, *GTP-dependent recognition of the methionine moiety on initiator tRNA by translation factor eIF2*. J Mol Biol, 2004. **335**(4): p. 923-36.
45. Erickson, F.L. and E.M. Hannig, *Ligand interactions with eukaryotic translation initiation factor 2: role of the gamma-subunit*. EMBO J, 1996. **15**(22): p. 6311-20.
46. Kapp, L.D., S.E. Kolitz, and J.R. Lorsch, *Yeast initiator tRNA identity elements cooperate to influence multiple steps of translation initiation*. RNA, 2006. **12**(5): p. 751-64.
47. Farruggio, D., et al., *The A1 x U72 base pair conserved in eukaryotic initiator tRNAs is important specifically for binding to the eukaryotic translation initiation factor eIF2*. Mol Cell Biol, 1996. **16**(8): p. 4248-56.
48. Nissen, P., et al., *Crystal structure of the ternary complex of Phe-tRNAPhe, EF-Tu, and a GTP analog*. Science, 1995. **270**(5241): p. 1464-72.
49. Shin, B.S., et al., *Initiation factor eIF2gamma promotes eIF2-GTP-Met-tRNAⁱ(Met) ternary complex binding to the 40S ribosome*. Nat Struct Mol Biol, 2011. **18**(11): p. 1227-34.
50. Hashem, Y., et al., *Structure of the mammalian ribosomal 43S preinitiation complex bound to the scanning factor DHX29*. Cell, 2013. **153**(5): p. 1108-19.
51. Conte, M.R., et al., *Structure of the eukaryotic initiation factor (eIF) 5 reveals a fold common to several translation factors*. Biochemistry, 2006. **45**(14): p. 4550-8.
52. Das, S., R. Ghosh, and U. Maitra, *Eukaryotic translation initiation factor 5 functions as a GTPase-activating protein*. J Biol Chem, 2001. **276**(9): p. 6720-6.
53. Paulin, F.E., et al., *Eukaryotic translation initiation factor 5 (eIF5) acts as a classical GTPase-activator protein*. Curr Biol, 2001. **11**(1): p. 55-9.
54. Bieniossek, C., et al., *The crystal structure of the carboxy-terminal domain of human translation initiation factor eIF5*. J Mol Biol, 2006. **360**(2): p. 457-65.
55. Singh, C.R., Y. Yamamoto, and K. Asano, *Physical association of eukaryotic initiation factor (eIF) 5 carboxyl-terminal domain with the lysine-rich eIF2beta segment strongly enhances its binding to eIF3*. J Biol Chem, 2004. **279**(48): p. 49644-55.
56. Asano, K., et al., *Multiple roles for the C-terminal domain of eIF5 in translation initiation complex assembly and GTPase activation*. EMBO J, 2001. **20**(9): p. 2326-37.
57. Yamamoto, Y., et al., *The eukaryotic initiation factor (eIF) 5 HEAT domain mediates multifactor assembly and scanning with distinct interfaces to eIF1, eIF2, eIF3, and eIF4G*. Proc Natl Acad Sci U S A, 2005. **102**(45): p. 16164-9.
58. Singh, C.R., et al., *Eukaryotic translation initiation factor 5 is critical for integrity of the scanning preinitiation complex and accurate control of GCN4 translation*. Mol Cell Biol, 2005. **25**(13): p. 5480-91.
59. Asano, K., et al., *A multifactor complex of eukaryotic initiation factors, eIF1, eIF2, eIF3, eIF5, and initiator tRNA^(Met) is an important translation initiation intermediate in vivo*. Genes Dev, 2000. **14**(19): p. 2534-46.
60. Dennis, M.D., M.D. Person, and K.S. Browning, *Phosphorylation of plant translation initiation factors by CK2 enhances the in vitro interaction of multifactor complex components*. J Biol Chem, 2009. **284**(31): p. 20615-28.
61. Sokabe, M., C.S. Fraser, and J.W. Hershey, *The human translation initiation multi-factor complex promotes methionyl-tRNAⁱ binding to the 40S ribosomal subunit*. Nucleic Acids Res, 2011. **40**(2): p. 905-13.
62. Valasek, L., et al., *Interactions of eukaryotic translation initiation factor 3 (eIF3) subunit NIP1/c with eIF1 and eIF5 promote preinitiation complex assembly and regulate start codon selection*. Mol Cell Biol, 2004. **24**(21): p. 9437-55.

References

63. Luna, R.E., et al., *The C-terminal domain of eukaryotic initiation factor 5 promotes start codon recognition by its dynamic interplay with eIF1 and eIF2beta*. Cell Rep, 2012. **1**(6): p. 689-702.
64. Algire, M.A., D. Maag, and J.R. Lorsch, *Pi release from eIF2, not GTP hydrolysis, is the step controlled by start-site selection during eukaryotic translation initiation*. Mol Cell, 2005. **20**(2): p. 251-62.
65. Alone, P.V. and T.E. Dever, *Direct binding of translation initiation factor eIF2gamma-G domain to its GTPase-activating and GDP-GTP exchange factors eIF5 and eIF2B epsilon*. J Biol Chem, 2006. **281**(18): p. 12636-44.
66. Hashimoto, N.N., L.S. Carnevalli, and B.A. Castilho, *Translation initiation at non-AUG codons mediated by weakened association of eukaryotic initiation factor (eIF) 2 subunits*. Biochem J, 2002. **367**(Pt 2): p. 359-68.
67. Huang, H.K., et al., *GTP hydrolysis controls stringent selection of the AUG start codon during translation initiation in Saccharomyces cerevisiae*. Genes Dev, 1997. **11**(18): p. 2396-413.
68. Singh, C.R., et al., *An eIF5/eIF2 complex antagonizes guanine nucleotide exchange by eIF2B during translation initiation*. EMBO J, 2006. **25**(19): p. 4537-46.
69. Jennings, M.D. and G.D. Pavitt, *eIF5 has GDI activity necessary for translational control by eIF2 phosphorylation*. Nature, 2010. **465**(7296): p. 378-81.
70. Gomez, E., S.S. Mohammad, and G.D. Pavitt, *Characterization of the minimal catalytic domain within eIF2B: the guanine-nucleotide exchange factor for translation initiation*. EMBO J, 2002. **21**(19): p. 5292-301.
71. Gomez, E. and G.D. Pavitt, *Identification of domains and residues within the epsilon subunit of eukaryotic translation initiation factor 2B (eIF2Bepsilon) required for guanine nucleotide exchange reveals a novel activation function promoted by eIF2B complex formation*. Mol Cell Biol, 2000. **20**(11): p. 3965-76.
72. Wortham, N.C., et al., *Analysis of the subunit organization of the eIF2B complex reveals new insights into its structure and regulation*. FASEB J, 2014. **28**(5): p. 2225-37.
73. Gordiyenko, Y., et al., *eIF2B is a decameric guanine nucleotide exchange factor with a gamma2epsilon2 tetrameric core*. Nat Commun, 2014. **5**: p. 3902.
74. Boesen, T., et al., *Structure of the catalytic fragment of translation initiation factor 2B and identification of a critically important catalytic residue*. J Biol Chem, 2004. **279**(11): p. 10584-92.
75. Mohammad-Qureshi, S.S., et al., *Critical contacts between the eukaryotic initiation factor 2B (eIF2B) catalytic domain and both eIF2beta and -2gamma mediate guanine nucleotide exchange*. Mol Cell Biol, 2007. **27**(14): p. 5225-34.
76. Mohammad-Qureshi, S.S., M.D. Jennings, and G.D. Pavitt, *Clues to the mechanism of action of eIF2B, the guanine-nucleotide-exchange factor for translation initiation*. Biochem Soc Trans, 2008. **36**(Pt 4): p. 658-64.
77. Dev, K., et al., *The beta/Gcd7 subunit of eukaryotic translation initiation factor 2B (eIF2B), a guanine nucleotide exchange factor, is crucial for binding eIF2 in vivo*. Mol Cell Biol, 2010. **30**(21): p. 5218-33.
78. Hinnebusch, A.G., *Gene-specific translational control of the yeast GCN4 gene by phosphorylation of eukaryotic initiation factor 2*. Mol Microbiol, 1993. **10**(2): p. 215-23.
79. Sonenberg, N. and A.G. Hinnebusch, *Regulation of translation initiation in eukaryotes: mechanisms and biological targets*. Cell, 2009. **136**(4): p. 731-45.
80. Hinnebusch, A.G., *Translational regulation of GCN4 and the general amino acid control of yeast*. Annu Rev Microbiol, 2005. **59**: p. 407-50.
81. Kyrpides, N.C. and C.R. Woese, *Universally conserved translation initiation factors*. Proc Natl Acad Sci U S A, 1998. **95**(1): p. 224-8.
82. Eiler, D., et al., *Initiation factor 2 crystal structure reveals a different domain organization from eukaryotic initiation factor 5B and mechanism among translational GTPases*. Proc Natl Acad Sci U S A, 2013.

83. Simonetti, A., et al., *Structure of the protein core of translation initiation factor 2 in apo, GTP-bound and GDP-bound forms*. Acta Crystallogr D Biol Crystallogr, 2013. **69**(Pt 6): p. 925-33.
84. Roll-Mecak, A., et al., *X-Ray structures of the universal translation initiation factor IF2/eIF5B: conformational changes on GDP and GTP binding*. Cell, 2000. **103**(5): p. 781-92.
85. Shin, B.S., et al., *Uncoupling of initiation factor eIF5B/IF2 GTPase and translational activities by mutations that lower ribosome affinity*. Cell, 2002. **111**(7): p. 1015-25.
86. Marintchev, A., et al., *Mapping the binding interface between human eukaryotic initiation factors 1A and 5B: a new interaction between old partners*. Proc Natl Acad Sci U S A, 2003. **100**(4): p. 1535-40.
87. Acker, M.G., et al., *Interaction between eukaryotic initiation factors 1A and 5B is required for efficient ribosomal subunit joining*. J Biol Chem, 2006. **281**(13): p. 8469-75.
88. Fringer, J.M., et al., *Coupled release of eukaryotic translation initiation factors 5B and 1A from 80S ribosomes following subunit joining*. Mol Cell Biol, 2007. **27**(6): p. 2384-97.
89. Olsen, D.S., et al., *Domains of eIF1A that mediate binding to eIF2, eIF3 and eIF5B and promote ternary complex recruitment in vivo*. EMBO J, 2003. **22**(2): p. 193-204.
90. Unbehaun, A., et al., *Position of eukaryotic initiation factor eIF5B on the 80S ribosome mapped by directed hydroxyl radical probing*. EMBO J, 2007. **26**(13): p. 3109-23.
91. Fernandez, I.S., et al., *Molecular architecture of a eukaryotic translational initiation complex*. Science, 2013. **342**(6160): p. 1240585.
92. Karaskova, M., et al., *Functional characterization of the role of the N-terminal domain of the c/Nip1 subunit of eukaryotic initiation factor 3 (eIF3) in AUG recognition*. J Biol Chem, 2012. **287**(34): p. 28420-34.
93. Das, S. and U. Maitra, *Mutational analysis of mammalian translation initiation factor 5 (eIF5): role of interaction between the beta subunit of eIF2 and eIF5 in eIF5 function in vitro and in vivo*. Mol Cell Biol, 2000. **20**(11): p. 3942-50.
94. Ryu, Y. and P.G. Schultz, *Efficient incorporation of unnatural amino acids into proteins in Escherichia coli*. Nat Methods, 2006. **3**(4): p. 263-5.
95. Kozakov, D., et al., *PIPER: an FFT-based protein docking program with pairwise potentials*. Proteins, 2006. **65**(2): p. 392-406.
96. Kozakov, D., et al., *Achieving reliability and high accuracy in automated protein docking: ClusPro, PIPER, SDU, and stability analysis in CAPRI rounds 13-19*. Proteins, 2010. **78**(15): p. 3124-30.
97. Acker, M.G., et al., *Reconstitution of yeast translation initiation*. Methods Enzymol, 2007. **430**: p. 111-45.
98. Gromadski, K.B., H.J. Wieden, and M.V. Rodnina, *Kinetic mechanism of elongation factor Ts-catalyzed nucleotide exchange in elongation factor Tu*. Biochemistry, 2002. **41**(1): p. 162-9.
99. Wagner, A., et al., *Interaction of guanosine nucleotides and their analogs with elongation factor Tu from Thermus thermophilus*. Biochemistry, 1995. **34**(39): p. 12535-42.
100. Lenzen, C., R.H. Cool, and A. Wittinghofer, *Analysis of intrinsic and CDC25-stimulated guanine nucleotide exchange of p21ras-nucleotide complexes by fluorescence measurements*. Methods Enzymol, 1995. **255**: p. 95-109.
101. Cherfils, J. and M. Zeghouf, *Regulation of small GTPases by GEFs, GAPs, and GDIs*. Physiol Rev, 2013. **93**(1): p. 269-309.
102. Gotze, M., et al., *StavroX--a software for analyzing crosslinked products in protein interaction studies*. J Am Soc Mass Spectrom, 2012. **23**(1): p. 76-87.
103. Luna, R.E., et al., *The interaction between eukaryotic initiation factor 1A and eIF5 retains eIF1 within scanning preinitiation complexes*. Biochemistry, 2013. **52**(52): p. 9510-8.
104. Reibarkh, M., et al., *Eukaryotic initiation factor (eIF) 1 carries two distinct eIF5-binding faces important for multifactor assembly and AUG selection*. J Biol Chem, 2008. **283**(2): p. 1094-103.

References

105. Jennings, M.D., et al., *eIF2B promotes eIF5 dissociation from eIF2*GDP to facilitate guanine nucleotide exchange for translation initiation*. *Genes Dev*, 2014. **27**(24): p. 2696-707.
106. Scheffzek, K., et al., *The Ras-RasGAP complex: structural basis for GTPase activation and its loss in oncogenic Ras mutants*. *Science*, 1997. **277**(5324): p. 333-8.
107. Grizot, S., et al., *Crystal structure of the Rac1-RhoGDI complex involved in nadph oxidase activation*. *Biochemistry*, 2001. **40**(34): p. 10007-13.
108. Kimple, R.J., et al., *Structural determinants for GoLoco-induced inhibition of nucleotide release by Galpha subunits*. *Nature*, 2002. **416**(6883): p. 878-81.
109. Willard, F.S., R.J. Kimple, and D.P. Siderovski, *Return of the GDI: the GoLoco motif in cell division*. *Annu Rev Biochem*, 2004. **73**: p. 925-51.
110. Hoffman, G.R., N. Nassar, and R.A. Cerione, *Structure of the Rho family GTP-binding protein Cdc42 in complex with the multifunctional regulator RhoGDI*. *Cell*, 2000. **100**(3): p. 345-56.
111. Gai, Z., et al., *The binding mechanism of eIF2beta with its partner proteins, eIF5 and eIF2Bepsilon*. *Biochem Biophys Res Commun*, 2012. **423**(3): p. 515-9.
112. Pavitt, G.D., et al., *eIF2 independently binds two distinct eIF2B subcomplexes that catalyze and regulate guanine-nucleotide exchange*. *Genes Dev*, 1998. **12**(4): p. 514-26.
113. Mueller, U., et al., *Facilities for macromolecular crystallography at the Helmholtz-Zentrum Berlin*. *J Synchrotron Radiat*, 2012. **19**(Pt 3): p. 442-9.
114. Kabsch, W., *Xds*. *Acta Crystallogr D Biol Crystallogr*, 2010. **66**(Pt 2): p. 125-32.
115. McCoy, A.J., et al., *Phaser crystallographic software*. *J Appl Crystallogr*, 2007. **40**(Pt 4): p. 658-674.
116. Emsley, P., et al., *Features and development of Coot*. *Acta Crystallogr D Biol Crystallogr*, 2010. **66**(Pt 4): p. 486-501.
117. Adams, P.D., et al., *PHENIX: a comprehensive Python-based system for macromolecular structure solution*. *Acta Crystallogr D Biol Crystallogr*, 2010. **66**(Pt 2): p. 213-21.
118. Fechter, P., et al., *Ribozyme processed tRNA transcripts with unfriendly internal promoter for T7 RNA polymerase: production and activity*. *FEBS Lett*, 1998. **436**(1): p. 99-103.
119. Kao, C.C., P. Singh, and D.J. Ecker, *De novo initiation of viral RNA-dependent RNA synthesis*. *Virology*, 2001. **287**(2): p. 251-60.
120. Shevchenko, A., et al., *Mass spectrometric sequencing of proteins silver-stained polyacrylamide gels*. *Anal Chem*, 1996. **68**(5): p. 850-8.
121. Levin, D.H., D. Kyner, and G. Acs, *Protein initiation in eukaryotes: formation and function of a ternary complex composed of a partially purified ribosomal factor, methionyl transfer RNA, and guanosine triphosphate*. *Proc Natl Acad Sci U S A*, 1973. **70**(1): p. 41-5.
122. Barrieux, A. and M.G. Rosenfeld, *Characterization of GTP-dependent Met-tRNA^f binding protein*. *J Biol Chem*, 1977. **252**(11): p. 3843-7.
123. Krishnamoorthy, T., et al., *Tight binding of the phosphorylated alpha subunit of initiation factor 2 (eIF2alpha) to the regulatory subunits of guanine nucleotide exchange factor eIF2B is required for inhibition of translation initiation*. *Mol Cell Biol*, 2001. **21**(15): p. 5018-30.
124. Sudhakar, A., et al., *Phosphorylation of serine 51 in initiation factor 2 alpha (eIF2 alpha) promotes complex formation between eIF2 alpha(P) and eIF2B and causes inhibition in the guanine nucleotide exchange activity of eIF2B*. *Biochemistry*, 2000. **39**(42): p. 12929-38.
125. Panniers, R., A.G. Rowlands, and E.C. Henshaw, *The effect of Mg²⁺ and guanine nucleotide exchange factor on the binding of guanine nucleotides to eukaryotic initiation factor 2*. *J Biol Chem*, 1988. **263**(12): p. 5519-25.
126. Andersen, G.R., et al., *Crystal structures of nucleotide exchange intermediates in the eEF1A-eEF1Balpha complex*. *Nat Struct Biol*, 2001. **8**(6): p. 531-4.
127. Kawashima, T., et al., *The structure of the Escherichia coli EF-Tu.EF-Ts complex at 2.5 A resolution*. *Nature*, 1996. **379**(6565): p. 511-8.

128. Rossman, K.L., et al., *A crystallographic view of interactions between Dbs and Cdc42: PH domain-assisted guanine nucleotide exchange*. EMBO J, 2002. **21**(6): p. 1315-26.
129. Boriack-Sjodin, P.A., et al., *The structural basis of the activation of Ras by Sos*. Nature, 1998. **394**(6691): p. 337-43.
130. Schummer, T., K.B. Gromadski, and M.V. Rodnina, *Mechanism of EF-Ts-catalyzed guanine nucleotide exchange in EF-Tu: contribution of interactions mediated by helix B of EF-Tu*. Biochemistry, 2007. **46**(17): p. 4977-84.
131. Zavialov, A.V., R.H. Buckingham, and M. Ehrenberg, *A posttermination ribosomal complex is the guanine nucleotide exchange factor for peptide release factor RF3*. Cell, 2001. **107**(1): p. 115-24.
132. Pavitt, G.D., *eIF2B, a mediator of general and gene-specific translational control*. Biochem Soc Trans, 2005. **33**(Pt 6): p. 1487-92.
133. Wang, X., et al., *Identification of residues that underpin interactions within the eukaryotic initiation factor (eIF2) 2B complex*. J Biol Chem, 2012. **287**(11): p. 8263-74.
134. Reid, P.J., S.S. Mohammad-Qureshi, and G.D. Pavitt, *Identification of intersubunit domain interactions within eukaryotic initiation factor (eIF) 2B, the nucleotide exchange factor for translation initiation*. J Biol Chem, 2012. **287**(11): p. 8275-85.
135. Pavitt, G.D., W. Yang, and A.G. Hinnebusch, *Homologous segments in three subunits of the guanine nucleotide exchange factor eIF2B mediate translational regulation by phosphorylation of eIF2*. Mol Cell Biol, 1997. **17**(3): p. 1298-313.
136. Price, N.T., et al., *eIF2B, the guanine nucleotide-exchange factor for eukaryotic initiation factor 2. Sequence conservation between the alpha, beta and delta subunits of eIF2B from mammals and yeast*. Biochem J, 1996. **318** (Pt 2): p. 637-43.
137. Craddock, B.L. and C.G. Proud, *The alpha-subunit of the mammalian guanine nucleotide-exchange factor eIF-2B is essential for catalytic activity in vitro*. Biochem Biophys Res Commun, 1996. **220**(3): p. 843-7.
138. Bogorad, A.M., et al., *Insights into the architecture of the eIF2Balpha/beta/delta regulatory subcomplex*. Biochemistry, 2014. **53**(21): p. 3432-45.
139. Hiyama, T.B., et al., *Crystal structure of the alpha subunit of human translation initiation factor 2B*. J Mol Biol, 2009. **392**(4): p. 937-51.
140. Dev, K., et al., *Archaeal aIF2B interacts with eukaryotic translation initiation factors eIF2alpha and eIF2Balpha: Implications for aIF2B function and eIF2B regulation*. J Mol Biol, 2009. **392**(3): p. 701-22.
141. Nakamura, A., et al., *Dynamic, ligand-dependent conformational change triggers reaction of ribose-1,5-bisphosphate isomerase from Thermococcus kodakarensis KOD1*. J Biol Chem, 2012. **287**(25): p. 20784-96.
142. Vazquez de Aldana, C.R. and A.G. Hinnebusch, *Mutations in the GCD7 subunit of yeast guanine nucleotide exchange factor eIF-2B overcome the inhibitory effects of phosphorylated eIF-2 on translation initiation*. Mol Cell Biol, 1994. **14**(5): p. 3208-22.
143. Hannig, E.M., et al., *The translational activator GCN3 functions downstream from GCN1 and GCN2 in the regulatory pathway that couples GCN4 expression to amino acid availability in Saccharomyces cerevisiae*. Genetics, 1990. **126**(3): p. 549-62.
144. Roll-Mecak, A., et al., *Engaging the ribosome: universal IFs of translation*. Trends Biochem Sci, 2001. **26**(12): p. 705-9.
145. Pestova, T.V., et al., *The joining of ribosomal subunits in eukaryotes requires eIF5B*. Nature, 2000. **403**(6767): p. 332-5.
146. Acker, M.G., et al., *Kinetic analysis of late steps of eukaryotic translation initiation*. J Mol Biol, 2009. **385**(2): p. 491-506.
147. Antoun, A., et al., *The roles of initiation factor 2 and guanosine triphosphate in initiation of protein synthesis*. EMBO J, 2003. **22**(20): p. 5593-601.

References

148. Benne, R., et al., *Recycling of initiation factors IF-1, IF-2 and IF-3*. Eur J Biochem, 1973. **32**(2): p. 372-80.
149. Dubnoff, J.S., A.H. Lockwood, and U. Maitra, *Studies on the role of guanosine triphosphate in polypeptide chain initiation in Escherichia coli*. J Biol Chem, 1972. **247**(9): p. 2884-94.
150. Tomsic, J., et al., *Late events of translation initiation in bacteria: a kinetic analysis*. EMBO J, 2000. **19**(9): p. 2127-36.
151. Fabbretti, A., et al., *Translation initiation without IF2-dependent GTP hydrolysis*. Nucleic Acids Res, 2012. **40**(16): p. 7946-55.
152. Allen, G.S., et al., *The cryo-EM structure of a translation initiation complex from Escherichia coli*. Cell, 2005. **121**(5): p. 703-12.
153. Haurlyuk, V., S. Hansson, and M. Ehrenberg, *Cofactor dependent conformational switching of GTPases*. Biophys J, 2008. **95**(4): p. 1704-15.
154. Pavlov, M.Y., et al., *Activation of initiation factor 2 by ligands and mutations for rapid docking of ribosomal subunits*. EMBO J, 2011. **30**(2): p. 289-301.
155. Laurberg, M., et al., *Structure of a mutant EF-G reveals domain III and possibly the fusidic acid binding site*. J Mol Biol, 2000. **303**(4): p. 593-603.
156. Harding, M.M., *Metal-ligand geometry relevant to proteins and in proteins: sodium and potassium*. Acta Crystallogr D Biol Crystallogr, 2002. **58**(Pt 5): p. 872-4.
157. Hilgenfeld, R., J.R. Mesters, and T. Hogg, *The Ribosome: Structure, Function, Antibiotics, and Cellular Interactions*. ASM Press, 2000.
158. Hendsch, Z.S. and B. Tidor, *Do salt bridges stabilize proteins? A continuum electrostatic analysis*. Protein Sci, 1994. **3**(2): p. 211-26.
159. Elcock, A.H., *The stability of salt bridges at high temperatures: implications for hyperthermophilic proteins*. J Mol Biol, 1998. **284**(2): p. 489-502.
160. Shin, B.S., et al., *Intragenic suppressor mutations restore GTPase and translation functions of a eukaryotic initiation factor 5B switch II mutant*. Mol Cell Biol, 2007. **27**(5): p. 1677-85.
161. Lee, J.H., et al., *Initiation factor eIF5B catalyzes second GTP-dependent step in eukaryotic translation initiation*. Proc Natl Acad Sci U S A, 2002. **99**(26): p. 16689-94.
162. Shin, B.S. and T.E. Dever, *Molecular genetic structure-function analysis of translation initiation factor eIF5B*. Methods Enzymol, 2007. **429**: p. 185-201.
163. Berchtold, H., et al., *Crystal structure of active elongation factor Tu reveals major domain rearrangements*. Nature, 1993. **365**(6442): p. 126-32.
164. Abrahamson, J.K., et al., *Direct determination of the association constant between elongation factor Tu X GTP and aminoacyl-tRNA using fluorescence*. Biochemistry, 1985. **24**(3): p. 692-700.
165. Louie, A. and F. Journak, *Kinetic studies of Escherichia coli elongation factor Tu-guanosine 5'-triphosphate-aminoacyl-tRNA complexes*. Biochemistry, 1985. **24**(23): p. 6433-9.
166. Delaria, K., et al., *Stabilization of the Escherichia coli elongation factor Tu-GTP-aminoacyl-tRNA complex*. Arch Biochem Biophys, 1991. **286**(1): p. 207-11.
167. Romero, G., V. Chau, and R.L. Biltonen, *Kinetics and thermodynamics of the interaction of elongation factor Tu with elongation factor Ts, guanine nucleotides, and aminoacyl-tRNA*. J Biol Chem, 1985. **260**(10): p. 6167-74.
168. Voorhees, R.M., et al., *The mechanism for activation of GTP hydrolysis on the ribosome*. Science, 2010. **330**(6005): p. 835-8.
169. Tourigny, D.S., et al., *Elongation factor G bound to the ribosome in an intermediate state of translocation*. Science, 2013. **340**(6140): p. 1235490.
170. Myasnikov, A.G., et al., *Conformational transition of initiation factor 2 from the GTP- to GDP-bound state visualized on the ribosome*. Nat Struct Mol Biol, 2005. **12**(12): p. 1145-9.

171. Wienk, H., et al., *Structural dynamics of bacterial translation initiation factor IF2*. J Biol Chem, 2012. **287**(14): p. 10922-32.
172. Simonetti, A., et al., *Structure of the 30S translation initiation complex*. Nature, 2008. **455**(7211): p. 416-20.
173. Julian, P., et al., *The Cryo-EM structure of a complete 30S translation initiation complex from Escherichia coli*. PLoS Biol, 2011. **9**(7): p. e1001095.
174. Antoun, A., et al., *Ribosome formation from subunits studied by stopped-flow and Rayleigh light scattering*. Biol Proced Online, 2004. **6**: p. 35-54.
175. Antoun, A., et al., *How initiation factors tune the rate of initiation of protein synthesis in bacteria*. EMBO J, 2006. **25**(11): p. 2539-50.
176. Mitkevich, V.A., et al., *Termination of translation in eukaryotes is mediated by the quaternary eRF1*eRF3*GTP*Mg2+ complex. The biological roles of eRF3 and prokaryotic RF3 are profoundly distinct*. Nucleic Acids Res, 2006. **34**(14): p. 3947-54.
177. Perozzo, R., G. Folkers, and L. Scapozza, *Thermodynamics of protein-ligand interactions: history, presence, and future aspects*. J Recept Signal Transduct Res, 2004. **24**(1-2): p. 1-52.
178. Prabhu, N.V. and K.A. Sharp, *Heat capacity in proteins*. Annu Rev Phys Chem, 2005. **56**: p. 521-48.
179. Jelesarov, I. and H.R. Bosshard, *Isothermal titration calorimetry and differential scanning calorimetry as complementary tools to investigate the energetics of biomolecular recognition*. J Mol Recognit, 1999. **12**(1): p. 3-18.
180. Spolar, R.S. and M.T. Record, Jr., *Coupling of local folding to site-specific binding of proteins to DNA*. Science, 1994. **263**(5148): p. 777-84.
181. Connelly, P.R. and J.A. Thomson, *Heat capacity changes and hydrophobic interactions in the binding of FK506 and rapamycin to the FK506 binding protein*. Proc Natl Acad Sci U S A, 1992. **89**(11): p. 4781-5.
182. Murphy, K.P. and E. Freire, *Thermodynamics of structural stability and cooperative folding behavior in proteins*. Adv Protein Chem, 1992. **43**: p. 313-61.
183. Paleskava, A., A.L. Konevega, and M.V. Rodnina, *Thermodynamics of the GTP-GDP-operated conformational switch of selenocysteine-specific translation factor SelB*. J Biol Chem, 2012. **287**(33): p. 27906-12.
184. Murphy, K.P., et al., *Molecular basis of co-operativity in protein folding. III. Structural identification of cooperative folding units and folding intermediates*. J Mol Biol, 1992. **227**(1): p. 293-306.
185. Frisch, C., et al., *Thermodynamics of the interaction of barnase and barstar: changes in free energy versus changes in enthalpy on mutation*. J Mol Biol, 1997. **267**(3): p. 696-706.
186. Faergeman, N.J., et al., *Thermodynamics of ligand binding to acyl-coenzyme A binding protein studied by titration calorimetry*. Biochemistry, 1996. **35**(45): p. 14118-26.
187. Holdgate, G.A., et al., *The entropic penalty of ordered water accounts for weaker binding of the antibiotic novobiocin to a resistant mutant of DNA gyrase: a thermodynamic and crystallographic study*. Biochemistry, 1997. **36**(32): p. 9663-73.
188. Schrift, G.L., et al., *Molecular basis for nucleotide-binding specificity: role of the exocyclic amino group "N2" in recognition by a guanylyl-ribonuclease*. J Mol Biol, 2006. **355**(1): p. 72-84.
189. Milon, P. and M.V. Rodnina, *Kinetic control of translation initiation in bacteria*. Crit Rev Biochem Mol Biol, 2012. **47**(4): p. 334-48.
190. Sundari, R.M., et al., *Interaction of bacterial initiation factor 2 with initiator tRNA*. J Biol Chem, 1976. **251**(11): p. 3338-45.
191. Petersen, H.U., et al., *Specific interaction of initiation factor IF2 of E. coli with formylmethionyl-tRNA f Met*. Biochem Biophys Res Commun, 1979. **91**(3): p. 1068-74.
192. Boelens, R. and C.O. Gualerzi, *Structure and function of bacterial initiation factors*. Curr Protein Pept Sci, 2002. **3**(1): p. 107-19.

References

193. Antoun, A., et al., *How initiation factors maximize the accuracy of tRNA selection in initiation of bacterial protein synthesis*. Mol Cell, 2006. **23**(2): p. 183-93.
194. Krafft, C., et al., *Interaction of fMet-tRNA(fMet) with the C-terminal domain of translational initiation factor IF2 from Bacillus stearothermophilus*. FEBS Lett, 2000. **471**(2-3): p. 128-32.
195. Spurio, R., et al., *The C-terminal subdomain (IF2 C-2) contains the entire fMet-tRNA binding site of initiation factor IF2*. J Biol Chem, 2000. **275**(4): p. 2447-54.
196. Guenneugues, M., et al., *Mapping the fMet-tRNA(f)(Met) binding site of initiation factor IF2*. EMBO J, 2000. **19**(19): p. 5233-40.
197. Meunier, S., et al., *Structure of the fMet-tRNA(fMet)-binding domain of B. stearothermophilus initiation factor IF2*. EMBO J, 2000. **19**(8): p. 1918-26.
198. Avarsson, A., *Structure-based sequence alignment of elongation factors Tu and G with related GTPases involved in translation*. J Mol Evol, 1995. **41**(6): p. 1096-104.
199. Choi, S.K., et al., *Promotion of met-tRNA^{iMet} binding to ribosomes by yIF2, a bacterial IF2 homolog in yeast*. Science, 1998. **280**(5370): p. 1757-60.
200. Pain, V.M., *Initiation of protein synthesis in eukaryotic cells*. Eur J Biochem, 1996. **236**(3): p. 747-71.
201. Kuhle, B. and R. Ficner, *eIF5B Employs a Novel Domain Release Mechanism to Catalyze Ribosomal Subunit Joining*. EMBO J, 2014.
202. Guillon, L., et al., *Initiator tRNA binding by e/aIF5B, the eukaryotic/archaeal homologue of bacterial initiation factor IF2*. Biochemistry, 2005. **44**(47): p. 15594-601.
203. Yamamoto, H., et al., *Structure of the mammalian 80S initiation complex with initiation factor 5B on HCV-IRES RNA*. Nat Struct Mol Biol, 2014. **21**(8): p. 721-7.
204. Nissen, P., et al., *The crystal structure of Cys-tRNA^{Cys}-EF-Tu-GDPNP reveals general and specific features in the ternary complex and in tRNA*. Structure, 1999. **7**(2): p. 143-56.
205. Murzin, A.G., *OB(oligonucleotide/oligosaccharide binding)-fold: common structural and functional solution for non-homologous sequences*. EMBO J, 1993. **12**(3): p. 861-7.
206. Theobald, D.L., R.M. Mitton-Fry, and D.S. Wuttke, *Nucleic acid recognition by OB-fold proteins*. Annu Rev Biophys Biomol Struct, 2003. **32**: p. 115-33.
207. Arcus, V., *OB-fold domains: a snapshot of the evolution of sequence, structure and function*. Curr Opin Struct Biol, 2002. **12**(6): p. 794-801.
208. Lupas, A.N., C.P. Ponting, and R.B. Russell, *On the evolution of protein folds: are similar motifs in different protein folds the result of convergence, insertion, or relics of an ancient peptide world?* J Struct Biol, 2001. **134**(2-3): p. 191-203.
209. Huber, C. and G. Wachtershauser, *Peptides by activation of amino acids with CO on (Ni,Fe)S surfaces: implications for the origin of life*. Science, 1998. **281**(5377): p. 670-2.
210. Wachtershauser, G., *Before enzymes and templates: theory of surface metabolism*. Microbiol Rev, 1988. **52**(4): p. 452-84.
211. Wachtershauser, G., *On the chemistry and evolution of the pioneer organism*. Chem Biodivers, 2007. **4**(4): p. 584-602.
212. Cavarelli, J., et al., *The active site of yeast aspartyl-tRNA synthetase: structural and functional aspects of the aminoacylation reaction*. EMBO J, 1994. **13**(2): p. 327-37.
213. Pettersen, E.F., et al., *UCSF Chimera--a visualization system for exploratory research and analysis*. J Comput Chem, 2004. **25**(13): p. 1605-12.
214. Edgar, R.C., *MUSCLE: a multiple sequence alignment method with reduced time and space complexity*. BMC Bioinformatics, 2004. **5**: p. 113.
215. Holm, L. and C. Sander, *Protein structure comparison by alignment of distance matrices*. J Mol Biol, 1993. **233**(1): p. 123-38.
216. Hansson, S., et al., *Crystal structure of a mutant elongation factor G trapped with a GTP analogue*. FEBS Lett, 2005. **579**(20): p. 4492-7.

217. Kong, C., et al., *Crystal structure and functional analysis of the eukaryotic class II release factor eRF3 from S. pombe*. Mol Cell, 2004. **14**(2): p. 233-45.
218. Leibundgut, M., et al., *Selenocysteine tRNA-specific elongation factor SelB is a structural chimaera of elongation and initiation factors*. EMBO J, 2005. **24**(1): p. 11-22.
219. Haurlyliuk, V., et al., *The pretranslocation ribosome is targeted by GTP-bound EF-G in partially activated form*. Proc Natl Acad Sci U S A, 2008. **105**(41): p. 15678-83.
220. Kuhle, B. and R. Ficner, *eIF5B employs a novel domain release mechanism to catalyze ribosomal subunit joining*. EMBO J, 2014. **33**(10): p. 1177-91.
221. Paleskava, A., A.L. Konevega, and M.V. Rodnina, *Thermodynamic and kinetic framework of selenocysteyl-tRNA^{Sec} recognition by elongation factor SelB*. J Biol Chem, 2010. **285**(5): p. 3014-20.
222. Wilden, B., et al., *Role and timing of GTP binding and hydrolysis during EF-G-dependent tRNA translocation on the ribosome*. Proc Natl Acad Sci U S A, 2006. **103**(37): p. 13670-5.
223. Haurlyliuk, V., et al., *Class-1 release factor eRF1 promotes GTP binding by class-2 release factor eRF3*. Biochimie, 2006. **88**(7): p. 747-57.
224. Burnett, B.J., et al., *Elongation factor Ts directly facilitates the formation and disassembly of the Escherichia coli elongation factor Tu.GTP.aminoacyl-tRNA ternary complex*. J Biol Chem, 2013. **288**(19): p. 13917-28.
225. Mesters, J.R., et al., *Synergism between the GTPase activities of EF-Tu.GTP and EF-G.GTP on empty ribosomes. Elongation factors as stimulators of the ribosomal oscillation between two conformations*. J Mol Biol, 1994. **242**(5): p. 644-54.
226. Liljas, A., M. Ehrenberg, and J. Aqvist, *Comment on "The mechanism for activation of GTP hydrolysis on the ribosome"*. Science, 2011. **333**(6038): p. 37; author reply 37.
227. Wallin, G., S.C. Kamerlin, and J. Aqvist, *Energetics of activation of GTP hydrolysis on the ribosome*. Nat Commun, 2013. **4**: p. 1733.
228. Aleksandrov, A. and M. Field, *Mechanism of activation of elongation factor Tu by ribosome: catalytic histidine activates GTP by protonation*. RNA, 2013. **19**(9): p. 1218-25.
229. Adamczyk, A.J. and A. Warshel, *Converting structural information into an allosteric-energy-based picture for elongation factor Tu activation by the ribosome*. Proc Natl Acad Sci U S A, 2011. **108**(24): p. 9827-32.
230. Gasper, R., et al., *It takes two to tango: regulation of G proteins by dimerization*. Nat Rev Mol Cell Biol, 2009. **10**(6): p. 423-9.
231. Scrima, A. and A. Wittinghofer, *Dimerisation-dependent GTPase reaction of MnmE: how potassium acts as GTPase-activating element*. EMBO J, 2006. **25**(12): p. 2940-51.
232. Chappie, J.S., et al., *G domain dimerization controls dynamin's assembly-stimulated GTPase activity*. Nature, 2010. **465**(7297): p. 435-40.
233. Rodnina, M.V., *Visualizing the protein synthesis machinery: new focus on the translational GTPase elongation factor Tu*. Proc Natl Acad Sci U S A, 2009. **106**(4): p. 969-70.
234. Kubarenko, A.V., P.V. Sergiev, and M.V. Rodnina, *GTPases of translational apparatus*. Mol Biol (Mosk), 2005. **39**(5): p. 746-61.
235. Mohr, D., W. Wintermeyer, and M.V. Rodnina, *GTPase activation of elongation factors Tu and G on the ribosome*. Biochemistry, 2002. **41**(41): p. 12520-8.
236. Wieden, H.J., W. Wintermeyer, and M.V. Rodnina, *A common structural motif in elongation factor Ts and ribosomal protein L7/12 may be involved in the interaction with elongation factor Tu*. J Mol Evol, 2001. **52**(2): p. 129-36.
237. Bondi, A., *van der Waals Volumes and Radii*. J. Phys. Chem., 1964. **68**(3): p. 441-451.
238. Shannon, R.D., *Revised Effective Ionic Radii and Systematic Studies of Interatomic Distances in Halides and Chalcogenides*. Acta Crystallogr A, 1976. **32**(Pt 5): p. 751-767.

References

239. Pisareva, V.P., C.U. Hellen, and T.V. Pestova, *Kinetic analysis of the interaction of guanine nucleotides with eukaryotic translation initiation factor eIF5B*. *Biochemistry*, 2007. **46**(10): p. 2622-9.
240. Gomez, J., et al., *The heat capacity of proteins*. *Proteins*, 1995. **22**(4): p. 404-12.
241. Conway, T.W., *On the Role of Ammonium or Potassium Ion in Amino Acid Polymerization*. *Proc Natl Acad Sci U S A*, 1964. **51**: p. 1216-20.
242. Conway, T.W. and F. Lipmann, *Characterization of a Ribosome-Linked Guanosine Triphosphatase in Escherichia Coli Extracts*. *Proc Natl Acad Sci U S A*, 1964. **52**: p. 1462-9.
243. Parmeggiani, A. and G. Sander, *Properties and regulation of the GTPase activities of elongation factors Tu and G, and of initiation factor 2*. *Mol Cell Biochem*, 1981. **35**(3): p. 129-58.
244. Fasano, O., E. De Vendittis, and A. Parmeggiani, *Hydrolysis of GTP by elongation factor Tu can be induced by monovalent cations in the absence of other effectors*. *J Biol Chem*, 1982. **257**(6): p. 3145-50.
245. Ash, M.R., et al., *The initiation of GTP hydrolysis by the G-domain of FeoB: insights from a transition-state complex structure*. *PLoS One*, 2011. **6**(8): p. e23355.
246. Chappie, J.S., et al., *A pseudoatomic model of the dynamin polymer identifies a hydrolysis-dependent powerstroke*. *Cell*, 2011. **147**(1): p. 209-22.
247. Kobayashi, K., et al., *Structural basis for mRNA surveillance by archaeal Pelota and GTP-bound EF1alpha complex*. *Proc Natl Acad Sci U S A*, 2010. **107**(41): p. 17575-9.
248. Kobayashi, K., et al., *Structural basis for translation termination by archaeal RF1 and GTP-bound EF1alpha complex*. *Nucleic Acids Res*, 2012. **40**(18): p. 9319-28.
249. Meyer, S., et al., *Kissing G domains of MnmE monitored by X-ray crystallography and pulse electron paramagnetic resonance spectroscopy*. *PLoS Biol*, 2009. **7**(10): p. e1000212.
250. Foucher, A.E., et al., *Potassium acts as a GTPase-activating element on each nucleotide-binding domain of the essential Bacillus subtilis EngA*. *PLoS One*, 2012. **7**(10): p. e46795.
251. Nagel, K. and J. Voigt, *Regulation of the uncoupled GTPase activity of elongation factor G (EF-G) by the conformations of the ribosomal subunits*. *Biochim Biophys Acta*, 1993. **1174**(2): p. 153-61.
252. Praefcke, G.J. and H.T. McMahon, *The dynamin superfamily: universal membrane tubulation and fission molecules?* *Nat Rev Mol Cell Biol*, 2004. **5**(2): p. 133-47.
253. Warnock, D.E., J.E. Hinshaw, and S.L. Schmid, *Dynamin self-assembly stimulates its GTPase activity*. *J Biol Chem*, 1996. **271**(37): p. 22310-4.
254. Das, S. and U. Maitra, *Functional significance and mechanism of eIF5-promoted GTP hydrolysis in eukaryotic translation initiation*. *Prog Nucleic Acid Res Mol Biol*, 2001. **70**: p. 207-31.
255. Ash, M.R., et al., *The cation-dependent G-proteins: in a class of their own*. *FEBS Lett*, 2012. **586**(16): p. 2218-24.
256. Perla-Kajan, J., et al., *Properties of Escherichia coli EF-Tu mutants designed for fluorescence resonance energy transfer from tRNA molecules*. *Protein Eng Des Sel*, 2009. **23**(3): p. 129-36.
257. Harding, M.M., *Geometry of metal-ligand interactions in proteins*. *Acta Crystallogr D Biol Crystallogr*, 2001. **57**(Pt 3): p. 401-11.
258. Ghosh, A., et al., *How guanylate-binding proteins achieve assembly-stimulated processive cleavage of GTP to GMP*. *Nature*, 2006. **440**(7080): p. 101-4.

Acknowledgements

This doctoral thesis was written during my time at the Department for Molecular Structural Biology of the Georg-August University Göttingen. First and foremost, I am grateful to Prof. Dr. Ralf Ficner for providing me with excellent working conditions and for his continuous and unreserved support throughout my time in his department. I would like to thank Prof. Dr. Marina Rodnina for the acceptance to be second reviewer of my thesis and for her comments on my work during the thesis committee meetings. Achim Dickmanns I thank for his support and discussions on countless occasions and his comments on various chapters presented in this thesis. Particularly indebted I am to Piotr Neumann for invaluable help during X-ray data collection and structure determination, as well as to Oliver Valerius for his contribution to the analysis of the crosslinking data. Finally, I thank Michael Franke for his excellent technical assistance. All former and current members of the research group for Applied Synthetic Biology and the MSB department, in particular my lab colleague Yi Liu, made the considerable amount of time I spent in lab or office worthwhile.

My parents provided me with indispensable advice and support. Moreover, I express my deep gratitude to Lili Dörfel, who contributed significantly to this thesis with her patience, her open ear regarding every detail of my work and for her critical comments on the many previous drafts of this manuscript.

Curriculum vitae

Persönliche Daten

Name: Bernhard Kuhle

Geburtsdatum: 06.12.1984

Geburtsort: Göttingen

Nationalität: deutsch

E-Mail: bkuhle@gwdg.de

Ausbildung

Schulbildung

1992-1996	Grundschule Waake
1996-1998	Orientierungsstufe Weende-Nord, Göttingen
2000-2001	Duluth Central High School, Minnesota, USA
1998-2004	Theodor-Heuss Gymnasium, Göttingen
2004	Allgemeine Hochschulreife (Abitur)

Studium

2004-2005	Physikstudium (Freie Universität Berlin)
2005-2010	Biologiestudium (Georg-August-Universität Göttingen)
2010	Diplom (Georg-August-Universität Göttingen)

Promotion

seit 07/2010	Promotion (Georg-August-Universität Göttingen)
--------------	--